Wetlands through time – modeling changes in area and greenhouse gas budgets from the past to the future

Inauguraldissertation

der Philosophisch–naturwissenschaftlichen Fakultät
der Universität Bern

vorgelegt von

Jurek Müller

aus Deutschland

Leiter der Arbeit:

Prof. Dr. Fortunat Joos

Abteilung für Klima– und Umweltphysik
Physikalisches Institut der Universität Bern

Wetlands through time – modeling changes in area and greenhouse gas budgets from the past to the future

Inauguraldissertation

der Philosophisch–naturwissenschaftlichen Fakultät
der Universität Bern

vorgelegt von

Jurek Müller

aus Deutschland

Leiter der Arbeit:

Prof. Dr. Fortunat Joos

Abteilung für Klima– und Umweltphysik
Physikalisches Institut der Universität Bern

Von der Philosophisch–naturwissenschaftlichen Fakultät angenommen.

Bern, 25.08.2021

Der Dekan
Prof. Dr. Zoltan Balogh

Even an entire society, a nation, or all simultaneously existing societies taken together, are not owners of the earth. They are simply its possessors, its beneficiaries, and have to bequeath it in an improved state to succeeding generations [..].

— Karl Marx, *Capital, Vol. 3*

Thesis overview and summary

The accelerated burning of fossil fuels and the large-scale transformation of forests into agricultural land since the industrial revolution have led to rapid climate warming which, if not mitigated, is threatening human life on Earth. The field of climate science strives to better understand the complex climate system and its internal feedbacks and with that be able to provide reliable projections of future changes. These depend most and foremost on societal and political dynamics. In the Paris Agreement, the global community has committed to limit warming below 2° C, which requires global net-zero greenhouse gas emissions until the year 2050. However, global efforts to reduce emissions are still by far insufficient to reach the agreed target.

Although climate science long has identified immediate emission reduction as the most important mitigation strategy, a multitude of internal feedbacks and processes are still poorly understood. This creates the need for further investigations into potential impacts of past and future emissions, not only on the climate but also on the global biosphere, including potential irreversible tipping points or mitigation opportunities. One important sub-system of the global climate system and carbon cycle that is expected to see increased pressures from anthropogenic disturbance and climate warming are global wetlands. Wetlands are sources of methane, an important greenhouse gas, and thus hold the potential to contribute to future warming. A special type of wetlands, peatlands, also act as long-term carbon stores and thus could both help to remove anthropogenic carbon from the atmosphere on long timescales or lead to large additional release of carbon into the atmosphere.

This thesis presents model investigations of wetland dynamics, using the dynamic global vegetation model LPX-Bern, which is developed and maintained at the University of Bern. LPX-Bern is used to investigate changes in wetland area and greenhouse gas budgets from the past to the future, with a particular focus on peatlands.

Chapter 1 gives an introduction to the key concepts discussed in this thesis. First, the global carbon cycle and its different components are introduced. Then wetlands, the main subject of this thesis, are defined and discussed in detail. Wetlands are a key component of the global carbon cycle as they function both as large carbon stores and sources of methane. The history of wetlands and their reconstruction through proxy evidence is discussed in the context of past climate variability. The past and potential future effects of human activities on wetlands are examined. Finally, the world of wetland modeling is introduced, giving an overview of the historic model development and different model complexities.

Chapter 2 then introduces the LPX-Bern and presents model adjustments that were implemented during this thesis. The modules representing peatlands and wetlands are discussed in detail, including the formulation for the dynamic calculation of wetland and peatland area and the new treatment of dynamic peatland area in case of prescribed land-use change. The discussion of the methane module includes the emission calculation for different types of wetlands, the implementation of methane emissions from fires, and the description of a re-calibration of key emission factors in preparation for the different modeling studies presented in the following chapters.

In **chapter 3**, a modeling study published in *Biogeosciences* is presented which investigates the transient history of peatlands from the Last Glacial Maximum (LGM), about 21,000 years ago, to the present. Transient LPX-Bern simulations suggest that peatland area was highly dynamic in the past and changes in area were driven mostly by changes in precipitation and temperature. The study argues that to determine the net peat carbon balance, the full history of peatlands has to be considered, including peatlands that vanished over time. The simulated transient evolution of today's northern peatlands is compared to data reconstructions and large model-data mismatches are found concerning the inception of peat in northern Asia. However, the simulated peatland distribution and carbon storage at present-day compare well to literature estimates. Additional time-slice simulations at the LGM show that uncertainties in the prescribed climate forcing propagate to large uncertainties in peatland variables.

Chapter 4 presents a follow-up study published in *Biogeosciences* which directly builds on results from the study presented in chapter 3. The transient simulation from the LGM to the present is taken as the basis for future projections of peatland dynamics. Different future climate and land-use scenarios are used to investigate potential future short-term and long-term changes in peatland area and carbon storage. The results suggest likely future losses of global peatland area and carbon, even under present-day climate, with large parts of today's northern peatlands at risk. Losses in response to future climate and land-use change are expected to increase with increasing future emissions. Uncertainties connected to uncertain climate anomalies are quantified by using output from a climate model ensemble as forcing.

In **chapter 5**, model investigations into past wetland methane emissions are presented. Results from transient LPX-Bern simulations from the LGM to the present are compared to the methane ice-core record. Large model-data mismatches are found, most notably the absence of a simulated increase in emissions from the LGM to the pre-industrial period (PI). Driver attribution reveals a small temperature sensitivity and large sea-level driven tropical wetland loss as potential sources of the small LGM-PI methane emission increase. Preliminary investigations into model adjustments, addressing the temperature dependence of methane production and the dynamic wetland model, show potential to increase the LGM-PI methane emission rise, but alone are not sufficient to close the model-date gap. Furthermore, the discussed model changes could worsen model performance in other respects which would need to be addressed.

Chapter 6 presents a selection of two collaborative studies for which LPX-Bern model output was provided. First, simulations that contributed to the Global Methane Budget, a community publication that is part of the Global Carbon Project, are discussed in detail, with a focus on comparing wetland methane emissions between LPX-Bern simulations with prescribed and dynamically calculated wetland area. Emissions are found to be globally comparable, but with regional biases in wetland prediction translating into large regional differences in simulated emissions. In the second part, simulations are presented that contributed to a model-intercomparison project investigating projected future changes in peatland net carbon balance and methane emissions under different scenarios. The LPX-Bern simulations in this study, where the peatland area is prescribed, are compared to similar LPX-Bern simulations from chapter 4, where the peatland area is calculated dynamically. Future peatland area loss is found to mostly lead to larger predicted carbon loss but also smaller peatland methane emissions than if peatland area is held constant.

Finally, **Chapter 7** gives an outlook over potential future model investigations and model development, progressing and building on the work presented in this thesis. An additional **appendix** describes the implementation of a new transient land-sea-ice mask for paleo simulations into the LPX-Bern, which however was not used in any simulations presented in the main text. The new implementation increases the update time-step and allows for variable grid cell land fractions.

Contents

Chapter 1

Introduction

Since the industrial revolution, the global climate system experiences rapid changes caused by the burning of fossil fuels and the large-scale reshaping of the terrestrial land surface by human activities (IPCC, 2013). The climate is a complex system with a multitude of processes and interconnected sub-systems that interact and feed back on each other. Solid knowledge about all components is required to quantify how a specific perturbation at one point of the system might propagate and change the state of the system as a whole. One of the most important elements of the climate system is the global carbon cycle, which is heavily disturbed by human-caused emissions of carbon dioxide (Ciais et al., 2013). Knowledge about the past, present, and future of the global carbon cycle is essential to understand how anthropogenic climate change impacts life on earth and to find effective mitigation strategies that avoid crossing irreversible tipping points of the climate system (Lowe & Bernie, 2018). One of the key components of the terrestrial carbon cycle are wetlands. This thesis provides detailed investigations of wetlands and their close relationship to the global carbon cycle and the climate system. Their dynamics have contributed to changes in the budgets of the greenhouse gases carbon dioxide and methane and thus have affected climate in the past and will continue to affect it in the future.

This chapter provides a general introduction to the concepts and processes that play an important role in the investigations presented in the following chapters. First, an overview of the global carbon cycle and its components is given in section 1.1, which serves as a backdrop for all model investigations presented in this thesis. Section 1.2 then defines and introduces the general concept of wetlands as the main subject of this thesis. Following, different aspects of global wetlands are introduced in detail. Section 1.3 presents the role of wetlands in the global carbon cycle. Section 1.4 gives a short introduction to past climate dynamics and explores how wetlands responded to past climate change and how these changes can be reconstructed from proxy records. Section 1.5 looks at how anthropogenic disturbance has affected wetlands in the recent past and might continue to affect wetlands in the future. Finally, section 1.6 discusses how wetlands and wetland processes are modeled and how these models are used in climate science.

1.1 The global carbon cycle

The global carbon cycle refers to the distribution and fluxes of carbon through, and its interaction with, the earth system. Carbon can be found in all spheres of the earth system. As an integral building block of life, the carbon cycle and the biosphere are deeply intertwined. Similar is true for the climate system, which is fundamentally shaped by two of the gaseous forms of carbon, carbon dioxide (CO_2) and methane (CH_4), due to their contribution to the greenhouse effect (Ciais et al., 2013). The greenhouse effect alters the energy balance of the earth by reducing the long-wave thermal radiation that escapes through the earths' atmosphere (Wild et al., 2013).

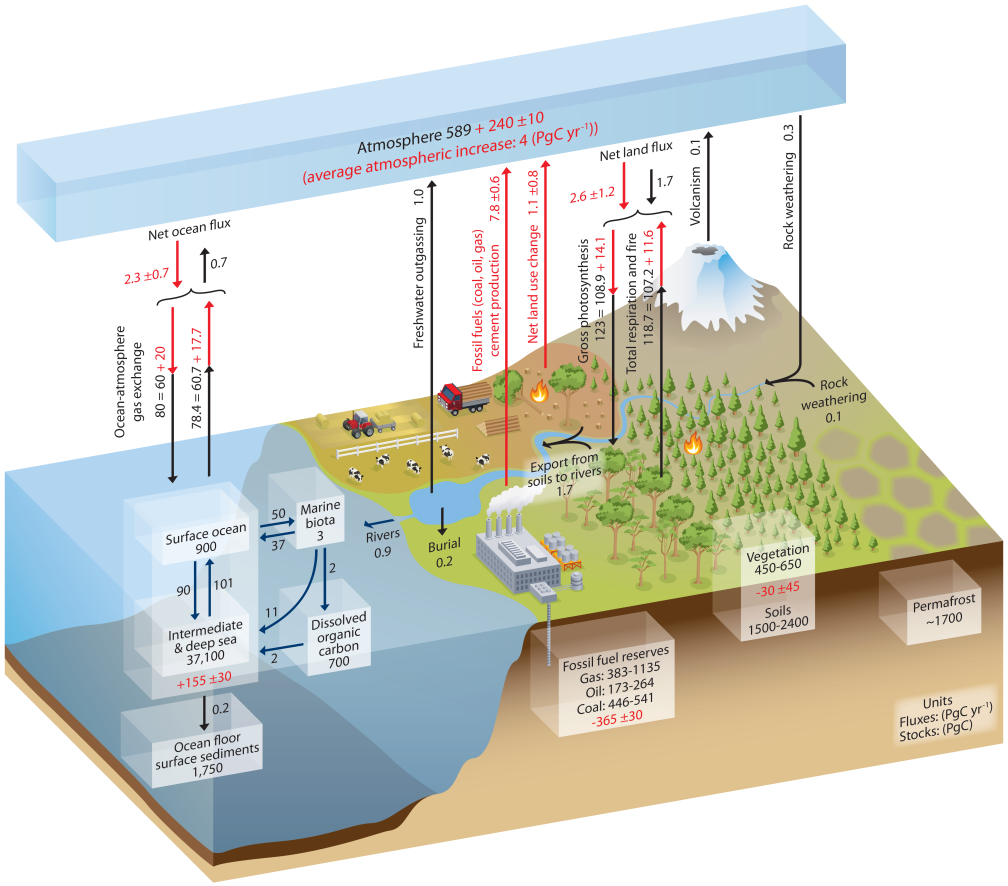

Figure 1.1: Simplified illustration of the main carbon pools (boxes) and fluxes (arrows) of the global carbon cycle from Ciais et al. (2013). Numbers for carbon pools are in the units petagrams of carbon (PgC), which can also be expressed as gigatons of carbon (GtC), and for fluxes in PgC yr^{-1}. Black numbers and arrows indicate the pre-industrial state (at 1750) and red numbers and arrows indicate the cumulative anthropogenic perturbation from 1750 to 2011 in case of carbon pools, and average perturbation over 2009–2011 in the case of fluxes. Updated numbers for selected fluxes from Friedlingstein et al. (2020) are given in the text.

Greenhouse gasses like water vapor, CO_2, CH_4, and nitrous oxide (N_2O) absorb part of the earth's thermal radiation and transform the atmosphere into an insulating layer resulting in a substantial increase of global surface temperature. Life on earth depends on this natural greenhouse effect, as mean global surface temperatures would be about 33° C lower without it (Schmidt et al., 2010). The majority of the natural greenhouse effect can be attributed to water vapor (about half), clouds (about a quarter), and CO_2 (about a fifth) (Huang et al., 2013). Other gasses such as CH_4 and N_2O play a smaller yet increasing role given anthropogenic emissions (Etminan et al., 2016).

The atmospheric concentrations of CO_2 and CH_4, and with them important controls on the global climate, are directly linked to the balance of carbon fluxes between all the spheres of the earth system. Before the industrial period, the global carbon cycle was in rough equilibrium entailing large gross carbon fluxes, but only small net carbon fluxes between atmosphere, land, and oceans (Ciais et al., 2013, Fig. 1.1). The anthropogenic disturbance of the carbon cycle since then mostly consisted in the burning of fossil fuels, which are inert deposits of organic carbon formed millions of years ago in the terrestrial biosphere and transformed into oil, coal, and methane. In addition, large-scale deforestation and other land-use changes released carbon stored in the land biosphere. This has shifted the balance of the global carbon fluxes and led to an almost doubling of atmospheric CO_2 concentrations since the pre-industrial period (Friedlingstein et al., 2020, Fig. 1.1).

Fossil fuel extraction and burning also releases large amounts of methane into the atmosphere (Ciais et al., 2013, Fig. 1.2). Other large anthropogenic sources include emissions from livestock, rice cultivation, biomass burning, and waste management. Together these disturbances of the methane budget led to an almost tripling of methane concentrations since the pre-industrial period (Saunois et al., 2020, Fig. 1.2).

Atmosphere

The atmosphere stores with 860 gigatons of carbon (GtC) only a small fraction of the global carbon, but acts as the main coupler of the carbon cycle, with large gross carbon fluxes between atmosphere, ocean, and land (Fig. 1.1 Friedlingstein et al., 2020). CO_2 is generally well mixed within the free atmosphere, with only small, but noticeable, regional differences. CO_2 has no major atmospheric sinks or sources and changes in its atmospheric concentration are thus determined by net fluxes between the atmosphere, oceans, and land and the anthropogenic input from fossil fuel burning. The seasonal cycle of atmospheric CO_2 concentrations is dominated by the exchange with the land biosphere in the northern hemisphere, where the landmass is the largest. During the growing season, the biosphere shows a net uptake of carbon, and during winter a net release.

Atmospheric CO_2 concentrations increased from about 277 parts per million (ppm) in 1750 (Joos & Spahni, 2008) to about 410 ppm in 2019, corresponding to an increase in atmospheric carbon storage of about 285 GtC (Friedlingstein et al., 2020). This represents only about 41 % of the total anthropogenic carbon released into the atmosphere since the pre-industrial period, with the rest taken up by the global oceans and the land biosphere. The annual atmospheric growth rate, however, has steadily increased reaching 5.1 GtC yr^{-1} in the years 2010–2019.

Methane, in contrast to CO_2, has a large atmospheric sink due to its reaction with hydroxyl radicals (OH). The majority of natural and anthropogenic methane sources are located on land, leading to a small inter hemispherical gradient with larger atmospheric methane concentrations in the northern hemisphere (Mayer et al., 1982). The lifetime of atmospheric methane is estimated to be 9–11 years (Prather et al., 2012; Voulgarakis et al., 2013; Maasakkers et al., 2019). Despite the short lifetime, the atmospheric concentrations have increased from about 700 parts per billion (ppb) in the pre-industrial period Schilt et al. (2010b) to 1879 ppb in 2020 (Ed Dlugokencky, 2021) due to large anthropogenic emissions (Saunois et al., 2020).

Oceans

The largest fraction of the carbon stored in the three relatively fast exchanging reservoirs - atmosphere, ocean, and land biosphere - is in the ocean (Fig. 1.1). The majority of that carbon, about 38,000 GtC, is stored as dissolved inorganic carbon (DIC), about 700 GtC are stored as dissolved organic carbon (DOC), and only about 3 GtC are stored in living marine biomass (Ciais et al., 2013). The three main parts of dissolved inorganic carbon, dissolved carbonic acid, bicarbonate, and carbonate ions, are all tightly coupled through acid-base chemistry (Sarmiento & Gruber, 2006). Apart from a small carbon input from rivers and carbon loss to sediments, the ocean exchanges carbon mainly with the atmosphere by air-sea gas exchange. This flux is driven by the air-sea difference in CO_2 partial pressure (pCO_2) and is on global average nearly balanced (Sarmiento & Gruber, 2006). The fast exchange of carbon between the surface ocean and the atmosphere tightly couples these two reservoirs.

The state of the ocean governs the natural atmospheric CO_2 inventory as the ocean holds much more carbon than the atmosphere. Surface-to-deep ocean gradients in carbon and alkalinity, and therefore also pCO_2 in the surface water are co-governed by the so-called solubility pump, biological pump, and carbonate pump (Volk & Hoffert, 1985; Denman et al., 2007). Due to the temperature dependence of the CO_2 solubility, cold waters can hold more DIC than warm waters.

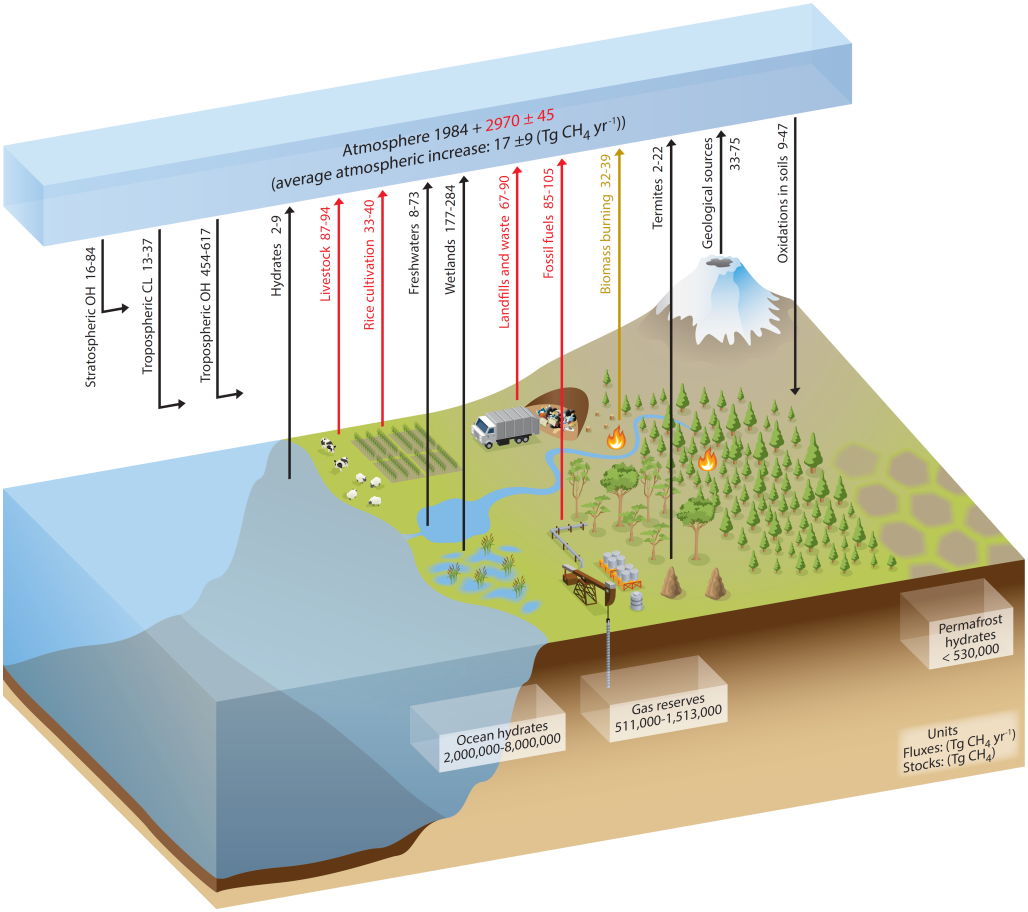

Figure 1.2: Simplified illustration of the main methane pools (boxes) and fluxes (arrows) of the global methane cycle from Ciais et al. (2013). Numbers for methane pools are in the units teragram of methane (Tg CH_4). Black arrows represent natural fluxes, with no direct anthropogenic interference. Red arrows represent anthropogenic methane fluxes, and the light brown arrow represents a combination of natural and anthropogenic fluxes. The increase in atmospheric methane since 1750 is given in red and the pre-industrial methane load in black. Updated numbers for selected fluxes from Saunois et al. (2020) are given in the text.

The surface ocean is on average warmer than the cold deep ocean and therefore depleted in DIC relative to the deep. The solubility pump is driven by water masses entering the deep ocean at deepwater formation zones in the Arctic regions of the North Atlantic and the Southern Ocean, where cool temperatures and high salinity lead to the sinking of cold, carbon-rich surface waters (Kuhlbrodt et al., 2007). In the case of up-welling of these carbon-rich waters in warmer tropical regions solubility decreases and CO_2 is out-gassed back to the atmosphere.

The biological pump also lowers DIC in the surface relative to the deep ocean. DIC is converted to organic carbon by plankton. A small but important fraction of this organic carbon is transported to the deep ocean in the form of gravitationally sinking particulate organic carbon or dissolved organic carbon. This organic carbon is remineralized to DIC in the thermocline and deep ocean and eventually transported back to the surface by the ocean circulation.

The carbonate pump is connected to marine biota which builds calcareous shells (Holligan & Robertson, 1996). Although these shells bind carbon, their formation increases the partial pressure of CO_2 through the carbon chemistry in the ocean, thus working against the biological pump with respect to CO_2. Calcareous shells are typically slowly remineralized after sinking to a depth below the saturation horizon of calcium carbonate. A small part of the organic carbon and calcareous shells reaches the seafloor, where it forms long term deposits. The calcium carbonate deposits can eventually form limestone and can reenter the carbon cycle in form

of rock weathering or volcanism (Denman et al., 2007). The sedimentation and weathering represent an important long-term control of the carbon cycle with timescales on the order of tens of thousands to millions of years (Jeltsch-Thömmes et al., 2019). Changes in these carbon pumps and geological fluxes were likely responsible for changes in atmospheric CO_2 over glacial-interglacial cycles of the order of 100 ppm (e.g. Sigman & Boyle, 2000; Sigman et al., 2010). Since the pre-industrial period, the ocean has taken up about 24 % of the anthropogenic carbon release corresponding to about 170 GtC (Friedlingstein et al., 2019). This uptake was mainly driven by the increase in atmospheric partial pressure due to the CO_2 input from fossil fuel burning and land use.

In terms of methane, the oceans represent a small source of about 13 teragrams of methane per year (Tg yr^{-1}) which is released from frozen methane hydrates and other geological and biogenic sources (Fig. 1.2 Saunois et al., 2020). Methane hydrates are solid crystalline structures formed out of water and methane, mostly found in the upper layers of the ocean sediments. They accumulate methane mostly formed by the microbial or thermal degradation of organic material in the sediments. It is estimated that they potentially hold 2000–9000 Gt of methane, which is about 390–1740 times more as currently present in the atmosphere (Ciais et al., 2013). Rising ocean temperatures can lead to the destabilization of methane hydrates, especially in shallower coastal regions, leading to the out-gassing of methane. However, in the case of gradual out-gassing most of the methane is respired to CO_2 by methanotrophs in the water column and little methane reaches the surface (Ruppel & Kessler, 2017). It has been suggested that the large continuous release of methane from hydrates could have driven large climate warming in the deep past such as during the Latest Paleocene Thermal Maximum about 55.6 million years ago (Dickens et al., 1995). However, in the future, the gradual methane release from hydrates is expected to remain moderate but could become important on geological timescales (Archer, 2007; O'Connor et al., 2010).

Land Biosphere

The carbon cycle of the terrestrial biosphere is tightly coupled to the terrestrial nutrient and water cycles (Fig. 1.1 Ciais et al., 2013). CO_2 is taken up from the atmosphere during plant photosynthesis. The solar energy is stored in carbohydrates. The carbohydrates are partly used immediately to drive plant metabolism, where the associated carbon is respired and released back to the atmosphere, and partly to build up biomass (Lambers et al., 2008). The total amount of carbon taken up by photosynthesis per unit time is referred to as gross primary production (GPP), and the fraction of organic carbon that remains after plant respiration and is used for plant growth is referred to as net primary production (NPP). Living vegetation stores about 450–650 GtC globally, with carbon densities varying between ecosystem types, such as grasslands and forests (Prentice et al., 2001). The heterotrophic part of the terrestrial biosphere, encompassing animals, fungi, and microorganisms gradually respires the organic carbon built up by plants within a complex food web. Turnover timescales vary between different carbon pools (Prentice et al., 2001). Plant litter that accumulates at the soil surface generally has a fast turnover time on the order of months to years, while a small, more stable, fraction of the organic carbon remains in the soils, where it has turnover times of decades to millennia. The difference between NPP and heterotrophic respiration (HR) per unit time is called net ecosystem productivity (NEP) and to a first degree determines the net carbon balance of the land biosphere. When considering also disturbances like wildfires, which lead to additional oxidation of organic carbon, the net carbon balance is denoted as net biome production (NBP).

Heterotrophic decay rates of organic carbon are modulated by a multitude of factors, such as temperature, moisture, species, and other soil properties (Rustad et al., 2000). Under the specific conditions in peatlands and permafrost soils, where heterotrophic respiration is reduced to a minimum, organic carbon can accumulate into large pools (see section 1.3.1). Global soils

are estimated to store about 1500 GtC up to a depth of 1 m (Scharlemann et al., 2014) and about 2300 GtC up to 3 m depth (Jobbágy & Jackson, 2000). About 600 GtC are stored in peatlands alone (Yu et al., 2010; Ribeiro et al., 2021; Hugelius et al., 2020). Perennially frozen permafrost soils constitute a second large soil carbon pool storing about 800 GtC (Hugelius et al., 2014). However, large uncertainties are connected especially to the estimates of peatland and permafrost carbon and some overlap between these pools exist.

Before the industrial period, the land was in rough equilibrium with the atmosphere, with only a small net carbon uptake partly driven by peatlands (Kleinen et al., 2010; Yu, 2011). Since then, drastic land-use changes and global warming have significantly disturbed the terrestrial carbon cycle. Deforestation and land-use change have contributed about 36 % to the anthropogenic emissions since 1750 corresponding to about 255 GtC, with estimated yearly emissions of 1.6 GtC between 2010–2019 (Friedlingstein et al., 2020). However, increases in global mean temperature, precipitation, and atmospheric CO_2 have also led to an increase in NPP, outweighing the concurrent increase in HR and disturbance fluxes. This land biosphere sink partly compensates for the anthropogenic emissions from land use, with a gross uptake of about 230 GtC since 1750 (Friedlingstein et al., 2020).

At present, the global land biosphere is thought to act as a net carbon sink with an average uptake of about 1.8 GtC yr^{-1} in the years 2010–2019, despite the continuing emissions from land use. The terrestrial carbon cycle thus provides a strong negative feedback to anthropogenic climate change, however, this net negative feedback could change in the future (Friedlingstein & Prentice, 2010; Schurgers et al., 2018). The so-called CO_2 fertilization effect increases productivity with rising atmospheric CO_2 concentrations by allowing to optimize CO_2 uptake and water loss (Schimel et al., 2015; Zhu et al., 2016), however, its effectiveness and restrictions due to nutrient limitations are debated (e.g. Gedalof & Berg, 2010; Terrer et al., 2016; He et al., 2017; Joos et al., 2020). Rising temperatures can result in longer growing seasons and increased NEP in some regions of the world, but reduced NEP in others (Gallego-Sala et al., 2018; Fernández-Martínez et al., 2019). High temperatures potentially also put large peatland and permafrost carbon pools at risk (Qiu et al., 2020; Hugelius et al., 2020), as discussed in chapter 4. Furthermore, continued deforestation and land-use change will increase anthropogenic land-use emissions and limit the ability of the land biosphere for future carbon uptake (Strassmann et al., 2008; Riahi et al., 2017; Popp et al., 2017).

In terms of methane, the natural terrestrial carbons cycle presents both a large source (about 134–215 Tg yr^{-1} in 2008–2017) and small sink (about 30–38 Tg yr^{-1}) (Fig. 1.2 Saunois et al., 2020). The methane is produced during the heterotrophic respiration of organic carbon under anoxic conditions and biomass burning. Wetlands are the largest natural source of methane (see section 1.3.2). Other sources include termites, ruminants, wildfires, freshwaters, and geological sources. A part of the methane produced in wetlands and wet soils is directly consumed by methanotrophic microorganisms. In dry soils, methanotrophs consume methane from the atmosphere forming the terrestrial methane sink. Similar to ocean sediments, frozen methane hydrates are thought to store large amounts (about 20 GtC) of accumulated methane in deep Arctic permafrost soils (Ruppel, 2015). For now, emissions from permafrost hydrates are estimated to be small (Saunois et al., 2020), however, the fate of this methane depends on the rate and extent of future permafrost thawing. Anthropogenic methane emissions mostly originate from fossil fuel burning, animal farming, landfills, and rice cultivation. They are estimated to amount to about 360 Tg yr^{-1} in the years 2008–2017 and thus surpass the natural emissions (Saunois et al., 2020).

Carbon isotopes

Carbon is present in the form of the stable isotopes ^{12}C and ^{13}C and the radioactive ^{14}C. Only about 1 % is present as ^{13}C and only a vanishing small fraction as ^{14}C ($^{14}C/C \sim 10^{-12}$). ^{13}C

and ^{14}C are subject to fractionation relative to ^{12}C during biological and physical processes. Measurements of their molar fractions in, e.g., atmospheric CO_2 or CH_4, ocean waters, and sediment cores, can thus be used to deduce carbon cycle properties during the past and at present (e.g. de Jong et al., 2010; Beck et al., 2018; Mackensen & Schmiedl, 2019). Due to its known half-life and atmospheric content, ^{14}C can be used to date the age of organic carbon and ocean waters (Jull et al., 2013). In this thesis, however, carbon isotopes are not part of the presented investigations and the reader is thus referred to the literature for more information (e.g. Griffiths, 1997).

1.2 Wetlands and peatlands

Wetlands are vegetated terrestrial ecosystems which are characterized by high permanent, seasonal, or intermitted soil moisture (Mitsch & Gosselink, 2015). The water table in wetlands is typically near or above the surface, for at least part of the year. Wetland plant species include trees, mangroves, shrubs, weeds, and mosses, and often show adaptations to moist conditions like aerenchyma, which allow for the transport of gasses to the roots. Wetlands can form in freshwater, saltwater, or brackish water, and can be found across all latitudes and altitudes. They can perform important environmental services including flood control, water purification, shoreline protection through buffering and filtering of water, biodiversity conservation as unique habitats, and climate change mitigation, through uptake and storage of carbon (Kimmel & Mander, 2010; Minayeva & Sirin, 2012; Xu et al., 2018a). At the same time, they are the largest natural source of methane, an important greenhouse gas (Saunois et al., 2020).

Wetlands are categorized, depending on water and vegetation characteristics, into swamps, marches, peatlands, and a multitude of subcategories (Mitsch & Gosselink, 2015). Swamps are wetlands dominated by trees, whereas marches are dominated by herbaceous vegetation. Wetlands that form peat are called peatlands and can range from moss-dominated boreal peatlands to tropical forested peat swamps (Moore, 1989; Rydin & Jeglum, 2013; Lindsay, 2018). Peat is formed by partially decomposed organic matter accumulating under waterlogged conditions, where decomposition is slowed by a large degree of anoxia (Blodau, 2002). Peat accumulation can continue over millennia and peat columns can reach depths of multiple meters. Due to the preservation of organic material in consecutive layers, peatland cores, drilled to reveal the full depth profile of a peatland, hold information about its history, the local vegetation, and climate, similar to cores drilled from ice cores or lake and marine sediments (Barber, 1993; de Jong et al., 2010). Radiocarbon dating and volcanic ash layers can be used to establish an age-depth model. Measurements of preserved pollen and plant fragments, charcoal, testate amoebae species compositions, and isotopic composition can then be used to make inferences about past vegetation, climate, and human activities in the region.

The most common processes for peatland inception are paludification, where peat forms on previously dry mineral soils, and terrestrialization, in which aquatic systems such as lakes or ponds slowly fill with organic material (Charman, 2002). Peatlands can be categorized into fens and bogs, depending on the source of water and nutrients (Lindsay, 2018). Fens are mineatrophic and are mostly fed by nutrient-rich ground and surface waters. In contrast, bogs are ombotrophic with a vegetation cover that is uncoupled from the groundwater and is mostly fed by nutrient-poor and acidic rainwater. These trophic differences translate to differences in plant species and carbon cycling. Bogs are often dominated by Sphagnum moss carpets, but in low latitudes can also be densely forested. Fens generally are characterized by larger plant diversity, including sedges, grasses, mosses, and trees, and see faster carbon cycling than bogs. Fens and bogs are often seen as two distinct phases of the peatland life cycle. The transition from fen to bog often happens rapidly and is based on the decoupling of the vegetation from the

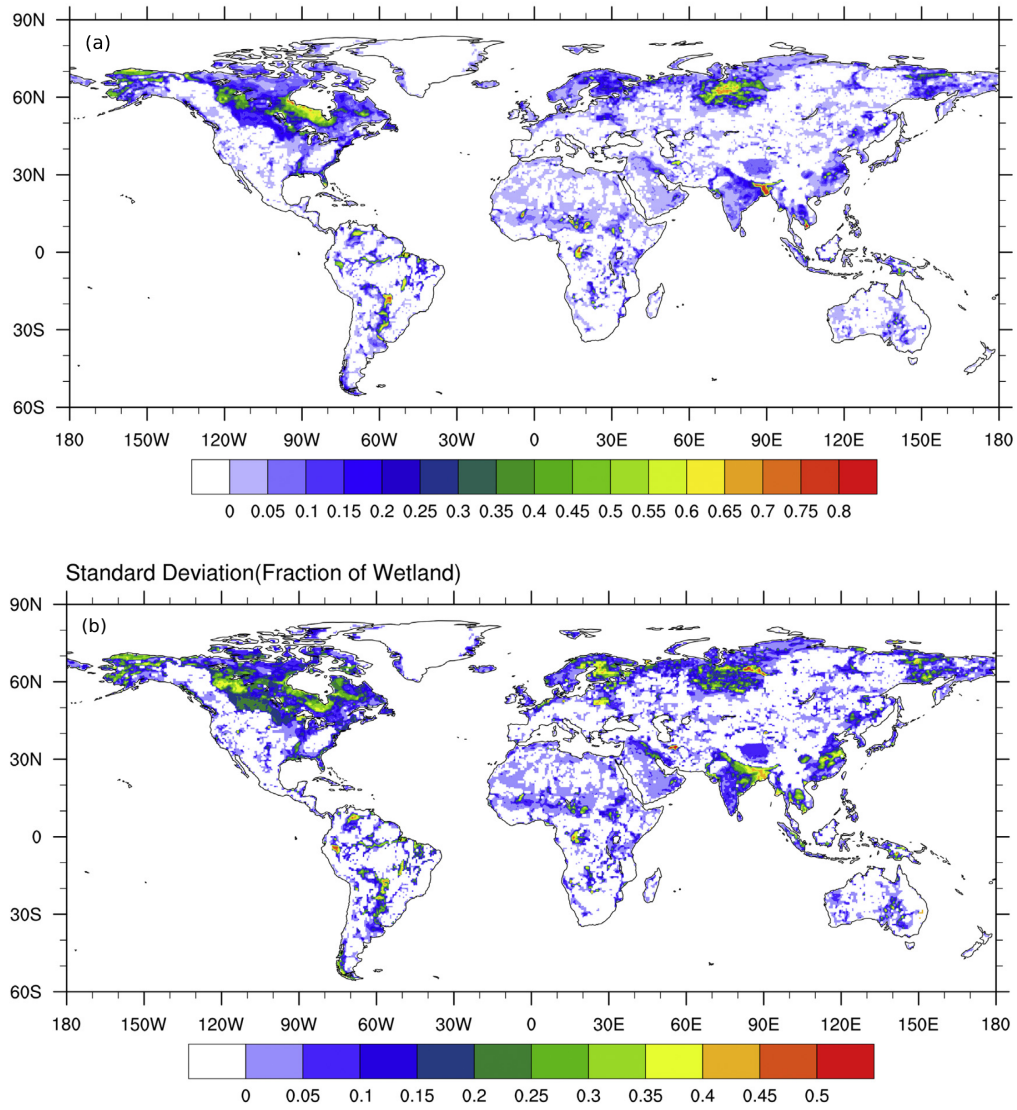

Figure 1.3: Mean maximum wetland area distribution (a) and standard deviation (b) based on five different wetland data sets described in Zhang et al. (2017). Units indicate the area fraction covered by wetlands. Figure adapted from Zhang et al. (2017).

groundwater, through the growth of the peat column itself, or through allogenic factors, such as changes in climate (Väliranta et al., 2017; Loisel & Bunsen, 2020).

Today, the global wetland area is estimated between 5.3–10.2 million square kilometers (Mkm^2; Zhang et al., 2017, Fig. 1.3). The large inconsistencies between wetland datasets can partly be explained by different wetland definitions (Hu et al., 2017a). Peatlands make up about half of all wetlands covering about 2.77–5.7 Mkm^2, when combining estimates for northern (Yu et al., 2010; Xu et al., 2018b; Hugelius et al., 2020) and tropical peatlands (Yu et al., 2010; Page et al., 2011; Gumbricht et al., 2017; Xu et al., 2018b). Most wetlands (∼56 %), and an even larger share of global peatlands (∼75 %) can be found in the northern mid and high latitudes with large wetland and peatland areas in the boreal regions of Canada, Europe, and Asia. A large part of these northern peatlands (∼46 %) is located within permafrost regions (Hugelius et al., 2020). Large tropical wetlands can be found in central Africa, South East Asia, and the Amazon basin, with a larger share of seasonally flooded wetlands that follow the rhythm of the monsoon.

1.3 The role of wetlands in the carbon cycle and the climate system

Wetlands play an important role in the global carbon cycle both as long-term carbon stores and as large methane sources. Both roles will be further explored in the main chapters of this thesis. To provide a general overview over the relations of wetlands to the global carbon cycle, section 1.3.1 will give an introduction to the role of peatlands as large terrestrial carbon stores and section 1.3.2 will introduce the role of wetlands as methane sources.

1.3.1 Peatlands as long term carbon stores

Most of today's peatlands formed over the past ten thousand years and have accumulated carbon over millennia (e.g. Yu et al., 2010; Morris et al., 2018). Although they cover only 3 % of the global land area (Xu et al., 2018b) they hold up to a third of the global soil organic carbon (Page et al., 2011; Yu, 2012). About 75 % of global peatlands can be found north of 30° N mostly in the northern parts of North America, Europe, and Asia. Traditionally northern peatlands have been studied much more intensively than peatlands in the tropics (30° S–30° N), leading to more robust estimates about area extent and carbon storage. Estimates for northern peatland carbon storage range between 270–604 GtC, using various methods and area estimates (see Yu (2012) and Yu et al. (2014) for a review), with the most recent credible estimates ranging between 415–436 GtC (Loisel et al., 2014; Hugelius et al., 2020). Estimates for organic carbon storage in tropical peatlands were recently revised upward to 70–288 GtC (Dargie et al., 2017; Ribeiro et al., 2021), compared to 44–92 GtC from earlier estimates (Yu et al., 2010; Page et al., 2011). The revision is the result of larger assumed peatland areas.

Most peatlands still functioned as net carbon sinks in recent centuries, with a collective yearly uptake of about 0.14 GtC yr^{-1} during the last millennium (Gallego-Sala et al., 2018). The potential cooling effect of peat carbon sequestration on the global climate can be partially offset by methane emission from wet peatlands (see also section 1.3.2). Given the short lifetime of the emitted methane versus the sustained long-term removal of carbon from the atmosphere, however, peatlands likely exerted a net cooling over most of the Holocene up to today (Frolking & Roulet, 2007). If subject to drainage and land-use change, the radiative balance, however, can quickly turn positive (Dommain et al., 2018).

Carbon accumulation rates (CARs) in peatlands, given in first order as the balance between NPP and HR, are driven by multiple factors including vegetation cover, water table, temperature, nutrient availability, and photosynthetically active radiation. For northern peatlands, temperature and photosynthetically active radiation were found to have the largest control, with higher temperatures leading to longer growing seasons and larger photosynthetic productivity (Charman et al., 2013, 2015; Gallego-Sala et al., 2018). High water tables are an important prerequisite for carbon accumulation and water table height has a positive correlation with peatland CARs (Potvin et al., 2015; Chimner et al., 2017). Additional to the external controls of peatland CARs, there is a multitude of internal feedbacks on peatland hydrology, vegetation, and energy balance that can affect peatland CARs (Morris et al., 2011; Waddington et al., 2015; Zhong et al., 2020).

These external and internal controls on peatland CARs, entail potential feedbacks to the global carbon cycle and climate system. Rising temperatures could increase heterotrophic respiration and, through the increase of evapotranspiration, lower the water tables exposing large amounts of carbon to oxic conditions and thus turning peatlands into net carbon sources (Ise et al., 2008). However, increasing temperatures and rising precipitation could also strengthen the carbon sink especially of northern peatlands through the increase in productivity (Charman et al., 2015; Gallego-Sala et al., 2018). Permafrost thaw could lead to new peatland formation

after initial carbon loss (Swindles et al., 2015; Jones et al., 2017; Magnússon et al., 2020) or even directly invigorate carbon accumulation (Estop-Aragonés et al., 2018). In chapter 4, the responses of peatlands and their carbon balance to past and future climate change are investigated in detail.

In the literature, different definitions of CARs are used in different contexts. Studies reporting results from peatland cores in the field often report so-called apparent CARs, given by the carbon density of peat layers and a radiocarbon-derived depth-age model (e.g. Turunen et al., 2002; Loisel et al., 2014; Loisel & Bunsen, 2020). These apparent CARs incorporate the integrated heterotrophic respiration of the respective layer from its formation to the present, and thus not only depend on the environmental conditions at the time of carbon deposition but also their changes since then and the time that has passed. Modeling studies, which have the full information of the model system available at every timestep often report CARs which represent the net carbon balance of the whole peat column at a given time (e.g. Frolking et al., 2010). The same models might have difficulties, depending on their soil column resolution, to resolve the state of carbon in particular layers (Spahni et al., 2013; Müller & Joos, 2020). Other definitions refer to an instantaneous CAR, meaning the rate of deposition of organic carbon on top of the peat layer, not considering peat decay from deeper layers (e.g. León et al., 2018). These diverging definitions are sometimes mixed and/or insufficiently specified (e.g. Marrs et al., 2019; Chaudhary et al., 2020), warranting care when comparing results from different studies (Young et al., 2019, 2021).

1.3.2 Methane emissions from wetlands

Wetlands are the largest natural source of terrestrial methane emissions (Saunois et al., 2020). The anoxic environment in the water-saturated soils favors methanogenic microorganisms that produce methane during the respiration of organic carbon. Methane emissions were found to be strongly temperature dependent, with emissions increasing faster than concurrent CO_2 emissions under rising temperatures (Yvon-Durocher et al., 2014; Turetsky et al., 2014). The temperature dependence of plant productivity, heterotrophic respiration, and methane production leads to generally higher emissions from low latitude wetlands. Higher water tables increase methane emissions (Turetsky et al., 2008), however, after reaching an optimum, further rising water tables reduce methane emissions possibly due to limiting diffusion and plant productivity (Turetsky et al., 2014).

Other environmental factors controlling wetland methane emissions include substrate availability and vegetation cover (Lai, 2009). Future climate change has thus both the potential to increase methane emissions through higher temperatures and wettening under increasing precipitation and reduce methane emissions in case of wetland drying. Section 6.2, briefly discusses future modeled methane emissions from peatlands under different scenarios.

Most methane that is produced in the soil, is directly oxidized by methanotrophic microorganisms in the soil or water column, using oxygen and other electron acceptors, before it can reach the atmosphere (Lai, 2009). The amount of methane that is emitted thus also depends on the speed of methane transport to the atmosphere. Methane can reach the atmosphere via diffusion through the soil column, out-gassing via bubbles (ebullition), or by being transported through plant tissues (Fig. 1.4 Carmichael et al., 2014). The latter requires vegetation that allows gas transport from the roots to the surface such as sedges with aerenchyma. Recently it has been found that in forested tropical wetlands large amounts of methane are transported by trees, which allows the methane to escape to the atmosphere despite water tables that seasonally can reach up to ten meters (Pangala et al., 2017). Similar, but smaller methane emissions from trees have also been found in forested mid-latitude wetlands and even uplands, suggesting possible production of methane within the stems (Barba et al., 2019). The differences in soil, vegetation,

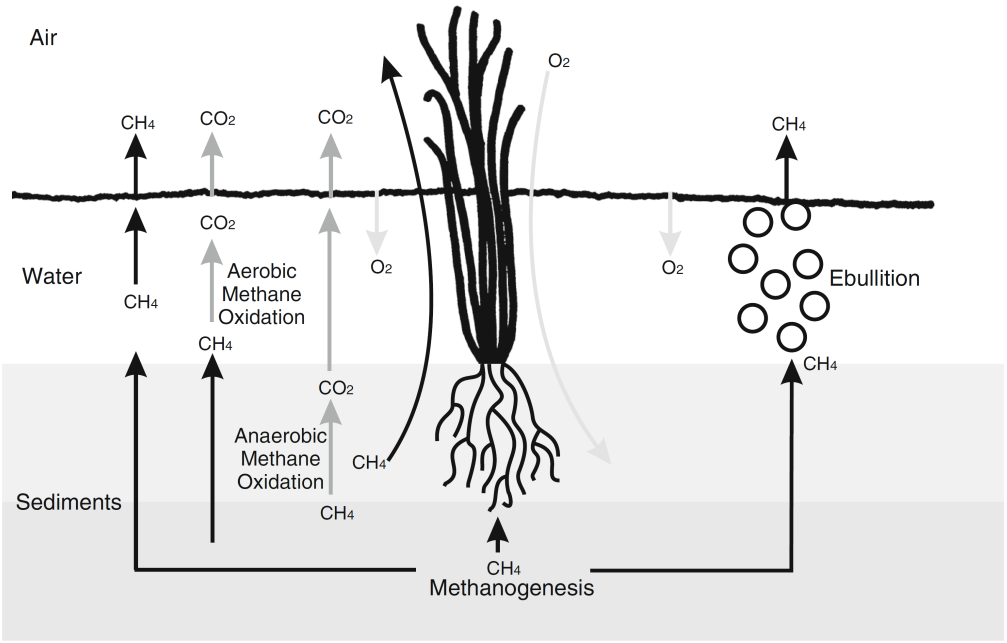

Figure 1.4: Simplified schematic of methane production, consumption, and transport pathways in wetlands. Depicted transport pathways for gasses consist of diffusion, plant transport, and outgassing via gas bubbles (ebullition). Methane consumption is dependent on the transport of Oxygen (O_2) into the soil. Figure from (Carmichael et al., 2014).

water table, and trophic regimes lead to differences in emissions from different wetland types (Turetsky et al., 2014). In mineatrophic fens, the faster production and respiration of organic carbon, together with higher water tables and a larger fraction of plants with aerenchyma, results in generally larger methane emissions than in ombotrophic bogs.

For the years 2008–2017, estimates of methane emissions from process-based models range between 102–182 Tg yr^{-1} while estimates from atmospheric inversions range between 159–200 Tg yr^{-1}, with most emissions originating in the tropics in both cases (Saunois et al., 2020). The partial mismatch between the estimate ranges is a reflection of the still persisting knowledge gaps about global wetland distribution and environmental controls on emissions, and the difficulty of partitioning between freshwater, wetland, and other natural sources. Past and present methane emissions from global wetlands are further discussed and investigated in chapter 5 and section 6.1.

1.4 Wetlands in the past

This thesis focuses in part on the past evolution of wetlands and their interactions with the carbon cycle. To place these investigations into the broader context of past climate variability, section 1.4.1 gives a brief introduction into the concepts of paleoclimate and glacial-interglacial cycles. Section 1.4.2 then gives a brief introduction to paleo wetlands over the last 21,000 years.

1.4.1 Paleoclimate overview

Proxy records allow the reconstruction of climate and environmental variables up to millions of years into the past (Masson-Delmotte et al., 2013). They can encompass a multitude of methods, including measurements of isotopes ratios, element ratios, or biological markers in sediments, ice cores, or speleothems, with new methods and proxies constantly being developed. Some

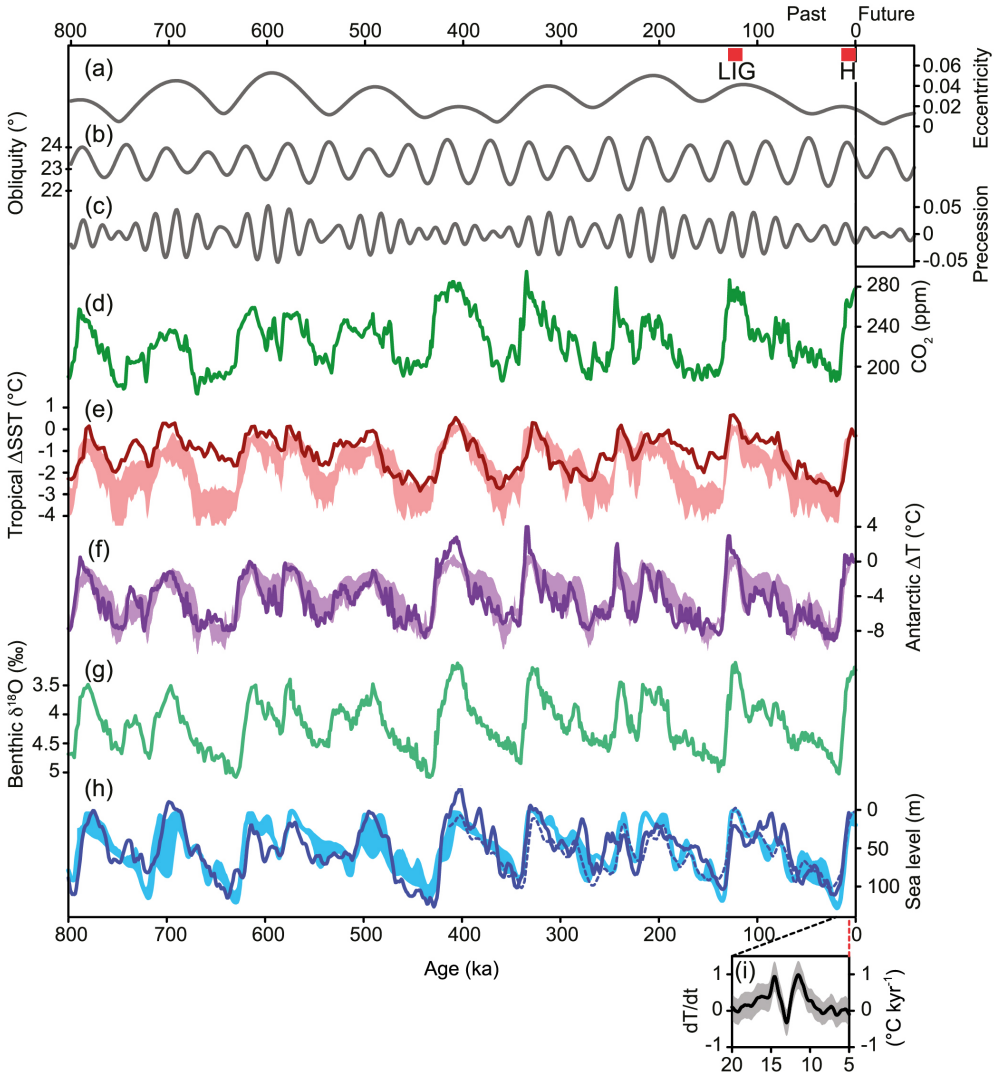

Figure 1.5: Orbital parameters and proxy records over the past 800,000 years. Shown are (a) eccentricity, (b) obliquity, and (c) precessional parameters. Proxy records include (d) atmospheric CO_2 concentration measured in Antarctic ice cores, (e) tropical sea surface temperature anomaly reconstructed from ocean sediments, (f) Antarctic temperature anomaly reconstructed from ice cores, (g) benthic $\delta^{18}O$ as a proxy for deep ocean temperature and global ice volume, (h) sea-level reconstruction from benthic $\delta^{18}O$, and (i) the rate of temperature change during the last deglaciation. Shaded areas indicate the ranges of modeling results. Figure from Masson-Delmotte et al. (2013). See there for references.

properties can even be measured directly, such as the atmospheric concentrations of gases that are preserved in continental ice sheets, where current records go back up to 800,000 years (e.g. Lüthi et al., 2008; Loulergue et al., 2008; Schilt et al., 2010a).

The comparison of different environmental variables reconstructed from independent proxies reveals a large correlated variability of global mean temperature, atmospheric concentrations of greenhouse gases, sea level, and ice volume over the last 800,000 years suggesting a highly dynamic earth system (Fig. 1.5, Masson-Delmotte et al., 2013). The variability is dominated by prominent glacial-interglacial cycles, where relatively short (∼10–30 kyrs) warm periods characterized by low global ice volume, high sea levels, and high atmospheric greenhouse gas concentrations, called interglacials, are separated by longer (∼70–90 kyrs) cold periods characterized by large global ice volume, low see levels, and low atmospheric greenhouse gas concentrations, called glacials (Masson-Delmotte et al., 2013; Past Interglacials Working Group of PAGES, 2016). This periodicity of about 100 kyrs can be observed back to the Mid-Pleistocene Transition

about 1.2–0.8 million years ago before which glacial-interglacial cycles had a periodicity of about 40 kyrs (Chalk et al., 2017).

The deglaciation, that is the transition from a glacial to an interglacial period, typically happens abrupt (over a few thousand years), with large parts of the global ice sheets relatively quickly collapsing, while the glaciations, that is the transition from an interglacial to a glacial, is more gradual, with the global ice sheets reforming over tens of thousands of years. Glacials are characterized by large instabilities, so-called Dansgaard-Oeschger events, which entail rapid Greenland warming, and gradual cooling on the timescales of centuries (e.g. Dansgaard et al., 1993; Erhardt et al., 2019; Li & Born, 2019).

It has to be noted that even in light of the past variability of the climate system various aspects of the anthropogenic disturbances are without analog. This is especially true for the rate of anthropogenic carbon release which is unprecedented during the past 20,000 years (Joos & Spahni, 2008) and compared to the large climate fluctuation at the Paleocene-Eocene Thermal Maximum around 55 million years ago (Zeebe et al., 2016). The large human-caused carbon release could lead to rates of ocean acidification unprecedented in the records of the past 65 million years (Ridgwell & Schmidt, 2010).

The main pacemaker of the glacial-interglacial cycles is the change in solar insolation on the northern hemisphere, which changes based on the orbital parameters: the orbital eccentricity, the axial tilt (obliquity), and the axial precession (Fig. 1.5 Hays et al., 1976; Imbrie et al., 1993). Although these parameters change on different timescales, their combined effect on the climate system resulted in a relatively regular 100,000 years periodicity of the glacial-interglacial cycles over the past 800,000 years (Jouzel et al., 2007; Loulergue et al., 2008). The exact mechanisms behind the glacial-interglacial cycles are still debated, however, there is consensus that the relatively small changes in solar forcing are amplified by a multitude of internal climate feedbacks related to ice sheet dynamics, ocean circulation changes, and atmospheric CO_2 and dust load (e.g. Ganopolski & Calov, 2011; van Nes et al., 2015; Weinans et al., 2021).

The transition from the Last Glacial Maximum (LGM) to the Holocene, the current interglacial, occurred roughly between 17.5 and 11.5 kyrs before present (BP, with present defined as the year 1950). It entailed an increase in global mean temperature of 3–8 $°C$, melting of large ice sheets over North America and Europe, a sea-level rise of about 120 meters, and increases of atmospheric greenhouse gas concentrations by about 80 ppm for CO_2 and about 300 ppb for methane (Masson-Delmotte et al., 2013; Köhler et al., 2017). The climatic changes drove large shifts in the terrestrial biosphere with a net land uptake of about 850 GtC (Jeltsch-Thömmes et al., 2019). The last deglaciation was not a continuous process but was divided into several northern hemisphere (NH) cold and warm phases. These are associated with a large-scale reorganization of the ocean circulation, thought to have been provoked by freshwater release from ice sheet melting leading to changes in the ocean heat transport (Stocker & Johnsen, 2003; Rasmussen et al., 2014). The NH climate swings entailed global changes, mediated by ocean currents and atmospheric circulation. For example, small changes in the Intertropical Convergence Zone, due to changing temperature gradients between high and low latitudes, probably led to substantial changes in tropical precipitation (McGee et al., 2014; Shi & Yan, 2019; Cao et al., 2019).

In this thesis, the time period since the LGM, including the deglaciation and the Holocene, is investigated in detail with respect to peatland evolution (chapter 3) and methane emissions from wetlands (chapter 5). The following sections give a short introduction to the available knowledge about wetlands during that period.

1.4.2 Paleo wetlands

Peatlands themselves, through their accumulation and preservation of organic material, are archives of environmental change, allowing the reconstruction of their evolution and the past environmental conditions they witnessed (Chambers & Charman, 2004). Most of today's peatlands are younger than 12,000 years and formed as a result of the climatic and environmental changes during the last deglaciation. This finding has been the result of an ever-expanding database of peatland basal ages, determined by the dating of the deepest part of peatland cores (e.g. Halsey et al., 2000; Gajewski et al., 2001; MacDonald et al., 2006; Gorham et al., 2007; Yu et al., 2010; Ruppel et al., 2013; Morris et al., 2018; Treat et al., 2019, Fig. 1.6). This basal age data can be used to reconstruct the initiation history and lateral expansion of the sampled active peatlands (Yu et al., 2010; Korhola et al., 2010; Ruppel et al., 2013; Dommain et al., 2014; Loisel et al., 2017). Peat initiation in the northern latitudes started at about 11–12 kyrs BP but initiation and lateral expansion continued to the present (Loisel et al., 2017). Expansion peaked at the beginning of the Holocene about 9–10 kyrs BP and slowed down since then.

In North America, peatland expansion followed the retreat of the Laurentide ice sheet with a delay of a few thousand years, leading to a delayed expansion peak around 8–5 kyrs BP (Gorham et al., 2007; Ruppel et al., 2013). In the Hudson Bay area, land emergence and peatland expansion continued after the ice sheet retreat due to isostatic adjustment which continues until today (Glaser et al., 2004). Besides the newly available land area, the strong warming at the beginning of the Holocene is identified as the main driver of peatland expansion, leading to longer growing seasons and high northern latitudes becoming hospitable for peat-forming vegetation (Morris et al., 2018). Concurrently increasing precipitation likely also played an important and, in some regions such as the Western Siberian Lowlands, a dominant role.

Peatland research has historically focused on the extensive peatlands in North America and northern Europe, with about 80 % of all peat cores drilled there (Fig. 1.6 Treat et al., 2019). This makes reconstructions of past peatland dynamics in other regions such as the tropics much more uncertain. Nonetheless, applying the same statistical approach to the few available tropical peat cores suggests a more or less continuous peatland expansion picking up after 18 kyr BP (Yu et al., 2010). However, a few tropical peatlands exist that are much older, initiating up to 50 kyrs ago (Treat et al., 2019). Given the sparse basal age data, Dommain et al. (2014) used a depth-age relation derived from regional accumulation rates to reconstruct peatland expansion in Indonesia. Their results suggest a much later peatland expansion than the statistical approach, with 90 % of peatlands establishing after 7 kyr BP and 60 % after 3 kyr BP. Local sea level was suggested as the main driver, with rising sea levels during the deglaciation and early Holocene enabling inland peatland formation through increased moisture availability and a lowering of the hydrological gradient. Sea-level stabilization and subsequent retreat after $\sim$4 kyr BP led to the establishment of today's extensive coastal peatlands.

The above-discussed reconstructions of peatland history, by design, focus only on peatlands still existing today. However, under a changing climate, not only new peatlands may form but conditions for existing peatlands might become unfavorable and the accumulated peat might degrade or become buried under mineral sediments (e.g. Talbot et al., 2010; Tchilinguirian et al., 2014; Campos et al., 2016; Lähteenoja et al., 2012; Tipping, 1995). Similarly, former coastal peatlands or peatlands on continental shelves might be flooded due to rising sea levels (Kreuzburg et al., 2018). Data about buried peat is still very sparse, as most buried peat layers are found incidentally in sediment and drilling cores instead of a targeted search (Fig. 1.6 Treat et al., 2019).

Treat et al. (2019) presented data of buried peat layers dating back up to the last interglacial, 130–116 kyrs ago. The presence of peatlands peaked during that time, with a decline towards the last glacial. Buried peat in the northern extratropics increases again between 57–29 kyrs

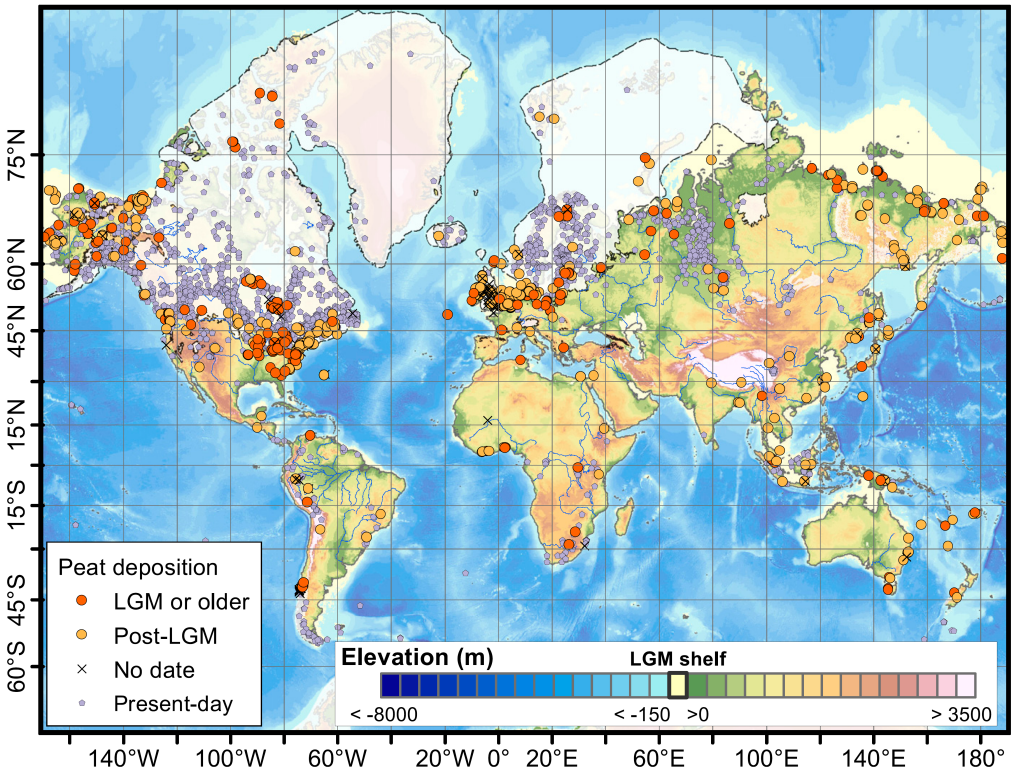

Figure 1.6: Peat core data of present-day peatlands (purple), buried peat older than 18 kyrs (orange), and buried peat younger then 18 kyrs (yellow). Figure from Treat et al. (2019).

BP corresponding to marine isotope stage 3, a period of slightly warmer mean temperatures compared to the LGM. Large buried peat deposits are again found dating from the deglaciation and throughout most of the Holocene, indicating a highly dynamic peatland area during the peak formation time of today's peatlands up to the middle and late Holocene. A large part of these buried peat deposits was found in northern and central Europe along the borders of the Fennoscandinavian ice sheet and in eastern North America along the borders of the Laurentide ice sheet (Fig. 1.6). This suggests peat accumulation at the LGM, which during the deglaciation shifted further North with time and under continually changing climate. North American pollen data of *Sphagnum* paints a similar picture (Halsey et al., 2000; Gajewski et al., 2001). In the tropics, only a small amount of dated buried peat layers exist (Treat et al., 2019). The buried peat mostly dates from after 60 kyrs BP and suggests tropical peatland area to have shifted continuously since then, with peat burial driven by climatic and sea-level changes. However, due to the limited amount of data, uncertainties are large.

Paleo wetlands that did not leave organic carbon in the form of peat behind are even harder to reconstruct. One approach is to use preserved pollen from aquatic vegetation as a proxy for wetland location and extent (e.g. Finkelstein & Cowling, 2011). Byun et al. (2021) used this approach on a regional scale and suggest a large expansion of wetlands in western North America during the Bølling-Allerød, a northern hemisphere warm period during the last deglaciation. These extensive wetlands (up to 60 % land cover) could have been supported by meltwater discharge from the Laurentide ice sheet. During the Younger Dryas, the following cold period, meltwater abruptly declined and wetlands retreated. These results are regionally and temporally in line with the evidence for peat.

Due to its short atmospheric lifetime, changes in source strength quickly manifest in changes in the atmospheric concentration of methane. The ice core record of atmospheric methane thus

can resolve abrupt environmental changes from the past on a high temporal resolution. This feature of the atmospheric methane record is often used to synchronize the timescales of different ice cores, even from different hemispheres (Blunier et al., 2007; Buizert et al., 2015). The abrupt changes seen in the atmospheric methane at the onset of interglacials or Dansgaard-Oeschger events are often connected to source changes in wetland emissions (e.g. Bock et al., 2017). Methane emission changes from boreal peatlands were also linked to the Northern Hemisphere cold event around 8.2 kyrs BP (Zürcher et al., 2013). However, the changes in methane emissions are suggested to be responses and positive feedbacks to environmental changes, rather than their drivers (e.g. Brook et al., 2000; Huber et al., 2006). There is evidence that in the deep past when wetlands were much more prominent, methane might have played a much more important role in shaping the climate of the earth (Beerling et al., 2009).

In chapter 3, a modeling study is presented, investigating peatland evolution since the LGM and comparing model results to the above-described reconstructions. In chapter 5, simulations over the same period are investigated with respect to wetland methane emissions, and model results are compared to the ice core record.

1.5 Wetlands in the Anthropocene

The Anthropocene is a term that has recently emerged to describe a new geological era that is fundamentally shaped by humanity (Lewis & Maslin, 2015). Human changes to the land surface and the unprecedented release of greenhouse gases have long-lasting effects that will be measurable in geological records for millions of years. This human influence extends to wetlands and peatlands, which have been subject to extensive drainage and land-use conversion in the recent past, and, in the future, will experience more and more pressure from a changing climate. With this, past and future disturbances put large carbon pools at risk (Goldstein et al., 2020).

Modeling studies suggest that a large part of natural wetlands have already been lost through human intervention (Hu et al., 2017b). Leifeld et al. (2019) estimate global peatland loss and suggest that 0.51 Mkm^2 of peatland area and 22 $\pm$ 5 GtC of peatland carbon was lost from 1850 to 2015 due to drainage and land-use conversion. Another modeling study estimates carbon loss from drained northern peatlands to about 72 GtC between 850–2010 (Qiu et al., 2021). Throughout most of the industrial period, peatland loss was largest in the northern mid and high latitudes, however, drainage in the tropics dramatically increased since the 1960s (Hergoualc'h & Verchot, 2011; Dohong et al., 2017; Leifeld et al., 2019; Dommain et al., 2018; Hoyt et al., 2020). If no action is taken, the degradation of former peatlands will release carbon for decades to come (Leifeld & Menichetti, 2018). However, immediate and resolute action towards restoration and re-wetting (Warren et al., 2017; Nugent et al., 2019; Günther et al., 2020) together with strong policies for protection (Humpenöder et al., 2020; Wibisana & Setyorini, 2021) could mitigate part of this committed and future carbon loss.

The impact of future anthropogenic climate change on wetlands depends among others on the changes in their moisture balance. Mean annual precipitation is projected to increase over large parts of the northern boreal regions, however, northern high latitudes are also expected to see disproportionately large warming due to the polar amplification (Collins et al., 2013). The temperature-driven increase in evapotranspiration could outweigh the increases in precipitation, especially in boreal peatlands, where evapotranspiration is more sensitive to temperature changes than in boreal forests (Helbig et al., 2020). Indeed, past climate change already led to an observed drying trend in peatlands in northern Europe (Swindles et al., 2019; ZHANG et al., 2020) and eastern Canada (Pellerin & Lavoie, 2003), with a shift in vegetation cover from moss-dominated to shrub- and tree-dominated (Pellerin & Lavoie, 2003; Talbot et al., 2010; Beauregard et al., 2020).

A decrease in the water table can expose deep peat layers to oxic conditions. Together with warmer soil temperatures, this could potentially lead to the release of large amounts of carbon (Ise et al., 2008; Hopple et al., 2020). Although deep peat carbon might be more robust to future warming than the surface peat carbon (Wilson et al., 2016). At the same time, warmer temperatures and higher atmospheric CO_2 concentrations could increase carbon uptake through increases in plant productivity (Charman et al., 2013; Gallego-Sala et al., 2018). Increased fire frequency due to low water tables poses another risk of carbon loss (Turetsky et al., 2015). In case of stable or even increasing water tables, wetland methane emissions are expected to substantially increase under future warming (Turetsky et al., 2014).

The responses and net feedbacks of wetlands and peatlands to future changes in climate, atmospheric CO_2, and the continued pressures from land-use conversion are still very uncertain as the different drivers potentially both increase and decrease wetland area and net carbon uptake. In chapter 4, a modeling study is presented that in detail investigates and discusses potential committed and future changes of global peatlands under different scenarios.

1.6 Modeling of wetlands

Process-based models are a reflection of the knowledge of a dynamical system. They can be used to test the process understanding by comparing model results to observations and to investigate process and system dynamics under various boundary conditions, including past and future climate states, for which observations are sparse, exist only as proxies, or are non-existent. The high temporal and spatial resolution of model output allows for a detailed analysis and the exploration of complex interactions between different processes.

In climate science, the use of models has a long history and they are used on all temporal, spatial, and process scales (Edwards, 2011). Physics-based models simulate ocean and atmospheric dynamics and the energy balance with varying spatial resolutions (e.g. Beadling et al., 2019), biochemistry models simulate the carbon and nitrogen cycles on land and in the ocean (Anav et al., 2013) often together with dynamic vegetation and ecology models simulating plant growth and species distribution (Prentice & Cowling, 2013), and socioeconomic models are used to simulate economic and societal dynamics (Nordhaus, 2017). Models for different processes are often coupled allowing for interactions and feedbacks between different sub-systems. Dynamic global vegetation models (DGVMs) often combine formulations for the terrestrial carbon, nutrient, and water cycles with simulated vegetation dynamics and soil physics. Finally, fully coupled earth system models strive to represent all parts of the earth system including ocean, atmosphere, land, and biosphere processes (Flato, 2011). Models of varying complexity and scope are used in different contexts. High-resolution earth system models are limited in their use by their computational cost and large data production and thus are mostly used for short transient or time-slice simulations (e.g. Eyring et al., 2016). Models of intermediate complexity can be used to explore system dynamics on long, e.g. glacial-interglacial, timescales and can be used to derive fundamental large-scale properties of the system (Claussen et al., 2002).

Process-based models used for wetland area prediction combine hydrological models with information about local topography, soil characteristics, and climate. They can vary from detailed catchment-scale models (e.g. Evenson et al., 2016; Lee et al., 2019) to simplified global scale models (e.g. Melton et al., 2013). Global wetland models are often integrated into DGVMs, where the spatial resolution is too coarse to resolve small-scale topography and where single grid cells might cover multiple unconnected catchments or large watersheds might be split into multiple grid cells. Most DGVMs thus simulate the terrestrial water cycle on a grid cell basis, with simulated water transport through the vertical soil column but often with no explicit

surface or groundwater flow between grid cells (e.g. Sitch et al., 2003; Hagemann & Stacke, 2015) and instead use a Topographic Index Model (TOPMODEL) approach to predict wetland area.

The TOPMODEL was developed as a simplified rainfall-runoff model that could predict the area of soil water saturation within a catchment based on topographic information and mean water storage deficit within the catchment (Beven & Kirkby, 1979). Originally designed for small to medium catchment areas, the model has been further developed and used in many different contexts since its development (Beven et al., 2021), including the adaptation for wetland area prediction on a global scale (e.g. Gedney & Cox, 2003; Kleinen et al., 2012; Stocker et al., 2014). The global TOPMODEL approach allows for a cost-efficient calculation of grid-cell wetland fraction in DGVMs, using sub-grid topography and the grid-cell mean water table which is dynamically simulated by the DGVM. In this thesis, the DGVM LPX-Bern v1.4 is used (Lienert & Joos, 2018), which also uses a wetland scheme that is based on the TOPMODEL approach (Stocker et al., 2014). The approach is discussed in detail in section 2.1.1.

Models of peat accumulation were first developed as one dimensional soil column models, which increased in complexity with time including processes such as water table and vegetation dynamics (e.g. Clymo, 1984; Frolking et al., 2010; Morris et al., 2011). Other models were developed to capture the two and three-dimensional aspects and ecohydrological feedbacks that play important roles in peat domes (e.g. Morris et al., 2012; Baird et al., 2012; Swinnen et al., 2019). Wania et al. (2009a,b) were the first to implement an explicit peatland representation of northern peatlands within a DGVM with dynamic soil freezing and explicit peatland vegetation. Their approach subsequently served as the basis for the implementation of peatland models in other DGVMs including the LPX-Bern (Kleinen et al., 2012; Spahni et al., 2013). Those models simulate peatland carbon accumulation with a simplified two-layer separating carbon pools for acrotelm and catotelm, respectively. Recently, integration of peatlands into DGVMs also include models where peat accumulation is simulated in distinct layers (Chaudhary et al., 2017; Largeron et al., 2018).

Another model development concerns the dynamic prediction of peatland area. While traditionally simulations of regional and global peatlands relied on prescribed maps of peatland area, a new generation of peatland models determine peatland area prognostically from environmental conditions. Peatland area can be determined by climatic envelope models alone (e.g. Gallego-Sala et al., 2016; Cong et al., 2020) or in combination with information about terrain morphology (Alexandrov et al., 2016). In DGVMs, including the LPX-Bern, models of dynamic peatland area are mostly based on the TOPMODEL approach described above. There, peatland area is determined from inundation persistency (Kleinen et al., 2012; Stocker et al., 2014; Largeron et al., 2018; Qiu et al., 2018). The integration of dynamic peatlands into DGVMs allows for the first time for large-scale model investigations of peatland dynamics under past (Kleinen et al., 2012; Treat et al., 2019; Chaudhary et al., 2020; Müller & Joos, 2020) and future (Qiu et al., 2020; Müller & Joos, 2021) environmental conditions. In this thesis, the LPX-Bern and its peatland module are used for model investigations of past peatland dynamics (chapter 3) and projections of future peatland dynamics (chapter 4). The respective peatland module of LPX-Bern is described in detail in section 2.1.1.

Modeling methane emissions from wetlands dates back almost four decades and includes models with varying complexities (Xu et al., 2016). As methane production depends on carbon cycle dynamics, most methane models are integrated into carbon cycle models or DGVMs. The simplest methane models diagnose emissions as a function of first-order determinants of the available substrate for methanogenesis such as NPP, HR, or soil carbon often dependent also on temperature or biome type (e.g. Christensen et al., 1996; Kaplan, 2002; Zhang et al., 2016). Most simple models, however, additionally consider the important control of soil moisture, with methanogenesis confined to the saturated part of the soil column (e.g. Cao et al., 1996; Gedney et al., 2004; Mokhov et al., 2007).

More complex models explicitly simulate the production and consumption of methane in the soil as well as various transport pathways of methane to the atmosphere, such as diffusion, ebullition, and plant transport, which determine methane residence time in the soil and consider specific flood-tolerant plant functional types (e.g. van Huissteden et al., 2006; Wania et al., 2010; Zürcher, 2013; Ringeval et al., 2014; Raivonen et al., 2017; Kleinen et al., 2020). Estimating methane emissions on a regional scale requires prescribed or simulated wetland area data, which is still one of the largest sources of uncertainty for large-scale emission estimates (Zhang et al., 2017; Melton et al., 2013; Liu et al., 2020). LPX-Bern includes formulations for methane emissions of different complexity for different wetland types, which are discussed in detail in section 2.1.2. Chapter 5 looks at methane emissions from the LGM to the present simulated by LPX-Bern and sections 6.1 and 6.2 discuss model results for the present and future, respectively.

Bibliography

Alexandrov, G. A., Brovkin, V. A., & Kleinen, T., 2016. The influence of climate on peatland extent in Western Siberia since the Last Glacial Maximum, *Sci. Rep.*, 6(October 2015), 6–11.

Anav, A., Friedlingstein, P., Kidston, M., Bopp, L., Ciais, P., Cox, P., Jones, C., Jung, M., Myneni, R., & Zhu, Z., 2013. Evaluating the land and ocean components of the global carbon cycle in the CMIP5 earth system models, *J. Clim.*, 26(18), 6801–6843.

Archer, D., 2007. Methane hydrate stability and anthropogenic climate change, *Biogeosciences*, 4(4), 521–544.

Baird, A. J., Morris, P. J., & Belyea, L. R., 2012. The DigiBog peatland development model 1: rationale, conceptual model, and hydrological basis, *Ecohydrology*, 5(3), 242–255.

Barba, J., Bradford, M. A., Brewer, P. E., Bruhn, D., Covey, K., van Haren, J., Megonigal, J. Â., Mikkelsen, T. N., Pangala, S. R., Pihlatie, M., Poulter, B., Rivas-Ubach, A., Schadt, C. W., Terazawa, K., Warner, D. L., Zhang, Z., & Vargas, R., 2019. Methane emissions from tree stems: a new frontier in the global carbon cycle, *New Phytol.*, 222(1), 18–28.

Barber, K. E., 1993. Peatlands as scientific archives of past biodiversity, *Biodivers. Conserv.*, 2(5), 474–489.

Beadling, R. L., Russell, J. L., Stouffer, R. J., Goodman, P. J., & Mazloff, M., 2019. Assessing the quality of Southern Ocean circulation in CMIP5 AOGCM and earth system model simulations, *J. Clim.*, 32(18), 5915–5940.

Beauregard, P., Lavoie, M., & Pellerin, S., 2020. Recent Gray Birch (Betula populifolia) Encroachment in Temperate Peatlands of Eastern North America, *Wetlands*, 40(2), 351–364.

Beck, J., Bock, M., Schmitt, J., Seth, B., Blunier, T., & Fischer, H., 2018. Bipolar carbon and hydrogen isotope constraints on the Holocene methane budget, *Biogeosciences*, 15(23), 7155–7175.

Beerling, D., Berner, R. A., Mackenzie, F. T., Harfoot, M. B., & Pyle, J. A., 2009. Methane and the CH 4-related greenhouse effect over the past 400 million years, *Am. J. Sci.*, 309(2), 97–113.

Beven, K. J. & Kirkby, M. J., 1979. A physically based, variable contributing area model of basin hydrology, *Hydrol. Sci. Bull.*, 24(1), 43–69.

Beven, K. J., Kirkby, M. J., Freer, J. E., & Lamb, R., 2021. A history of TOPMODEL, *Hydrol. Earth Syst. Sci.*, 25(2), 527–549.

Blodau, C., 2002. Carbon cycling in peatlands - A review of processes and controls, *Environ. Rev.*, 10(2), 111–134.

Blunier, T., Spahni, R., Barnola, J. M., Chappellaz, J., Loulergue, L., & Schwander, J., 2007. Synchronization of ice core records via atmospheric gases, *Clim. Past*, 3(2), 325–330.

Bock, M., Schmitt, J., Beck, J., Seth, B., Chappellaz, J., & Fischer, H., 2017. Glacial/interglacial wetland, biomass burning, and geologic methane emissions constrained by dual stable isotopic CH4 ice core records, *Proc. Natl. Acad. Sci.*, 114(29), E5778–E5786.

Brook, E. J., Harder, S., Severinghaus, J., Steig, E. J., & Sucher, C. M., 2000. On the origin and timing of rapid changes in atmospheric methane during the Last Glacial Period, *Global Biogeochem. Cycles*, 14(2), 559–572.

Buizert, C., Cuffey, K. M., Severinghaus, J. P., Baggenstos, D., Fudge, T. J., Steig, E. J., Markle, B. R., Winstrup, M., Rhodes, R. H., Brook, E. J., Sowers, T. A., Clow, G. D., Cheng, H., Edwards, R. L., Sigl, M., McConnell, J. R., & Taylor, K. C., 2015. The WAIS Divide deep ice core WD2014 chronology – Part 1: Methane synchronization (68-31 ka BP) and the gas age-ice age difference, *Clim. Past*, 11(2), 153–173.

Byun, E., Sato, H., Cowling, S. A., & Finkelstein, S. A., 2021. Extensive wetland development in mid-latitude North America during the Bølling-Allerød, *Nat. Geosci.*, 14(1), 30–35.

Campos, J. R. d. R., Silva, A. C., Slater, L., Nanni, M. R., & Vidal-Torrado, P., 2016. Stratigraphic control and chronology of peat bog deposition in the Serra do Espinhaço Meridional, Brazil, *CATENA*, 143, 167–173.

Cao, J., Wang, B., & Ma, L., 2019. Attribution of Global Monsoon Response to the Last Glacial Maximum Forcings, *J. Clim.*, 32(19), 6589–6605.

Cao, M., Marshall, S., & Gregson, K., 1996. Global carbon exchange and methane emissions from natural wetlands: Application of a process-based model, *J. Geophys. Res. Atmos.*, 101(D9), 14399–14414.

Carmichael, M. J., Bernhardt, E. S., Bräuer, S. L., & Smith, W. K., 2014. The role of vegetation in methane flux to the atmosphere: Should vegetation be included as a distinct category in the global methane budget?, *Biogeochemistry*, 119(1-3), 1–24.

Chalk, T. B., Hain, M. P., Foster, G. L., Rohling, E. J., Sexton, P. F., Badger, M. P., Cherry, S. G., Hasenfratz, A. P., Haug, G. H., Jaccard, S. L., Martínez-García, A., Pälike, H., Pancost, R. D., & Wilson, P. A., 2017. Causes of ice age intensification across the mid-pleistocene transition, *Proc. Natl. Acad. Sci. U. S. A.*, 114(50), 13114–13119.

Chambers, F. M. & Charman, D. J., 2004. Holocene environmental change: Contributions from the peatland archive, *Holocene*, 14(1), 1–6.

Charman, D., 2002. *Peatlands and environmental change*, John Wiley & Sons Ltd, United Kingdom.

Charman, D. J., Beilman, D. W., Blaauw, M., Booth, R. K., Brewer, S., Chambers, F. M., Christen, J. A., Gallego-Sala, A., Harrison, S. P., Hughes, P. D., Jackson, S. T., Korhola, A., Mauquoy, D., Mitchell, F. J., Prentice, I. C., Van Der Linden, M., De Vleeschouwer, F., Yu, Z. C., Alm, J., Bauer, I. E., Corish, Y. M., Garneau, M., Hohl, V., Huang, Y., Karofeld, E., Le Roux, G., Loisel, J., Moschen, R., Nichols, J. E., Nieminen, T. M., MacDonald, G. M., Phadtare, N. R., Rausch, N., Sillasoo, U., Swindles, G. T., Tuittila, E. S., Ukonmaanaho, L., Väliranta, M., Van Bellen, S., Van Geel, B., Vitt, D. H., & Zhao, Y., 2013. Climate-related changes in peatland carbon accumulation during the last millennium, *Biogeosciences*, 10(2), 929–944.

Charman, D. J., Amesbury, M. J., Hinchliffe, W., Hughes, P. D., Mallon, G., Blake, W. H., Daley, T. J., Gallego-Sala, A. V., & Mauquoy, D., 2015. Drivers of Holocene peatland carbon accumulation across a climate gradient in northeastern North America, *Quat. Sci. Rev.*, 121, 110–119.

Chaudhary, N., Miller, P. A., & Smith, B., 2017. Modelling past, present and future peatland carbon accumulation across the pan-Arctic region, *Biogeosciences*, 14(18), 4023–4044.

Chaudhary, N., Westermann, S., Lamba, S., Shurpali, N., Sannel, A. B. K., Schurgers, G., Miller, P. A., & Smith, B., 2020. Modelling past and future peatland carbon dynamics across the pan-Arctic, *Glob. Chang. Biol.*, 26(7), 4119–4133.

Chimner, R. A., Pypker, T. G., Hribljan, J. A., Moore, P. A., & Waddington, J. M., 2017. Multi-decadal Changes in Water Table Levels Alter Peatland Carbon Cycling, *Ecosystems*, 20(5), 1042–1057.

Christensen, T. R., Prentice, I. C., Kaplan, J., Haxeltine, A., & Sitch, S., 1996. Methane flux from northern wetlands and tundra: An ecosystem source modelling approach, *Tellus, Ser. B Chem. Phys. Meteorol.*, 48(5), 652–661.

Ciais, P., Sabine, C., Bala, G., Bopp, L., Brovkin, V., Canadell, J., Chhabra, A., DeFries, R., Galloway, J., Heimann, M., Jones, C., Quéré, C. L., Myneni, R., Piao, S., & Thornton, P., 2013. Carbon and Other Biogeochemical Cycles, in *Clim. Chang. 2013 Phys. Sci. Basis Work. Gr. I Contrib. to Fifth Assess. Rep. Intergov. Panel Clim. Chang.*, pp. 465–570, eds Stocker, T., Qin, D., Plattner, G.-K., Tignor, M., Allen, S., Boschung, J., Nauels, A., Xia, Y., Bex, V., & Midgley, P., Cambridge University Press, Cambridge.

Claussen, M., Mysak, L., Weaver, A., Crucifix, M., Fichefet, T., Loutre, M. F., Weber, S., Alcamo, J., Alexeev, V., Berger, A., Calov, R., Ganopolski, A., Goosse, H., Lohmann, G., Lunkeit, F., Mokhov, I., Petoukhov, V., Stone, P., & Wang, Z., 2002. Earth system models of intermediate complexity: Closing the gap in the spectrum of climate system models, *Clim. Dyn.*, 18(7), 579–586.

Clymo, R. S., 1984. The Limits to Peat Bog Growth, *Philos. Trans. R. Soc. B Biol. Sci.*, 303(1117), 605–654.

Collins, M., Knutti, R., Arblaster, J., Dufresne, J.-L., Fichefet, T., Friedlingstein, P., Gao, X., Gutowski, W., Johns, T., Krinner, G., Shongwe, M., Tebaldi, C., Weaver, A., & Wehner, M., 2013. Long-term Climate Change: Projections, Commitments and Irreversibility, in *Clim. Chang. 2013 Phys. Sci. Basis. Contrib. Work. Gr. I to Fifth Assess. Rep. Intergov. Panel Clim. Chang.*, eds Stocker, T., Qin, D., Plattner, G.-K., Tignor, M., Allen, S., Boschung, J., Nauels, A., Xia, Y., Bex, V., & Midgley, P., Cambridge University Press, Cambridge.

Cong, M., Xu, Y., Tang, L., Yang, W., & Jian, M., 2020. Predicting the dynamic distribution of Sphagnum bogs in China under climate change since the last interglacial period, *PLoS One*, 15(4), e0230969.

Dansgaard, W., Johnsen, S. J., Clausen, H. B., Dahl-Jensen, D., Gundestrup, N. S., Hammer, C. U., Hvidberg, C. S., Steffensen, J. P., Sveinbjörnsdottir, A. E., Jouzel, J., & Bond, G., 1993. Evidence for general instability of past climate from a 250-kyr ice-core record, *Nature*, 364(6434), 218–220.

Dargie, G. C., Lewis, S. L., Lawson, I. T., Mitchard, E. T., Page, S. E., Bocko, Y. E., & Ifo, S. A., 2017. Age, extent and carbon storage of the central Congo Basin peatland complex, *Nature*, 542(7639), 86–90.

de Jong, R., Blaauw, M., Chambers, F. M., Christensen, T. R., de Vleeschouwer, F., Finsinger, W., Fronzek, S., Johansson, M., Kokfelt, U., Lamentowicz, M., Le Roux, G., Mauquoy, D., Mitchell, E. A., Nichols, J. E., Samaritani, E., & van Geel, B., 2010. Climate and Peatlands, in *Chang. Clim. Earth Syst. Soc.*, pp. 85–121, ed. Dodson, J., Springer Netherlands, Dordrecht.

Denman, K., Brasseur, G., Chidthaisong, A., Ciais, P., Cox, P., Dickinson, R., Hauglustaine, D., Heinze, C., Holland, E., Jacob, D., Lohmann, U., Ramachandran, S., Dias, P. d. S., Wofsy, S., & Zhang, X., 2007. Couplings between changes in the climate system and biogeochemistry, in *Clim. Chang. 2007 Phys. Sci. basis. Contrib. Work. Gr. I to Fourth Assess. Rep. Intergov. Panel Clim. Chang.*, pp. 499–587, Cambridge University Press.

Dickens, G. R., O'Neil, J. R., Rea, D. K., & Owen, R. M., 1995. Dissociation of oceanic methane hydrate as a cause of the carbon isotope excursion at the end of the Paleocene, *Paleoceanography*, 10(6), 965–971.

Dohong, A., Aziz, A. A., & Dargusch, P., 2017. A review of the drivers of tropical peatland degradation in South-East Asia, *Land use policy*, 69(October), 349–360.

Dommain, R., Couwenberg, J., Glaser, P. H., Joosten, H., & Suryadiputra, I. N. N., 2014. Carbon storage and release in Indonesian peatlands since the last deglaciation, *Quat. Sci. Rev.*, 97, 1–32.

Dommain, R., Frolking, S., Jeltsch-Thömmes, A., Joos, F., Couwenberg, J., & Glaser, P. H., 2018. A radiative forcing analysis of tropical peatlands before and after their conversion to agricultural plantations, *Glob. Chang. Biol.*, 24(11), 5518–5533.

Ed Dlugokencky, 2021. NOAA/GML (www.esrl.noaa.gov/gmd/ccgg/trends_ch4/).

Edwards, P. N., 2011. History of climate modeling, *Wiley Interdiscip. Rev. Clim. Chang.*, 2(1), 128–139.

Erhardt, T., Capron, E., Olander Rasmussen, S., Schüpbach, S., Bigler, M., Adolphi, F., & Fischer, H., 2019. Decadal-scale progression of the onset of Dansgaard-Oeschger warming events, *Clim. Past*, 15(2), 811–825.

Estop-Aragonés, C., Cooper, M. D., Fisher, J. P., Thierry, A., Garnett, M. H., Charman, D. J., Murton, J. B., Phoenix, G. K., Treharne, R., Sanderson, N. K., Burn, C. R., Kokelj, S. V., Wolfe, S. A., Lewkowicz, A. G., Williams, M., & Hartley, I. P., 2018. Limited release of previously-frozen C and increased new peat formation after thaw in permafrost peatlands, *Soil Biol. Biochem.*, 118(August 2017), 115–129.

Etminan, M., Myhre, G., Highwood, E. J., & Shine, K. P., 2016. Radiative forcing of carbon dioxide, methane, and nitrous oxide: A significant revision of the methane radiative forcing, *Geophys. Res. Lett.*, 43(24), 12,614–12,623.

Evenson, G. R., Golden, H. E., Lane, C. R., & D'Amico, E., 2016. An improved representation of geographically isolated wetlands in a watershed-scale hydrologic model, *Hydrol. Process.*, 30(22), 4168–4184.

Eyring, V., Bony, S., Meehl, G. A., Senior, C. A., Stevens, B., Stouffer, R. J., Taylor, K. E., Dynamique, D. M., Pierre, I., Laplace, S., & Ipsl, L. M. D., 2016. Overview of the Coupled Model Intercomparison Project Phase 6 (CMIP6) experimental design and organization, *Geosci. Model Dev*, (9), 1937–1958.

Fernández-Martínez, M., Sardans, J., Chevallier, F., Ciais, P., Obersteiner, M., Vicca, S., Canadell, J. G., Bastos, A., Friedlingstein, P., Sitch, S., Piao, S. L., Janssens, I. A., & Peñuelas, J., 2019. Global trends in carbon sinks and their relationships with CO2 and temperature, *Nat. Clim. Chang.*, 9(1), 73–79.

Finkelstein, S. A. & Cowling, S. A., 2011. Wetlands, temperature, and atmospheric CO2and CH4coupling over the past two millennia, *Global Biogeochem. Cycles*, 25(1), 1–7.

Flato, G. M., 2011. Earth system models: An overview, *Wiley Interdiscip. Rev. Clim. Chang.*, 2(6), 783–800.

Friedlingstein, P. & Prentice, I. C., 2010. Carbon-climate feedbacks: A review of model and observation based estimates, *Curr. Opin. Environ. Sustain.*, 2(4), 251–257.

Friedlingstein, P., Jones, M. W., O'Sullivan, M., Andrew, R. M., Hauck, J., Peters, G. P., Peters, W., Pongratz, J., Sitch, S., Le Quéré, C., Bakker, D. C. E., Canadell, J. G., Ciais, P., Jackson, R. B., Anthoni, P., Barbero, L., Bastos, A., Bastrikov, V., Becker, M., Bopp, L., Buitenhuis, E., Chandra, N., Chevallier, F., Chini, L. P., Currie, K. I., Feely, R. A., Gehlen, M., Gilfillan, D., Gkritzalis, T., Goll, D. S., Gruber, N., Gutekunst, S., Harris, I., Haverd, V., Houghton, R. A., Hurtt, G., Ilyina, T., Jain, A. K., Joetzjer, E., Kaplan, J. O., Kato, E., Klein Goldewijk, K., Korsbakken, J. I., Landschützer, P., Lauvset, S. K., Lefèvre, N., Lenton, A., Lienert, S., Lombardozzi, D., Marland, G., McGuire, P. C., Melton, J. R., Metzl, N., Munro, D. R., Nabel, J. E. M. S.,

Nakaoka, S.-I., Neill, C., Omar, A. M., Ono, T., Peregon, A., Pierrot, D., Poulter, B., Rehder, G., Resplandy, L., Robertson, E., Rödenbeck, C., Séférian, R., Schwinger, J., Smith, N., Tans, P. P., Tian, H., Tilbrook, B., Tubiello, F. N., van der Werf, G. R., Wiltshire, A. J., & Zaehle, S., 2019. Global Carbon Budget 2019, *Earth Syst. Sci. Data*, 11(4), 1783–1838.

Friedlingstein, P., O'Sullivan, M., Jones, M. W., Andrew, R. M., Hauck, J., Olsen, A., Peters, G. P., Peters, W., Pongratz, J., Sitch, S., Le Quéré, C., Canadell, J. G., Ciais, P., Jackson, R. B., Alin, S., Aragão, L. E. O. C., Arneth, A., Arora, V., Bates, N. R., Becker, M., Benoit-Cattin, A., Bittig, H. C., Bopp, L., Bultan, S., Chandra, N., Chevallier, F., Chini, L. P., Evans, W., Florentie, L., Forster, P. M., Gasser, T., Gehlen, M., Gilfillan, D., Gkritzalis, T., Gregor, L., Gruber, N., Harris, I., Hartung, K., Haverd, V., Houghton, R. A., Ilyina, T., Jain, A. K., Joetzjer, E., Kadono, K., Kato, E., Kitidis, V., Korsbakken, J. I., Landschützer, P., Lefèvre, N., Lenton, A., Lienert, S., Liu, Z., Lombardozzi, D., Marland, G., Metzl, N., Munro, D. R., Nabel, J. E. M. S., Nakaoka, S.-I., Niwa, Y., O'Brien, K., Ono, T., Palmer, P. I., Pierrot, D., Poulter, B., Resplandy, L., Robertson, E., Rödenbeck, C., Schwinger, J., Séférian, R., Skjelvan, I., Smith, A. J. P., Sutton, A. J., Tanhua, T., Tans, P. P., Tian, H., Tilbrook, B., van der Werf, G., Vuichard, N., Walker, A. P., Wanninkhof, R., Watson, A. J., Willis, D., Wiltshire, A. J., Yuan, W., Yue, X., & Zaehle, S., 2020. Global Carbon Budget 2020, *Earth Syst. Sci. Data*, 12(4), 3269–3340.

Frolking, S. & Roulet, N. T., 2007. Holocene radiative forcing impact of northern peatland carbon accumulation and methane emissions, *Glob. Chang. Biol.*, 13(5), 1079–1088.

Frolking, S., Roulet, N. T., Tuittila, E., Bubier, J. L., Quillet, A., Talbot, J., & Richard, P. J. H., 2010. A new model of Holocene peatland net primary production, decomposition, water balance, and peat accumulation, *Earth Syst. Dyn.*, 1(1), 1–21.

Gajewski, K., Viau, A., Sawada, M., Atkinson, L. J., & Wilson, S., 2001. Sphagnum peatland distribution in North America and Eurasia during the past 21 , 000 years, *Carbon N. Y.*, 15(2), 297–310.

Gallego-Sala, A. V., Charman, D. J., Harrison, S. P., Li, G., & Prentice, I. C., 2016. Climate-driven expansion of blanket bogs in Britain during the Holocene, *Clim. Past*, 12(1), 129–136.

Gallego-Sala, A. V., Charman, D. J., Brewer, S., Page, S. E., Colin Prentice, I., Friedlingstein, P., Moreton, S., Amesbury, M. J., Beilman, D. W., Bjamp, S., Blyakharchuk, T., Bochicchio, C., Booth, R. K., Bunbury, J., Camill, P., Carless, D., Chimner, R. A., Clifford, M., Cressey, E., Courtney-Mustaphi, C., Vleeschouwer, O., Jong, R., Fialkiewicz-Koziel, B., Finkelstein, S. A., Garneau, M., Githumbi, E., Hribjlan, J., Holmquist, J., M Hughes, P. D., Jones, C., Jones, M. C., Karofeld, E., Klein, E. S., Kokfelt, U., Korhola, A., Lacourse, T., Roux, G., Lamentowicz, M., Large, D., Lavoie, M., Loisel, J., Mackay, H., MacDonald, G. M., Makila, M., Magnan, G., Marchant, R., Marcisz, K., Martamp, A., Cortizas, N., Massa, C., Mathijssen, P., Mauquoy, D., Mighall, T., G Mitchell, F. J., Moss, P., Nichols, J., Oksanen, P. O., Orme, L., Packalen, M. S., Robinson, S., Roland, T. P., Sanderson, N. K., Britta Sannel, A. K., Steinberg, N., Swindles, G. T., Edward Turner, T., Uglow, J., Vamp, M., Bellen, S., Linden, M., Geel, B., Wang, G., Yu, Z., Zaragoza-Castells, J., & Zhao, Y., 2018. Latitudinal limits to the predicted increase of the peatland carbon sink with warming, *Nat. Clim. Chang.*, 8(October), 907–914.

Ganopolski, A. & Calov, R., 2011. The role of orbital forcing, carbon dioxide and regolith in 100 kyr glacial cycles, *Clim. Past*, 7(4), 1415–1425.

Gedalof, Z. & Berg, A. A., 2010. Tree ring evidence for limited direct CO2 fertilization of forests over the 20th century, *Global Biogeochem. Cycles*, 24(3), 2–7.

Gedney, N. & Cox, P. M., 2003. The Sensitivity of Global Climate Model Simulations to the Representation of Soil Moisture Heterogeneity, *J. Hydrometeorol.*, 4(6), 1265–1275.

Gedney, N., Cox, P. M., & Huntingford, C., 2004. Climate feedback from wetland methane emissions, *Geophys. Res. Lett.*, 31(20), 1–4.

Glaser, P. H., Hansen, B. C., Siegel, D. I., Reeve, A. S., & Morin, P. J., 2004. Rates, pathways and drivers for peatland development in the Hudson Bay Lowlands, northern Ontario, Canada, *J. Ecol.*, 92(6), 1036–1053.

Goldstein, A., Turner, W. R., Spawn, S. A., Anderson-Teixeira, K. J., Cook-Patton, S., Fargione, J., Gibbs, H. K., Griscom, B., Hewson, J. H., Howard, J. F., Ledezma, J. C., Page, S., Koh, L. P., Rockström, J., Sanderman, J., & Hole, D. G., 2020. Protecting irrecoverable carbon in Earth's ecosystems, *Nat. Clim. Chang.*, 10(4), 287–295.

Gorham, E., Lehman, C., Dyke, A., Janssens, J., & Dyke, L., 2007. Temporal and spatial aspects of peatland initiation following deglaciation in North America, *Quat. Sci. Rev.*, 26(3-4), 300–311.

Griffiths, H., 1997. *Stable Isotopes: The Integration of Biological, Ecological and Geochemical Processes*, Garland Science.

Gumbricht, T., Roman-Cuesta, R. M., Verchot, L., Herold, M., Wittmann, F., Householder, E., Herold, N., & Murdiyarso, D., 2017. An expert system model for mapping tropical wetlands and peatlands reveals South America as the largest contributor, *Glob. Chang. Biol.*, 23(9), 3581–3599.

Günther, A., Barthelmes, A., Huth, V., Joosten, H., Jurasinski, G., Koebsch, F., & Couwenberg, J., 2020. Prompt rewetting of drained peatlands reduces climate warming despite methane emissions, *Nat. Commun.*, 11(1), 1–5.

Hagemann, S. & Stacke, T., 2015. Impact of the soil hydrology scheme on simulated soil moisture memory, *Clim. Dyn.*, 44(7-8), 1731–1750.

Halsey, L. A., Vitt, D. H., Gignac, L. D., Bryologist, T., & Summer, N., 2000. Sphagnum-Dominated Peatlands in North America since the Last Glacial Maximum : Their Occurrence and Extent Sphagnum-dominated Peatlands in North America Since the Last Glacial Maximum : Their Occurrence and Extent, *Bryologist*, 103(2), 334–352.

Hays, J. D., Imbrie, J., & Shackleton, N. J., 1976. Variations in the earth's orbit: Pacemaker of the ice ages, *Science*, 194(4270), 1121–1132.

He, L., Chen, J. M., Croft, H., Gonsamo, A., Luo, X., Liu, J., Zheng, T., Liu, R., & Liu, Y., 2017. Nitrogen Availability Dampens the Positive Impacts of CO2 Fertilization on Terrestrial Ecosystem Carbon and Water Cycles, *Geophys. Res. Lett.*, 44(22), 11,590–11,600.

Helbig, M., Waddington, J. M., Alekseychik, P., Amiro, B. D., Aurela, M., Barr, A. G., Black, T. A., Blanken, P. D., Carey, S. K., Chen, J., Chi, J., Desai, A. R., Dunn, A., Euskirchen, E. S., Flanagan, L. B., Forbrich, I., Friborg, T., Grelle, A., Harder, S., Heliasz, M., Humphreys, E. R., Ikawa, H., Isabelle, P. E., Iwata, H., Jassal, R., Korkiakoski, M., Kurbatova, J., Kutzbach, L., Lindroth, A., Löfvenius, M. O., Lohila, A., Mammarella, I., Marsh, P., Maximov, T., Melton, J. R., Moore, P. A., Nadeau, D. F., Nicholls, E. M., Nilsson, M. B., Ohta, T., Peichl, M., Petrone, R. M., Petrov, R., Prokushkin, A., Quinton, W. L., Reed, D. E., Roulet, N. T., Runkle, B. R., Sonnentag, O., Strachan, I. B., Taillardat, P., Tuittila, E. S., Tuovinen, J. P., Turner, J., Ueyama, M., Varlagin, A., Wilmking, M., Wofsy, S. C., & Zyrianov, V., 2020. Increasing contribution of peatlands to boreal evapotranspiration in a warming climate, *Nat. Clim. Chang.*, 10(6), 555–560.

Hergoualc'h, K. & Verchot, L. V., 2011. Stocks and fluxes of carbon associated with land use change in Southeast Asian tropical peatlands: A review, *Global Biogeochem. Cycles*, 25(2).

Holligan, P. M. & Robertson, J. E., 1996. Significance of ocean carbonate budgets for the global carbon cycle, *Glob. Chang. Biol.*, 2(2), 85–95.

Hopple, A. M., Wilson, R. M., Kolton, M., Zalman, C. A., Chanton, J. P., Kostka, J., Hanson, P. J., Keller, J. K., & Bridgham, S. D., 2020. Massive peatland carbon banks vulnerable to rising temperatures, *Nat. Commun.*, 11(1), 2373.

Hoyt, A. M., Chaussard, E., Seppalainen, S. S., & Harvey, C. F., 2020. Widespread subsidence and carbon emissions across Southeast Asian peatlands, *Nat. Geosci.*, 13(6), 435–440.

Hu, S., Niu, Z., & Chen, Y., 2017a. Global Wetland Datasets: a Review, *Wetlands*, 37(5), 807–817.

Hu, S., Niu, Z., Chen, Y., Li, L., & Zhang, H., 2017b. Global wetlands: Potential distribution, wetland loss, and status, *Sci. Total Environ.*, 586, 319–327.

Huang, J., Mendoza, B., Daniel, J. S., Nielsen, C. J., Rotstayn, L., & Wild, O., 2013. Anthropogenic and natural radiative forcing, *Clim. Chang. 2013 Phys. Sci. Basis Work. Gr. I Contrib. to Fifth Assess. Rep. Intergov. Panel Clim. Chang.*, 9781107057, 659–740.

Huber, C., Leuenberger, M., Spahni, R., Flückiger, J., Schwander, J., Stocker, T. F., Johnsen, S., Landais, A., & Jouzel, J., 2006. Isotope calibrated Greenland temperature record over Marine Isotope Stage 3 and its relation to CH4, *Earth Planet. Sci. Lett.*, 243(3-4), 504–519.

Hugelius, G., Strauss, J., Zubrzycki, S., Harden, J. W., Schuur, E. A., Ping, C. L., Schirrmeister, L., Grosse, G., Michaelson, G. J., Koven, C. D., O'Donnell, J. A., Elberling, B., Mishra, U., Camill, P., Yu, Z., Palmtag, J., & Kuhry, P., 2014. Estimated stocks of circumpolar permafrost carbon with quantified uncertainty ranges and identified data gaps, *Biogeosciences*, 11(23), 6573–6593.

Hugelius, G., Loisel, J., Chadburn, S., Jackson, R. B., Jones, M., MacDonald, G., Marushchak, M., Olefeldt, D., Packalen, M., Siewert, M. B., Treat, C., Turetsky, M., Voigt, C., & Yu, Z., 2020. Large stocks of peatland carbon and nitrogen are vulnerable to permafrost thaw, *Proc. Natl. Acad. Sci. U. S. A.*, 117(34), 20438–20446.

Humpenöder, F., Karstens, K., Lotze-Campen, H., Leifeld, J., Menichetti, L., Barthelmes, A., & Popp, A., 2020. Peatland protection and restoration are key for climate change mitigation, *Environ. Res. Lett.*, 15(10), 104093.

Imbrie, J., Berger, A., Boyle, E. A., Clemens, S. C., Duffy, A., Howard, W. R., Kukla, G., Kutzbach, J., Martinson, D. G., McIntyre, A., Mix, A. C., Molfino, B., Morley, J. J., Peterson, L. C., Pisias, N. G., Prell, W. L., Raymo, M. E., Shackleton, N. J., & Toggweiler, J. R., 1993. On the structure and origin of major glaciation cycles 2. The 100,000-year cycle, *Paleoceanography*, 8(6), 699–735.

IPCC, 2013. *Climate Change 2013: The Physical Science Basis. Contribution of Working Group I to the Fifth Assessment Report of the Intergovernmental Panel on Climate Change*, Cambridge University Press, Cambridge.

Ise, T., Dunn, A. L., Wofsy, S. C., & Moorcroft, P. R., 2008. High sensitivity of peat decomposition to climate change through water-table feedback, *Nat. Geosci.*, 1(11), 763–766.

Jeltsch-Thömmes, A., Battaglia, G., Cartapanis, O., Jaccard, S. L., & Joos, F., 2019. Low terrestrial carbon storage at the Last Glacial Maximum: Constraints from multi-proxy data, *Clim. Past*, 15(2), 849–879.

Jobbágy, E. G. & Jackson, R. B., 2000. The vertical distribution of soil organic carbon and its relation to climate and vegetation, *Ecol. Appl.*, 10(2), 423–436.

Jones, M. C., Harden, J., O'Donnell, J., Manies, K., Jorgenson, T., Treat, C., & Ewing, S., 2017. Rapid carbon loss and slow recovery following permafrost thaw in boreal peatlands, *Glob. Chang. Biol.*, 23(3), 1109–1127.

Joos, F. & Spahni, R., 2008. Rates of change in natural and anthropogenic radiative forcing over the past 20,000 years, *Proc. Natl. Acad. Sci. U. S. A.*, 105(5), 1425–1430.

Joos, F., Spahni, R., D. Stocker, B., Lienert, S., Müller, J., Fischer, H., Schmitt, J., Colin Prentice, I., Otto-Bliesner, B., & Liu, Z., 2020. N2O changes from the Last Glacial Maximum to the preindustrial - Part 2: Terrestrial N2O emissions and carbon-nitrogen cycle interactions, *Biogeosciences*, 17(13), 3511–3543.

Jouzel, J., Masson-Delmotte, V., Cattani, O., Dreyfus, G., Falourd, S., Hoffmann, G., Minster, B., Nouet, J., Barnola, J. M., Chappellaz, J., Fischer, H., Gallet, J. C., Johnsen, S., Leuenberger, M., Loulergue, L., Luethi, D., Oerter, H., Parrenin, F., Raisbeck, G., Raynaud, D., Schilt, A., Schwander, J., Selmo, E., Souchez, R., Spahni, R., Stauffer, B., Steffensen, J. P., Stenni, B., Stocker, T. F., Tison, J. L., Werner, M., & Wolff, E. W., 2007. Orbital and Millennial Antarctic Climate Variability over the Past 800,000 Years, *Science*, 317(5839), 793–796.

Jull, A. J., Burr, G. S., & Hodgins, G. W., 2013. Radiocarbon dating, reservoir effects, and calibration, *Quat. Int.*, 299, 64–71.

Kaplan, J. O., 2002. Wetlands at the Last Glacial Maximum: Distribution and methane emissions, *Geophys. Res. Lett.*, 29(6), 3–1–3–4.

Kimmel, K. & Mander, Ü., 2010. Ecosystem services of peatlands: Implications for restoration, *Prog. Phys. Geogr.*, 34(4), 491–514.

Kleinen, T., Brovkin, V., Bloh, W., Archer, D., & Munhoven, G., 2010. Holocene carbon cycle dynamics, *Geophys. Res. Lett.*, 37(2), 1–5.

Kleinen, T., Brovkin, V., & Schuldt, R. J., 2012. A dynamic model of wetland extent and peat accumulation: Results for the Holocene, *Biogeosciences*, 9(1), 235–248.

Kleinen, T., Mikolajewicz, U., & Brovkin, V., 2020. Terrestrial methane emissions from the Last Glacial Maximum to the preindustrial period, *Clim. Past*, 16(2), 575–595.

Köhler, P., Nehrbass-Ahles, C., Schmitt, J., Stocker, T. F., & Fischer, H., 2017. A 156 kyr smoothed history of the atmospheric greenhouse gases CO2, CH4, and N2O and their radiative forcing, *Earth Syst. Sci. Data*, 9(1), 363–387.

Korhola, A., Ruppel, M., Seppä, H., Väliranta, M., Virtanen, T., & Weckström, J., 2010. The importance of northern peatland expansion to the late-Holocene rise of atmospheric methane, *Quat. Sci. Rev.*, 29(5-6), 611–617.

Kreuzburg, M., Ibenthal, M., Janssen, M., Rehder, G., Voss, M., Naumann, M., & Feldens, P., 2018. Sub-marine Continuation of Peat Deposits From a Coastal Peatland in the Southern Baltic Sea and its Holocene Development, *Front. Earth Sci.*, 6(July), 103.

Kuhlbrodt, T., Griesel, A., Montoya, M., Levermann, A., Hofmann, M., & Rahmstorf, S., 2007. On the driving processes of the Atlantic meridional overturning circulation, *Rev. Geophys.*, 45(2).

Lähteenoja, O., Reátegui, Y. R., Räsänen, M., Torres, D. D. C., Oinonen, M., & Page, S., 2012. The large Amazonian peatland carbon sink in the subsiding Pastaza-Marañón foreland basin, Peru, *Glob. Chang. Biol.*, 18(1), 164–178.

Lai, D., 2009. Methane Dynamics in Northern Peatlands: A Review, *Pedosphere*, 19(4), 409–421.

Lambers, H., Chapin, F. S., & Pons, T. L., 2008. Photosynthesis, in *Plant Physiol. Ecol.*, pp. 11–99, Springer New York, New York, NY.

Largeron, C., Krinner, G., Ciais, P., & Brutel-Vuilmet, C., 2018. Implementing northern peatlands in a global land surface model: Description and evaluation in the ORCHIDEE high-latitude version model (ORC-HL-PEAT), *Geosci. Model Dev.*, 11(8), 3279–3297.

Lee, S., Yeo, I. Y., Lang, M. W., McCarty, G. W., Sadeghi, A. M., Sharifi, A., Jin, H., & Liu, Y., 2019. Improving the catchment scale wetland modeling using remotely sensed data, *Environ. Model. Softw.*, 122.

Leifeld, J. & Menichetti, L., 2018. The underappreciated potential of peatlands in global climate change mitigation strategies, *Nat. Commun.*, 9(1), 1071.

Leifeld, J., Wüst-Galley, C., & Page, S., 2019. Intact and managed peatland soils as a source and sink of GHGs from 1850 to 2100, *Nat. Clim. Chang.*, 9(12), 945–947.

León, C. A., Benitez-Mora, A., & Oliván, G., 2018. Update of recent rates of carbon accumulation in bogs of Northern patagonia-Chile, *J. Soil Sci. Plant Nutr.*, 18(4), 977–988.

Lewis, S. L. & Maslin, M. A., 2015. Defining the Anthropocene, *Nature*, 519(7542), 171–180.

Li, C. & Born, A., 2019. Coupled atmosphere-ice-ocean dynamics in Dansgaard-Oeschger events, *Quat. Sci. Rev.*, 203(5020), 1–20.

Lienert, S. & Joos, F., 2018. A Bayesian ensemble data assimilation to constrain model parameters and land-use carbon emissions, *Biogeosciences*, 15(9), 2909–2930.

Lindsay, R., 2018. Peatland Classification, in *Wetl. B.*, pp. 1515–1528, Springer Netherlands, Dordrecht.

Liu, L., Zhuang, Q., Oh, Y., Shurpali, N. J., Kim, S., & Poulter, B., 2020. Uncertainty Quantification of Global Net Methane Emissions From Terrestrial Ecosystems Using a Mechanistically Based Biogeochemistry Model, *J. Geophys. Res. Biogeosciences*, 125(6), 1–19.

Loisel, J. & Bunsen, M., 2020. Abrupt Fen-Bog Transition Across Southern Patagonia: Timing, Causes, and Impacts on Carbon Sequestration, *Front. Ecol. Evol.*, 8(August), 1–19.

Loisel, J., Yu, Z., Beilman, D. W., Camill, P., Alm, J., Amesbury, M. J., Anderson, D., Andersson, S., Bochicchio, C., Barber, K., Belyea, L. R., Bunbury, J., Chambers, F. M., Charman, D. J., De Vleeschouwer, F., Fiałkiewicz-Kozieł, B., Finkelstein, S. A., Gałka, M., Garneau, M., Hammarlund, D., Hinchcliffe, W., Holmquist, J., Hughes, P., Jones, M. C., Klein, E. S., Kokfelt, U., Korhola, A., Kuhry, P., Lamarre, A., Lamentowicz, M., Large, D., Lavoie, M., MacDonald, G., Magnan, G., Mäkilä, M., Mallon, G., Mathijssen, P., Mauquoy, D., McCarroll, J., Moore, T. R., Nichols, J., O'Reilly, B., Oksanen, P., Packalen, M., Peteet, D., Richard, P. J., Robinson, S., Ronkainen, T., Rundgren, M., Sannel, A. B. K., Tarnocai, C., Thom, T., Tuittila, E.-S., Turetsky, M., Väliranta, M., van der Linden, M., van Geel, B., van Bellen, S., Vitt, D., Zhao, Y., & Zhou, W., 2014. A database and synthesis of northern peatland soil properties and Holocene carbon and nitrogen accumulation, *The Holocene*, 24(9), 1028–1042.

Loisel, J., van Bellen, S., Pelletier, L., Talbot, J., Hugelius, G., Karran, D., Yu, Z., Nichols, J., & Holmquist, J., 2017. Insights and issues with estimating northern peatland carbon stocks and fluxes since the Last Glacial Maximum, *Earth-Science Rev.*, 165, 59–80.

Loulergue, L., Schilt, A., Spahni, R., Masson-Delmotte, V., Blunier, T., Lemieux, B., Barnola, J.-M., Raynaud, D., Stocker, T. F., & Chappellaz, J., 2008. Orbital and millennial-scale features of atmospheric CH4 over the past 800,000 years, *Nature*, 453(7193), 383–386.

Lowe, J. A. & Bernie, D., 2018. The impact of Earth system feedbacks on carbon budgets and climate response, *Philos. Trans. R. Soc. A Math. Phys. Eng. Sci.*, 376(2119).

Lüthi, D., Le Floch, M., Bereiter, B., Blunier, T., Barnola, J. M., Siegenthaler, U., Raynaud, D., Jouzel, J., Fischer, H., Kawamura, K., & Stocker, T. F., 2008. High-resolution carbon dioxide concentration record 650,000-800,000 years before present, *Nature*, 453(7193), 379–382.

Maasakkers, J. D., Jacob, D. J., Sulprizio, M. P., Scarpelli, T. R., Nesser, H., Sheng, J.-X., Zhang, Y., Hersher, M., Bloom, A. A., Bowman, K. W., Worden, J. R., Janssens-Maenhout, G., & Parker, R. J., 2019. Global distribution of methane emissions, emission trends, and OH concentrations and trends inferred from an inversion of GOSAT satellite data for 2010–2015, *Atmos. Chem. Phys. Discuss.*, pp. 1–36.

MacDonald, G. M., Beilman, D. W., Kremenetski, K. V., Sheng, Y., Smith, L. C., & Velichko, A. A., 2006. Rapid Early Development of Circumarctic Peatlands and Atmospheric CH4 and CO2 Variations, *Science*, 314(5797), 285–288.

Mackensen, A. & Schmiedl, G., 2019. Stable carbon isotopes in paleoceanography: atmosphere, oceans, and sediments, *Earth-Science Rev.*, 197(June), 102893.

Magnússon, R. Í., Limpens, J., Huissteden, J., Kleijn, D., Maximov, T. C., Rotbarth, R., Sass-Klaassen, U., & Heijmans, M. M. P. D., 2020. Rapid Vegetation Succession and Coupled Permafrost Dynamics in Arctic Thaw Ponds in the Siberian Lowland Tundra, *J. Geophys. Res. Biogeosciences*, 125(7), 1–20.

Marrs, R. H., Marsland, E. L., Lingard, R., Appleby, P. G., Piliposyan, G. T., Rose, R. J., O'Reilly, J., Milligan, G., Allen, K. A., Alday, J. G., Santana, V., Lee, H., Halsall, K., & Chiverrell, R. C., 2019. Experimental evidence for sustained carbon sequestration in fire-managed, peat moorlands, *Nat. Geosci.*, 12(2), 108–112.

Masson-Delmotte, V., Schulz, M., Abe-Ouchi, A., Beer, J., Ganopolski, A., Rouco, J. G., Jansen, E., Lambeck, K., Luterbacher, J., Naish, T., Osbor, T., Otto-Bliesner, B., Quinn, T., Ramesh, R., Rojas, M., Shao, X., & Timmermann, A., 2013. Information from Paleoclimate Archives, in *Clim. Chang. 2013 Phys. Sci. Basis. Contrib. Work. Gr. I to Fifth Assess. Rep. Intergov. Panel Clim. Chang.*, pp. 383–464, eds Stocker, T., D. Qin, G.-K. P., Tignor, M., Allen, S., Boschung, J., Nauels, A., Xia, Y., Bex, V., & Midgley, P., Cambridge University Press, Cambridge.

Mayer, E. W., Blake, D. R., Tyler, S. C., Makide, Y., Montague, D. C., & Rowland, F. S., 1982. Methane: Interhemispheric concentration gradient and atmospheric residence time, *Proc. Natl. Acad. Sci.*, 79(4), 1366–1370.

McGee, D., Donohoe, A., Marshall, J., & Ferreira, D., 2014. Changes in ITCZ location and cross-equatorial heat transport at the Last Glacial Maximum, Heinrich Stadial 1, and the mid-Holocene, *Earth Planet. Sci. Lett.*, 390, 69–79.

Melton, J. R., Wania, R., Hodson, E. L., Poulter, B., Ringeval, B., Spahni, R., Bohn, T., Avis, C. A., Beerling, D. J., Chen, G., Eliseev, A. V., Denisov, S. N., Hopcroft, P. O., Lettenmaier, D. P., Riley, W. J., Singarayer, J. S., Subin, Z. M., Tian, H., Zürcher, S., Brovkin, V., van Bodegom, P. M., Kleinen, T., Yu, Z. C., & Kaplan, J. O., 2013. Present state of global wetland extent and wetland methane modelling: conclusions from a model inter-comparison project (WETCHIMP), *Biogeosciences*, 10(2), 753–788.

Minayeva, T. Y. & Sirin, A. A., 2012. Peatland biodiversity and climate change, *Biol. Bull. Rev.*, 2(2), 164–175.

Mitsch, W. J. & Gosselink, J. G., 2015. *Wetlands*, John Wiley & Sons.

Mokhov, I. I., Eliseev, A. V., & Denisov, S. N., 2007. Model diagnostics of variations in methane emissions by wetlands in the second half of the 20th century based on reanalysis data, *Dokl. Earth Sci.*, 417(1), 1293–1297.

Moore, P. D., 1989. The ecology of peat-forming processes: a review, *Int. J. Coal Geol.*, 12(1-4), 89–103.

Morris, P. J., Belyea, L. R., & Baird, A. J., 2011. Ecohydrological feedbacks in peatland development: A theoretical modelling study, *J. Ecol.*, 99(5), 1190–1201.

Morris, P. J., Baird, A. J., & Belyea, L. R., 2012. The DigiBog peatland development model 2: ecohydrological simulations in 2D, *Ecohydrology*, 5(3), 256–268.

Morris, P. J., Swindles, G. T., Valdes, P. J., Ivanovic, R. F., Gregoire, L. J., Smith, M. W., Tarasov, L., Haywood, A. M., & Bacon, K. L., 2018. Global peatland initiation driven by regionally asynchronous warming, *Proc. Natl. Acad. Sci.*, 115(19), 4851–4856.

Müller, J. & Joos, F., 2020. Global peatland area and carbon dynamics from the Last Glacial Maximum to the present - a process-based model investigation, *Biogeosciences*, 17(21), 5285–5308.

Müller, J. & Joos, F., 2021. Committed and projected future changes in global peatlands - continued transient model simulations since the Last Glacial Maximum, *Biogeosciences*, 18(12), 3657–3687.

Nordhaus, W., 2017. Integrated assessment models of climate change, *NBER Report.*, (3), 16–20.

Nugent, K. A., Strachan, I. B., Roulet, N. T., Strack, M., Frolking, S., & Helbig, M., 2019. Prompt active restoration of peatlands substantially reduces climate impact, *Environ. Res. Lett.*, 14(12), 124030.

O'Connor, F. M., Boucher, O., Gedney, N., Jones, C. D., Folberth, G. a., Coppell, R., Friedlingstein, P., Collins, W. J., Chappellaz, J., Ridley, J., Johnson, C. E., Connor, F. M. O., Boucher, O., Gedney, N., Jones, C. D., Folberth, G. a., Coppell, R., Friedlingstein, P., Collins, W. J., Chappellaz, J., Ridley, J., & Johnson, C. E., 2010. Possible Role of Wetlands , Permafrost , and Methane Hydrates in the Methane Cycle Under Future Climate Change : a Review, *Rev. Geophys.*, 48(4), 1–33.

Page, S. E., Rieley, J. O., & Banks, C. J., 2011. Global and regional importance of the tropical peatland carbon pool, *Glob. Chang. Biol.*, 17(2), 798–818.

Pangala, S. R., Enrich-Prast, A., Basso, L. S., Peixoto, R. B., Bastviken, D., Hornibrook, E. R., Gatti, L. V., Marotta, H., Calazans, L. S. B., Sakuragui, C. M., Bastos, W. R., Malm, O., Gloor, E., Miller, J. B., & Gauci, V., 2017. Large emissions from floodplain trees close the Amazon methane budget, *Nature*, 552(7684), 230–234.

Past Interglacials Working Group of PAGES, 2016. Interglacials of the last 800,000 years, *Rev. Geophys.*, 54, 162–219.

Pellerin, S. & Lavoie, C., 2003. Recent expansion of jack pine in peatlands of southeastern Québec: A paleoecological study, *Écoscience*, 10(2), 247–257.

Popp, A., Calvin, K., Fujimori, S., Havlik, P., Humpenöder, F., Stehfest, E., Bodirsky, B. L., Dietrich, J. P., Doelmann, J. C., Gusti, M., Hasegawa, T., Kyle, P., Obersteiner, M., Tabeau, A., Takahashi, K., Valin, H., Waldhoff, S., Weindl, I., Wise, M., Kriegler, E., Lotze-Campen, H., Fricko, O., Riahi, K., & van Vuuren, D. P., 2017. Land-use futures in the shared socio-economic pathways, *Glob. Environ. Chang.*, 42, 331–345.

Potvin, L. R., Kane, E. S., Chimner, R. A., Kolka, R. K., & Lilleskov, E. A., 2015. Effects of water table position and plant functional group on plant community, aboveground production, and peat properties in a peatland mesocosm experiment (PEATcosm), *Plant Soil*, 387(1-2), 277–294.

Prather, M. J., Holmes, C. D., & Hsu, J., 2012. Reactive greenhouse gas scenarios: Systematic exploration of uncertainties and the role of atmospheric chemistry, *Geophys. Res. Lett.*, 39(9), 6–10.

Prentice, I., Farquhar, G., Fasham, M., Goulden, M., Heimann, M., Jaramillo, V., Kheshgi, H., Le Quéré, C., Scholes, R., & Wallace, D., 2001. The carbon cycle and atmospheric carbon dioxide, in *Clim. Chang. 2001 Sci. Basis*, pp. 183–237, eds Houghton, J., Ding, Y., Griggs, D., Noguer, M., van der Linden, P., Dai, X., Maskell, K., & Johnson, C., Cambridge University Press, United Kingdom.

Prentice, I. C. & Cowling, S. A., 2013. Dynamic Global Vegetation Models, *Encycl. Biodivers. Second Ed.*, 2, 670–689.

Qiu, C., Zhu, D., Ciais, P., Guenet, B., Krinner, G., Peng, S., Aurela, M., Bernhofer, C., Brümmer, C., Bret-Harte, S., Chu, H., Chen, J., Desai, A. R., Dušek, J., Euskirchen, E. S., Fortuniak, K., Flanagan, L. B., Friborg, T., Grygoruk, M., Gogo, S., Grünwald, T., Hansen, B. U., Holl, D., Humphreys, E., Hurkuck, M., Kiely, G., Klatt, J., Kutzbach, L., Largeron, C., Laggoun-Défarge, F., Lund, M., Lafleur, P. M., Li, X., Mammarella, I., Merbold, L., Nilsson, M. B., Olejnik, J., Ottosson-Löfvenius, M., Oechel, W., Parmentier, F. J. W., Peichl, M., Pirk, N., Peltola, O., Pawlak, W., Rasse, D., Rinne, J., Shaver, G., Peter Schmid, H., Sottocornola, M., Steinbrecher, R., Sachs, T., Urbaniak, M., Zona, D., & Ziemblinska, K., 2018. ORCHIDEE-PEAT (revision 4596), a model for northern peatland CO2, water, and energy fluxes on daily to annual scales, *Geosci. Model Dev.*, 11(2), 497–519.

Qiu, C., Zhu, D., Ciais, P., Guenet, B., & Peng, S., 2020. The role of northern peatlands in the global carbon cycle for the 21st century, *Glob. Ecol. Biogeogr.*, 29(5), 956–973.

Qiu, C., Ciais, P., Zhu, D., Guenet, B., Peng, S., Petrescu, A. M. R., Lauerwald, R., Makowski, D., Gallego-Sala, A. V., Charman, D. J., & Brewer, S. C., 2021. Large historical carbon emissions from cultivated northern peatlands, *Sci. Adv.*, 7(23).

Raivonen, M., Smolander, S., Backman, L., Susiluoto, J., Aalto, T., Markkanen, T., Mäkelä, J., Rinne, J., Peltola, O., Aurela, M., Lohila, A., Tomasic, M., Li, X., Larmola, T., Juutinen, S., Tuittila, E.-S., Heimann, M., Sevanto, S., Kleinen, T., Brovkin, V., & Vesala, T., 2017. HIMMELI v1.0: HelsinkI Model of MEthane buiLd-up and emIssion for peatlands, *Geosci. Model Dev.*, 10(12), 4665–4691.

Rasmussen, S. O., Bigler, M., Blockley, S. P., Blunier, T., Buchardt, S. L., Clausen, H. B., Cvijanovic, I., Dahl-Jensen, D., Johnsen, S. J., Fischer, H., Gkinis, V., Guillevic, M., Hoek, W. Z., Lowe, J. J., Pedro, J. B., Popp, T., Seierstad, I. K., Steffensen, J. P., Svensson, A. M., Vallelonga, P., Vinther, B. M., Walker, M. J., Wheatley, J. J., & Winstrup, M., 2014. A stratigraphic framework for abrupt climatic changes during the Last Glacial period based on three synchronized Greenland ice-core records: refining and extending the INTIMATE event stratigraphy, *Quat. Sci. Rev.*, 106, 14–28.

Riahi, K., van Vuuren, D. P., Kriegler, E., Edmonds, J., O'Neill, B. C., Fujimori, S., Bauer, N., Calvin, K., Dellink, R., Fricko, O., Lutz, W., Popp, A., Cuaresma, J. C., KC, S., Leimbach, M., Jiang, L., Kram, T., Rao, S., Emmerling, J., Ebi, K., Hasegawa, T., Havlik, P., Humpenöder, F., Da Silva, L. A., Smith, S., Stehfest, E., Bosetti, V., Eom, J., Gernaat, D., Masui, T., Rogelj, J., Strefler, J., Drouet, L., Krey, V., Luderer, G., Harmsen, M., Takahashi, K., Baumstark, L., Doelman, J. C., Kainuma, M., Klimont, Z., Marangoni, G., Lotze-Campen, H., Obersteiner, M., Tabeau, A., & Tavoni, M., 2017. The Shared Socioeconomic Pathways and their energy, land use, and greenhouse gas emissions implications: An overview, *Glob. Environ. Chang.*, 42, 153–168.

Ribeiro, K., Pacheco, F. S., Ferreira, J. W., de Sousa-Neto, E. R., Hastie, A., Krieger Filho, G. C., Alvalá, P. C., Forti, M. C., & Ometto, J. P., 2021. Tropical peatlands and their contribution to the global carbon cycle and climate change, *Glob. Chang. Biol.*, 27(3), 489–505.

Ridgwell, A. & Schmidt, D. N., 2010. Past constraints on the vulnerability of marine calcifiers to massive carbon dioxide release, *Nat. Geosci.*, 3(3), 196–200.

Ringeval, B., Houweling, S., Van Bodegom, P. M., Spahni, R., Van Beek, R., Joos, F., & Röckmann, T., 2014. Methane emissions from floodplains in the Amazon Basin: Challenges in developing a process-based model for global applications, *Biogeosciences*, 11(6), 1519–1558.

Ruppel, C., 2015. Permafrost-associated gas hydrate: Is it really approximately 1 % of the global system?, *J. Chem. Eng. Data*, 60(2), 429–436.

Ruppel, C. D. & Kessler, J. D., 2017. The interaction of climate change and methane hydrates, *Rev. Geophys.*, 55(1), 126–168.

Ruppel, M., Väliranta, M., Virtanen, T., & Korhola, A., 2013. Postglacial spatiotemporal peatland initiation and lateral expansion dynamics in North America and northern Europe, *Holocene*, 23(11), 1596–1606.

Rustad, L. E., Huntington, T. G., & Boone, D., 2000. Controls on Soil Respiration: Implications for Climate Change, *Biogeochemistry*, 48(1), 1–6.

Rydin, H. & Jeglum, J. K., 2013. *The Biology of Peatlands*, Oxford University Press.

Sarmiento, J. L. & Gruber, N., 2006. *Ocean Biogeochemical Dynamics*, Princeton University Press.

Saunois, M., Stavert, A. R., Poulter, B., Bousquet, P., Canadell, J. G., Jackson, R. B., Raymond, P. A., Dlugokencky, E. J., Houweling, S., Patra, P. K., Ciais, P., Arora, V. K., Bastviken, D., Bergamaschi, P., Blake, D. R., Brailsford, G., Bruhwiler, L., Carlson, K. M., Carrol, M., Castaldi, S., Chandra, N., Crevoisier, C., Crill, P. M., Covey, K., Curry, C. L., Etiope, G., Frankenberg, C., Gedney, N., Hegglin, M. I., Höglund-Isaksson, L., Hugelius, G., Ishizawa, M., Ito, A., Janssens-Maenhout, G., Jensen, K. M., Joos, F., Kleinen, T., Krummel, P. B., Langenfelds, R. L., Laruelle, G. G., Liu, L., Machida, T., Maksyutov, S., McDonald, K. C., McNorton, J., Miller, P. A., Melton, J. R., Morino, I., Müller, J., Murguia-Flores, F., Naik, V., Niwa, Y., Noce, S., O'Doherty, S., Parker, R. J., Peng, C., Peng, S., Peters, G. P., Prigent, C., Prinn, R., Ramonet, M., Regnier, P., Riley, W. J., Rosentreter, J. A., Segers, A., Simpson, I. J., Shi, H., Smith, S. J., Steele, L. P., Thornton, B. F., Tian, H., Tohjima, Y., Tubiello, F. N., Tsuruta, A., Viovy, N., Voulgarakis, A., Weber, T. S., van Weele, M., van der Werf, G. R., Weiss, R. F., Worthy, D., Wunch, D., Yin, Y., Yoshida, Y., Zhang, W., Zhang, Z., Zhao, Y., Zheng, B., Zhu, Q., Zhu, Q., & Zhuang, Q., 2020. The Global Methane Budget 2000-2017, *Earth Syst. Sci. Data*, 12(3), 1561–1623.

Scharlemann, J. P., Tanner, E. V., Hiederer, R., & Kapos, V., 2014. Global soil carbon: Understanding and managing the largest terrestrial carbon pool, *Carbon Manag.*, 5(1), 81–91.

Schilt, A., Baumgartner, M., Blunier, T., Schwander, J., Spahni, R., Fischer, H., & Stocker, T. F., 2010a. Glacial-interglacial and millennial-scale variations in the atmospheric nitrous oxide concentration during the last 800,000 years, *Quat. Sci. Rev.*, 29(1-2), 182–192.

Schilt, A., Baumgartner, M., Schwander, J., Buiron, D., Capron, E., Chappellaz, J., Loulergue, L., Schüpbach, S., Spahni, R., Fischer, H., & Stocker, T. F., 2010b. Atmospheric nitrous oxide during the last 140,000 years, *Earth Planet. Sci. Lett.*, 300(1-2), 33–43.

Schimel, D., Stephens, B. B., & Fisher, J. B., 2015. Effect of increasing CO2 on the terrestrial carbon cycle, *Proc. Natl. Acad. Sci. U. S. A.*, 112(2), 436–441.

Schmidt, G. A., Ruedy, R. A., Miller, R. L., & Lacis, A. A., 2010. Attribution of the present-day total greenhouse effect, *J. Geophys. Res. Atmos.*, 115(20), 1–6.

Schurgers, G., Ahlström, A., Arneth, A., Pugh, T. A., & Smith, B., 2018. Climate Sensitivity Controls Uncertainty in Future Terrestrial Carbon Sink, *Geophys. Res. Lett.*, 45(9), 4329–4336.

Shi, J. & Yan, Q., 2019. Evolution of the Asian-African Monsoonal Precipitation over the last 21 kyr and the Associated Dynamic Mechanisms, *J. Clim.*, 32(19), 6551–6569.

Sigman, D. M. & Boyle, E. A., 2000. Glacial/Interglacial changes in atmospheric carbon dioxide, *Nature*, 407(October), 859–869.

Sigman, D. M., Hain, M. P., & Haug, G. H., 2010. The polar ocean and glacial cycles in atmospheric CO2 concentration, *Nature*, 466(7302), 47–55.

Sitch, S., Smith, B., Prentice, I. C., Arneth, A., Bondeau, A., Cramer, W., Kaplan, J. O., Levis, S., Lucht, W., Sykes, M. T., Thonicke, K., & Venevsky, S., 2003. Evaluation of ecosystem dynamics, plant geography and terrestrial carbon cycling in the LPJ dynamic global vegetation model, *Glob. Chang. Biol.*, 9(2), 161–185.

Spahni, R., Joos, F., Stocker, B. D., Steinacher, M., & Yu, Z. C., 2013. Transient simulations of the carbon and nitrogen dynamics in northern peatlands: From the Last Glacial Maximum to the 21st century, *Clim. Past*, 9(3), 1287–1308.

Stocker, B. D., Spahni, R., & Joos, F., 2014. DYPTOP: A cost-efficient TOPMODEL implementation to simulate sub-grid spatio-temporal dynamics of global wetlands and peatlands, *Geosci. Model Dev.*, 7(6), 3089–3110.

Stocker, T. F. & Johnsen, S. J., 2003. A minimum thermodynamic model for the bipolar seesaw, *Paleoceanography*, 18(4), 1–9.

Strassmann, K. M., Joos, F., & Fischer, G., 2008. Simulating effects of land use changes on carbon fluxes: Past contributions to atmospheric CO2 increases and future commitments due to losses of terrestrial sink capacity, *Tellus, Ser. B Chem. Phys. Meteorol.*, 60(4), 583–603.

Swindles, G. T., Morris, P. J., Mullan, D., Watson, E. J., Turner, T. E., Roland, T. P., Amesbury, M. J., Kokfelt, U., Schoning, K., Pratte, S., Gallego-Sala, A., Charman, D. J., Sanderson, N., Garneau, M., Carrivick, J. L., Woulds, C., Holden, J., Parry, L., & Galloway, J. M., 2015. The long-term fate of permafrost peatlands under rapid climate warming, *Sci. Rep.*, 5(November), 1–6.

Swindles, G. T., Morris, P. J., Mullan, D. J., Payne, R. J., Roland, T. P., Amesbury, M. J., Lamentowicz, M., Turner, T. E., Gallego-Sala, A., Sim, T., Barr, I. D., Blaauw, M., Blundell, A., Chambers, F. M., Charman, D. J., Feurdean, A., Galloway, J. M., Gałka, M., Green, S. M., Kajukało, K., Karofeld, E., Korhola, A., Lamentowicz, Ł., Langdon, P., Marcisz, K., Mauquoy, D., Mazei, Y. A., McKeown, M. M., Mitchell, E. A. D., Novenko, E., Plunkett, G., Roe, H. M., Schoning, K., Sillasoo, Ü., Tsyganov, A. N., van der Linden, M., Väliranta, M., & Warner, B., 2019. Widespread drying of European peatlands in recent centuries, *Nat. Geosci.*, 12(11), 922–928.

Swinnen, W., Broothaerts, N., & Verstraeten, G., 2019. Modelling long-term blanket peatland development in eastern Scotland, *Biogeosciences*, 16(20), 3977–3996.

Talbot, J., Richard, P., Roulet, N., & Booth, R., 2010. Assessing long-term hydrological and ecological responses to drainage in a raised bog using paleoecology and a hydrosequence, *J. Veg. Sci.*, 21(1), 143–156.

Tchilinguirian, P., Morales, M., Oxman, B., Lupo, L., Olivera, D., & Yacobaccio, H., 2014. Early to Middle Holocene transition in the Pastos Chicos record, dry Puna of Argentina, *Quat. Int.*, 330(1), 171–182.

Terrer, C., Vicca, S., Hungate, B. A., Phillips, R. P., & Prentice, I. C., 2016. Mycorrhizal association as a primary control of the CO 2 fertilization effect, *Science*, 353(6294), 72–74.

Tipping, R., 1995. Holocene evolution of a lowland Scottish landscape: Kirkpatrick Fleming. Part I, peat- and pollen-stratigraphic evidence for raised moss development and climatic change, *The Holocene*, 5(1), 69–81.

Treat, C. C., Kleinen, T., Broothaerts, N., Dalton, A. S., Dommain, R., Douglas, T. A., Drexler, J. Z., Finkelstein, S. A., Grosse, G., Hope, G., Hutchings, J., Jones, M. C., Kuhry, P., Lacourse, T., Lähteenoja, O., Loisel, J., Notebaert, B., Payne, R. J., Peteet, D. M., Sannel, A. B. K., Stelling, J. M., Strauss, J., Swindles, G. T., Talbot, J., Tarnocai, C., Verstraeten, G., Williams, C. J., Xia, Z., Yu, Z., Väliranta, M., Hättestrand, M., Alexanderson, H., & Brovkin, V., 2019. Widespread global peatland establishment and persistence over the last 130,000 y, *Proc. Natl. Acad. Sci.*, 116(11), 201813305.

Turetsky, M. R., Treat, C. C., Waldrop, M. P., Waddington, J. M., Harden, J. W., & McGuire, A. D., 2008. Short-term response of methane fluxes and methanogen activity to water table and soil warming manipulations in an Alaskan peatland, *J. Geophys. Res.*, 113(G3).

Turetsky, M. R., Kotowska, A., Bubier, J., Dise, N. B., Crill, P., Hornibrook, E. R., Minkkinen, K., Moore, T. R., Myers-Smith, I. H., Nykänen, H., Olefeldt, D., Rinne, J., Saarnio, S., Shurpali, N., Tuittila, E. S., Waddington, J. M., White, J. R., Wickland, K. P., & Wilmking, M., 2014. A synthesis of methane emissions from 71 northern, temperate, and subtropical wetlands, *Glob. Chang. Biol.*, 20(7), 2183–2197.

Turetsky, M. R., Benscoter, B., Page, S., Rein, G., Van Der Werf, G. R., & Watts, A., 2015. Global vulnerability of peatlands to fire and carbon loss, *Nat. Geosci.*, 8(1), 11–14.

Turunen, J., Tolonen, K., Tomppo, E., & Reinikainen, A., 2002. Estimating carbon accumulation rates of undrained mires in Finland - Application to boreal and subarctic regions, *Holocene*, 12(1), 69–80.

Väliranta, M., Salojärvi, N., Vuorsalo, A., Juutinen, S., Korhola, A., Luoto, M., & Tuittila, E. S., 2017. Holocene fen-bog transitions, current status in Finland and future perspectives, *Holocene*, 27(5), 752–764.

van Huissteden, J., van den Bos, R., & Marticorena Alvarez, I., 2006. Modelling the effect of water-table management on CO2 and CH4 fluxes from peat soils, *Geol. en Mijnbouw/Netherlands J. Geosci.*, 85(1), 3–18.

van Nes, E. H., Scheffer, M., Brovkin, V., Lenton, T. M., Ye, H., Deyle, E., & Sugihara, G., 2015. Causal feedbacks in climate change, *Nat. Clim. Chang.*, 5(5), 445–448.

Volk, T. & Hoffert, M. I., 1985. Ocean Carbon Pumps: Analysis of Relative Strengths and Efficiencies in Ocean-Driven Atmospheric CO 2 Changes, in *The Carbon Cycle and Atmospheric CO2: Natural Variations Archean to Present*, pp. 99–110, eds Sundquist, E. & Broecker, W., American Geophysical Union (AGU).

Voulgarakis, A., Naik, V., Lamarque, J. F., Shindell, D. T., Young, P. J., Prather, M. J., Wild, O., Field, R. D., Bergmann, D., Cameron-Smith, P., Cionni, I., Collins, W. J., Dalsøren, S. B., Doherty, R. M., Eyring, V., Faluvegi, G., Folberth, G. A., Horowitz, L. W., Josse, B., MacKenzie, I. A., Nagashima, T., Plummer, D. A., Righi, M., Rumbold, S. T., Stevenson, D. S., Strode, S. A., Sudo, K., Szopa, S., & Zeng, G., 2013. Analysis of present day and future OH and methane lifetime in the ACCMIP simulations, *Atmos. Chem. Phys.*, 13(5), 2563–2587.

Waddington, J. M., Morris, P. J., Kettridge, N., Granath, G., Thompson, D. K., & Moore, P. A., 2015. Hydrological feedbacks in northern peatlands, *Ecohydrology*, 8(1), 113–127.

Wania, R., Ross, I., & Prentice, I. C., 2009a. Integrating peatlands and permafrost into a dynamic global vegetation model: 2. Evaluation and sensitivity of vegetation and carbon cycle processes, *Global Biogeochem. Cycles*, 23(3).

Wania, R., Ross, L., & Prentice, I. C., 2009b. Integrating peatlands and permafrost into a dynamic global vegetation model: 1. Evaluation and sensitivity of physical land surface processes, *Global Biogeochem. Cycles*, 23(3), 1–19.

Wania, R., Ross, I., & Prentice, I. C., 2010. Implementation and evaluation of a new methane model within a dynamic global vegetation model: LPJ-WHyMe v1.3.1, *Geosci. Model Dev.*, 3(2), 565–584.

Warren, M., Frolking, S., Dai, Z., & Kurnianto, S., 2017. Impacts of land use, restoration, and climate change on tropical peat carbon stocks in the twenty-first century: implications for climate mitigation, *Mitig. Adapt. Strateg. Glob. Chang.*, 22(7), 1041–1061.

Weinans, E., Omta, A. W., van Voorn, G. A. K., & van Nes, E. H., 2021. A potential feedback loop underlying glacial-interglacial cycles, *Clim. Dyn.*.

Wibisana, A. G. & Setyorini, S. N., 2021. Peatland Protection in Indonesia: Toward the Right Direction?, in *Springer Clim.*, pp. 301–328, Springer International Publishing.

Wild, M., Folini, D., Schär, C., Loeb, N., Dutton, E. G., & König-Langlo, G., 2013. The global energy balance from a surface perspective, *Clim. Dyn.*, 40(11-12), 3107–3134.

Wilson, R. M., Hopple, A. M., Tfaily, M. M., Sebestyen, S. D., Schadt, C. W., Pfeifer-Meister, L., Medvedeff, C., McFarlane, K. J., Kostka, J. E., Kolton, M., Kolka, R., Kluber, L. A., Keller, J. K., Guilderson, T. P., Griffiths, N. A., Chanton, J. P., Bridgham, S. D., & Hanson, P. J., 2016. Stability of peatland carbon to rising temperatures, *Nat. Commun.*, 7(1), 13723.

Xu, J., Morris, P. J., Liu, J., & Holden, J., 2018a. Hotspots of peatland-derived potable water use identified by global analysis, *Nat. Sustain.*, 1(5), 246–253.

Xu, J., Morris, P. J., Liu, J., & Holden, J., 2018b. PEATMAP: Refining estimates of global peatland distribution based on a meta-analysis, *CATENA*, 160(September 2017), 134–140.

Xu, X., Yuan, F., Hanson, P. J., Wullschleger, S. D., Thornton, P. E., Riley, W. J., Song, X., Graham, D. E., Song, C., & Tian, H., 2016. Reviews and syntheses: Four decades of modeling methane cycling in terrestrial ecosystems, *Biogeosciences*, 13(12), 3735–3755.

Young, D. M., Baird, A. J., Charman, D. J., Evans, C. D., Gallego-Sala, A. V., Gill, P. J., Hughes, P. D. M., Morris, P. J., & Swindles, G. T., 2019. Misinterpreting carbon accumulation rates in records from near-surface peat, *Sci. Rep.*, 9(1), 17939.

Young, D. M., Baird, A. J., Gallego-Sala, A. V., & Loisel, J., 2021. A cautionary tale about using the apparent carbon accumulation rate (aCAR) obtained from peat cores, *Sci. Rep.*, 11(1), 1–12.

Yu, Z., 2011. Holocene carbon flux histories of the world's peatlands: Global carbon-cycle implications, *Holocene*, 21(5), 761–774.

Yu, Z., Loisel, J., Brosseau, D. P., Beilman, D. W., & Hunt, S. J., 2010. Global peatland dynamics since the Last Glacial Maximum, *Geophys. Res. Lett.*, 37(13), 1–5.

Yu, Z., Loisel, J., Charman, D. J., Beilman, D. W., & Camill, P., 2014. Holocene peatland carbon dynamics in the circum-Arctic region: An introduction, *Holocene*, 24(9), 1021–1027.

Yu, Z. C., 2012. Northern peatland carbon stocks and dynamics: A review, *Biogeosciences*, 9(10), 4071–4085.

Yvon-Durocher, G., Allen, A. P., Bastviken, D., Conrad, R., Gudasz, C., St-Pierre, A., Thanh-Duc, N., & Del Giorgio, P. A., 2014. Methane fluxes show consistent temperature dependence across microbial to ecosystem scales, *Nature*, 507(7493), 488–491.

Zeebe, R. E., Ridgwell, A., & Zachos, J. C., 2016. Anthropogenic carbon release rate unprecedented during the past 66 million years, *Nat. Geosci.*, 9(4), 325–329.

Zhang, B., Tian, H., Lu, C., Chen, G., Pan, S., Anderson, C., & Poulter, B., 2017. Methane emissions from global wetlands: An assessment of the uncertainty associated with various wetland extent data sets, *Atmos. Environ.*, 165, 310–321.

ZHANG, Q., LI, T.-T., ZHANG, Q., WANG, G.-C., YU, L.-J., GUO, B., & HAN, P.-F., 2020. Accuracy analysis in CH4MODwetland in the simulation of CH4 emissions from Chinese wetlands, *Adv. Clim. Chang. Res.*, 11(1), 52–59.

Zhang, Z., Zimmermann, N. E., Kaplan, J. O., & Poulter, B., 2016. Modeling spatiotemporal dynamics of global wetlands: Comprehensive evaluation of a new sub-grid TOPMODEL parameterization and uncertainties, *Biogeosciences*, 13(5), 1387–1408.

Zhong, Y., Jiang, M., & Middleton, B. A., 2020. Effects of water level alteration on carbon cycling in peatlands, *Ecosyst. Heal. Sustain.*, 6(1), 1806113.

Zhu, Z., Piao, S., Myneni, R. B., Huang, M., Zeng, Z., Canadell, J. G., Ciais, P., Sitch, S., Friedlingstein, P., Arneth, A., Cao, C., Cheng, L., Kato, E., Koven, C., Li, Y., Lian, X., Liu, Y., Liu, R., Mao, J., Pan, Y., Peng, S., Peuelas, J., Poulter, B., Pugh, T. A., Stocker, B. D., Viovy, N., Wang, X., Wang, Y., Xiao, Z., Yang, H., Zaehle, S., & Zeng, N., 2016. Greening of the Earth and its drivers, *Nat. Clim. Chang.*, 6(8), 791–795.

Zürcher, S., 2013. *Methane Emissions and Isotopes of Northern Peatlands in a Global Vegetation Model*, Ph.D. thesis.

Zürcher, S., Spahni, R., Joos, F., Steinacher, M., & Fischer, H., 2013. Impact of an abrupt cooling event on interglacial methane emissions in northern peatlands, *Biogeosciences*, 10(3), 1963–1981.

Chapter 2

Methods

The work presented in this thesis is based on the Land-surface Processes and eXchanges (LPX-Bern) dynamic global vegetation model (DGVM) version 1.4 (Lienert & Joos, 2018), which is developed and maintained in Bern. This chapter gives an overview of this model (section 2.1) and a detailed look at the modules most used in this thesis, together with the discussion of various model changes. The peatland module is discussed in section 2.1.1 and the methane module is discussed in section 2.1.2.

2.1 LPX-Bern description

LPX-Bern is based on the Lund-Potsdam-Jena (LPJ) model (Sitch et al., 2003). LPX-Bern can be run coupled to the ocean-atmosphere model Bern3D (Ritz et al., 2011), which is also developed in Bern, to form the earth system model of intermediate complexity Bern3D-LPX. In this thesis, however, LPX-Bern was used standalone in the so-called offline mode. Prescribed atmospheric CO_2 concentrations, anthropogenic land cover, and soil properties together with monthly input fields of near-surface temperature, precipitation, cloud cover, and nitrogen deposition are used to interactively simulate vegetation dynamics, wetland and peatland extent, and, on a daily basis, the carbon-, water- and nitrogen cycle, and fluxes of the greenhouse gases CO_2, CH_4, and N_2O.

Carbon and nitrogen are distributed and transferred between pools of living biomass (roots, leaves, sapwood, and heartwood), slow and fast overturning litter and soil carbon pools. Decay rates depend on the pool type and are modulated by soil temperature and soil moisture. The simulated soil column of 2 m is subdivided into two water buckets connected via percolation. To accurately simulate thermal properties throughout the soil column and the freezing and thawing in different depths, the heat diffusion is calculated based on eight soil layers with varying depths (0.1, 0.1, 0.1, 0.2, 0.2, 0.3, 0.5, and 0.5 m) and an additional four layer soil padding reaching from 2 m to 10 m in depth (Wania et al., 2009b). Thermal properties are dependent on the soil type and water-, ice-, and air content. Individual soil layers can freeze and thaw independently. Vegetation composition is simulated with plant functional types (PFTs), which compete for water, light, and nutrients (Sitch et al., 2003; Xu-Ri et al., 2012; Spahni et al., 2013).

The model can be adapted to run on any grid-cell resolution. In this thesis, a relatively high ($0.5° \times 0.5°$), medium ($1° \times 1°$), and coarse ($3.75°$ longitudinal and $2.5°$ latitudinal) resolutions are used. Prescribed land fractions can range between 0–1 in the case of high and medium resolution and are fixed to 1 in case of the coarse resolution. For the coarse resolution, a transient land-sea-ice mask based on (Peltier, 2004) allows for transient simulations over the past 22,000 years. The land-sea-ice mask is updated every 1000 years with yearly linearly interpolated area changes. In chapter A, the implementation of an updated transient land-sea-ice mask is

discussed, reducing the timestep and introducing variable land fractions. The updated version, however, was not yet used for any simulations.

Each grid cell is partitioned into different independent land classes, that can include natural vegetation, land-use areas, and peatlands. Each land class is described with its own carbon, water, and nutrient pools and vegetation is represented by land-class specific PFTs. Wetland and peatland area can be prescribed or calculated dynamically using the Dynamical Peatland Model Based on TOPMODEL (DYPTOP) module (Stocker et al., 2014b). A methane module calculates the soil sink and emissions both from peatlands (Wania et al., 2010) and inundated mineral soils as well as from wet mineral soils (Spahni et al., 2011). For this thesis, the peatland and methane modules are especially important. They are described in detail below, together with additional adjustments of these modules performed as part of this thesis.

2.1.1 Peatland module

The peatland module is based on the LPJ-WHyMe model (Wania et al., 2009a,b) and was originally designed to model northern high latitude peatlands. The two original PFTs represent *Sphagnum* moss and flood-tolerant graminoids. The module was later expanded for global use (Stocker et al., 2014b), with the addition of three PFTs representing tropical peatland vegetation: flood-tolerant tropical evergreen and deciduous tree PFTs, and a flood-tolerant C4-type grass. Soil water- and carbon pools are modeled based on the distinction between the catotelm and acrotelm of peatlands. The catotelm is often defined as the deep permanently water-saturated part of the peat column, where decomposition of organic material is almost halted (Ingram, 1978). In LPX-Bern, the catotelm is defined as spanning the soil column from 0.3 m to 2 m depth and is per definition permanently saturated. Above that, the acrotelm is subject to water table fluctuations and in the model is defined as the upper 0.3 m of the soil column. Decomposition in the acrotelm is much faster than in the catotelm with soil moisture and temperature modulating the decay rates. The carbon flux between the acrotelm and catotelm (F_{AC}) is determined by an average acrotelm carbon density of 18.7 kg C m^{-2} derived from (Belyea & Clymo, 2001). If at the end of the year the acrotelm carbon density exceeds this value, the excess carbon is transferred to the slow overturning catotelm throughout the next year and vice versa (Spahni et al., 2013). If the litter input to the acrotelm exceeds acrotelm decay, this leads to a buildup of peat in the catotelm. If however acrotelm decay dominates, e.g. if the peatland dries out, this can lead to a gradual loss of accumulated catotelm carbon.

TOPMODEL

The DYPTOP module developed by Stocker et al. (2014b) determines the monthly inundated grid-cell fraction (f_i) using the TOPMODEL approach, which in turn is used to calculate the potential peatland fraction (f_{pp}). The TOPMODEL approach (Beven & Kirkby, 1979) is based on compound topographic indices (CTIs) given on a sub-grid resolution (∼1×1 km), which provide topographically derived information about floodability. They are defined as:

$$CTI = \ln\left(\frac{a}{\tan\beta}\right), \tag{2.1}$$

where a represents the area that drains into or through the respective sub-grid pixel divided by the pixel contour length and β represents the slope of the pixel. The sub-grid CTIs are used to relate the mean grid-cell water table position (WTP), which is defined as negative below the surface, to f_i. Based on WTP, a threshold (CTI^*) is calculated:

$$CTI^* = \overline{CTI}_b - M \cdot WTP, \tag{2.2}$$

where $\overline{CTI}_b$ is the mean CTI, averaged over the entire primary catchment area in which the respective grid cell is located and M is a tunable parameter. Sub-grid pixels with $CTI > CTI^*$ are assumed to be flooded. Sub-grid pixels with a $CTI < CTI_{min}$ are assumed unfloodable irrespective of the water table position, with CTI_{min} being the second tunable parameter. The flooded grid-cell fraction f_i is then determined as the proportion of flooded sub-grid pixels within the respective grid cell. Stocker et al. (2014b) tuned the free parameters to $CTI_{min} = 12$ and $M = 8$. To simplify the resource-intensive calculation on the sub-grid level, in every grid cell an asymmetric sigmoid function is fitted to the characteristic relationship between WTP and f_i, which is then used to determine monthly inundated area fractions in place of the sub-grid calculation during simulations.

The calculation of WTP was slightly changed in this thesis compared to Stocker et al. (2014b). LPX-Bern calculates drainage and surface runoff as the excess water above the water holding capacity of the lower and upper water bucket of the two-bucket hydrological scheme. As runoff occurs instantaneously in LPX-Bern, the excess water is lost immediately and the calculated WTP would be limited by the soil water holding capacity in case the runoff is not considered. Previously, drainage and surface runoff were both added directly to the calculated WTP. Drainage runoff, however, which extends the water saturation into soil layers below the simulated soil column, should not affect the water table position which is defined as the distance from the surface to the zone of water saturation. The exception would be if the excess water can not leave the simulated soil column because of water-impermeable soil layers, however, such cases are not considered in LPX-Bern. Drainage runoff was thus excluded from the calculation and only surface runoff is added to the calculated WTP.

Furthermore, the calculation of transpiration and interception loss for tropical peatland tree PFTs was updated. Previously, evapotranspiration from peatlands was calculated using an empirical relationship derived for moss-dominated peatlands, only depending on the equilibrium evapotranspiration and the peatland water table, but irrespective of actual peatland vegetation cover (Wania et al., 2009b). This formulation was not updated after the introduction of tree PFTs on tropical peatlands. Here, the calculation of transpiration for tropical tree peatland PFTs was adjusted to be in line with the calculations for the standard tree PFTs based on water demand and supply (Sitch et al., 2003). The previous calculation is continued to be used for all herbaceous and moss peatland PFTs and for evaporation from peatland soils without vegetation cover. Furthermore, interception loss is now also calculated for peatland tree PFTs, analogue to the calculation for standard tree PFTs. These updates slightly change the peatland water balance and thus indirectly also the calculated grid-cell WTP.

Criteria for peatland presence

Potential peatland area is determined by inundation persistence, with f_{pp} equal to the area flooded at least $N = 18$ months in the previous 31 years. Potential peatland area thus changes with changes in inundated area, with a 31-year memory.

The existence of peatlands is further limited by moisture and carbon balance criteria. Water balance is defined as annual precipitation over annual evapotranspiration (POAET) and is required to be larger than one. Newly establishing peatlands are required to have a positive net ecosystem balance (NEP) and a large enough average acrotelm to catotelm flux ($F_{AC} > 10$ g m^{-2} yr^{-1}), except for the model spinup, where alternatively a peatland soil carbon density above 50 kg m^{-2} suffices. Once established, peatlands that do not fulfill these carbon balance criteria, e.g. when they are near equilibrium or lose carbon, are required to remain above a soil carbon density of 50 kg m^{-2} or suffer a reduction in potential area. For a peat C stock, C_{peat}, from 50 kg m^{-2} to about 45 kg m^{-2} f_{pp} is reduced to an actual potential peatland

fraction, f_{app}, according to a sigmoid function:

$$f_{app} = \begin{cases} f_{pp} \cdot \frac{1}{1+20\, e^{-2.4\,(C_{peat}-45)}} & | \; if \; C_{peat} < 50 \text{ kg m}^{-2}, \\ f_{pp} & | \; if \; C_{peat} > 50 \text{ kg m}^{-2}. \end{cases} \tag{2.3}$$

For peatland establishment the criteria are evaluated based on a small peatland seed, with peatland fraction $f_p = 1e^{-5}$, that is present in all grid cells. The carbon balance criteria used in this thesis differ slightly to Stocker et al. (2014b), where the soil carbon criteria of $C_{peat} > 50$ kg m^{-2} was a strict threshold that also applied for peatland initiation. With the updated criteria, abrupt peatland collapse due to carbon loss and sudden peatland initiation due to slow carbon buildup in the peatland seeds are prevented.

Peatland area dynamics

Given that all criteria are fulfilled and $f_{app} > 0$, peatland fraction, f_p, is free to grow or shrink to approach f_{app} with a rate of 1 % of its current size. Area changes of small peatlands thus are much slower than those of already large peatlands. In the case of peatland retreat, the lost grid-cell fraction is treated as a separate land class for former peatlands. It inherits the carbon stocks of the shrinking peatland and is subsequently treated in the same way as the mineral soils regarding vegetation, hydrology, and carbon cycling. Growing active peatlands first expand on former peatlands inheriting the remaining carbon there. This treatment prevents carbon dissolution into mineral soils due to area fluctuations. Using postprocessing described in chapters 3 and 4 it is possible to track the peatland carbon through the different land classes even after peatland retreat.

Effect of peatland module changes

Figure 2.1 shows the peatland area simulated from the Last Glacial Maximum as discussed in chapter 3 next to the same simulation with an LPX-Bern model version prior to minor bug fixes and the changes to the water table calculation and peatland presence criteria described above.

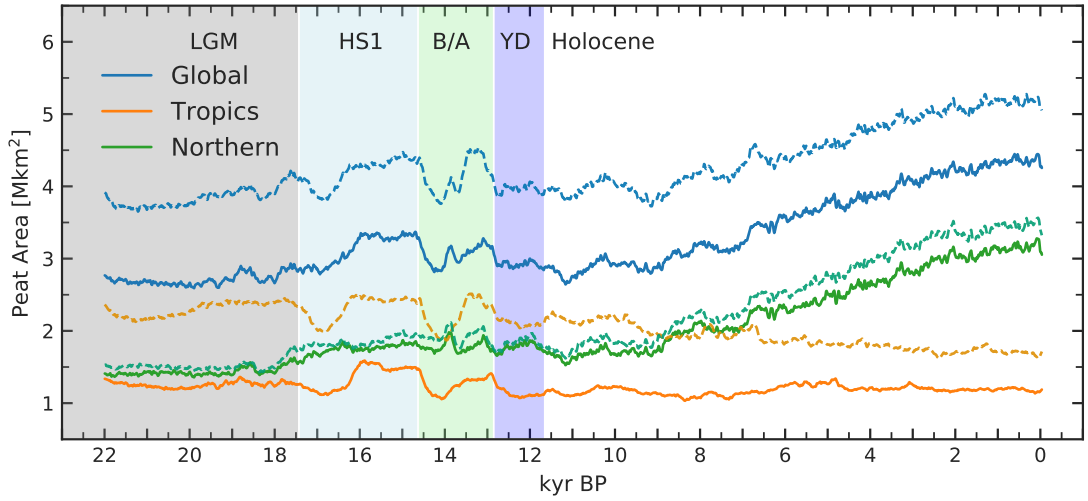

Figure 2.1: Peatland area dynamics since the Last Glacial Maximum simulated with the LPX-Bern after (solid lines) and before (dotted lines) the implementation of changes in the water table calculation and peatland presence criteria described in the main text, and additional minor bug fixes. Forcings and model setup are identical to simulations presented in chapter 3.

The changes lead to a substantial reduction in tropical peatland area, with only a small reduction in northern high latitudes during the Holocene. The largest effect comes from the

exclusion of drainage runoff from the WTP calculation, which leads to a decrease in peatland area, especially in the tropics. As discussed in chapters 3 and 4, present-day peatland area distribution is shifted towards the tropics compared to most estimates, even after the model changes. The changes to the peatland module thus bring the modeled tropical peatland area closer to the observational estimates.

Peatland and land-use change

Land-use and land-use change are tested and often used features of LPX-Bern (Stocker et al., 2014a; Lienert & Joos, 2018). However, up to now, simulations with land-use change could not be used together with the dynamic peatland module DYPTOP and vice versa. For chapter 4 the option of land-use change with dynamic peatlands was added to LPX-Bern and its following description is partly adopted from Müller & Joos (2021).

Land-use area in the model is represented by three specific land classes: pasture, cropland, and urban (Lienert & Joos, 2018). Pastures and croplands have specific vegetation represented by two PFTs each. Changes in land-use area are treated as net changes, where all growing land classes proportionally inherit the carbon, water, and nutrients of all shrinking land classes. In the absence of gross change information, three assumptions were made: 1) Changes within the three land-use classes that do not affect the total land-use area are assumed as shifts between land-use types (e.g. shift from pasture to cropland). 2) Increases in total land-use area reduce all other land classes proportionally, including peatlands. 3) Peatland area that is converted to land-use area can not be reclaimed by expanding peatlands at a later stage. For this, the peatland area fraction converted to land-use area f_{ptl} is tracked and subtracted from the actual potential peatland fraction f_{app}. Without this restriction, peatlands would quickly recover by expanding on the remaining non-land-use mineral soils, as their target area (f_{app}) would remain unchanged.

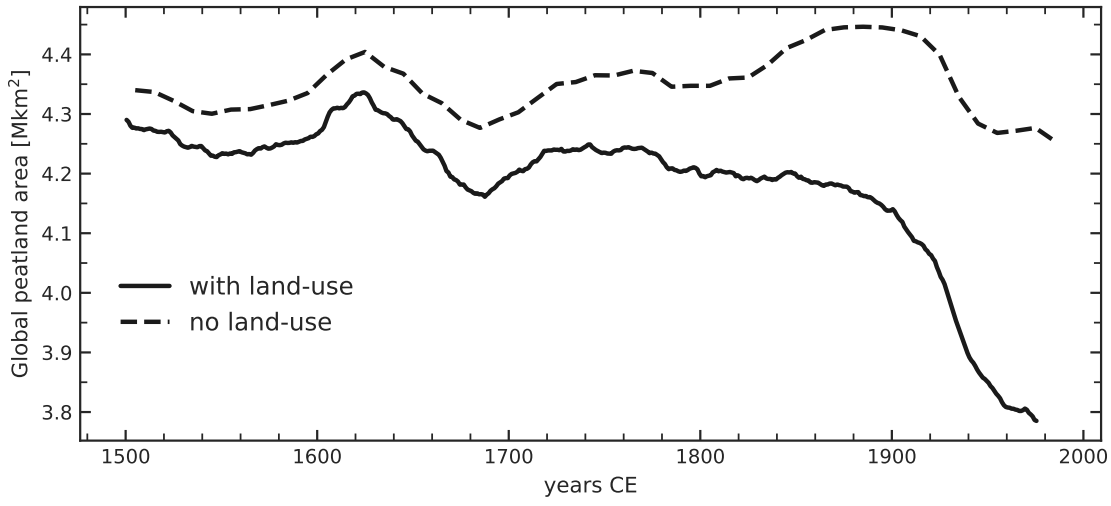

Figure 2.2: Global simulated peatland area from 1500 to present without (dashed line; setup as in chapter 3) and with land-use and land-use change since 1500 (solid line; setup as in chapter 4).

Figure 2.2 shows the difference between simulated global peatland evolution since 1500 without (as in chapter 3) and with land-use and land-use change (as in chapter 4). Future data synthesis focusing on information about global gross peatland to land-use conversions could enable additional implementation of land-use gross changes as they are already in use for mineral soil only simulations with the LPX-Bern (Stocker et al., 2014a).

2.1.2 Methane module

The modeling of methane emissions from peatlands in LPX-Bern is based on the LPJ-WhyMe implementation by Wania et al. (2010). Emissions from flooded mineral soils, wet mineral soils, and rice paddies as well as the soil methane uptake were later added (Spahni et al., 2011). In the following, the important parts of these different components are described together with developments made during this thesis, including the addition of temperature-dependent methane production, methane emissions from fire, and an updated wetland emission calibration. Emissions from rice paddies are not considered throughout the thesis and are thus excluded from the model description.

2.1.2.1 Methane emissions from peatlands

The calculation of Methane emissions from peatlands is based on Wania et al. (2010) and has the most sophisticated representation of all methane source types in LPX-Bern. This section gives an overview of the simulated processes, starting with methane production in the soil based on anaerobic heterotrophic respiration, followed by a description of the various transport pathways of methane to the atmosphere, and finally short descriptions of how available oxygen (O_2) is used for methane oxidization and how peatland microtopography is handled.

Production

Methane production in the model is directly linked to the modeled heterotrophic respiration in litter and soil pools as well as the respiration of root exudates. The root distribution and potential frozen layers are used to distribute production over different soil layers. The ratio r_p between carbon released as methane (CH_4) and as carbon dioxide (CO_2) in peatlands is a tunable parameter in the model (see Sect. 2.1.2.3). This ratio is weighted by the degree of anoxia α, with $\alpha = 1 - f_{air}$. The air fraction, f_{air}, of each soil layer, is dependent on soil porosity and water and ice fractions.

Originally no explicit temperature dependence of the methane production was included (Wania et al., 2010). Production of methane is only indirectly affected by temperature through the temperature dependence of heterotrophic respiration. However, methane emissions have been found to often respond much stronger to increases in temperature compared to the concurrent CO_2 emissions (Yvon-Durocher et al., 2014; Turetsky et al., 2014). This suggests that the CH_4/CO_2 production ratio has an explicit temperature dependence. Various methane models thus additionally scale the CH_4/CO_2 ratio with soil temperature (Melton et al., 2013; Xu et al., 2016). For the investigations discussed in chapter 5, an additional temperature modifier m_T was added to the methane production calculation. The temperature modifier is calculated based on an Arrhenius equation following Lloyd & Taylor (1994), which is also used for modulating heterotrophic respiration:

$$m_T = e^{E_o\left(\frac{1}{T_{ref}-T_o}-\frac{1}{T_{soil}-T_o}\right)}, \tag{2.4}$$

where T_{soil}, T_{ref}, and T_0 are the soil temperature, the reference temperature at which $m_T = 1$, and a calibration temperature determined to $T_0 = 227.13K$ in Lloyd & Taylor (1994). E_o is linked to the activation energy and determines the slope of the function, analog to a Q10 factor. With the application of the temperature modifier the produced methane, P_{CH_4}, thus is determined as:

$$P_{CH_4} = R_p \cdot r_p \cdot (1 - f_{air}) \cdot \boldsymbol{m_T}, \tag{2.5}$$

where R_p is the heterotrophic respiration of the peatland. For the results reported in this thesis, the additional temperature modifier is only used for the investigations in chapter 5 and is set to $m_T = 1$ otherwise.

Transport

LPX-Bern simulates three transport pathways of peatland methane and other gasses between the soil and the atmosphere: diffusion, plant transport, and ebullition. Diffusion through the soil layers is based on the same Crank-Nicolson numerical scheme as for the heat diffusion (Wania et al., 2009b), with an increased time resolution of one-hundredth of a day. Diffusion at the water-air boundary of the top layer is solved analytically (Wania et al., 2010). Diffusion is calculated for the gases CH_4, CO_2, and O_2. Diffusivities depend on soil temperature, porosity, and water- and air content. All gasses can diffuse out and into the soil, depending on the concentration gradient. However, in most cases, CH_4 and CO_2 diffuse out of the soil into the atmosphere whereas O_2 diffuses into the soil where it is consumed.

Transport via vascular plants is the second pathway for gas diffusion in and out of the soil. Of the five peatland PFTs, only the extratropical flood-tolerant graminoid is considered for plant transport. Recently methane emissions from tropical wetland tree stems and leaves have identified tree-mediated emissions as one of the most important emission pathways in tropical wetlands (Pangala et al., 2017). Future development thus should strive to include plant methane transport also for tropical peatland PFTs. For now plant transport of CH_4, CO_2, and O_2 is limited to graminoids. Over the area available for plant transport, determined by abundance and phenology, diffusion is handled similar to the diffusion at the water-air boundary of the first soil layer.

The third emission pathway of CH_4 and CO_2 is ebullition, first introduced in Wania et al. (2010) and further developed in Zürcher et al. (2013). The gasses CH_4, CO_2, and N_2 are separated in a dissolved and a gaseous part. If the sum of partial pressures of the gaseous part of CH_4, CO_2, and N_2 exceeds the sum of atmospheric and hydraulic pressures, CH_4 and CO_2 can be released via bubbles directly from deeper soil layers to the atmosphere. The total amount of N_2 is assumed to be constant. In LPX-Bern, ebullition is the dominant emission pathway and plant transport is the rarest (Zürcher, 2013).

Oxidation

The O_2 that enters the soil via diffusion and plant transport is used to oxidize CH_4 stored in the soil layers. It is assumed, that two-third of the oxygen is consumed by roots and non-methanotrophic microbes. The rest is used to oxidize the CH_4 to CO_2 in the soil layers with two moles of O_2 per mole of CH_4. If enough O_2 is present, all CH_4 is oxidized.

Microtopography

Peatlands are a heterogeneous landscape with a rich microtopography of hummocks, lawns, and hollows, which influences methane emissions (Cresto Aleina et al., 2015). To account for the effects of local differences in substrate, water table, vegetation, and soil conditions on large-scale methane emissions, a microtopography scaling factor, mt_p, is used. This factor is tuned based on regional methane budgets (see chapter 5) and is applied after the calculation of peatland methane emissions described above.

2.1.2.2 Methane on mineral soils

Spahni et al. (2011) added methane emissions from seasonally inundated mineral soils and wet mineral soils to LPX-Bern. The inundated fraction is prescribed or determined by the DYPTOP

module. Soil moisture determines emissions from non-inundated mineral soils. The soil sink, i.e. methane uptake and oxidation in mineral soils is calculated separately and can occur in the same grid cell alongside wet mineral soil emissions.

Inundated mineral soils

The prescribed or prognostically determined inundation fraction is assumed to first flood any existing peatlands. Only the inundation fraction f_{i_m} that exceeds peatland extent, and thus forms seasonal wetlands on mineral soils and land-use areas, is used for the simplified calculation of inundation methane emissions E_{i_m}:

$$E_{i_m} = R_i \cdot r_i \cdot \boldsymbol{m_T}, \tag{2.6}$$

where R_i is the area-weighted heterotrophic respiration averaged over all land class fractions that are inundated by f_{i_m} and r_i is the tunable CH_4/CO_2 ratio for inundation methane emissions (see section 2.1.2.3). Emissions from seasonal wetlands on mineral soils are thus directly proportional to the respiration and the inundated area fraction. The temperature modifier m_T is the same as for peatlands and is only used for the investigations in chapter 5. In all other cases $m_T = 1$.

Wet mineral soils

Wet mineral soils in LPX-Bern can be a source of methane even when they are not fully inundated. The grid-cell fraction covered by wet soils f_w is determined by a threshold of 95 % soil saturation in the first soil layer. Peatlands and inundated soils are excluded. Wet mineral soil emissions E_w are then given by:

$$E_w = \begin{cases} R_w \cdot W_1 \cdot r_w \cdot \boldsymbol{m_T} & \mid if\ W_1 \geq 0.95 \cdot W_{sat}, \\ 0 & \mid \text{otherwise} \end{cases} \tag{2.7}$$

where R_w is the total heterotrophic respiration on f_w, W_1 is the water fraction of the first soil layer, W_{sat} is the soil type dependent water fraction at field capacity, and r_w is the tunable CH_4/CO_2 ratio for methane emissions from wet mineral soils. The temperature modifier m_T is the same as described above.

Soil sink

The uptake of methane by mineral soils is calculated on the grid-cell fraction that is neither peatland nor inundated mineral soil. That means that methane uptake can also occur on methane emitting mineral soils but is reduced due to dependencies of diffusivity and oxidation rate on soil moisture. The soil uptake, U_s, is modeled after Curry (2007):

$$U_s = g_0 \cdot C_{atm} \cdot (D_{soil} \cdot k_o)^{1/2}, \tag{2.8}$$

where g_0 is a constant factor that transforms the atmospheric methane concentration C_{atm} into an intake flux. This flux is further modulated by the diffusivity of the first soil layer D_{soil} and the oxidation rate k_o. Diffusivity and oxidation rate are parametrized after Curry (2007) and depend on water content and soil temperature.

2.1.2.3 Emission Calibration

The parameters of the methane module described above were updated for chapter 5 and chapter 6. Re-tuning became necessary due to a recent parameter update to key LPX-Bern parameters through data assimilation by Lienert & Joos (2018). Updated parameters included parameters affecting vegetation productivity, heterotrophic respiration, and nitrogen cycling, which all have a direct or indirect effect on methane emissions. The re-tuning procedure was in part based on previous versions in Wania et al. (2010), Zürcher et al. (2013) and Spahni et al. (2011). Re-tuning was performed in three successive steps for three parameters: 1) the CH_4/CO_2 ratio in peatland methane production, r_p, based on site data 2) the microtopography scaling factor in peatland methane production, mt_p, based on a Hudson Bay Lowland budget, and the CH_4/CO_2 ratio in methane production on inundated mineral soils, r_i, based on an Amazon basin budget.

1) Tuning of r_p based on site data

The emission data for the six sites used to determine r_p is identical to Wania et al. (2010) and Zürcher et al. (2013) (see table 2.1 for references). The Abisko site (Jackowicz-Korczyński et al., 2010), was excluded due to lack of data at the time.

Model simulations for all six sites were first done with a starting value of $r_p = 0.2$. Monthly input of temperature, precipitation, cloud cover, and wet days was taken from the reanalysis product of the Climatic Research Unit (CRU) version 3.26 on a $0.5° \times 0.5°$ resolution. Simulations ranged from 1901–2017, but only years corresponding to the measurement years were evaluated. To evaluate model performance, the root mean squared error normalized by the site mean and weighted by observation length ($RMSENW$) was used as distance measure between modeled emissions and monthly mean observational site data. Emissions were scaled to minimize $RMSENW$ towards the observations. The resulting scaling factor was then applied to r_p resulting in $r_p = 0.088$ with $RMSENW = 0.31$. A second iteration of simulation and optimization proved this value of r_p to be robust. Figure 2.3 shows the simulated site emissions before and after tuning of r_p compared to observations.

Summer methane emissions at the Michigan site are underestimated and simulated peak emissions in the Degeroe site are shifted towards the autumn compared to observations. Both biases were also seen in a previous version (Zürcher et al., 2013). Emissions at the Sanjiang site are also underestimated, however, observation length is the shortest of all sites, which resulted in a low priority for optimization. For the Minnesota site agreement of modeled emissions with observations increased in the spring compared to Zürcher et al. (2013).

2) Tuning of mt_p based on regional budget

In a second step, the microtopography scaling factor mt_p for peatland methane emissions was determined based on a regional emission budget for the peatland-dominated Hudson Bay

Table 2.1: Site data used for tuning of r_p, similar to Wania et al. (2010) and Zürcher et al. (2013).

Cite Name	Year	Country	Coordinates	Reference
Boreas	1996	Canada	56° N, 99° W	Bubier et al. (1998)
Sanjiang	2002	China	33° N, 103° E	Ding et al. (2004)
Salmisuo	1993	Finland	63° N, 31° E	Saarnio et al. (1997)
Degerö	1996	Sweden	64° N, 20° E	Granberg et al. (2001)
Michigan	1991	USA	42° N, 84° W	Shannon et al. (2009)
Minnesota	1989	USA	47° N, 93° W	Dise (1993)

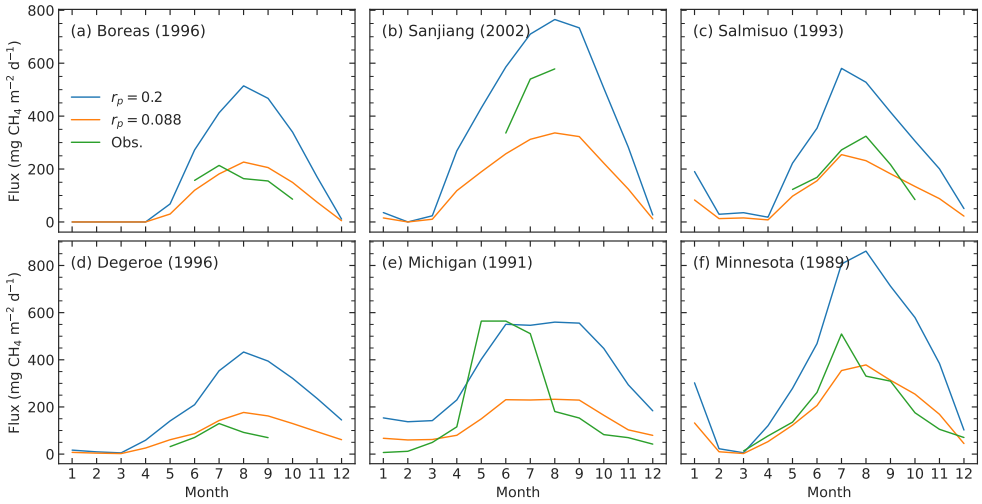

Figure 2.3: Observed and simulated site emissions before ($r_p = 0.2$) and after ($r_p = 0.088$) tuning for the sites in table 2.1.

Lowland (HBL). Pickett-Heaps et al. (2011) estimate HBL methane emission between 2004–2008 using aircraft measurements, surface observations, and a chemical transport model. The region of the HBL is defined as 50° N–60° N, 75° W—96° W. A regional HBL simulation with prescribed peatland area (Xu et al., 2018) and 0.5° × 0.5° resolution was performed with the value of r_p determined in step 1. Emissions from peatlands were then scaled with mt_p so that:

$$E_{HBL} = mt_p \cdot E_{peat} + E_{wet} - S_{soil}, \tag{2.9}$$

where E_{peat} and E_{wet} are simulated emissions from peatlands and wet mineral soils, S_{soil} is the simulated soil sink, and E_{HBL} is the HBL emission budget estimated by Pickett-Heaps et al. (2011). During the time of tuning, E_{HBL} between 2004–2008 was assumed to be 2.9 teragrams of methane per year (Tg yr^{-1}) resulting in $mt_p = 0.197$. Upon revisiting, however, E_{HBL} should have been taken as 2.3 Tg yr^{-1}, as this is the best guess estimate in Pickett-Heaps et al. (2011) after data constraining, whereas the higher value is prior to constraining. The lower E_{HBL} would result in $mt_p = 0.157$.

3) Tuning of r_i based on regional budget

In a third step, the CH_4/CO_2 ratio r_i which scales methane emissions from inundated mineral soils was determined based on a regional budget for the Amazon basin (AB). Pangala et al. (2017) presented a top-down and a detailed bottom-up estimate for the period 2010–2013 based on measurements, including measurements of emissions via tree stems. A regional AB simulation with prescribed peatland area (Xu et al., 2018) and 0.5° × 0.5° resolution was performed with the values of r_p and mt_p determined in step 1 and 2. Taking the top-down estimate of 42.7 Tg yr^{-1} and subtracting bottom-up estimates for sources not simulated by LPX-Bern (open water with 1.2 Tg yr^{-1} and river channels with 0.4 Tg yr^{-1}), results in an AB wetland emission budget of 41 Tg yr^{-1}. The extent of the simulated AB, determined based on the HYDRO1K basin map (EROS, 2013), was 10.6 % smaller than the reported $6.7 \times 10^6\, km^2$ reported in Pangala et al. (2017). Taking the smaller area into account, the target emission budget, E_{AB}, between 2010–2013 is 36.6 Tg yr^{-1}. To reach this target, emissions from inundated mineral soils were scaled with r_i so that:

$$E_{AB} = r_i \cdot E_{in}|_{r_i=1} + E_{peat} + E_{wet}, \tag{2.10}$$

where E_{peat} and $E_{wetsoil}$ are simulated emissions from peatlands and wet mineral soils and $E_{in}|_{r_i=1}$ are the un-scaled emissions from inundated mineral soils. Optimization of r_i according to equation 2.10 results in $r_i = 0.058$. At time of tuning the simulated soil sink was not considered in this step. In retrospect, the soil sink should have been included similar to step 2, as the top-down target emission budget was based on atmospheric measurements. Including the soil sink would increase r_i to $r_i = 0.065$. If additionally in step two the lower E_{HBL} is used with $mt_p = 0.157$, r_i would increase to $r_i = 0.070$.

Summary of emission calibration

The three tuning parameters were determined to: $r_p = 0.088$, $mt_p = 0.197$, and $r_i = 0.058$. These parameters were used in simulations for model intercomparison projects in sections 6.1 and 6.2, where the resulting global wetland emission from LPX-Bern are presented and compared to results from other methane models. Upon revisiting, two easy to fix shortcomings of the tuning procedure were identified leading to updated posterior scaling factors: $mt_p = 0.157$ and $r_i = 0.070$. These updated parameters were used for the simulations in chapter 5, where the resulting global emissions for present day are discussed and compared to observations and estimates. The tuning procedure described above has multiple additional shortcomings that could be addressed in a future iteration. Step 1 included only six stations of which only two provided data for all twelve months of the year. Additionally, all stations are located north of 30° N, and thus no information about tropical peatland sites was used. The inclusion of more site data with the full seasonal cycle both from the tropics and the northern extratropics would give a more accurate picture of the performance of LPX-Bern on a global scale. In the next tuning iteration, step 2 should be done with the best guess emission budget from Pickett-Heaps et al. (2011) and optimally validated with regional budgets from other regions. As tropical and high-latitude peatlands have very different structures, it might be necessary to determine mt_p independently for different zones. Additionally, the scaling factors mt_p and r_i could be dependent on the spatial model resolution, which was not considered here. Separate tuning for different model resolutions could improve inter-resolution consistency. Furthermore, a sensible approach to optimize emissions from wet mineral soils should be integrated into the procedure described above.

2.1.2.4 Methane emissions from fire

During this thesis, a simple parametrization for methane emissions from wildfires was added to LPX-Bern. Fire occurrence and frequency in LPX-Bern are limited by the amount of biomass fuel and litter moisture. The carbon lost by fire further depends on PFT-specific fire resistances. All burned carbon is released into the atmosphere as CO_2. To diagnose the amount of methane emitted by wildfires, emission factors were taken from (Andreae & Merlet, 2001). Emission factors are reported in gram species per kilogram dry matter burned and for three biomes, savanna and grassland (CO_2: 1613 ± 95; CH_4: 2.3 ± 0.9), tropical forest (CO_2: 1580 ± 90; CH_4: 6.8 ± 2.0), and extratropical forest (CO_2: 1550 ± 95; CH_4: 6.1 ± 2.2). For the same biomes, estimates for dry matter burned yearly in the late 1990s are given as 3160 Tg, 1330 Tg, and 640 Tg for savanna and grassland, tropical forest, and extratropical forest respectively. Average global emission factors for CH_4 and CO_2 were calculated by averaging over biomes, weighted by burned biomass, and then converted to units of gram carbon per kilogram dry matter burned. In LPX-Bern, only the amount of carbon burned is calculated. To convert to model units the ratio of the observational emission factors is assumed to be equal to the ratio in model emission

factors:

$$\frac{E^m_{CH_4}}{E^m_{CO_2}} = \frac{E^o_{CH_4}}{E^o_{CO_2}}, \tag{2.11}$$

where $E^o_{CH_4}$ and $E^o_{CO_2}$ are the emission factors of CH_4 and CO_2 derived from observations in grams carbon per kilogram dry matter burned, and $E^m_{CH_4}$ and $E^m_{CO_2}$ are the model emission factors in grams carbon per grams carbon. This results in an LPX-Bern emission factor of $8.56 \cdot 10^{-4}$ gC released as methane for every gram carbon released as CO_2. For the output, emissions are converted from grams of carbon to grams of methane.

Figure 2.4 shows global methane emissions from fire in a simulation over the historical period with dynamic peatlands and land-use, CO_2, N-deposition, and CRU climate forcing. Average emissions from 2000–2009 are 3.67 Tg yr^{-1} and thus within the range of other bottom-up estimates of 1 to 5 Tg yr^{-1} over the same period (Kirschke et al., 2013). Further development should aim to substitute the global emission factor averaged over biomes by PFT-specific emission factors.

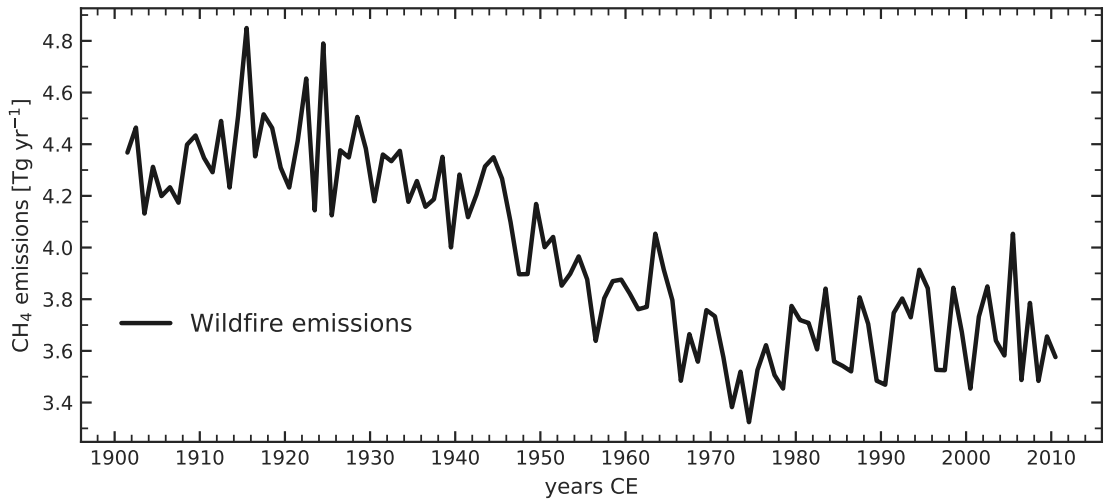

Figure 2.4: Global simulated methane emissions from wildfires in a simulation over the historical period with CO_2, N-deposition, land-use, and CRU climate forcing.

Bibliography

Andreae, M. O. & Merlet, P., 2001. Emission of trace gases and aerosols from biomass burning, *Biogeochemistry*, 15(4), 955–966.

Belyea, L. R. & Clymo, R. S., 2001. Feedback control of the rate of peat formation, *Proc. R. Soc. B Biol. Sci.*, 268(1473), 1315–1321.

Beven, K. J. & Kirkby, M. J., 1979. A physically based, variable contributing area model of basin hydrology, *Hydrol. Sci. Bull.*, 24(1), 43–69.

Bubier, J. L., Crill, P. M., Moore, T. R., Savage, K., & Varner, R. K., 1998. Seasonal patterns and controls on net ecosystem CO2 exchange in a boreal peatland complex, *Global Biogeochem. Cycles*, 12(4), 703–714.

Cresto Aleina, F., Runkle, B. R., Kleinen, T., Kutzbach, L., Schneider, J., & Brovkin, V., 2015. Modeling micro-topographic controls on boreal peatland hydrology and methane fluxes, *Biogeosciences*, 12(19), 5689–5704.

Curry, C. L., 2007. Modeling the soil consumption at atmospheric methane at the global scale, *Global Biogeochem. Cycles*, 21(4), 1–15.

Ding, W., Cai, Z., & Wang, D., 2004. Preliminary budget of methane emissions from natural wetlands in China, *Atmos. Environ.*, 38(5), 751–759.

Dise, N. B., 1993. Methane emission from Minnesota peatlands: Spatial and seasonal variability, *Global Biogeochem. Cycles*, 7(1), 123–142.

EROS, 2013. HYDRO1K (https://www.usgs.gov/centers/eros/science/usgs-eros-archive-digital-elevation-hydro1k).

Granberg, G., Ottosson-Löfvenius, M., Grip, H., Sundh, I., & Nilsson, M., 2001. Effect of climatic variability from 1980 to 1997 on simulated methane emission from a boreal mixed mire in northern Sweden, *Global Biogeochem. Cycles*, 15(4), 977–991.

Ingram, H. A. P., 1978. Soil layers in mires: Function and terminology, *J. Soil Sci.*, 29(2), 224–227.

Jackowicz-Korczyński, M., Christensen, T. R., Bäckstrand, K., Crill, P., Friborg, T., Mastepanov, M., & Ström, L., 2010. Annual cycle of methane emission from a subarctic peatland, *J. Geophys. Res. Biogeosciences*, 115(G2).

Kirschke, S., Bousquet, P., Ciais, P., Saunois, M., Canadell, J. G., Dlugokencky, E. J., Bergamaschi, P., Bergmann, D., Blake, D. R., Bruhwiler, L., Cameron-Smith, P., Castaldi, S., Chevallier, F., Feng, L., Fraser, A., Heimann, M., Hodson, E. L., Houweling, S., Josse, B., Fraser, P. J., Krummel, P. B., Lamarque, J.-F., Langenfelds, R. L., Le Quéré, C., Naik, V., O'Doherty, S., Palmer, P. I., Pison, I., Plummer, D., Poulter, B., Prinn, R. G., Rigby, M., Ringeval, B., Santini, M., Schmidt, M., Shindell, D. T., Simpson, I. J., Spahni, R., Steele, L. P., Strode, S. A., Sudo, K., Szopa, S., van der Werf, G. R., Voulgarakis, A., van Weele, M., Weiss, R. F., Williams, J. E., & Zeng, G., 2013. Three decades of global methane sources and sinks, *Nat. Geosci.*, 6(10), 813–823.

Lienert, S. & Joos, F., 2018. A Bayesian ensemble data assimilation to constrain model parameters and land-use carbon emissions, *Biogeosciences*, 15(9), 2909–2930.

Lloyd, J. & Taylor, J. A., 1994. On the temperature-dependence of soil respiration, *Funct. Ecol.*, 8(3), 315–323.

Melton, J. R., Wania, R., Hodson, E. L., Poulter, B., Ringeval, B., Spahni, R., Bohn, T., Avis, C. A., Beerling, D. J., Chen, G., Eliseev, A. V., Denisov, S. N., Hopcroft, P. O., Lettenmaier, D. P., Riley, W. J., Singarayer, J. S., Subin, Z. M., Tian, H., Zürcher, S., Brovkin, V., van Bodegom, P. M., Kleinen, T., Yu, Z. C., & Kaplan, J. O., 2013. Present state of global wetland extent and wetland methane modelling: conclusions from a model inter-comparison project (WETCHIMP), *Biogeosciences*, 10(2), 753–788.

Müller, J. & Joos, F., 2021. Committed and projected future changes in global peatlands - continued transient model simulations since the Last Glacial Maximum, *Biogeosciences*, 18(12), 3657–3687.

Pangala, S. R., Enrich-Prast, A., Basso, L. S., Peixoto, R. B., Bastviken, D., Hornibrook, E. R., Gatti, L. V., Marotta, H., Calazans, L. S. B., Sakuragui, C. M., Bastos, W. R., Malm, O., Gloor, E., Miller, J. B., & Gauci, V., 2017. Large emissions from floodplain trees close the Amazon methane budget, *Nature*, 552(7684), 230–234.

Peltier, W., 2004. Global glacial isostasy and the surface of the ice-age eart: The ICE-5G (VM2) Model and GRACE, *Annu. Rev. Earth Planet. Sci.*, 32(1), 111–149.

Pickett-Heaps, C. A., Jacob, D. J., Wecht, K. J., Kort, E. A., Wofsy, S. C., Diskin, G. S., Worthy, D. E. J., Kaplan, J. O., Bey, I., & Drevet, J., 2011. Magnitude and seasonality of wetland methane emissions from the Hudson Bay Lowlands (Canada), *Atmos. Chem. Phys.*, 11(8), 3773–3779.

Ritz, S. P., Stocker, T. F., & Joos, F., 2011. A coupled dynamical ocean-energy balance atmosphere model for paleoclimate studies, *J. Clim.*, 24(2), 349–375.

Saarnio, S., Alm, J., Silvola, J., Lohila, A., Nykänen, H., & Martikainen, P. J., 1997. Seasonal variation in CH 4 emissions and production and oxidation potentials at microsites on an oligotrophic pine fen, *Oecologia*, 110(3), 414–422.

Shannon, R. D., White, J. R., Lawson, J. E., & Gilmour, B. S., 2009. Methane Efflux from Emergent Vegetation in Peatlands Published by : British Ecological Society Stable URL : http://www.jstor.org/stable/2261359, 84(2), 239–246.

Sitch, S., Smith, B., Prentice, I. C., Arneth, A., Bondeau, A., Cramer, W., Kaplan, J. O., Levis, S., Lucht, W., Sykes, M. T., Thonicke, K., & Venevsky, S., 2003. Evaluation of ecosystem dynamics, plant geography and terrestrial carbon cycling in the LPJ dynamic global vegetation model, *Glob. Chang. Biol.*, 9(2), 161–185.

Spahni, R., Wania, R., Neef, L., Van Weele, M., Pison, I., Bousquet, P., Frankenberg, C., Foster, P. N., Joos, F., Prentice, I. C., & Van Velthoven, P., 2011. Constraining global methane emissions and uptake by ecosystems, *Biogeosciences*, 8(6), 1643–1665.

Spahni, R., Joos, F., Stocker, B. D., Steinacher, M., & Yu, Z. C., 2013. Transient simulations of the carbon and nitrogen dynamics in northern peatlands: From the Last Glacial Maximum to the 21st century, *Clim. Past*, 9(3), 1287–1308.

Stocker, B. D., Feissli, F., Strassmann, K. M., Spahni, R., & Joos, F., 2014a. Past and future carbon fluxes from land use change, shifting cultivation and wood harvest, *Tellus, Ser. B Chem. Phys. Meteorol.*, 66(1).

Stocker, B. D., Spahni, R., & Joos, F., 2014b. DYPTOP: A cost-efficient TOPMODEL implementation to simulate sub-grid spatio-temporal dynamics of global wetlands and peatlands, *Geosci. Model Dev.*, 7(6), 3089–3110.

Turetsky, M. R., Kotowska, A., Bubier, J., Dise, N. B., Crill, P., Hornibrook, E. R., Minkkinen, K., Moore, T. R., Myers-Smith, I. H., Nykänen, H., Olefeldt, D., Rinne, J., Saarnio, S., Shurpali, N., Tuittila, E. S., Waddington, J. M., White, J. R., Wickland, K. P., & Wilmking, M., 2014. A synthesis of methane emissions from 71 northern, temperate, and subtropical wetlands, *Glob. Chang. Biol.*, 20(7), 2183–2197.

Wania, R., Ross, I., & Prentice, I. C., 2009a. Integrating peatlands and permafrost into a dynamic global vegetation model: 2. Evaluation and sensitivity of vegetation and carbon cycle processes, *Global Biogeochem. Cycles*, 23(3).

Wania, R., Ross, L., & Prentice, I. C., 2009b. Integrating peatlands and permafrost into a dynamic global vegetation model: 1. Evaluation and sensitivity of physical land surface processes, *Global Biogeochem. Cycles*, 23(3), 1–19.

Wania, R., Ross, I., & Prentice, I. C., 2010. Implementation and evaluation of a new methane model within a dynamic global vegetation model: LPJ-WHyMe v1.3.1, *Geosci. Model Dev.*, 3(2), 565–584.

Xu, J., Morris, P. J., Liu, J., & Holden, J., 2018. PEATMAP: Refining estimates of global peatland distribution based on a meta-analysis, *CATENA*, 160(September 2017), 134–140.

Xu, X., Yuan, F., Hanson, P. J., Wullschleger, S. D., Thornton, P. E., Riley, W. J., Song, X., Graham, D. E., Song, C., & Tian, H., 2016. Reviews and syntheses: Four decades of modeling methane cycling in terrestrial ecosystems, *Biogeosciences*, 13(12), 3735–3755.

Xu-Ri, Prentice, I. C., Spahni, R., & Niu, H. S., 2012. Modelling terrestrial nitrous oxide emissions and implications for climate feedback, *New Phytol.*, 196(2), 472–488.

Yvon-Durocher, G., Allen, A. P., Bastviken, D., Conrad, R., Gudasz, C., St-Pierre, A., Thanh-Duc, N., & Del Giorgio, P. A., 2014. Methane fluxes show consistent temperature dependence across microbial to ecosystem scales, *Nature*, 507(7493), 488–491.

Zürcher, S., 2013. *Methane Emissions and Isotopes of Northern Peatlands in a Global Vegetation Model*, Ph.D. thesis.

Zürcher, S., Spahni, R., Joos, F., Steinacher, M., & Fischer, H., 2013. Impact of an abrupt cooling event on interglacial methane emissions in northern peatlands, *Biogeosciences*, 10(3), 1963–1981.

Chapter 3

Global peatland area and carbon dynamics from the Last Glacial Maximum to the present - a process-based model investigation

3.1 Main article

Jurek Müller and Fortunat Joos

Published in *Biogeosciences*, Volume 17, 5285-5308, 2020.

Biogeosciences, 17, 5285–5308, 2020
https://doi.org/10.5194/bg-17-5285-2020

Biogeosciences Open Access EGU

Global peatland area and carbon dynamics from the Last Glacial Maximum to the present – a process-based model investigation

Jurek Müller[1,2] **and Fortunat Joos**[1,2]

[1]Climate and Environmental Physics, Physics Institute, University of Bern, Bern, Switzerland
[2]Oeschger Centre for Climate Change Research, University of Bern, Bern, Switzerland

Correspondence: Jurek Müller (jurek.mueller@climate.unibe.ch)

Received: 26 March 2020 – Discussion started: 26 April 2020
Revised: 3 September 2020 – Accepted: 24 September 2020 – Published: 5 November 2020

Abstract. Peatlands are an essential part of the terrestrial carbon cycle and the climate system. Understanding their history is key to understanding future and past land–atmosphere carbon fluxes. We performed transient simulations over the last 22 000 years with a dynamic global peat and vegetation model forced by Earth system model climate output, thereby complementing data-based reconstructions for peatlands. Our novel results demonstrate a highly dynamic evolution with concomitant gains and losses of active peatland areas. Modeled gross area changes exceed net changes several fold, while net peat area increases by 60 % over the deglaciation. Peatlands expand to higher northern latitudes in response to warmer and wetter conditions and retreating ice sheets, and they are partly lost in midlatitude regions. In the tropics, peatlands are partly lost due to the flooding of continental shelves and are regained through nonlinear responses to the combined changes in temperature, precipitation, and CO_2. Large north–south shifts of tropical peatlands are driven by shifts in the position of the intertropical convergence zone associated with the abrupt climate events of the glacial termination. Time slice simulations for the Last Glacial Maximum (LGM) demonstrate large uncertainties in modeled peatland extent (global range from 1.5 to 3.4 Mkm^2, million square kilometers) stemming from uncertainties in climate forcing. The net uptake of atmospheric CO_2 by peatlands, modeled at 351 GtC since the LGM, considers decay from former peatlands. Carbon uptake would be misestimated, in particular during periods of rapid climate change and subsequent shifts in peatland distribution, when considering only changes in the area of currently active peatlands. Our study highlights the dynamic nature of peatland distribution and calls for an improved understanding of former peatlands to better constrain peat carbon sources and sinks.

1 Introduction

Peatlands are a wetland landscape type that is characterized by permanently waterlogged conditions, resulting in accumulation of dead plant material as peat (Gorham, 1957; Moore, 1989; Blodau, 2002). Peatlands are globally distributed and can take multiple forms from minerotrophic fens to ombrotrophic bogs and forested tropical peat swamps (Rydin and Jeglum, 2013; Page and Baird, 2016; Lindsay, 2018). Peatlands cover less than 3 % of the global land area (Xu et al., 2018), but they store a share of the total global soil organic carbon that is up to an order of magnitude higher (Page et al., 2011; Yu, 2012). At the same time, they are a significant carbon sink (e.g., Gorham et al., 2012; Lähteenoja et al., 2012; Leifeld et al., 2019) and a large natural source of methane (e.g., Frolking and Roulet, 2007; LAI, 2009; Korhola et al., 2010; Yu et al., 2013; Packalen et al., 2014); thus, they are an integral part of the terrestrial carbon cycle (Gorham, 1991; Yu, 2011; Page et al., 2011). Most of today's peatlands, formed over the past 12 000 years as a result of deglacial climate change and ice sheet retreat (e.g., Halsey et al., 2000; Gajewski et al., 2001; MacDonald et al., 2006; Gorham et al., 2007; Yu et al., 2010; Ruppel et al., 2013; Morris et al., 2018; Treat et al., 2019). Since then, northern peatlands alone have sequestered about 500 GtC (Yu et al., 2010; Yu, 2012), resulting in a net cooling effect on the climate (Frolking and Roulet, 2007). The drainage and conversion of existing peatlands to plantations or other forms of

land use leads to release of peat carbon into the atmosphere, adding to the ongoing global warming trend (Dommain et al., 2018; Leifeld et al., 2019). Additionally, global warming will likely diminish the net carbon sink of remaining global peatlands (Spahni et al., 2013; Gallego-Sala et al., 2018; Wang et al., 2018; Leifeld et al., 2019; Ferretto et al., 2019), despite a possible increase in the sink of some northern peatlands (Swindles et al., 2015; Chaudhary et al., 2017a).

Despite their global importance, peat research has long focused almost exclusively on northern high-latitude peatlands with about 80 % of dated peat cores taken in Europe and North America, which only covers roughly 40 % of global peat area (Xu et al., 2018; Treat et al., 2019). Although research on tropical peatlands has increased in recent years (e.g., Page et al., 2011; Dommain et al., 2011, 2014; Lawson et al., 2015; Silvestri et al., 2019; Gumbricht et al., 2017; Cobb and Harvey, 2019; Leng et al., 2019; Illés et al., 2019), our understanding about tropical peatlands, including their dynamics and life cycles, is still limited. This also entails ongoing new discoveries of previously unknown peatland complexes such as in the Congo Basin (Dargie et al., 2017). The tendency to search for the deepest core within a peatland (Loisel et al., 2017) and the acute lack of information about the fate of old and buried peat (Treat et al., 2019) represent additional sampling biases that contribute to our limited understanding of peatland evolution and its drivers. These gaps in our understanding are also reflected in the large ranges of estimates of today's peatland area (e.g., Yu et al., 2010; Page et al., 2011; Loisel et al., 2017; Xu et al., 2018) and peatland carbon (e.g., Tarnocai et al., 2009; Yu et al., 2010; Yu, 2012; Page et al., 2011; Gumbricht et al., 2017) in the literature. Only recently, a highly contested study proposed a doubling of conventional northern high-latitude peat carbon stock estimates (Nichols and Peteet, 2019; Yu, 2019). Refining our understanding and estimates of peatland carbon dynamics is timely, as the potential past and future effects of peatlands on the global carbon cycle are substantial, and knowledge of the amount, timing, and speed of carbon removal and release is crucial to constrain them.

Results from process-based models can offer an independent perspective on the transient evolution of global peatlands and peat carbon stocks, complementing data-based reconstructions of global peatland expansion and carbon accumulation (e.g., MacDonald et al., 2006; Gorham et al., 2007; Yu et al., 2010; Ruppel et al., 2013; Dommain et al., 2014; Loisel et al., 2017; Treat et al., 2019). Efforts to model peatlands and processes within them exist at the site level (e.g., Frolking et al., 2010; Morris et al., 2011; Baird et al., 2012; Morris et al., 2012; Kurnianto et al., 2015; Cresto Aleina et al., 2015; Chaudhary et al., 2017b; Cobb and Harvey, 2019) as well as on regional to global scales (e.g., Wania et al., 2009a,b; Kleinen et al., 2012; Spahni et al., 2013; Gallego-Sala et al., 2016; Alexandrov et al., 2016; Chaudhary et al., 2017a; Stocker et al., 2017; Largeron et al., 2018; Qiu et al., 2019; Swinnen et al., 2019). Although still small, the number of dynamic global vegetation models (DGVMs) with integrated peatland modules and dynamic peatland area is increasing (Kleinen et al., 2012; Stocker et al., 2014; Largeron et al., 2018; Qiu et al., 2018) enabling, for the first time, a hindcast of past and a prediction of future peatlands on large spatial and temporal scales. Representations of peatlands have also been developed for the inclusion in the land modules of complex Earth system models (Lawrence and Slater, 2008; Schuldt et al., 2013). However, peatlands are generally still prominently missing from the newest generation of Earth system models (ESMs) taking part in the sixth phase of the Climate Model Intercomparison Project (CMIP6), which is the main source for future climate and carbon cycle projections used for the determination of international climate mitigation targets (Eyring et al., 2016). Thus, rigorous testing and improvement of the existing peat modules not only has the potential to yield further insights into peatland dynamics but can also pave the way for the integration of peat into the next generation of ESMs for improved climate projections.

Peatlands and their carbon stocks evolve dynamically through time and over glacial cycles. Peatlands may disintegrate or be buried by mineral sediments when climatic conditions become locally unfavorable for peat growth or local hydrologic conditions change (e.g., Talbot et al., 2010; Tchilinguirian et al., 2014; Campos et al., 2016; Lähteenoja et al., 2012; Tipping, 1995). Peatlands on exposed coastal shelves may be flooded during periods of rising sea levels (Kreuzburg et al., 2018), and new peatlands may form in areas previously covered by continental ice sheets or in areas that were previously too cold or too dry for peat establishment. Therefore, net changes in peat extent are the difference of concomitant gains and losses in peatland area. Similarly, the net flux of CO_2 from the atmosphere to peat carbon is the sum of complex changes. Peat carbon accumulates on active and expanding peatlands. Dying peatlands may lose some of the accumulated carbon to the atmosphere through degradation whereas another part might be buried and, thus, conserved on long timescales. Estimating peat carbon stocks for today's active peatlands is an important but insufficient step to fully constrain the influence of peat carbon changes on the atmospheric carbon balance. At the same time, peatlands are, in the absence of abrupt anthropogenic disturbance, slowly reacting systems with process timescales ranging from years to millennia. Thus, the present distribution of peatland and peat carbon and their future fate depend on past peatland dynamics and legacy effects from the last glacial–interglacial climate transition as well as the current interglacial (Holocene). However, model studies that thoroughly investigate the establishment and the disintegration of global peatlands constraining the total carbon balance transiently over the deglaciation are still lacking.

Here, our goal is to present a rigorous model investigation of peatland area and carbon dynamics since the Last Glacial Maximum (LGM), 21 000 years before present (BP).

We use a DGVM to simulate the LGM peatland distribution and assess uncertainties stemming from the climate forcing. Transient model and factorial simulations from the LGM to the present are analyzed to learn about past peatland dynamics, underlying drivers, and the net peatland carbon balance. Model results are compared to available data for the present and the LGM as well as to reconstructions of modern-day peatland initiation and development.

2 Methods

2.1 Model description

The simulations presented here were performed with the Land surface Processes and eXchanges (LPX-Bern) dynamic global vegetation model (DGVM) version 1.4 (Lienert and Joos, 2018). It includes an interactive carbon, water, and nitrogen cycle and simulates dynamic vegetation composition with plant functional types (PFTs), which compete for water, light, and nutrients (Sitch et al., 2003; Xu-Ri et al., 2012; Spahni et al., 2013). The implementation of permafrost and peatlands as long-term carbon stores are based on the Lund–Potsdam–Jena Wetland Hydrology and Methane (LPJ-WHyMe) model (Wania et al., 2009a,b) and a module to simulate peat area dynamically (Stocker et al., 2014). Peatlands are represented as a separate land class within a grid cell. The area of each grid cell is split into a fraction covered by the "peat", "mineral soils", and "old peat" (formerly active peat now treated as mineral soils) land classes. In this study, anthropogenic land use and land use change and corresponding land classes are not considered. Estimates of peat carbon loss through land use only exist for the industrial period. Leifeld et al. (2019) estimate that about 22 ± 5 GtC of peat carbon was lost globally between 1850 and 2015. Houghton and Nassikas (2017) used results from Randerson et al. (2015) and Hooijer et al. (2010) to estimate carbon loss from the draining and burning of peatlands for oil palm plantations in Southeast Asia. Losses are negligible before 1980, and they amount to about 6 GtC for the period from 1980 to 2015. These estimates of the loss of peat carbon through land use, although substantial, are still small compared with the total pool sizes. Peatland vegetation is represented by five peat PFTs: *Sphagnum* and flood tolerant graminoids, as mostly indicative of high-latitude peatlands, and flood tolerant tropical evergreen and deciduous tree PFTs as well as a flood tolerant version of the C4 grass PFT, as mostly indicative of tropical peatlands (Stocker et al., 2014). Carbon cycling in peat soils is based on the distinction between a lower, fully water-saturated slow overturning pool (catotelm) and an upper, fast overturning pool (acrotelm) with a fluctuating water table position (WTP; Spahni et al., 2013). For the determination of the carbon flux between acrotelm and catotelm a fixed average acrotelm carbon (C) density ($18.7\,\mathrm{kg\,C\,m^{-3}}$) is used, along with a fixed acrotelm depth of 0.3 m. The difference between this target acrotelm density and the actual average acrotelm density, determined by carbon influx from the litter pools and heterotrophic respiration within the acrotelm, is used to determine the size and sign of the daily flux between acrotelm and catotelm (Spahni et al., 2013). Decay rates are modulated by temperature in the catotelm and by temperature and the WTP in the acrotelm (Wania et al., 2009a).

The area fraction covered by peat (f_{peat}) in a given grid cell is determined dynamically with the DYPTOP (Dynamical Peatland Model Based on TOPMODEL) module (Stocker et al., 2014). The TOPMODEL approach (Beven and Kirkby, 1979) is used to predict the monthly inundated area fraction given sub-grid-scale topographic information and mean grid cell WTP. Here, the WTP calculation of mineral soils has changed slightly with respect to Stocker et al. (2014), with drainage runoff excluded from the calculation. The area potentially available for peatlands (f_{pot}) is then determined by inundation persistency. Peatlands expand or shrink towards a changing f_{pot} at a rate of 1 % of the current f_{peat} per year. The grid cell fraction lost during peatland retreat is treated as a separate land use class named "old peat"; it inherits the carbon stocks of the dying peat and is subsequently treated in the same way as the mineral soils regarding vegetation, hydrology, and carbon cycling. Growing active peatlands first expand on eventual old peat, inheriting the remaining carbon there.

As vegetation growth and carbon cycling continues normally on the old peat fraction, the carbon inherited by the former peatland, which would form distinct organic soil layers in the real world, can not be distinguished from new carbon accumulated by new non-peatland vegetation in the model. The same is true for grid cells that get flooded by rising sea levels. Given the evidence of coastal peat carbon deposits (Kreuzburg et al., 2018; Treat et al., 2019), we assume that most of the carbon is buried within sediments rather than released to the atmosphere during flooding. In case of flooding in the model, carbon from all land use classes in the respective cell is combined into a single "flooded" land use class, where it slowly decays with a mean lifetime of 15 kyr. Despite this mixing of carbon from different sources, we can track peat carbon in post-processing using the transient model output for peatland area changes, decay rates of slow pool carbon, and carbon input into the catotelm of the active peatlands. Area changes are used to transfer carbon between active, old, and flooded peatlands. Transient decay rates are used to decay the carbon in the respective pools. Thus, carbon is tracked from the entry into the catotelm of an active peatland until decay in either an active peatland, an old peatland, or peatland flooded by ocean. This approach can not take the acrotelm carbon into account; however acrotelm carbon constitutes only a small part of total peat carbon (5 % in the preindustrial (PI) period, and we can assume that this carbon at the peat surface is quickly respired after peatland transformation. The "old peat carbon" calculated this way represents the remaining peatland carbon after peatland death

and is used in the calculation of the peatland carbon balance (see Sect. 3.3.5).

Peatland existence, beyond a small peatland "seed" ($f_{peat} = 10^{-5}$) in every grid cell, is further limited by criteria on its carbon (C) and water balance. In this study, the evapotranspiration for peatland tree PFTs is now calculated analogously to non-peatland tree PFTs using demand and supply functions (Sitch et al., 2003). The determination of the criterion of a positive water balance (precipitation over evapotranspiration ratio in peat > 1), however, was kept functionally unchanged to Stocker et al. (2014). The C criteria were slightly improved in this study. The peat establishment and persistence criterion on the C balance during the spin-up is a positive net ecosystem production (NEP) and an acrotelm to catotelm flux higher than $10\,g\,m^{-2}\,yr^{-1}$, or C stocks of the peat seed exceeding $50\,kg\,m^{-2}$ as in Stocker et al. (2014). During the transient run this criterion is changed so that peat establishment depends on the acrotelm to catotelm flux alone. For peat persistence, the sharp C stock threshold is softened. For a peat C stock from $50\,kg\,m^{-2}$ to about $45\,kg\,m^{-2}$, f_{pot} is reduced to an actual potential peatland fraction (f_{apot}) according to a sigmoid function:

$$f_{apot} = f_{pot} \times \frac{1}{1 + 20\ e^{-2.4\,(C_{peat}-46)}} \quad | \text{ if } C_{peat} < 50\ kg\,m^{-2}, \tag{1}$$

where C_{peat} represents the peatland soil carbon pool in units of kilograms per square meter ($kg\,m^{-2}$). This avoids peatland collapse due to a sharp threshold. Peatlands can now endure short periods of carbon loss, even with C pools falling below the threshold of $50\,kg\ m^{-2}$, but they have to suffer area losses as a consequence, as f_{peat} now approaches f_{apot}.

The representation of peatlands in the LPX described above is a simplification in many respects. The absence of local processes and information like lateral water flow, the influence of sea level variations on the water balance, local soil features, or the influence of animals by grazing and river damming can limit the ability of the TOPMODEL approach to predict peatlands on a regional to local scale. Further, direct anthropogenic influences such as land use, drainage, or peat mining are not considered. The lack of a distinction and transition between different peatland types, like fens, bogs, blanket bogs, or marshes, neglects possible differences in the constraints on their formation and evolution. The treatment of acrotelm and catotelm as single carbon pools and the absence of strong disturbances such as peat fires constitute limits on the comparability of the model results to peat core carbon profiles. This simplified representation, however, has been shown to reproduce peatland area and carbon accumulation well within the observational constraints (Wania et al., 2009a; Spahni et al., 2013; Stocker et al., 2014, 2017) while using a minimal set of free parameters. Our efficient representation allows for long transient paleo-simulations and sensitivity studies such as those we present here.

2.2 Simulation setup

The transient LPX simulations from the Last Glacial Maximum (LGM), 22 kyr before present (BP), until present were run with a model resolution of 2.5° latitude × 3.75° longitude and were forced with CO_2 (Joos and Spahni, 2008), temperature, and precipitation fields as well as transient evolving orbital parameters influencing available photosynthetic active radiation. Temperature and precipitation anomalies are taken from the transient CCSM3 run TraCE21k (Liu et al., 2009). The TraCE21k experiment constitutes a unique climate forcing, not only because it is currently the only published transient simulation over the deglaciation using a fully coupled general circulation model (GCM) but also because the meltwater forcing in TraCE21k was chosen, using sensitivity experiments, to best reproduce the abrupt climate events such as the Bølling–Allerød (BA) and the Younger Dryas (YD) (He, 2011). The TraCE21k anomalies are imposed on the CRU TS 3.1 (Mitchell and Jones, 2005) base climate from 1960 to 1990. Thus, interannual variability is adopted from TraCE21k. The land–sea–ice mask is changes every 1 kyr according to Peltier (2004) and is interpolated in between. The model is spun up under LGM conditions for 2.5 kyr before starting the transient simulations.

In addition to the standard LPX transient simulation, five transient factorial simulations were performed using the same setup but keeping one of the five transient forcings (land–sea–ice mask, orbital, CO_2, precipitation, and temperature) constant at LGM levels for each simulation. These were used to identify the dominant drivers and driver contributions through time by comparing the factorial and standard runs (see Sect. 3.3).

To investigate the uncertainty stemming from the choice of climate forcing, seven additional LGM time slice simulations were performed. Mean LGM climate anomalies from six different PMIP3 models (including CCSM4, COSMOS-ASO, IPSL-CM5A-LR, MIROC-ESM, MPI-ESM-P, and MRI-CGCM3; Braconnot et al., 2012) and the mean LGM anomaly of the TraCE21k simulation were imposed on the CRU 3.1 climatology from 1901 to 1931. Thus, interannual variability is adopted from CRU. CO_2, ice-sea-land mask, and orbital parameters are set to LGM levels (in this case 21 kyr BP). Two of the eight available LGM simulations from phase 3 of the Paleoclimate Modelling Intercomparison Project (PMIP3) were not used (FGOALS-g2 and CNRM-CM5) due to their poor performance compared to observational data, especially in the variables of temperature and precipitation (Harrison et al., 2014). Simulations are spun up for 2.5 kyr and run for an additional 2 kyr under unchanged conditions. In the analysis, the temporal mean over the last 2 kyr is used.

2.3 Validation data

Even estimates for the current global peatland area are still subject to large uncertainties as peatlands often lie in remote, inaccessible, or understudied regions, such as the tropical forests or the Arctic tundra. Even estimates for the relatively well-studied northern high-latitude peatlands have a range from 2.4 to 4.0 M km^2 (see Loisel et al., 2017 for a review). The total area of tropical peatlands is even less well defined and estimates range from 0.37 to 1.7 M km^2 (Yu et al., 2010; Page et al., 2011; Gumbricht et al., 2017). The upper end of this range is given by an estimate that uses an expert system method, combining hydrological modeling, satellite imaging, and topographic data and, thus, tries to also account for currently undiscovered peatlands (Gumbricht et al., 2017). The most extensive and comprehensive compilation of known peatlands to date is the recent PEATMAP by Xu et al. (2018). PEATMAP shows a distribution shifted more towards the tropics than previous estimates from the literature. For example, Yu et al. (2010) estimates the area of northern peatlands to be 4 M km^2 and the area of tropical peatlands to be 0.37 M km^2, whereas PEATMAP gives 3.18 and 0.99 M km^2, respectively. In Fig. 1, Table 1, and Sect. 3.1, the LPX present-day peatland extent and global distribution are compared against a $0.5^\circ \times 0.5^\circ$ gridded version of PEATMAP.

Measured peat core basal dates have long been used to estimate northern peat initiation and lateral expansion through time. Yu et al. (2013) compiled a dataset containing 2808 basal dates combining published datasets from MacDonald et al. (2006), Gorham et al. (2007), and Korhola et al. (2010). Loisel et al. (2017) used this dataset (MGK13) to produce a version with only the oldest date per $1^\circ \times 1^\circ$ grid cell (MGK13G), as a proxy for peatland initiation. The MGK13G dataset is used in this study for comparison with simulated northern peat initiation (see Sect. 3.3.4). Multiple local basal dates are needed to disentangle lateral expansion from initiation. Loisel et al. (2017) compiled a reconstruction based on the gridded MGK13 dataset, but only grid cells with three or more peat cores were considered (MGK13S). Expansion curves were built regionally and then stacked to compensate for regional sampling bias. Korhola et al. (2010) used a similar approach utilizing 954 basal dates from 138 sites, with at least three dated cores per site. Their expansion reconstruction (KOR10) shows delayed expansion compared with Loisel et al. (2017) and the fastest expansion between 3 and 5 kyr BP. Both MGK13S and KOR10 are compared to the expansion simulated by LPX for currently existing northern peatlands (see Sect. 3.3.4), thereby not including area changes of peatlands that had previously existed but have already disappeared.

3 Results and discussion

3.1 Distribution and carbon inventories of present-day peatlands

3.1.1 Peatland area

The modern peatland distribution simulated by LPX-Bern (standard run) compares well to the distribution given by PEATMAP (see Fig. 1 and Table 1). LPX and PEATMAP yield a very similar global peatland area, with respective values of 4.37 and 4.23 M km^2. The same is true for the latitudinal distribution. LPX simulates 3.2 M km^2 in the high latitudes ($> 30^\circ$ N) and 1.15 M km^2 in the tropics (30° S–30° N), whereas PEATMAP gives 3.18 and 0.99 M km^2, respectively. This broad-scale agreement between LPX and PEATMAP notably emerges without any tuning of LPX against PEATMAP. These results are similar to previous results using the LPX (Stocker et al., 2014) with slightly larger tropical peatland coverage in the current study. Differences are due to a new model version after data assimilation, LPX v1.4, (Lienert and Joos, 2018) and the additional model changes described in Sect. 2.1.

Minor and major differences in peatland area between LPX and PEATMAP are seen on the local to regional scale (Fig. 1 and Table 1). In the tropics, LPX simulates more peat in South America and Southeast Asia than PEATMAP indicates. Compared to the estimate of Gumbricht et al. (2017), the LPX peatland extent is similar for South America and a factor of 2 smaller for Southeast Asia. The vast peatland complex in the Congo Basin is almost absent in LPX. In the northern mid to high latitudes, LPX seems to underestimate European peatland area by a factor of 2 and slightly overestimates peatland area in northern Asia, mostly west and east of the western Siberian lowland (WSL) peat complex. In North America, LPX simulates more peat in Alaska and Quebec and less in Western Canada than PEATMAP.

Other modeling studies present results from prognostic simulations of Northern Hemisphere peatlands. Kleinen et al. (2012) simulated peatland dynamics and carbon accumulation over the past 8000 years using the coupled climate carbon cycle model CLIMBER2-LPJ. However, no quantitative results in terms of peatland area were reported. Qiu et al. (2019) used the ORCHIDEE-PEAT DGVM (Qiu et al., 2018) to simulate northern ($> 30^\circ$ N) peat expansion over the Holocene. Their simulated northern present-day peatland area is, at 3.9 M km^2, slightly larger than in LPX. They find similar regional discrepancies between simulated and observation-based peat area in North America, northern Europe, and Asia, as described above for LPX. Peat area dynamics in ORCHIDEE-PEAT are also using the TOPMODEL approach following Stocker et al. (2014), with some different expansion criteria. This might indicate that these discrepancies could have their source in the TOPMODEL approach and its limitations. Another major source of un-

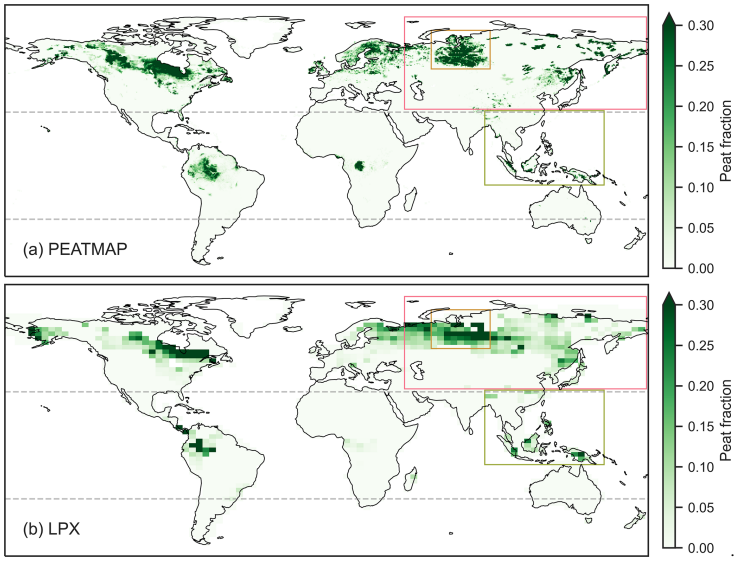

Figure 1. Global present-day peatland distribution according to PEATMAP (Xu et al., 2018) in a $0.5^\circ \times 0.5^\circ$ gridded version **(a)** and simulated by LPX-Bern after the transient "standard" setup simulation from 22 kyr BP to present **(b)**. The colored rectangles show three of the regions listed in Table 1: northern Asia (red), the western Siberian lowland (orange) region, and Southeast Asia (green)

certainties is in the climate data used to force LPX (see also Sect. 3.2.2). In particular, precipitation data show large discrepancies between available observational products (Sun et al., 2018).

3.1.2 Peatland carbon

Total peat carbon estimates are closely linked to the estimates for area and, thus, inherit their uncertainties. Additional assumptions on bulk density and peat depth introduce additional uncertainties. Therefore, the ranges of both carbon estimates and area estimates are large (Gorham, 1991; Turunen et al., 2002; Yu et al., 2010). The research bias allows for more constrained estimates in well-studied regions such as Europe and North America and less constrained estimates in the tropics and northern Asia. Estimates for northern peatlands range from 270 to 604 GtC and were obtained using various methods and area estimates (see Yu, 2012 and Yu et al., 2014 for a review). The modern carbon inventory of northern peatlands simulated by LPX at the end of the transient standard run from the LGM until present is, at 361 GtC, well within this observational range. In the tropics, LPX simulates a peat carbon inventory of 136 GtC which is substantially larger than classical estimates from the literature that range from 50 to 87 GtC (Yu et al., 2010; Page et al., 2011). These, however, also assume a substantially smaller tropical peatland area than LPX or PEATMAP suggest (see Sect. 3.1.1). Including estimates for the newly discovered peat in the Congo Basin, Dargie et al. (2017) estimate a tropical peat inventory of 69.6–129.8 GtC, which is closer to the LPX results. Gumbricht et al. (2017) calculate an even larger area than LPX, and combining their area estimate with the peat properties assumed by Page et al. (2011) would result in a tropical peat inventory of 350 GtC.

Previous studies with LPX-Bern reported somewhat different carbon inventories than given here. Stocker et al. (2014) reported 460 and 88 GtC for northern and tropical peatlands, respectively. Differences stem from an updated model version, also resulting in different areas as mentioned in the previous section. Additionally, their carbon stocks were the results of an accelerated spin-up scheme, whereas the pools in this study are filled over a transient run. Spahni et al. (2013) also report northern peatland carbon stocks after a transient LPX run from the LGM, although with prescribed not prognostic peatland area. Their simulation resulted in 365 GtC stored in northern peatlands.

Other model studies with dynamic peatland area reported 317 GtC after an 8 kyr Holocene run (Kleinen et al., 2012) and 463 GtC after a 12 kyr Holocene run (Qiu et al., 2019) in northern peatlands.

Table 1. Peatland area for different regions and latitudinal bands as given by PEATMAP (Xu et al., 2018) for today and peatland area and their carbon stocks as simulated by LPX-Bern for the preindustrial (PI) period and the Last Glacial Maximum (LGM) in the transient "standard" setup simulation from 22 kyr BP to present. The extent of the northern Asia, western Siberian (WS) lowland, and Southeast Asia regions are shown in Fig. 1.

Region	PEATMAP	LPX (PI)		LPX (LGM)	
	($M km^2$)	($M km^2$)	(GtC)	($M km^2$)	(GtC)
Global	4.232	4.366	499.3	2.687	275.6
Northern (> 30° N)	3.168	3.202	361.4	1.430	142.1
Tropics (30° S to 30° N)	0.976	1.151	135.7	1.236	131.6
North America	1.330	1.294	99.2	0.823	86.4
South America	0.489	0.744	94.9	0.634	62.7
Europe	0.414	0.231	19.6	0.331	30.8
Northern Asia	1.467	1.685	243.4	0.301	27.0
WS lowland region	0.624	0.691	108.9	0.030	2.5
Africa	0.189	0.050	3.9	0.115	7.0
Southeast Asia	0.273	0.349	36.1	0.471	60.4

3.2 Peatlands during the Last Glacial Maximum

3.2.1 Peatland distribution and carbon storage

Under LGM conditions, global simulated peatland area and carbon inventories are reduced compared with the preindustrial period (Table 1). Globally, simulated peatland area and the peat C inventory are 38 % and 45 % smaller at the LGM than during the PI period, respectively. This reduction is dominated by the northern extra-tropics, where peat extent and the C inventory are almost 60 % smaller at the LGM than during the PI period. In contrast, the peat C inventory in the tropics is only about 3 % smaller, and the tropical peat area is even 7 % larger at the LGM than during the PI period. This difference in the tropics is mostly linked to large peatlands simulated on flat exposed continental shelves in Southeast Asia at the LGM, which were subsequently flooded during the deglaciation. Another modeling study by Kaplan (2002) also suggests extensive wetlands on the flat Sunda Shelf, but reconstructions of Indonesian peatlands suggest that vast peat presence in Indonesia during the LGM is unlikely (Dommain et al., 2014). Establishment of now existing inland peatlands seems to be connected to rising sea level (Dommain et al., 2011). In sediment cores from the now submerged Sunda Shelf, there is little evidence of peatlands during the LGM (Hanebuth et al., 2011). Dommain et al. (2014) suggest that the shelf, although with a small topographic gradient, had an effective drainage system with deeply incised river valleys, preventing the formation of large wetlands. Both the hydrological feedback of rising sea level and deep river systems are not represented in LPX and, thus, might limit the models ability to reproduce peat and wetland dynamics in this region correctly.

Simulated peatland coverage in northern mid and high latitudes is smaller and is shifted southwards at the LGM compared with the PI period. Ice sheets covered large parts of Europe and North America during the LGM preventing vegetation and peat from growing. However, peat is also mostly absent in northern Asia and the WSL due to the substantially colder and dryer conditions compared with today. On the other hand, large peatland complexes are simulated along the southern ice sheet margins in North America and in Europe (Fig. 2), in regions where modeled peatlands are mostly absent under current conditions. This even leads to a simulated net increase of peatland area in Europe (+43 %) compared with the present. Verifying the existence of these extensive LGM peatlands that do not exist under present conditions (compare Fig. 1) is difficult, as existing compilations of peat core dates focus almost exclusively on today's existing peatlands (MacDonald et al., 2006; Gorham et al., 2007; Yu et al., 2010; Loisel et al., 2017). In a recent study, Treat et al. (2019) presented a compilation of dated buried peat deposits and simulated peatland area and carbon stocks. Their simulation also suggests large midlatitude peatlands in North America in agreement with our results. Their peat deposits data for the LGM (Fig. 2; dots), together with pollen analyses suggesting the presence of at least some *Sphagnum* in eastern North America (Halsey et al., 2000; Gajewski et al., 2001), provide plausible evidence for the existence of midlatitude LGM peatlands in North America and Europe. Their extent, however, is probably overestimated in our simulation. Comparisons between the North American LGM hydroclimate in TraCE21k and proxy reconstructions have resulted in a poor skill score, especially in eastern North America (Lora and Ibarra, 2019). Bad performance in this region is shared with all PMIP3 models (Lora and Lora, 2018).

3.2.2 Uncertainties from climate forcing

The peat distribution as simulated by LPX-Bern for the LGM and the past 20 000 years is subject to many uncertainties. Uncertainties arise from model parameterizations, not only

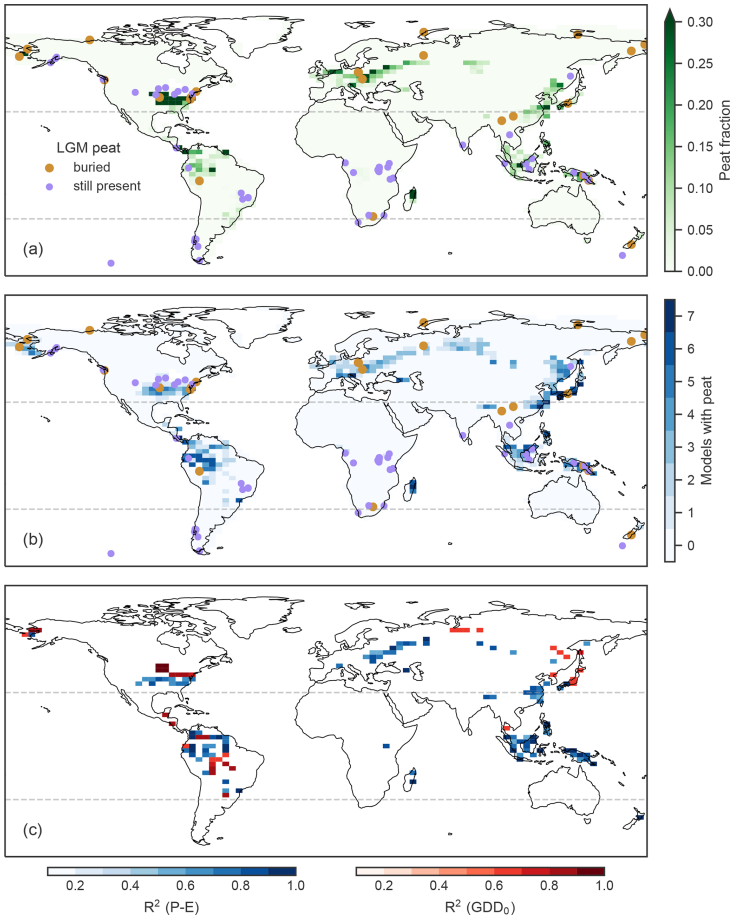

Figure 2. Peatland distribution at the Last Glacial Maximum (LGM) as simulated by LPX-Bern in the standard setup **(a)**, agreement (as number of models simulating peat in given grid cell) between LGM time slice simulations run with LPX and forced with different climates anomalies from six PMIP3 models as well as the TraCE21k anomaly **(b)**, and the squared correlation coefficient for a linear regression between physical properties of the different time slice simulations (precipitation minus evapotranspiration, P−E, and growing degree days above 0 °C) and peat fraction in the respective cells. Only cells with significant correlation ($p > 0.05$) are plotted. The colored shading in panel **(b)** indicates how many time slice simulations show a peat fraction of > 0.05 in the respective cell. The color code in panel **(c)** denotes the dominant predictor in the respective cell. Dots in panels **(a)** and **(b)** show buried and still active peat deposits that indicate active peat accumulation during the LGM (24.5–17.5 kyr BP). Peat core data are from Treat et al. (2019).

in the peat module but through all components of the model, and are often hard to quantify. Data assimilation, as done recently for the LPX in Lienert and Joos (2018) to constrain model parameters, is an approach to improve model performance in the light of uncertain key parameters. Another source of uncertainty stems from uncertainties in the prescribed forcings. The orbital parameters, atmospheric CO_2 mixing ratio, and land–sea–ice mask for the LGM and their deglacial evolution are all well constrained for the purpose of peat modeling, in contrast to the climate anomalies. Although there are paleoclimate reconstructions for the LGM (Bartlein et al., 2011; Schmittner et al., 2011; Annan and

Hargreaves, 2013), 6 k (Bartlein et al., 2011) and the last millennium (Hakim et al., 2016; Tardif et al., 2019), they lack the temporal resolution and/or spatial coverage needed for a global transient simulation from the LGM to present. Climate models can fill these gaps; however, climate anomalies are model dependent, and model performance differs between variables, regions, and the simulated time period (Harrison et al., 2014). These differences in climate models have been shown to propagate large uncertainties into carbon cycle projections (Stocker et al., 2013; Ahlström et al., 2017).

We assess the uncertainty in peatland area and peat carbon stemming from climate forcing uncertainties. Climate anomalies from seven different models are used to force the LPX into seven different LGM states (see Sect. 2.2). This yields a very wide range for global mean inundated area (2.6–3.6 M km^2), peat area (1.5–3.4 M km^2), and peat carbon (147–347 GtC). Interestingly, simulated wetland and peatland area and the peat C inventory for the 21 kyr BP period are also substantially different between the standard transient simulation using temporally evolving climate anomalies from the TraCE21k simulation compared with the time slice simulation forced with TraCE21k anomalies (Fig. 3, gray star versus gray dot). This highlights both the influence of different methods of input preparation, with slightly different treatment of anomalies and an interannual variability taken from TraCE21k in the transient simulation and from CRU 3.1 for the time slice, as well as the importance of memory effects for a slowly reacting system such as peatlands.

Agreement on the simulated peat extent among the seven simulations differs among regions (Fig. 2b). It tends to be higher in the tropics and East Asia and lower in North America, Europe, and western Siberia. Differences in temperature and precipitation anomalies propagate into differences in the water balance and productivity, partly limited by growing season length, and thus into differences in peat abundance and extent.

A statistical analysis of the differences in climatic drivers and simulated peat area reveals regionally different mechanisms (Fig. 2c). Temperature, precipitation, precipitation minus evapotranspiration (P−E), and growing degree days over 0 °C (GDD_0) are considered as climatic predictor variables for the peat fraction within a grid cell. We correlated, for each grid cell, the seven climatological mean values of a selected predictor with the modeled peat fraction from each of the seven time slice simulations. P−E and GDD_0 show significant correlations ($p < 0.05$) in more grid cells than precipitation and temperature, respectively. Both moisture balance and GDD_0 have been shown to be among the most important predictors of northern peat initiation and carbon accumulation in the past (Morris et al., 2018; Charman et al., 2013). In LPX the water balance, influenced by P−E, and the carbon balance, influenced by temperature and growing season length, define thresholds on peatland existence and size. In eastern Europe, differences in peat extent between the seven LGM time slice simulations are mostly driven by differences in local precipitation anomalies driving P−E. The same is true in the tropics, with MRI-CGCM3 and IPSL-CM5A-LR being the driest models with the least tropical peatlands and TraCE21k and COSMOS-ASO being the wettest with the largest tropical peatlands. However, in parts of central South America, temperature is the dominant predictor signaling a fragile carbon balance, where peat presence in some of the model climates is possible because of cooler conditions and, thus, reduced respiration. In the south of North America, moisture balance, with contributions of both P and E, is the dominant determinant of the inter-model differences. The time slice forced with TraCE21k climate shows the peatland distribution in North America more shifted to the east compared with most other PIMP3 forcings alongside warmer and wetter conditions (see also Lora and Lora, 2018). The peatland extent in the north of North America is sensitive to temperature differences with longer growing season allowing for increased productivity and, therefore, peat formation. In the MRI-CGCM3 time slice, temperature anomalies with respect to the preindustrial period are lowest and peat is subsequently shifted northwards compared with other time slices. Similar is true for northern and East Asia where lower temperature anomalies allow for more peatlands. Large areas in central Europe, East Asia, and South America show differences in peatland extent induced by differences in climate forcings, but no significant correlations between peat fraction and predictor variables are found. This might be the result of nonlinear interactions and threshold behaviors not captured by our linear regression approach. Taken together, these findings demonstrate a strong sensitivity of simulated peat extent and the C inventory to the prescribed climate fields and a strong dependence of the results on the choice of climate model output used to force LPX. In other words, caution is warranted when interpreting model results for times and regions in which proxy records or observations are sparse and have limited power to constrain the actual climate conditions. This holds not only in the context of this study but also for global peat and carbon cycle model studies in general.

3.3 Transient peat evolution

Figure 4a shows the peatland evolution in the transient model run. The model simulates the establishment and expansion of peatlands under favorable conditions as well as the decay and disappearance of peatlands under unfavorable conditions. Both processes can happen simultaneously on a global as well as a regional scale (Fig. A1). To treat carbon storage in a consistent manner, we distinguish between the active peatlands, which are treated as peatlands in the LPX, and old peatlands, which are treated as mineral soils. Old peatlands inherit the carbon stocks of the peatlands that are shrinking or vanishing. Similarly, growing active peatlands first expand onto the area of old peatlands, inheriting the remaining carbon stored there (see also Sect. 3.3.5). In the analysis, we decompose the net changes of peatland area into gross positive

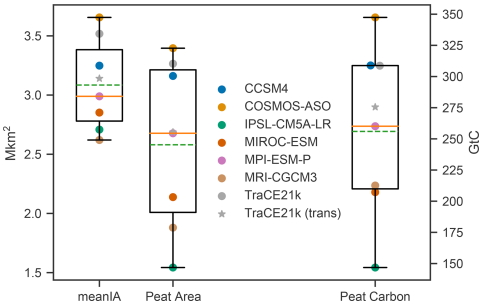

Figure 3. Spread of the global annual mean inundated area (meanIA), peatland area, and peatland carbon during the LGM (21 kyr BP) in time slices forced with climate anomalies from seven different climate models (see Sect. 2.2). The box, the solid line, and the dashed line indicate the interquartile range, the median, and the mean from the seven simulations, respectively. The star indicates the values of the transient simulation for the same time period using climate anomalies from TraCE21k.

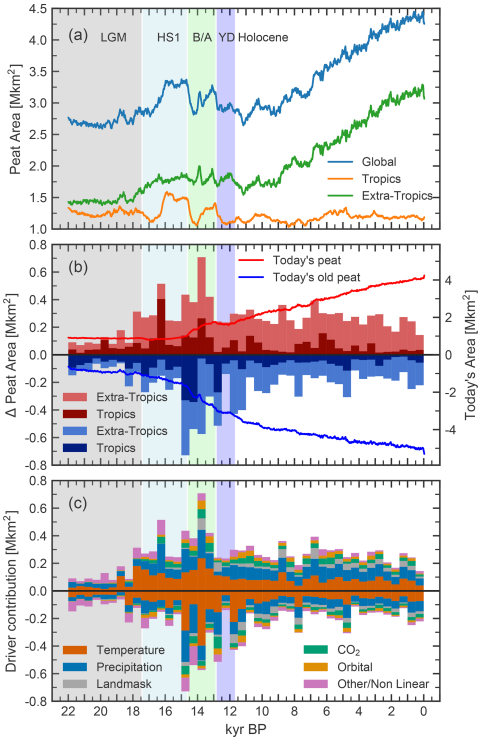

Figure 4. Simulated peatland area over time **(a)**, gross positive and negative peatland area changes in 0.5 kyr bins, the evolution of today's simulated peatland area and old peat area **(b)**, and driver contributions to the same changes **(c)**, calculated using factorial simulations (see Sect. 2.2). Contributions by regions **(b)** and by drivers **(c)** are plotted cumulatively. Vertical bars indicate the Last Glacial Maximum (LGM) period, the Heinrich Stadial 1 (HS1) Northern Hemisphere cold phase, the Bølling–Allerød (BA) Northern Hemisphere warm phase, and the Younger Dryas (YD) Northern Hemisphere cold phase.

and negative changes. This allows for a deeper insight into the underlying temporal dynamics (Fig. 4b). Transient factorial runs, performed over the same time period as the standard setup (see Sect. 2.2), allow us to attribute driver contributions to the simulated changes (Figs. 4c, 6).

3.3.1 22–17.43 kyr BP

Global changes in peatland area and carbon before the onset of the Heinrich Stadial 1 (HS1) are small, due to the relatively small changes in the main drivers. There is initial carbon loss in some regions of the tropics, due to some grid cells still approaching equilibrium after the spin-up (Fig. A1). North America already sees an accelerating carbon accumulation with unchanging area before the HS1, driven mostly by increasing temperature. Carbon and area also increase in Europe with large temperature-driven fluctuations

3.3.2 17.43–11.65 kyr BP

Three main features characterize the peat area evolution over the last glacial termination: (i) a northward shift in the distribution of northern extra-tropical peatlands, including peat expansion in northern Asia; (ii) dipole-like north–south shifts in tropical South America, associated with north–south shifts of the rain belts of the intertropical convergence zone (ITCZ); and (iii) flooding of peatlands on continental shelves, mostly in Southeast Asia, due to rising sea levels.

The last termination represents the transition of the climate system from the last glacial to the current interglacial, accompanied by large warming, ocean circulation changes, and an increase in atmospheric CO_2 (Monnin et al., 2001; Shakun and Carlson, 2010; Ritz et al., 2013). The termination is divided into the Heinrich Stadial 1 (HS1, 17.43–14.63 kyr BP) Northern Hemisphere (NH) cold period, the Bølling–Allerød (BA, 14.63–12.85 kyr BP) NH warm period, and the Younger Dryas (YD, 12.85–11.65 kyr BP) NH cold period (Rasmussen et al., 2014). These NH cold–warm swings are associated with a large-scale reorganization of ocean circulation, which is thought to have been provoked by freshwater release from ice sheet melting leading to changes in the ocean heat transport (Stocker and Johnsen, 2003). With changing low- to high-latitude temperature gradients, the ITCZ shifted and with it the high precipitation zones in

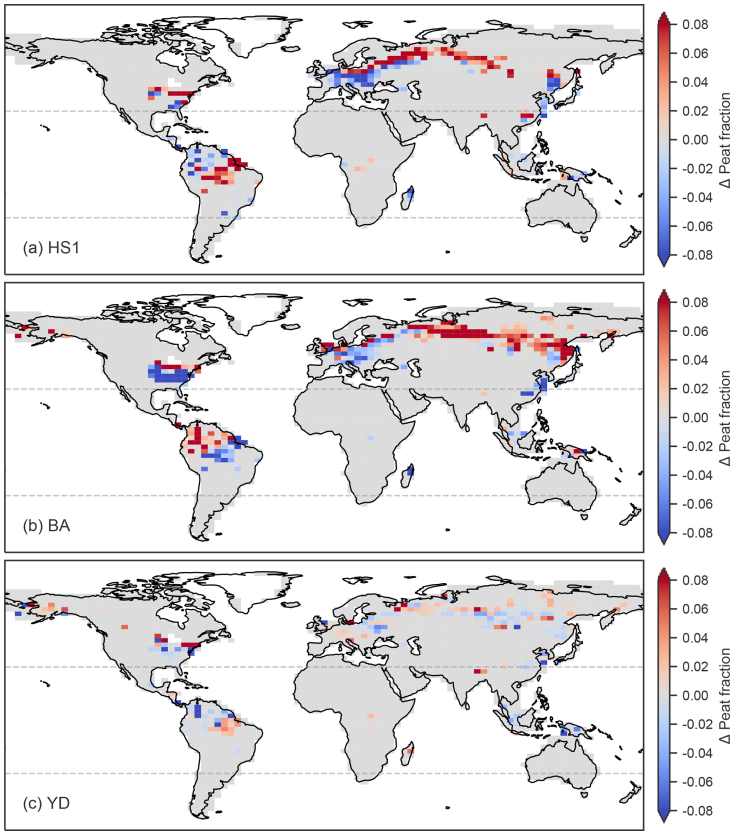

Figure 5. Maps showing the changes in the peatland fraction during three periods of past substantial climate change: **(a)** the Heinrich Stadial 1 (HS1, 17.43–14.63 kyr BP), **(b)** the Bølling–Allerød Northern Hemisphere warm period (BA, 14.63–12.85 kyr BP), and **(c)** the Younger Dryas Northern Hemisphere cold period (YD, 12.85–11.65 kyr BP).

the tropics (McGee et al., 2014; Shi and Yan, 2019; Cao et al., 2019). These climate dynamics are well captured by the transient TraCE21k simulation (Liu et al., 2009).

The responses of peatlands in LPX to these climatic changes are drastic. Large shifts in peatland area start to set in at the onset of the HS1 and increase into the BA. During the BA, peatlands show the fastest gross positive and negative area changes throughout the simulation (see Fig. 4b). In the northern mid and high latitudes, peatlands shift north and eastward (see Figs. 5, A2). Peatlands disappear in midlatitude North America and Europe, and new peatlands emerge at higher latitudes and in cold continental regions of Asia. These new peatlands include the large peat complex in the western Siberian lowland (WSL) region. Some of the peatlands established in northern Europe during HS1 vanish again during the BA. The described changes are driven by the TraCE21k climate which shows a substantial warming and wetting of the Northern Hemisphere beginning during the HS1. Temperature is the dominant driver for peat loss and expansion in Europe and North America. The loss of old peat is especially abrupt in North America (see Fig. A1b). Here, precipitation decreases and temperature increases abruptly over southwestern North America at 13 870 BP. Both changes decrease the water balance given by P−E which leads to a decrease in potential peat area and, thus, loss of the previous extensive peat complexes. As this abrupt climate change occurs at a discontinuity of the trace boundary conditions (changes in ice sheet configuration

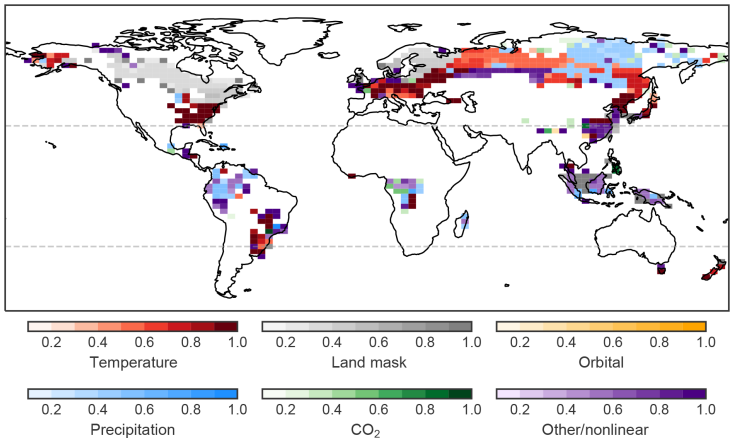

Figure 6. Drivers of the change in peatland area from LGM to present. Colors indicate the most important driver, and colored shading shows the contribution of the respective driver on a scale from 0 (no contribution) to 1 (only contributor).

and freshwater forcing), the speed of this change is probably drastically overestimated. In northern Asia both temperature and precipitation drive the peatland expansion. This expansion sees a pronounced halt during the YD where the Northern Hemisphere climate briefly returns to more glacial conditions (see Fig. A2e).

In the tropics, the area and carbon changes are mostly driven by precipitation changes. Largest changes are simulated in South America, where precipitation patterns respond to changes in ITCZ position (see Fig. 5). During the HS1 and the YD where the Atlantic meridional overturning circulation (AMOC) is in a reduced state, peatland area shifts to the south following the southward shift of the ITCZ. During the BA the AMOC is strong and precipitation and peatland area shift back north. In Africa half the peatland area is lost during the BA mostly driven by drying. In Southeast Asia peatlands are lost over the whole termination due to precipitation changes and the onset of sea level rise, which starts to flood the large continental shelves at about 16 kyr BP.

The shifts in peatland distribution result in a similar global peatland area at the beginning of the Holocene compared with the LGM and at the onset of the HS1. However, much less carbon is stored in active peatlands at the beginning of the Holocene than during the LGM and at the onset of the HS1. Thus, the carbon density per unit area is much lower for the newly established peatlands than for the lost LGM peatlands.

3.3.3 11.65–0 kyr BP

Modeled peatlands in the Holocene show a continuous net expansion in the northern extra-tropics, with newly forming peatlands more than balancing the loss of peatlands elsewhere. The Holocene experienced relative stability in climate and CO_2 levels compared with the termination. The early to mid Holocene was likely characterized by warmer summer temperatures than the preindustrial period with a larger seasonality in the Northern Hemisphere (Marcott et al., 2013; Liu et al., 2014; Samartin et al., 2017). Ice sheet retreat and sea level rise lagged behind the deglacial temperature increase and was mostly completed at about 7 kyr BP (Peltier, 2004). Locally, new land keeps emerging to this day due to isostatic rebound. This effect is especially pronounced in the Hudson Bay lowlands, where new land emerges at a rate of up to 12 mm yr^{-1} (Henton et al., 2006).

For northern peatlands, positive area changes are consistently larger than negative changes throughout most of the Holocene (see Fig. 4a). This leads to a large continuous area expansion. Old peatland area is also simulated to increase continuously during the Holocene (Fig. 4b), showing that the parallel positive and negative changes are more than mere fluctuations of existing peat but that there is actual continuous peatland loss and growth. Net area increase picks up at about 9 kyr BP, decreases in the late Holocene, and turns into a net area reduction in the last millennium. This late Holocene slowdown and reversal of net peatland area growth is most pronounced in northern Asia where increasing negative changes start to balance and eventually offset the still large positive changes (Figs. A1 and A2). Here, both negative and positive dynamics are driven by temperature and precipitation. The early, fast expansion in northern Asia is offset by a temperature-driven net area loss in Europe which is recovered partly towards the late Holocene. Net area increase in

North America is delayed by continued loss of midlatitude peat and the slow retreat of the Laurentide Ice Sheet, which limits the establishment of new peatlands. Today's peatlands in North America start to establish after about 9 kyr BP with most of today's peatlands forming between 7 and 2 kyr BP. Carbon stocks follow these regional trends but with larger relative increases especially towards the late Holocene. As the timescale for building up carbon pools is generally much longer than the timescale of potential area changes, fluctuations in area, mostly by young peatlands, are smoothed in the carbon stocks (see, e.g., Fig. A1b).

The tropical peatland area is simulated to stay relatively stable throughout the Holocene, with positive changes balancing negative changes. Southeast Asia sees a reduction in area in the early Holocene due to continued sea level rise and a subsequent gradual recovery of integrated peat area driven by precipitation and nonlinear effects. Peat area in South America increases slightly over the Holocene with mostly precipitation-driven fluctuations in between. On the other hand, fluctuations in region-integrated peat carbon stocks are largely absent in South America, as carbon, with changing area, is shifted between peat and old peat pools. Peat carbon stocks in South America show a large relative increase following a near-linear path. Africa sees an increase in area at about 10 kyr BP driven by precipitation and enabled by high CO_2 concentrations. The new area gradually degrades again until 3 kyr BP with another peak at 0.5 kyr BP.

3.3.4 Model versus reconstructions

The study of peatland initiation, life cycle, dynamics, and responses to external forcing has been focused on today's existing and active peatlands. This work includes large compilations of peat core basal dates (MacDonald et al., 2006; Gorham et al., 2007; Yu et al., 2010) which are used to reconstruct initiation dates and lateral expansion (Yu et al., 2010; Korhola et al., 2010; Dommain et al., 2014; Loisel et al., 2017) of the sampled active peatlands. This approach, however, does not include earlier peatlands that dried out, were buried or flooded, or otherwise ceased to be active accumulating peatlands. Treat et al. (2019) presented a first compilation of dated buried peat layers, but the small sample size make quantitative reconstructions difficult. Thus, we limit most of the model–data comparison of the transient behavior to today's existing peatlands. Figures 7 and 8c show modeled initiation date frequency, area, and carbon dynamics of northern peatlands that are still active at present.

Figure 7a compares LPX results to a gridded "oldest age" dataset compiled by Loisel et al. (2017), and Fig. 7b and c compare LPX results to two different reconstructions for lateral expansion (Loisel et al., 2017; Korhola et al., 2010) based on similar methods but different underlying peat core datasets (see Sect. 2.3). The two reconstructions for peat expansion agree on a limited pre-Holocene expansion, but they disagree substantially on the timing of fastest expansion during the Holocene (Fig. 7). Both simulated initiation and peat expansion have peaks about 4 kyr earlier than the reconstructions. The model simulates early initiation of today's northern peatlands, already beginning in HS1, and a large expansion during BA. The reconstructions, on the other hand, suggest lateral peat expansion picking up only with the transition into the Holocene. Agreement between model and reconstructions becomes good in the mid to late Holocene.

The early expansion in the model also propagates to the carbon balance for presently active peatlands. The model simulates earlier accumulation extending into the HS1 and slower accumulation during the early Holocene than suggested by net carbon balance (NCB) reconstructions by Yu (2011) (Fig. 7c). The summed simulated carbon increase from the LGM to the PI period in today's northern peatlands amounts to 313 GtC (Fig. 8c).

The early expansion of northern peatlands in the simulation is mostly dominated by peat establishment in western Siberian lowland (WSL) region and northern Asia in general (see Sect. 3.3.2 and Fig. A1). The dominant drivers of this expansion are temperature and precipitation, which, according to TraCE21k, both increase substantially over northern Asia during the HS1 and BA. A similar simulated early expansion into the WSL was reported by Treat et al. (2019), with the coupled CLIMBER2-LPJ setup. Morris et al. (2018) investigated possible climatic drivers for peat initiation in a modeling study using the HadCM3 model. They suggest that the WSL responded to an increase in effective precipitation at about 11.5 kyr BP, instead of the early warming. One source of the model data mismatch could lie in the uncertainties in climate anomalies discussed in Sect. 3.2.2. Especially at high latitudes, climate anomalies can vary greatly between climate models, and model performance at one point in time does not always correspond to performance at another point in time (Harrison et al., 2014). Although the freshwater change in TraCE21k was designed to capture the rapid climate events during the glaciation, the magnitude and timing of regional or even hemispheric changes can still have large biases. To date, TraCE21k is the only available transient GCM simulation, but new simulations under the umbrella of PMIP4 might shed more light on the model dependence of the warming pattern in question (Ivanovic et al., 2016). Another source of the mismatch could lie in the simple representation of peatlands in the model, which might be unsuitable to reproduce specific initiation and expansion pathways, like terrestrialization and fen–bog transition that might have been important controlling factors in that time and region (Kremenetski et al., 2003). One example could be the relative weakness of the initiation criteria on the moisture balance (precipitation over evapotranspiration > 1), which is almost always weaker than the indirectly mediated condition on inundation persistence. This might pose a problem, especially in the WSL where moisture balance might have been the driving factor for peat initiation (Morris et al., 2018). Lastly, although the WSL is relatively densely sampled and reconstructions of peat initiation are ro-

bust, other areas of northern Asia are vastly under sampled and reconstructions are less reliable.

Throughout the tropics dated buried and active peat cores already show peatland presence during and preceding the LGM. However, peatland extent or evolution towards the presence are not well constrained and are subject to large uncertainties. The small number of available dated tropical peat cores impedes a statistical approach. Applied nevertheless, it indicates a more or less continuous growth of today's peatlands since about 19 kyr BP with the largest expansion rates between 8 and 4 kyr BP (Yu et al., 2010). Dommain et al. (2014) reconstructed the evolution of Indonesian peatlands using a combination of dated cores and a transfer function between depth and age. They argue for a peat expansion much later than that inferred by basal ages alone, with 90 % of today's peat establishing after 7 kyr BP and 60 % after 3 kyr BP. In this study, the dominant control on peatland area was found to be local sea level. Rising sea level during the termination and the early Holocene triggered the establishment of inland peatlands through alterations in moisture availability and the hydrological gradient, and the stabilization of sea level and subsequent sea level regression after 4 kyr BP prompted the establishment of coastal peatlands. In contrast to these reconstructions, the transient simulation shows that 60 % of today's tropical peatland area is already present in the LGM and only small expansion during the recent millennia. The sparsity of the data warrants caution when comparing reconstructions to model results. However, in Southeast Asia, this discrepancy could indicate the importance of the feedback of sea level on local hydrology, which is missing in LPX.

3.3.5 Transient carbon balance of peatland soils and the land biosphere as seen by the atmosphere

In this section, we address how carbon stored in soils of active peatlands and carbon stored in the remains of former peat soils changed over time. Thus, we quantify the overall contribution of peatland soils and peat carbon to the changes in the global carbon inventory of the land biosphere.

When trying to quantify the net effect of peatlands on the atmosphere, looking only at carbon stored in today's active peatlands can be misleading. Former active peatlands have transformed into other landscapes. Organic-rich peat layers may now be buried under mineral soils on land or in coastal ocean sediments (Treat et al., 2019; Kreuzburg et al., 2018). When analyzing the transient carbon balance of global peatlands such "old peat carbon" pools have to be considered.

Figure 8b shows the temporal evolution of carbon stored in soils of active peatlands, old peat soil carbon remaining on former peatlands, and old peat carbon stored on flooded continental shelves. Here, the old peat pools presented exclusively include the carbon from the organic-rich layers of formerly active peatlands that remain after accounting for decomposition over time (see Sect. 2.1). In the PI period, 499,

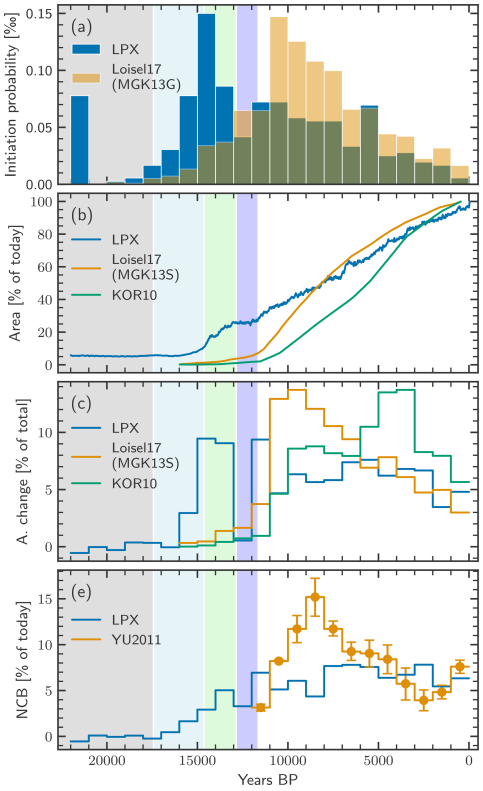

Figure 7. Simulated and reconstructed dynamics of today's existing northern peatlands: **(a)** peatland initiation frequency (two overlapping histograms), **(b)** peatland area expansion and **(c)** expansion rate, and **(d)** the net carbon balance (NCB) normalized by respective estimates of today's carbon pool. The reconstruction datasets are described in Sect. 2.3. The background colors indicate different time periods, as in Fig. 4

139, and 22 GtC of peat carbon are stored in their respective pools. The total simulated increase in peat carbon from the LGM to the PI period within these three pools is 351 GtC. This represents the simulated net carbon accumulation of global peat and, thus, the net amount of carbon sequestered from the atmosphere by peat. When only considering carbon stored in active peatlands, we would underestimate the deglacial peat carbon change with a value of 224 GtC. On the other hand, if we only consider the carbon stored in today's active peatlands, the inferred deglacial change amounts to 365 GtC (Fig. 8c), and we would overestimate the net peat accumulation since the LGM. While the latter differ-

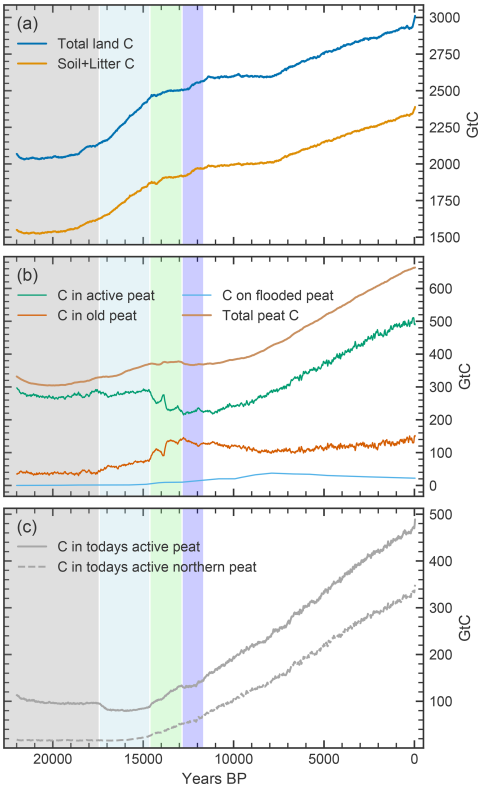

Figure 8. Carbon on global land (soil + litter + vegetation) **(a)**; on active peatland areas, old peatland areas, and on flooded continental shelves **(b)**; and in today's active peatlands **(c)**. The brown line in panel **(b)** represents global carbon that originated from peatlands, even if it is not part of an active peatland anymore. The background colors indicate different time periods, as in Fig. 4

ence in net peat carbon accumulation between the complete and incomplete accounting scheme appears small for the total deglacial change, the difference can be substantial and relevant for other periods. For example, a particular large difference is identified for the phase of high peatland expansion and loss rates as simulated from the Bølling–Allerød to the Preboreal in our model. Here, the carbon balance is given as 12 GtC when including old peat, versus 102 GtC when only looking at the carbon in today's active peat for the period from 14.6 to 10 kyr BP.

Peatlands contribute about 40 % to the total land biosphere carbon increase of 893 GtC. The result for the total land carbon increase between the LGM and the PI period is in good accordance with a recent estimate, integrating multiple proxy constraints (median: 850 GtC; 450–1250 GtC ± 1 standard deviation) (Jeltsch-Thömmes et al., 2019). The model also simulates the total change of the land biosphere carbon inventory between the beginning of the Holocene and the preindustrial period in reasonable agreement with the reconstruction by Elsig et al. (2009). The simulated temporal evolution, however, is different, with a rapid uptake in the early Holocene in the reconstruction compared with a delayed uptake in the mid to late Holocene in the simulation.

4 Conclusions

We used the LPX-Bern dynamic global vegetation model to produce an in-depth model analysis of the transient area and carbon dynamics of global peatlands from the Last Glacial Maximum (LGM) to the present. For the LGM, peatland area, reduced to the tropics and northern midlatitudes, is predicted at 2.687 Mkm^2 in the transient run, storing 275.6 GtC of carbon. Under LGM climatic conditions, LPX-Bern predicts peatlands in areas with low or no peat cover at present or on currently submerged continental shelves. Uncertainty from the climate forcing was assessed by using, in addition to the TraCE21k, climate anomalies from six different time slice simulations for the LGM from phase 3 of the Paleoclimate Modelling Intercomparison Project (PMIP3). This results in a peat area range of 1.5–3.4 Mkm^2 with a carbon storage of 147–347 GtC. This large range illustrates the dependence of results on, uncertain, LGM climate conditions and the sensitivity of simulated peatlands to these differences. Sparse data on paleo-peatlands, on their extent, and on their carbon storage make it difficult to further constrain this range. At the same time, there are currently only a few coupled climate simulations for the LGM and only one transient simulation with an atmosphere–ocean general circulation model available for the period from the LGM to present.

A driver attribution of the simulated transient evolution of peatlands using factorial simulations showed regional and temporal differences. Modeled changes in the tropics were dominated by shifts in the position of the intertropical convergence zone and associated precipitation changes during the last glacial termination as well as by rising sea level. Changes in the northern high latitudes are mostly driven by temperature and precipitation increases. The largest model mismatches to available area reconstructions can be seen in the onset and timing of the earliest expansion of today's northern peatlands. A strong warming in the climate forcing during Heinrich Stadial 1 and the Bølling–Allerød triggers a first expansion into northern Asia, which according to reconstructions only starts during the Preboreal, about 4 kyr later.

The simulated transient evolution of peatlands is characterized by continuous and simultaneous increases and decreases of area and carbon, with the fastest positive and negative changes happening during the termination (Hein-

rich Stadial 1 and Bølling–Allerød). This reveals a different perspective from the commonly assumed linear and continuous growth of global peatlands. Instead peatlands become a dynamic, growing, dying, and shifting landscape. Carbon in soils of formerly active peatlands can be trapped in mineral soils or ocean sediments. Thus, when assessing the net carbon balance of global peatlands over time, accounting for paleo-peatlands and their remains becomes essential. In our transient simulation the LGM to the PI period net peat carbon balance is predicted at 351 GtC, with 499, 139, and 22 GtC stored in the PI period in soils of still active peatlands, in the remains of former peat soils on land, and in the remains on submerged shelves, respectively. For today's active northern peatlands, simulated peat area and carbon is in good accordance with the range of estimates from the literature, whereas predictions for the tropics are larger than most estimates. However, data constraints in the tropics are significantly weaker, as peatland science has long focused on the northern high latitudes and has only began accelerating its effort in the tropics over the last few decades. Even fewer data are available to constrain old peat carbon that remains outside of today's active peatlands.

Taken together, our study provides an in-depth model analysis of peatland development, the associated drivers, and the uncertainties on a global scale. It contributes to a foundation for a better understanding of past peat dynamics and emphasizes the importance of treating and understanding peatlands as dynamic and evolving systems. In a next step, the results presented here can serve as a starting point for projections of future peat dynamics under different scenarios.

A growing database of buried peat and knowledge emerging from the growing literature on anthropogenically drained peatlands might shed more light on the fate of old peat carbon and inform future modeling studies. New time slice and transient climate model simulations under PMIP4 (Ivanovic et al., 2016; Kageyama et al., 2017) as well as an increased effort from the peat community to fill gaps in sample coverage both for today's peatlands and buried peat layers, especially in North America, northern Asia, and the tropics, might help to constrain past peat dynamics further and to test the robustness of the results presented here. At the same time, there is potential for improvements to the LPX-Bern that could decrease model data mismatches, especially on the regional scale. Future improvements could include refining the moisture balance criteria on peat initiation, improving hydrology and boundary conditions on continental shelves, and finding key processes that might benefit from a more complex representation, such as a multilayer peat profile and distinctions between different peatland types.

Appendix A

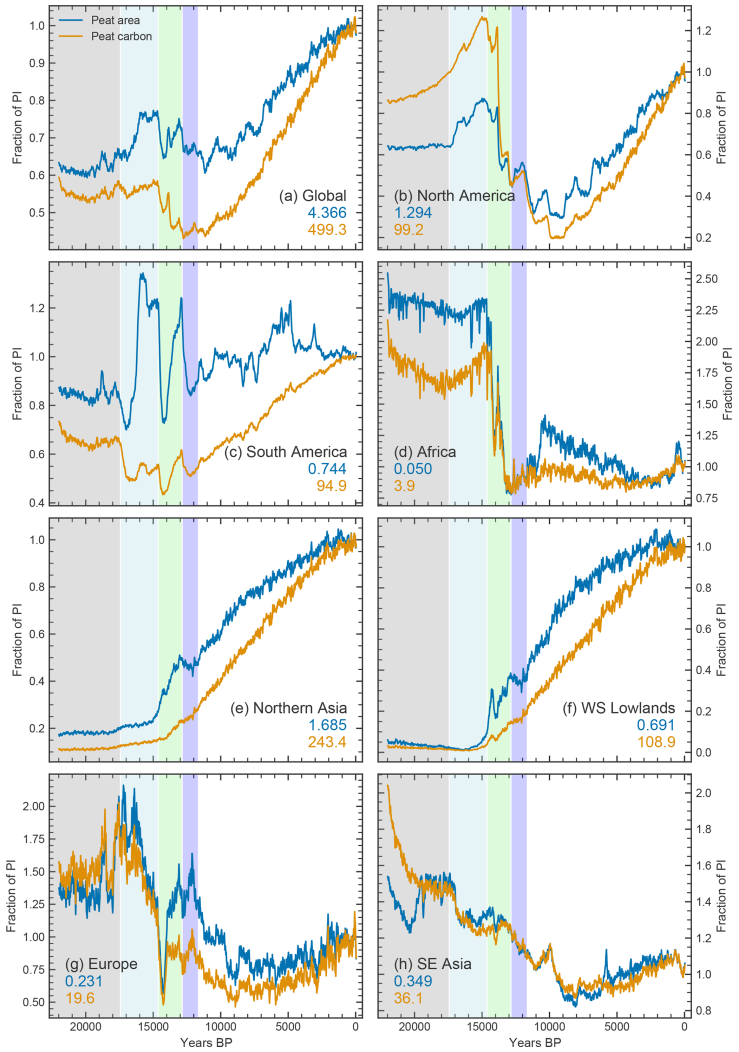

Figure A1. Simulated global and regional peatland area and carbon dynamics over time, relative to PI levels. PI levels are given in millions of square kilometers ($M km^2$) for peat area and in gigatons of carbon (GtC) for peat carbon. The extent of the northern Asia, western Siberian (WS) lowlands, and Southeast Asia regions are shown in Fig. 1. The background colors indicate different time periods, as in Fig. 4

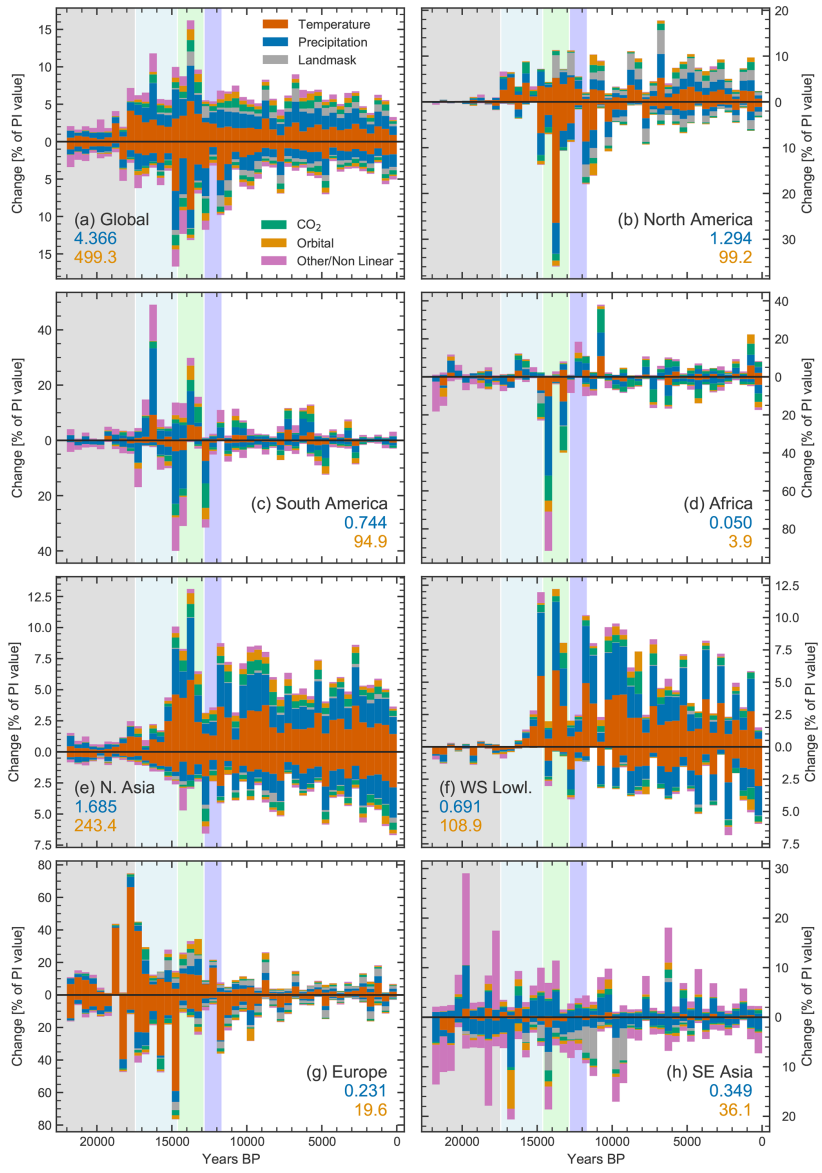

Figure A2. Simulated global and regional gross positive and negative changes in peatland area in 0.5 kyr bins, relative to PI levels. PI levels are given in millions of square kilometers ($M\,km^2$) for peat area and in gigatons of carbon (GtC) for peat carbon. Colors indicate driver contributions to changes attributed using factorial simulations. The extent of the northern Asia, western Siberian (WS) lowland, and Southeast Asia regions are shown in Fig. 1. The background colors indicate different time periods, as in Fig. 4

Data availability. Data from the main text figures are available as electronic supplementary material, and further data are available from the authors upon request.

Author contributions. JM and FJ designed the study. JM performed the simulations and the analyses in consultation with FJ. JM prepared the figures and wrote the paper with input from FJ.

Competing interests. The authors declare that they have no conflict of interest.

Acknowledgements. We thank Sebastian Lienert for fruitful discussion and support regarding LPX-Bern.

Financial support. This research has been supported by the Swiss National Science Foundation (grant no. 200020_172476).

Review statement. This paper was edited by Jens-Arne Subke and reviewed by Thomas Kleinen and one anonymous referee.

References

Ahlström, A., Schurgers, G., and Smith, B.: The large influence of climate model bias on terrestrial carbon cycle simulations, Environ. Res. Lett., 12, 014004, https://doi.org/10.1088/1748-9326/12/1/014004, 2017.

Alexandrov, G. A., Brovkin, V. A., and Kleinen, T.: The influence of climate on peatland extent in Western Siberia since the Last Glacial Maximum, Sci. Rep., 6, 6–11, https://doi.org/10.1038/srep24784, 2016.

Annan, J. D. and Hargreaves, J. C.: A new global reconstruction of temperature changes at the Last Glacial Maximum, Clim. Past, 9, 367–376, https://doi.org/10.5194/cp-9-367-2013, 2013.

Baird, A. J., Morris, P. J., and Belyea, L. R.: The DigiBog peatland development model 1: rationale, conceptual model, and hydrological basis, Ecohydrology, 5, 242–255, https://doi.org/10.1002/eco.230, 2012.

Bartlein, P. J., Harrison, S. P., Brewer, S., Connor, S., Davis, B. A., Gajewski, K., Guiot, J., Harrison-Prentice, T. I., Henderson, A., Peyron, O., Prentice, I. C., Scholze, M., Seppä, H., Shuman, B., Sugita, S., Thompson, R. S., Viau, A. E., Williams, J., and Wu, H.: Pollen-based continental climate reconstructions at 6 and 21 ka: A global synthesis, Clim. Dyn., 37, 775–802, https://doi.org/10.1007/s00382-010-0904-1, 2011.

Beven, K. J. and Kirkby, M. J.: A physically based, variable contributing area model of basin hydrology, Hydrol. Sci. Bull., 24, 43–69, https://doi.org/10.1080/02626667909491834, 1979.

Blodau, C.: Carbon cycling in peatlands – A review of processes and controls, Environ. Rev., 10, 111–134, https://doi.org/10.1139/a02-004, 2002.

Braconnot, P., Harrison, S. P., Kageyama, M., Bartlein, P. J., Masson-Delmotte, V., Abe-Ouchi, A., Otto-Bliesner, B., and Zhao, Y.: Evaluation of climate models using palaeoclimatic data, Nat. Clim. Change, 2, 417–424, https://doi.org/10.1038/nclimate1456, 2012.

Campos, J. R. d. R., Silva, A. C., Slater, L., Nanni, M. R., and Vidal-Torrado, P.: Stratigraphic control and chronology of peat bog deposition in the Serra do Espinhaço Meridional, Brazil, CATENA, 143, 167–173, https://doi.org/10.1016/j.catena.2016.04.009, 2016.

Cao, J., Wang, B., and Ma, L.: Attribution of Global Monsoon Response to the Last Glacial Maximum Forcings, J. Clim., 32, 6589–6605, https://doi.org/10.1175/jcli-d-18-0871.1, 2019.

Charman, D. J., Beilman, D. W., Blaauw, M., Booth, R. K., Brewer, S., Chambers, F. M., Christen, J. A., Gallego-Sala, A., Harrison, S. P., Hughes, P. D., Jackson, S. T., Korhola, A., Mauquoy, D., Mitchell, F. J., Prentice, I. C., Van Der Linden, M., De Vleeschouwer, F., Yu, Z. C., Alm, J., Bauer, I. E., Corish, Y. M., Garneau, M., Hohl, V., Huang, Y., Karofeld, E., Le Roux, G., Loisel, J., Moschen, R., Nichols, J. E., Nieminen, T. M., MacDonald, G. M., Phadtare, N. R., Rausch, N., Sillasoo, U., Swindles, G. T., Tuittila, E. S., Ukonmaanaho, L., Väliranta, M., Van Bellen, S., Van Geel, B., Vitt, D. H., and Zhao, Y.: Climate-related changes in peatland carbon accumulation during the last millennium, Biogeosciences, 10, 929–944, https://doi.org/10.1016/j.protis.2013.07.005, 2013.

Chaudhary, N., Miller, P. A., and Smith, B.: Modelling past, present and future peatland carbon accumulation across the pan-Arctic region, Biogeosciences, 14, 4023–4044, https://doi.org/10.5194/bg-14-4023-2017, 2017a.

Chaudhary, N., Miller, P. A., and Smith, B.: Modelling Holocene peatland dynamics with an individual-based dynamic vegetation model, Biogeosciences, 14, 2571–2596, https://doi.org/10.5194/bg-14-2571-2017, 2017b.

Cobb, A. R. and Harvey, C. F.: Scalar Simulation and Parameterization of Water Table Dynamics in Tropical Peatlands, Water Resour. Res., 55, 9351–9377, https://doi.org/10.1029/2019WR025411, 2019.

Cresto Aleina, F., Runkle, B. R., Kleinen, T., Kutzbach, L., Schneider, J., and Brovkin, V.: Modeling micro-topographic controls on boreal peatland hydrology and methane fluxes, Biogeosciences, 12, 5689–5704, https://doi.org/10.5194/bg-12-5689-2015, 2015.

Dargie, G. C., Lewis, S. L., Lawson, I. T., Mitchard, E. T., Page, S. E., Bocko, Y. E., and Ifo, S. A.: Age, extent and carbon storage of the central Congo Basin peatland complex, Nature, 542, 86–90, https://doi.org/10.1038/nature21048, 2017.

Dommain, R., Couwenberg, J., and Joosten, H.: Development and carbon sequestration of tropical peat domes in south-east Asia: Links to post-glacial sea-level changes and Holocene climate variability, Quaternary Sci. Rev., 30, 999–1010, https://doi.org/10.1016/j.quascirev.2011.01.018, 2011.

Dommain, R., Couwenberg, J., Glaser, P. H., Joosten, H., and Suryadiputra, I. N. N.: Carbon storage and release in Indonesian peatlands since the last deglaciation, Quaternary Sci. Rev., 97, 1–32, https://doi.org/10.1016/j.quascirev.2014.05.002, 2014.

Dommain, R., Frolking, S., Jeltsch-Thömmes, A., Joos, F., Couwenberg, J., and Glaser, P. H.: A radiative forcing analysis of tropical peatlands before and after their conversion to agricultural plantations, Glob. Change Biol., 24, 5518–5533, https://doi.org/10.1111/gcb.14400, 2018.

Elsig, J., Schmitt, J., Leuenberger, D., Schneider, R., Eyer, M., Leuenberger, M., Joos, F., Fischer, H., and Stocker, T. F.: Stable isotope constraints on Holocene carbon cycle changes from an Antarctic ice core, Nature, 461, 507–510, https://doi.org/10.1038/nature08393, 2009.

Eyring, V., Bony, S., Meehl, G. A., Senior, C. A., Stevens, B., Stouffer, R. J., and Taylor, K. E.: Overview of the Coupled Model Intercomparison Project Phase 6 (CMIP6) experimental design and organization, Geosci. Model Dev., 9, 1937–1958, https://doi.org/10.5194/gmd-9-1937-2016, 2016.

Ferretto, A., Brooker, R., Aitkenhead, M., Matthews, R., and Smith, P.: Potential carbon loss from Scottish peatlands under climate change, Reg. Environ. Chang., 19, 2101–2111, https://doi.org/10.1007/s10113-019-01550-3, 2019.

Frolking, S. and Roulet, N. T.: Holocene radiative forcing impact of northern peatland carbon accumulation and methane emissions, Glob. Change Biol., 13, 1079–1088, https://doi.org/10.1111/j.1365-2486.2007.01339.x, 2007.

Frolking, S., Roulet, N. T., Tuittila, E., Bubier, J. L., Quillet, A., Talbot, J., and Richard, P. J. H.: A new model of Holocene peatland net primary production, decomposition, water balance, and peat accumulation, Earth Syst. Dynam., 1, 1–21, https://doi.org/10.5194/esd-1-1-2010, 2010.

Gajewski, K., Viau, A., Sawada, M., Atkinson, L. J., and Wilson, S.: Sphagnum peatland distribution in North America and Eurasia during the past 21 000 years, Carbon NY, 15, 297–310, 2001.

Gallego-Sala, A. V., Charman, D. J., Harrison, S. P., Li, G., and Prentice, I. C.: Climate-driven expansion of blanket bogs in Britain during the Holocene, Clim. Past, 12, 129–136, https://doi.org/10.5194/cp-12-129-2016, 2016.

Gallego-Sala, A. V., Charman, D. J., Brewer, S., Page, S. E., Colin Prentice, I., Friedlingstein, P., Moreton, S., Amesbury, M. J., Beilman, D. W., Bjamp, S., Blyakharchuk, T., Bochicchio, C., Booth, R. K., Bunbury, J., Camill, P., Carless, D., Chimner, R. A., Clifford, M., Cressey, E., Courtney-Mustaphi, C., ois Vleeschouwer, Jong, R., Fialkiewicz-Koziel, B., Finkelstein, S. A., Garneau, M., Githumbi, E., Hribjlan, J., Holmquist, J., M Hughes, P. D., Jones, C., Jones, M. C., Karofeld, E., Klein, E. S., Kokfelt, U., Korhola, A., Lacourse, T., Roux, G., Lamentowicz, M., Large, D., Lavoie, M., Loisel, J., Mackay, H., MacDonald, G. M., Makila, M., Magnan, G., Marchant, R., Marcisz, K., Martamp, A., nez Cortizas, Massa, C., Mathijssen, P., Mauquoy, D., Mighall, T., G Mitchell, F. J., Moss, P., Nichols, J., Oksanen, P. O., Orme, L., Packalen, M. S., Robinson, S., Roland, T. P., Sanderson, N. K., Britta Sannel, A. K., Steinberg, N., Swindles, G. T., Edward Turner, T., Uglow, J., Vamp, M., Bellen, S., Linden, M., Geel, B., Wang, G., Yu, Z., Zaragoza-Castells, J., and Zhao, Y.: Latitudinal limits to the predicted increase of the peatland carbon sink with warming, Nat. Clim. Change, 8, 907–914, https://doi.org/10.1038/s41558-018-0271-1, 2018.

Gorham, E.: The Development of Peat Lands, Q. Rev. Biol., 32, 145–166, https://doi.org/10.1086/401755, 1957.

Gorham, E.: Northern Peatlands: Role in the Carbon Cycle and Probable Responses to Climatic Warming, Ecol. Appl., 1, 182–195, https://doi.org/10.2307/1941811, 1991.

Gorham, E., Lehman, C., Dyke, A., Janssens, J., and Dyke, L.: Temporal and spatial aspects of peatland initiation following deglaciation in North America, Quaternary Sci. Rev., 26, 300–311, https://doi.org/10.1016/j.quascirev.2006.08.008, 2007.

Gorham, E., Lehman, C., Dyke, A., Clymo, D., and Janssens, J.: Long-term carbon sequestration in North American peatlands, Quateranry Sci. Rev., 58, 77–82, https://doi.org/10.1016/j.quascirev.2012.09.018, 2012.

Gumbricht, T., Roman-Cuesta, R. M., Verchot, L., Herold, M., Wittmann, F., Householder, E., Herold, N., and Murdiyarso, D.: An expert system model for mapping tropical wetlands and peatlands reveals South America as the largest contributor, Glob. Change Biol., 23, 3581–3599, https://doi.org/10.1111/gcb.13689, 2017.

Hakim, G. J., Emile-Geay, J., Steig, E. J., Noone, D., Anderson, D. M., Tardif, R., Steiger, N., and Perkins, W. A.: The last millennium climate reanalysis project: Framework and first results, J. Geophys. Res., 121, 6745–6764, https://doi.org/10.1002/2016JD024751, 2016.

Halsey, L. A., Vitt, D. H., Gignac, L. D., Bryologist, T., and Summer, N.: Sphagnum-Dominated Peatlands in North America since the Last Glacial Maximum : Their Occurrence and Extent Sphagnum-dominated Peatlands in North America Since the Last Glacial Maximum: Their Occurrence and Extent, Bryologist, 103, 334–352, 2000.

Hanebuth, T. J., Voris, H. K., Yokoyama, Y., Saito, Y., and Okuno, J.: Formation and fate of sedimentary depocentres on Southeast Asia's Sunda Shelf over the past sea-level cycle and biogeographic implications, Earth-Sci. Rev., 104, 92–110, https://doi.org/10.1016/j.earscirev.2010.09.006, 2011.

Harrison, S. P., Bartlein, P. J., Brewer, S., Prentice, I. C., Boyd, M., Hessler, I., Holmgren, K., Izumi, K., and Willis, K.: Climate model benchmarking with glacial and mid-Holocene climates, Clim. Dynam., 43, 671–688, https://doi.org/10.1007/s00382-013-1922-6, 2014.

He, F.: Simulating Transient Climate Evolution of the Last deglaciation with CCSM3, Ph. d., University of Wisconsin-Madison, 2011.

Henton, J. A., Craymer, M. R., Ferland, R., Dragert, H., Mazzotti, S., and Forbes, D. L.: C Rustal Motion and Deformation, Geomatica, 60, 173–191, 2006.

Hooijer, A., Page, S., Canadell, J. G., Silvius, M., Kwadijk, J., Wösten, H., and Jauhiainen, J.: Current and future CO_2 emissions from drained peatlands in Southeast Asia, Biogeosciences, 7, 1505–1514, https://doi.org/10.5194/bg-7-1505-2010, 2010.

Houghton, R. A. and Nassikas, A. A.: Global and regional fluxes of carbon from land use and land cover change 1850–2015, Global Biogeochem. Cy., 31, 456–472, https://doi.org/10.1002/2016GB005546, 2017.

Illés, G., Sutikno, S., Szatmári, G., Sandhyavitri, A., Pásztor, L., Kristijono, A., Molnár, G., Yusa, M., and Székely, B.: Facing the peat CO_2 threat: digital mapping of Indonesian peatlands – a proposed methodology and its application, J. Soils Sediments, 19, 3663–3678, https://doi.org/10.1007/s11368-019-02328-0, 2019.

Ivanovic, R. F., Gregoire, L. J., Kageyama, M., Roche, D. M., Valdes, P. J., Burke, A., Drummond, R., Peltier, W. R., and Tarasov, L.: Transient climate simulations of the deglaciation 21-9 thousand years before present (version 1) – PMIP4 Core experiment design and boundary conditions, Geosci. Model Dev., 9, 2563–2587, https://doi.org/10.5194/gmd-9-2563-2016, 2016.

Jeltsch-Thömmes, A., Battaglia, G., Cartapanis, O., Jaccard, S. L., and Joos, F.: Low terrestrial carbon storage at the Last Glacial

Maximum: Constraints from multi-proxy data, Clim. Past, 15, 849–879, https://doi.org/10.5194/cp-15-849-2019, 2019.

Joos, F. and Spahni, R.: Rates of change in natural and anthropogenic radiative forcing over the past 20,000 years, P. Natl. Acad. Sci. USA, 105, 1425–1430, https://doi.org/10.1073/pnas.0707386105, 2008.

Kageyama, M., Albani, S., Braconnot, P., Harrison, S. P., Hopcroft, P. O., Ivanovic, R. F., Lambert, F., Marti, O., Peltier, W. R., Peterschmitt, J.-Y., Roche, D. M., Tarasov, L., Zhang, X., Brady, E. C., Haywood, A. M., LeGrande, A. N., Lunt, D. J., Mahowald, N. M., Mikolajewicz, U., Nisancioglu, K. H., Otto-Bliesner, B. L., Renssen, H., Tomas, R. A., Zhang, Q., Abe-Ouchi, A., Bartlein, P. J., Cao, J., Li, Q., Lohmann, G., Ohgaito, R., Shi, X., Volodin, E., Yoshida, K., Zhang, X., and Zheng, W.: The PMIP4 contribution to CMIP6 – Part 4: Scientific objectives and experimental design of the PMIP4-CMIP6 Last Glacial Maximum experiments and PMIP4 sensitivity experiments, Geosci. Model Dev., 10, 4035–4055, https://doi.org/10.5194/gmd-10-4035-2017, 2017.

Kaplan, J. O.: Wetlands at the Last Glacial Maximum: Distribution and methane emissions, Geophys. Res. Lett., 29, 3-1–3-4, https://doi.org/10.1029/2001GL013366, 2002.

Kleinen, T., Brovkin, V., and Schuldt, R. J.: A dynamic model of wetland extent and peat accumulation: Results for the Holocene, Biogeosciences, 9, 235–248, https://doi.org/10.5194/bg-9-235-2012, 2012.

Korhola, A., Ruppel, M., Seppä, H., Väliranta, M., Virtanen, T., and Weckström, J.: The importance of northern peatland expansion to the late-Holocene rise of atmospheric methane, Quaternanry Sci. Rev., 29, 611–617, https://doi.org/10.1016/j.quascirev.2009.12.010, 2010.

Kremenetski, K. V., Velichko, A. A., Borisova, O. K., MacDonald, G. M., Smith, L. C., Frey, K. E., and Orlova, L. A.: Peatlands of the Western Siberian lowlands: Current knowledge on zonation, carbon content and Late Quaternary history, Quaternary Sci. Rev., 22, 703–723, https://doi.org/10.1016/S0277-3791(02)00196-8, 2003.

Kreuzburg, M., Ibenthal, M., Janssen, M., Rehder, G., Voss, M., Naumann, M., and Feldens, P.: Sub-marine Continuation of Peat Deposits From a Coastal Peatland in the Southern Baltic Sea and its Holocene Development, Front. Earth Sci., 6, 103 pp., https://doi.org/10.3389/feart.2018.00103, 2018.

Kurnianto, S., Warren, M., Talbot, J., Kauffman, B., Murdiyarso, D., and Frolking, S.: Carbon accumulation of tropical peatlands over millennia: A modeling approach, Glob. Change Biol., 21, 431–444, https://doi.org/10.1111/gcb.12672, 2015.

Lähteenoja, O., Reátegui, Y. R., Räsänen, M., Torres, D. D. C., Oinonen, M., and Page, S.: The large Amazonian peatland carbon sink in the subsiding Pastaza-Marañón foreland basin, Peru, Glob. Change Biol., 18, 164–178, https://doi.org/10.1111/j.1365-2486.2011.02504.x, 2012.

LAI, D.: Methane Dynamics in Northern Peatlands: A Review, Pedosphere, 19, 409–421, https://doi.org/10.1016/S1002-0160(09)00003-4, 2009.

Largeron, C., Krinner, G., Ciais, P., and Brutel-Vuilmet, C.: Implementing northern peatlands in a global land surface model: Description and evaluation in the ORCHIDEE high-latitude version model (ORC-HL-PEAT), Geosci. Model Dev., 11, 3279–3297, https://doi.org/10.5194/gmd-11-3279-2018, 2018.

Lawrence, D. M. and Slater, A. G.: Incorporating organic soil into a global climate model, Clim. Dynam., 30, 145–160, https://doi.org/10.1007/s00382-007-0278-1, 2008.

Lawson, I. T., Kelly, T. J., Aplin, P., Boom, A., Dargie, G., Draper, F. C., Hassan, P. N., Hoyos-Santillan, J., Kaduk, J., Large, D., Murphy, W., Page, S. E., Roucoux, K. H., Sjögersten, S., Tansey, K., Waldram, M., Wedeux, B. M., and Wheeler, J.: Improving estimates of tropical peatland area, carbon storage, and greenhouse gas fluxes, Wetl. Ecol. Manag., 23, 327–346, https://doi.org/10.1007/s11273-014-9402-2, 2015.

Leifeld, J., Wüst-Galley, C., and Page, S.: Intact and managed peatland soils as a source and sink of GHGs from 1850 to 2100, Nat. Clim. Change, 9, 945–947, https://doi.org/10.1038/s41558-019-0615-5, 2019.

Leng, L. Y., Ahmed, O. H., and Jalloh, M. B.: Brief review on climate change and tropical peatlands, Geosci. Front., 10, 373–380, https://doi.org/10.1016/j.gsf.2017.12.018, 2019.

Lienert, S. and Joos, F.: A Bayesian ensemble data assimilation to constrain model parameters and land-use carbon emissions, Biogeosciences, 15, 2909–2930, https://doi.org/10.5194/bg-15-2909-2018, 2018.

Lindsay, R.: Peatland Classification, in: The Wetland Book, Springer Netherlands, Dordrecht, 1515–1528, https://doi.org/10.1007/978-90-481-9659-3_341, 2018.

Liu, Z., Otto-Bliesner, B. L., He, F., Brady, E. C., Tomas, R., Clark, P. U., Carlson, A. E., Lynch-Stieglitz, J., Curry, W., Brook, E., Erickson, D., Jacob, R., Kutzbach, J., and Cheng, J.: Transient simulation of last deglaciation with a new mechanism for bolling-allerod warming, Science, 325, 310–314, https://doi.org/10.1126/science.1171041, 2009.

Liu, Z., Zhu, J., Rosenthal, Y., Zhang, X., Otto-Bliesner, B. L., Timmermann, A., Smith, R. S., Lohmann, G., Zheng, W., and Timm, O. E.: The Holocene temperature conundrum, P. Natl. Acad. Sci. USA, 111, E3501–E3505, https://doi.org/10.1073/pnas.1407229111, 2014.

Loisel, J., van Bellen, S., Pelletier, L., Talbot, J., Hugelius, G., Karran, D., Yu, Z., Nichols, J., and Holmquist, J.: Insights and issues with estimating northern peatland carbon stocks and fluxes since the Last Glacial Maximum, Earth-Sci. Rev., 165, 59–80, https://doi.org/10.1016/j.earscirev.2016.12.001, 2017.

Lora, J. M. and Ibarra, D. E.: The North American hydrologic cycle through the last deglaciation, Quaternary Sci. Rev., 226, 105991, https://doi.org/10.1016/j.quascirev.2019.105991, 2019.

Lora, J. M. and Lora, J. M.: Components and Mechanisms of Hydrologic Cycle Changes over North America at the Last Glacial Maximum, J. Clim., 31, 7035–7051, https://doi.org/10.1175/JCLI-D-17-0544.1, 2018.

MacDonald, G. M., Beilman, D. W., Kremenetski, K. V., Sheng, Y., Smith, L. C., and Velichko, A. A.: Rapid Early Development of Circumarctic Peatlands and Atmospheric CH4 and CO2 Variations, Science, 314, 285–288, https://doi.org/10.1126/science.1131722, 2006.

Marcott, S. a., Shakun, J. D., Clark, P. U., and Mix, A. C.: A Reconstruction of Regional and Global Temperature for the Past 11,300 Years, Science, 339, 1198–1201, https://doi.org/10.1126/science.1228026, 2013.

McGee, D., Donohoe, A., Marshall, J., and Ferreira, D.: Changes in ITCZ location and cross-equatorial heat transport at the Last Glacial Maximum, Heinrich Stadial 1,

and the mid-Holocene, Earth Planet. Sc. Lett., 390, 69–79, https://doi.org/10.1016/j.epsl.2013.12.043, 2014.

Mitchell, T. D. and Jones, P. D.: An improved method of constructing a database of monthly climate observations and associated high-resolution grids, Int. J. Climatol., 25, 693–712, https://doi.org/10.1002/joc.1181, 2005.

Monnin, E., Indermühle, A., Dällenbach, A., Flückiger, J., Stauffer, B., Stocker, T. F., Raynaud, D., and Barnola, J. M.: Atmospheric CO_2 concentrations over the last glacial termination, Science, 291, 112–114, https://doi.org/10.1126/science.291.5501.112, 2001.

Moore, P. D.: The ecology of peat-forming processes: a review, Int. J. Coal Geol., 12, 89–103, https://doi.org/10.1016/0166-5162(89)90048-7, 1989.

Morris, P. J., Belyea, L. R., and Baird, A. J.: Ecohydrological feedbacks in peatland development: A theoretical modelling study, J. Ecol., 99, 1190–1201, https://doi.org/10.1111/j.1365-2745.2011.01842.x, 2011.

Morris, P. J., Baird, A. J., and Belyea, L. R.: The DigiBog peatland development model 2: ecohydrological simulations in 2D, Ecohydrology, 5, 256–268, https://doi.org/10.1002/eco.229, 2012.

Morris, P. J., Swindles, G. T., Valdes, P. J., Ivanovic, R. F., Gregoire, L. J., Smith, M. W., Tarasov, L., Haywood, A. M., and Bacon, K. L.: Global peatland initiation driven by regionally asynchronous warming, P. Natl. Acad. Sci. USA, 115, 4851–4856, https://doi.org/10.1073/pnas.1717838115, 2018.

Nichols, J. E. and Peteet, D. M.: Rapid expansion of northern peatlands and doubled estimate of carbon storage, Nat. Geosci., 12, 917–922, https://doi.org/10.1038/s41561-019-0454-z, 2019.

Packalen, M. S., Finkelstein, S. A., and McLaughlin, J. W.: Carbon storage and potential methane production in the Hudson Bay Lowlands since mid-Holocene peat initiation, Nat. Commun., 5, 1–8, https://doi.org/10.1038/ncomms5078, 2014.

Page, S. and Baird, A.: Peatlands and Global Change: Response and Resilience, Ssrn, Annu. Rev. Environ. Res., 41, 35–57, https://doi.org/10.1146/annurev-environ-110615-085520, 2016.

Page, S. E., Rieley, J. O., and Banks, C. J.: Global and regional importance of the tropical peatland carbon pool, Glob. Change Biol., 17, 798–818, https://doi.org/10.1111/j.1365-2486.2010.02279.x, 2011.

Peltier, W.: Global glacial isostasy and the surface of the ice-age earth: The ICE-5G (VM2) Model and GRACE, Annu. Rev. Earth Pl. Sc., 32, 111–149, https://doi.org/10.1146/annurev.earth.32.082503.144359, 2004.

Qiu, C., Zhu, D., Ciais, P., Guenet, B., Krinner, G., Peng, S., Aurela, M., Bernhofer, C., Brümmer, C., Bret-Harte, S., Chu, H., Chen, J., Desai, A. R., Dušek, J., Euskirchen, E. S., Fortuniak, K., Flanagan, L. B., Friborg, T., Grygoruk, M., Gogo, S., Grünwald, T., Hansen, B. U., Holl, D., Humphreys, E., Hurkuck, M., Kiely, G., Klatt, J., Kutzbach, L., Largeron, C., Laggoun-Défarge, F., Lund, M., Lafleur, P. M., Li, X., Mammarella, I., Merbold, L., Nilsson, M. B., Olejnik, J., Ottosson-Löfvenius, M., Oechel, W., Parmentier, F. J. W., Peichl, M., Pirk, N., Peltola, O., Pawlak, W., Rasse, D., Rinne, J., Shaver, G., Peter Schmid, H., Sottocornola, M., Steinbrecher, R., Sachs, T., Urbaniak, M., Zona, D., and Ziemblinska, K.: ORCHIDEE-PEAT (revision 4596), a model for northern peatland CO_2, water, and energy fluxes on daily to annual scales, Geosci. Model Dev., 11, 497–519, https://doi.org/10.5194/gmd-11-497-2018, 2018.

Qiu, C., Zhu, D., Ciais, P., Guenet, B., Peng, S., Krinner, G., Tootchi, A., Ducharne, A., and Hastie, A.: Modelling northern peatland area and carbon dynamics since the Holocene with the ORCHIDEE-PEAT land surface model (SVN r5488), Geosci. Model Dev., 12, 2961–2982, https://doi.org/10.5194/gmd-12-2961-2019, 2019.

Randerson, J. T., van der Werf, G. R., Giglio, L., Collatz, G. J., and Kasibhatla, P. S.: Global Fire Emissions Database, Version 4 (GFEDv4), https://doi.org/10.3334/ORNLDAAC/1293, 2015.

Rasmussen, S. O., Bigler, M., Blockley, S. P., Blunier, T., Buchardt, S. L., Clausen, H. B., Cvijanovic, I., Dahl-Jensen, D., Johnsen, S. J., Fischer, H., Gkinis, V., Guillevic, M., Hoek, W. Z., Lowe, J. J., Pedro, J. B., Popp, T., Seierstad, I. K., Steffensen, J. P., Svensson, A. M., Vallelonga, P., Vinther, B. M., Walker, M. J., Wheatley, J. J., and Winstrup, M.: A stratigraphic framework for abrupt climatic changes during the Last Glacial period based on three synchronized Greenland ice-core records: refining and extending the INTIMATE event stratigraphy, Quaternary Sci. Rev., 106, 14–28, https://doi.org/10.1016/j.quascirev.2014.09.007, 2014.

Ritz, S. P., Stocker, T. F., Grimalt, J. O., Menviel, L., and Timmermann, A.: Estimated strength of the Atlantic overturning circulation during the last deglaciation, Nat. Geosci., 6, 208–212, https://doi.org/10.1038/ngeo1723, 2013.

Ruppel, M., Väliranta, M., Virtanen, T., and Korhola, A.: Post-glacial spatiotemporal peatland initiation and lateral expansion dynamics in North America and northern Europe, Holocene, 23, 1596–1606, https://doi.org/10.1177/0959683613499053, 2013.

Rydin, H. and Jeglum, J. K.: The Biology of Peatlands, Oxford University Press, https://doi.org/10.1093/acprof:osobl/9780199602995.001.0001, 2013.

Samartin, S., Heiri, O., Joos, F., Renssen, H., Franke, J., Brönnimann, S., and Tinner, W.: Warm Mediterranean mid-Holocene summers inferred from fossil midge assemblages, Nat. Geosci., 10, 207–212, https://doi.org/10.1038/ngeo2891, 2017.

Schmittner, A., Urban, N. M., Shakun, J. D., Mahowald, N. M., Clark, P. U., Bartlein, P. J., Mix, A. C., and Rosell-Mele, A.: Climate Sensitivity Estimated from Temperature Reconstructions of the Last Glacial Maximum, Science, 334, 1385–1388, https://doi.org/10.1126/science.1203513, 2011.

Schuldt, R. J., Brovkin, V., Kleinen, T., and Winderlich, J.: Modelling Holocene carbon accumulation and methane emissions of boreal wetlands-an Earth system model approach, Biogeosciences, 10, 1659–1674, https://doi.org/10.5194/bg-10-1659-2013, 2013.

Shakun, J. D. and Carlson, A. E.: A global perspective on Last Glacial Maximum to Holocene climate change, Quaternary Sci. Rev., 29, 1801–1816, https://doi.org/10.1016/j.quascirev.2010.03.016, 2010.

Shi, J. and Yan, Q.: Evolution of the Asian–African Monsoonal Precipitation over the last 21 kyr and the Associated Dynamic Mechanisms, J. Clim., 32, 6551–6569, https://doi.org/10.1175/jcli-d-19-0074.1, 2019.

Silvestri, S., Knight, R., Viezzoli, A., Richardson, C. J., Anshari, G. Z., Dewar, N., Flanagan, N., and Comas, X.: Quantification of Peat Thickness and Stored Carbon at the Landscape Scale in Tropical Peatlands: A Comparison of Airborne Geophysics and

an Empirical Topographic Method, J. Geophys. Res.-Earth, 124, 3107–3123, https://doi.org/10.1029/2019JF005273, 2019.

Sitch, S., Smith, B., Prentice, I. C., Arneth, A., Bondeau, A., Cramer, W., Kaplan, J. O., Levis, S., Lucht, W., Sykes, M. T., Thonicke, K., and Venevsky, S.: Evaluation of ecosystem dynamics, plant geography and terrestrial carbon cycling in the LPJ dynamic global vegetation model, Glob. Change Biol., 9, 161–185, https://doi.org/10.1046/j.1365-2486.2003.00569.x, 2003.

Spahni, R., Joos, F., Stocker, B. D., Steinacher, M., and Yu, Z. C.: Transient simulations of the carbon and nitrogen dynamics in northern peatlands: From the Last Glacial Maximum to the 21st century, Clim. Past, 9, 1287–1308, https://doi.org/10.5194/cp-9-1287-2013, 2013.

Stocker, B. D., Roth, R., Joos, F., Spahni, R., Steinacher, M., Zaehle, S., Bouwman, L., Xu-Ri, and Prentice, I. C.: Multiple greenhouse-gas feedbacks from the land biosphere under future climate change scenarios, Nat. Clim. Change, 3, 666–672, https://doi.org/10.1038/nclimate1864, 2013.

Stocker, B. D., Spahni, R., and Joos, F.: DYPTOP: A cost-efficient TOPMODEL implementation to simulate sub-grid spatio-temporal dynamics of global wetlands and peatlands, Geosci. Model Dev., 7, 3089–3110, https://doi.org/10.5194/gmd-7-3089-2014, 2014.

Stocker, B. D., Yu, Z., Massa, C., and Joos, F.: Holocene peatland and ice-core data constraints on the timing and magnitude of CO2 emissions from past land use, P. Natl. Acad. Sci. USA, 114, 1492–1497, https://doi.org/10.1073/pnas.1613889114, 2017.

Stocker, T. F. and Johnsen, S. J.: A minimum thermodynamic model for the bipolar seesaw, Paleoceanography, 18, 1–9, https://doi.org/10.1029/2003PA000920, 2003.

Sun, Q., Miao, C., Duan, Q., Ashouri, H., Sorooshian, S., and Hsu, K.: A Review of Global Precipitation Data Sets: Data Sources, Estimation, and Intercomparisons, Rev. Geophys., 56, 79–107, https://doi.org/10.1002/2017RG000574, 2018.

Swindles, G. T., Morris, P. J., Mullan, D., Watson, E. J., Turner, T. E., Roland, T. P., Amesbury, M. J., Kokfelt, U., Schoning, K., Pratte, S., Gallego-Sala, A., Charman, D. J., Sanderson, N., Garneau, M., Carrivick, J. L., Woulds, C., Holden, J., Parry, L., and Galloway, J. M.: The long-term fate of permafrost peatlands under rapid climate warming, Sci. Rep., 5, 1–6, https://doi.org/10.1038/srep17951, 2015.

Swinnen, W., Broothaerts, N., and Verstraeten, G.: Modelling long-term blanket peatland development in eastern Scotland, Biogeosciences, 16, 3977–3996, https://doi.org/10.5194/bg-16-3977-2019, 2019.

Talbot, J., Richard, P., Roulet, N., and Booth, R.: Assessing long-term hydrological and ecological responses to drainage in a raised bog using paleoecology and a hydrosequence, J. Veg. Sci., 21, 143–156, https://doi.org/10.1111/j.1654-1103.2009.01128.x, 2010.

Tardif, R., Hakim, G. J., Perkins, W. A., Horlick, K. A., Erb, M. P., Emile-Geay, J., Anderson, D. M., Steig, E. J., and Noone, D.: Last Millennium Reanalysis with an expanded proxy database and seasonal proxy modeling, Clim. Past, 15, 1251–1273, https://doi.org/10.5194/cp-15-1251-2019, 2019.

Tarnocai, C., Canadell, J. G., Schuur, E. A. G., Kuhry, P., Mazhitova, G., and Zimov, S.: Soil organic carbon pools in the northern circumpolar permafrost region, Global Biogeochem. Cy., 23, 1–11, https://doi.org/10.1029/2008GB003327, 2009.

Tchilinguirian, P., Morales, M., Oxman, B., Lupo, L., Olivera, D., and Yacobaccio, H.: Early to Middle Holocene transition in the Pastos Chicos record, dry Puna of Argentina, Quaternary Int., 330, 171–182, https://doi.org/10.1016/j.quaint.2012.03.006, 2014.

Tipping, R.: Holocene evolution of a lowland Scottish landscape: Kirkpatrick Fleming, Part I, peat- and pollen-stratigraphic evidence for raised moss development and climatic change, Holocene, 5, 69–81, https://doi.org/10.1177/095968369500500108, 1995.

Treat, C. C., Kleinen, T., Broothaerts, N., Dalton, A. S., Dommain, R., Douglas, T. A., Drexler, J. Z., Finkelstein, S. A., Grosse, G., Hope, G., Hutchings, J., Jones, M. C., Kuhry, P., Lacourse, T., Lähteenoja, O., Loisel, J., Notebaert, B., Payne, R. J., Peteet, D. M., Sannel, A. B. K., Stelling, J. M., Strauss, J., Swindles, G. T., Talbot, J., Tarnocai, C., Verstraeten, G., Williams, C. J., Xia, Z., Yu, Z., Väliranta, M., Hättestrand, M., Alexanderson, H., and Brovkin, V.: Widespread global peatland establishment and persistence over the last 130,000 y, P. Natl. Acad. Sci. USA, 116, 201813305, https://doi.org/10.1073/pnas.1813305116, 2019.

Turunen, J., Tolonen, K., Tomppo, E., and Reinikainen, A.: Estimating carbon accumulation rates of undrained mires in Finland – Application to boreal and subarctic regions, Holocene, 12, 69–80, https://doi.org/10.1191/0959683602hl522rp, 2002.

Wang, S., Zhuang, Q., Lähteenoja, O., Draper, F. C., and Cadillo-Quiroz, H.: Potential shift from a carbon sink to a source in Amazonian peatlands under a changing climate, P. Natl. Acad. Sci. USA, 115, 12407–12412, https://doi.org/10.1073/pnas.1801317115, 2018.

Wania, R., Ross, I., and Prentice, I. C.: Integrating peatlands and permafrost into a dynamic global vegetation model: 2. Evaluation and sensitivity of vegetation and carbon cycle processes, Global Biogeochem. Cy., 23, https://doi.org/10.1029/2008GB003413, 2009a.

Wania, R., Ross, L., and Prentice, I. C.: Integrating peatlands and permafrost into a dynamic global vegetation model: 1. Evaluation and sensitivity of physical land surface processes, Global Biogeochem. Cy., 23, 1–19, https://doi.org/10.1029/2008GB003412, 2009b.

Xu, J., Morris, P. J., Liu, J., and Holden, J.: PEATMAP: Refining estimates of global peatland distribution based on a meta-analysis, CATENA, 160, 134–140, https://doi.org/10.1016/j.catena.2017.09.010, 2018.

Xu-Ri, Prentice, I. C., Spahni, R., and Niu, H. S.: Modelling terrestrial nitrous oxide emissions and implications for climate feedback, New Phytol., 196, 472–488, https://doi.org/10.1111/j.1469-8137.2012.04269.x, 2012.

Yu, Z.: Holocene carbon flux histories of the world's peatlands: Global carbon-cycle implications, Holocene, 21, 761–774, https://doi.org/10.1177/0959683610386982, 2011.

Yu, Z.: No support for carbon storage of >1000 GtC in northern peatlands Comment on the paper by Nichols & Peteet (2019) in Nature Geoscience (12: 917–921), Nat. Geosci., in review, https://doi.org/10.31223/osf.io/hynm7, 2019.

Yu, Z., Loisel, J., Brosseau, D. P., Beilman, D. W., and Hunt, S. J.: Global peatland dynamics since the Last Glacial Maximum, Geophys. Res. Lett., 37, 1–5, https://doi.org/10.1029/2010GL043584, 2010.

Yu, Z., Loisel, J., Turetsky, M. R., Cai, S., Zhao, Y., Frolking, S., MacDonald, G. M., and Bubier, J. L.: Evidence for elevated emissions from high-latitude wetlands contributing to high atmospheric CH_4 concentration in the early Holocene, Global Biogeochem. Cy., 27, 131–140, https://doi.org/10.1002/gbc.20025, 2013.

Yu, Z., Loisel, J., Charman, D. J., Beilman, D. W., and Camill, P.: Holocene peatland carbon dynamics in the circum-Arctic region: An introduction, Holocene, 24, 1021–1027, https://doi.org/10.1177/0959683614540730, 2014.

Yu, Z. C.: Northern peatland carbon stocks and dynamics: A review, Biogeosciences, 9, 4071–4085, https://doi.org/10.5194/bg-9-4071-2012, 2012.

Chapter 4

Committed and projected future changes in global peatlands - continued transient model simulations since the Last Glacial Maximum

4.1 Main article

Jurek Müller and Fortunat Joos

Published in *Biogeosciences*, Volume 18, 3657-3687, 2021.

Biogeosciences, 18, 3657–3687, 2021
https://doi.org/10.5194/bg-18-3657-2021

Biogeosciences Open Access EGU

Committed and projected future changes in global peatlands – continued transient model simulations since the Last Glacial Maximum

Jurek Müller[1,2] **and Fortunat Joos**[1,2]

[1]Climate and Environmental Physics, Physics Institute, University of Bern, Bern, Switzerland
[2]Oeschger Centre for Climate Change Research, University of Bern, Bern, Switzerland

Correspondence: Jurek Müller (jurek.mueller@climate.unibe.ch)

Received: 30 March 2021 – Discussion started: 6 April 2021
Revised: 19 May 2021 – Accepted: 22 May 2021 – Published: 18 June 2021

Abstract. Peatlands are diverse wetland ecosystems distributed mostly over the northern latitudes and tropics. Globally they store a large portion of the global soil organic carbon and provide important ecosystem services. The future of these systems under continued anthropogenic warming and direct human disturbance has potentially large impacts on atmospheric CO_2 and climate.

We performed global long-term projections of peatland area and carbon over the next 5000 years using a dynamic global vegetation model forced with climate anomalies from 10 models of the Coupled Model Intercomparison Project (CMIP6) and three standard future scenarios. These projections are seamlessly continued from a transient simulation from the Last Glacial Maximum to the present to account for the full transient history and are continued beyond 2100 with constant boundary conditions.

Our results suggest short to long-term net losses of global peatland area and carbon, with higher losses under higher-emission scenarios. Large parts of today's active northern peatlands are at risk, whereas peatlands in the tropics and, in case of mitigation, eastern Asia and western North America can increase their area and carbon stocks.

Factorial simulations reveal committed historical changes and future rising temperature as the main driver of future peatland loss and increasing precipitations as the driver for regional peatland expansion.

Additional simulations forced with climate anomalies from a subset of climate models which follow the extended CMIP6 scenarios, transient until 2300, show qualitatively similar results to the standard scenarios but highlight the importance of extended transient future scenarios for long-term carbon cycle projections.

The spread between simulations forced with different climate model anomalies suggests a large uncertainty in projected peatland changes due to uncertain climate forcing.

Our study highlights the importance of quantifying the future peatland feedback to the climate system and its inclusion into future earth system model projections.

1 Introduction

Peatlands are a wetland type that is characterized by thick layers of accumulated organic matter facilitated by permanently waterlogged conditions (Moore, 1989; Blodau, 2002). Suitable conditions can vary globally and can depend on local hydrology, topography, climate, and vegetation (Gorham, 1957), resulting in multiple forms from minerotrophic fens to ombrotrophic bogs and forested tropical peat swamps (Rydin and Jeglum, 2013; Page and Baird, 2016; Lindsay, 2018). Although peatlands cover only 3 % of the global land area (Xu et al., 2018b), they have an integral role in the global carbon cycle (Gorham, 1991; Yu, 2011; Page et al., 2011). They function as long-term carbon stores holding up to a third of the total global soil organic carbon (Page et al., 2011; Yu, 2012). Most of today's peatlands formed and accumulated carbon over the last 12 000 years, driven by deglacial climate change and ice sheet retreat (e.g., Halsey et al., 2000; Gajewski et al., 2001; MacDonald et al., 2006; Gorham et al., 2007; Yu et al., 2010; Ruppel et al., 2013; Morris et al., 2018;

Treat et al., 2019; Müller and Joos, 2020). Peatlands often are at the same time long-term sinks of carbon (e.g., Gorham et al., 2012; Lähteenoja et al., 2012; Leifeld et al., 2019) as well as large natural sources of methane (e.g., Frolking and Roulet, 2007; LAI, 2009; Korhola et al., 2010; Yu et al., 2013; Packalen et al., 2014; Dommain et al., 2018). The net radiative effect over the Holocene has been a cooling (Frolking and Roulet, 2007).

Apart from their function as long-term carbon stores, and net carbon sinks, peatlands provide many more important ecosystem services (Kimmel and Mander, 2010; Page and Baird, 2016). Peatlands act as hydrological buffers providing purified drinking water (Xu et al., 2018a). As unique ecosystems, peatlands are a habitat to many rare and specialized species and thus preserve global biodiversity (Minayeva and Sirin, 2012). Culturally they can serve recreational and spiritual functions. For environmental researchers, they provide a unique archive for environmental and cultural change over millennia (de Jong et al., 2010).

Direct and indirect anthropogenic disturbances, however, have exerted increasing pressures on global peatlands, threatening their important ecosystem services and potentially putting large carbon stocks at risk (Posa et al., 2011; Goldstein et al., 2020). Direct disturbances include peatland drainage for land-use conversion and peat mining, which has led to large carbon losses in temperate and tropical regions (Hergoualc'h and Verchot, 2011; Dohong et al., 2017; Leifeld et al., 2019; Dommain et al., 2018; Hoyt et al., 2020). Low water tables after drainage also facilitate increased peat burning (Turetsky et al., 2015; Page and Hooijer, 2016). Drainage of agricultural areas can also affect neighboring unmanaged peatlands (Beauregard et al., 2020). Degradation following past land-use conversion will continue to release large amounts of carbon over decades to come (Leifeld and Menichetti, 2018). Given prompt action, this committed and additional carbon loss could be partly mitigated with large-scale restoration and re-wetting efforts (Warren et al., 2017; Nugent et al., 2019; Günther et al., 2020) in conjunction with strong protection policies (Humpenöder et al., 2020; Wibisana and Setyorini, 2021).

Indirect human disturbances are mediated through anthropogenic climate change which is rapidly changing the boundary conditions for global peatlands. Mean annual precipitation is projected to increase in regions of large peatland extent such as the northern high latitudes and Southeast Asia (Collins et al., 2013), possibly improving conditions for peatland development and carbon accumulation. However, increases in precipitation are often offset by increased evapotranspiration under a warmer climate. Temperatures are projected to disproportionately increase in the northern high latitudes (Collins et al., 2013), where the largest portion of global peatlands reside (Xu et al., 2018b). Industrial warming has already led to increases in peatland evapotranspiration (Helbig et al., 2020b), leading to a widespread drying trend in the peatlands of northern Europe (Swindles et al., 2019; Zhang et al., 2020) and eastern Canada peatlands (Pellerin and Lavoie, 2003). The water table is an important regulator in peatland ecosystems with complex feedbacks to vegetation and carbon cycling (Sawada et al., 2003; Zhong et al., 2020). A water table drawdown leads to increased fire frequency (Turetsky et al., 2015) and a shift in vegetation cover from moss-dominated to shrub- and tree-dominated (Pellerin and Lavoie, 2003; Talbot et al., 2010; Pinceloup et al., 2020; Beauregard et al., 2020). Lower water tables also lead to the exposure of progressively deeper peat layers to oxic conditions, increasing decomposition (Ise et al., 2008; Zhong et al., 2020). Higher temperatures also generally lead to higher decomposition rates with increases in both measured CO_2 (Hopple et al., 2020; Kluber et al., 2020) and methane emissions (Turetsky et al., 2014). Although some studies suggest deep peat carbon to be robust under future warming (Wilson et al., 2016). In the northern high latitudes, this might be offset by increases in plant productivity, even leading to net increases in carbon accumulation (Charman et al., 2013; Gallego-Sala et al., 2018).

About 46 % of northern peatlands are underlain by permafrost (Hugelius et al., 2020), which in some regions is quickly thawing as a response to global warming (Camill, 2005; Lara et al., 2016; Mamet et al., 2017). Permafrost thaw is projected to accelerate dramatically depending on the future scenario (Lawrence et al., 2012; Guo and Wang, 2016). Permafrost peatlands have been found to often collapse after thaw and form thermokarst landscapes and collapse-scar wetlands (Payette et al., 2004; Olefeldt et al., 2016; Magnússon et al., 2020) characterized by carbon loss and high methane emissions (Jiang et al., 2020; Voigt et al., 2019; Turetsky et al., 2020; Estop-Aragonés et al., 2020). Given sustained inundation, renewed and invigorated accumulation is assumed to set in after collapse, leading to an eventual return to a net cooling effect after decades to millennia of net warming (Swindles et al., 2015; Jones et al., 2017; Magnússon et al., 2020). However, some peatlands show an increase in carbon accumulation already directly after thaw (Estop-Aragonés et al., 2018).

Investigating the potential future trajectories of global peatlands is of great importance, given the multiple pressures on peatlands as unique ecosystems and carbon stores, which will further increase with future climate and land-use change. Although the potential feedbacks between peatlands, the carbon cycle, and the climate system could be immense, peatlands are in general still not included in state-of-the-art earth system models (ESMs) (Loisel and Bunsen, 2020), with only a few exceptions (Schuldt et al., 2013). A large part of the global carbon cycle is thus also missing in the future climate and carbon cycle projections used for the determination of international climate mitigation targets, such as the sixth phase of the Coupled Model Intercomparison Project (CMIP6) (Eyring et al., 2016). Different approaches have been used to independently project different aspects of future peatland dynamics under future scenarios. Paleo-data-driven

approaches can be used to investigate future peatland carbon accumulation rates (Gallego-Sala et al., 2018). Bioclimatic envelope models enable estimates of regional peatland area changes in blanket bogs in the United Kingdom (Gallego-Sala et al., 2016; Ferretto et al., 2019) and China (Cong et al., 2020). Process-based models provide another way to project potential futures of complex systems under changing boundary conditions. Peatland projections, however, have mostly focused on peatland area (Alexandrov et al., 2016) and peatland carbon dynamics (Spahni et al., 2013; Warren et al., 2017; Wang et al., 2018; Chaudhary et al., 2017; Voigt et al., 2019; Swinnen et al., 2019; Chaudhary et al., 2020) independently. A still limited but increasing number of dynamic global vegetation models (DGVMs) with dynamically determined peatland area (Kleinen et al., 2012; Stocker et al., 2014b; Largeron et al., 2018; Qiu et al., 2018) enables, for the first time, the projection of peatland area and carbon dynamics on a large spatial scale (Qiu et al., 2020). The focus, however, is still often put on northern boreal peatlands alone (Chaudhary et al., 2020; Qiu et al., 2020).

The dynamic simulation of peatlands is complicated by the non-trivial model spinup. Peatland initiation, expansion, and peat carbon accumulation and loss occurred at different times in different regions during the glacial termination and the Holocene as climate and environmental conditions changed. However, peat models are typically spun up uniformly for all regions, over a constant period, and by applying constant preindustrial climate and environmental (e.g., CO_2, total land area, and land-use area) conditions. This common spinup approach does not fully account for the transient and gradual evolution of peatlands, driven and constrained by transient climate evolution, ice sheet retreat, and sea-level rise (Loisel et al., 2017). In a system with long timescales such as peatlands, the system's history might be a strong determinant of future changes.

Here we present the first combined projection of global peatland area and carbon dynamics. A previously published transient simulation from the Last Glacial Maximum (LGM, 22 000 years before present) to the present (Müller and Joos, 2020) is used to base the projections on a fully transient spinup. This allows not only the consideration of all legacy effects of the transient peatland development but also the consideration of former peatlands in the carbon balance calculation. Committed and future peatland responses to three different standard future emission and land-use scenarios are investigated using the DGVM LPX-Bern. Simulations are continued with constant forcing beyond 2100 to reveal delayed long-term effects on peatlands over the next 5000 years. Standard simulations are compared to additional simulations with extended transient scenario forcing until 2300 and constant forcing thereafter. Uncertainties and drivers are analyzed using multiple climate model forcings and factorial simulations.

2 Methods

2.1 Model description

All simulations were performed with the Land surface Processes and eXchanges (LPX-Bern) dynamic global vegetation model (DGVM) version 1.4 (Lienert and Joos, 2018). The model setup is mostly identical to Müller and Joos (2020), which is briefly described below. LPX-Bern includes an interactive carbon, water, and nitrogen cycle and simulates dynamic vegetation composition with plant functional types (PFTs), which compete for water, light, and nutrients (Sitch et al., 2003; Xu-Ri et al., 2012; Spahni et al., 2013). The implementation of permafrost and peatlands as long-term carbon stores is based on the LPJ-WHyMe model (Wania et al., 2009a, b) with the addition of dynamic peatland area (Stocker et al., 2014b).

Peatland vegetation is represented by five peat plant functional types (PFTs): *Sphagnum* and flood-tolerant graminoids as indicative mostly for high-latitude peatlands, and flood-tolerant tropical evergreen, deciduous tree PFTs, and a flood-tolerant C_4 type grass as indicative mostly for tropical peatlands (Stocker et al., 2014b). Carbon cycling in peat soils is based on the distinction between a lower, fully water saturated slow overturning pool (catotelm; from 0.3 to 2 m of the soil column) and an upper, fast-overturning pool (acrotelm; upper 0.3 m of the soil column) with fluctuating water table position (WTP) (Spahni et al., 2013). Decay rates are modulated by temperature in the catotelm and by temperature and WTP in the acrotelm (Wania et al., 2009a). The size and sign of the carbon flux between acrotelm and catotelm are determined by the acrotelm carbon balance. Methane emissions from peatlands are simulated but not part of the analysis in this study.

The area fraction covered by peat in a given grid cell is determined dynamically with the DYPTOP module (Dynamical Peatland Model Based on TOPMODEL) (Stocker et al., 2014b). The TOPMODEL approach (Beven and Kirkby, 1979) is used to predict the monthly inundated area fraction given sub-grid-scale topographic information and mean grid cell WTP, averaged over all land classes. The area potentially available for peatlands is then determined by inundation persistency. Peatlands expand or shrink towards a changing potential extent with a rate of 1 % of their current grid cell fraction per year. The grid cell fraction lost during peatland retreat is treated as a separate land class for former peatlands. It inherits the carbon stocks of the shrinking peatland and is subsequently treated in the same way as the mineral soils regarding vegetation, hydrology, and carbon cycling. Growing active peatlands first expand on former peatlands inheriting the remaining carbon there. This treatment prevents carbon dissolution into mineral soils due to fluctuations in peatland area.

Different to Müller and Joos (2020) we also consider changing land-use area in our simulations. Land-use area in

the model is represented by three specific land classes: pasture, cropland, and urban (Lienert and Joos, 2018). Pastures and croplands have specific vegetation represented by two herbaceous PFTs each. Changes in land-use area are treated as net changes, where all growing land classes proportionally inherit the carbon, water, and nutrients of all shrinking land classes. A more complex implementation, which considers gross changes, exists but is not compatible with the peatland module used here (Stocker et al., 2014a). In the absence of gross change information, three assumptions were made. (1) Changes within the three land-use classes that do not affect the total land-use area are assumed as shifts between land-use types (e.g., shift from pasture to cropland). (2) Increases in total land-use area reduce all other land classes proportionally, including peatlands. (3) Peatland area that is converted to land-use area cannot be reclaimed by expanding peatlands at a later stage. These assumptions are simplifications that fail especially in areas where peatlands are preferentially targeted for land-use conversion, such as in Indonesia (Dommain et al., 2018; Hoyt et al., 2020), or are subject to restoration efforts after conversion (e.g., Haapalehto et al., 2011; Young et al., 2017). However, given the technical restrictions and the lack of detailed worldwide information about gross land-use changes on peatlands, we think this simplified approach is the most robust.

The above-described representation of peatlands in the LPX is a simplification in many respects. The absence of local processes and information such as lateral water flow, local soil features, or influence of animals by grazing and river damming can limit the ability of the TOPMODEL approach to predict peatlands on a regional to local scale. Further, direct human-caused influences such as land use, drainage, or peat mining are only considered in a strongly simplified way. The lack of a distinction and transition between different peatland types like fens, bogs, blanket bogs, or marshes neglects possible differences in the constraints on their formation and evolution. The treatment of acrotelm and catotelm as single carbon pools, and the absence of strong disturbances such as peat fires, constitute limits on the comparability of the model results to peat core carbon profiles. This simplified representation, nevertheless, has been shown to reproduce peatland area and carbon accumulation well within the observational constraints (Wania et al., 2009a; Spahni et al., 2013; Stocker et al., 2014b, 2017; Müller and Joos, 2020) while using a minimal set of free parameters.

2.2 Calculation of peat carbon

Peat carbon can be present not only in soils of active but also in the soils of former peatlands. Peat may be preserved during peatland conversion and form distinct organic soil layers on non-peatland areas (Lähteenoja et al., 2012; Broothaerts et al., 2014; Xu et al., 2016; Campos et al., 2016; Treat et al., 2019). In the model, subsequent land classes inherit the soil carbon from former peatlands, including peatlands converted to land-use areas. Yet, this peat carbon is mixed within the model's soil pools and cannot be directly distinguished from carbon transferred to soils from more recently established vegetation. It is, however, possible to track peat carbon that at one point was sequestered in the catotelm of active peatlands through the soil pools of other land classes using post processing. For this, transient model output for peatland area changes, the decay rates of slow overturning pools, and the carbon input into the catotelm of active peatlands is needed. Area changes are used to transfer carbon between active peatlands, former peatlands, land-use areas, and natural vegetation classes. Transient decay rates are used to decay the carbon in the respective pools. Carbon is thus tracked from its entry into the catotelm of an actively accumulating peatland until its decay there or in a former peatland or land-use area. This approach cannot take account of the acrotelm carbon. However, acrotelm carbon constitutes only a small part of simulated total peatland carbon (5 % at 1975), and we can assume that this carbon at the peat surface is quickly respired after peatland transformation. For the analysis, we refer to two different variables related to peat carbon: (1) *peatland carbon*, which refers to the carbon stored in the acrotelm and catotelm pools of active peatlands, and (2) *total peat carbon*, which is calculated in post-processing and represents all carbon in the catotelm of active peatlands and organic, not-yet-decomposed carbon that was at some point sequestered into a catotelm on peatlands transformed to land-use areas and other former peatlands. After ecosystem transformation, depending on the transition and the conditions thereafter, former peatlands can see a fast collapse or erosion of carbon stocks (Hoyt et al., 2020; Li et al., 2018) as well as buried peat carbon layers preserved for millennia (Treat et al., 2019). The two carbon variables can be interpreted as two bounding cases to the fate of peat carbon in former peatlands. Changes in the variable *peatland carbon* can represent a fast emission bounding case where peatland carbon is lost immediately after ecosystem or land-use transformation. The slow emission bounding case, with peat carbon decaying in former peatlands over a long timescale, can be represented by changes in the variable *total peat carbon*. The true fate of peat carbon in former peatlands in most cases will lie somewhere in between these worst- and best-case scenarios.

2.3 Simulation setup

The simulations presented here are a direct continuation of a transient simulation from the Last Glacial Maximum (LGM) to the present, which was discussed in detail in Müller and Joos (2020). This enables future projections starting from a truly transient spinup, including all potential legacy effects of the past 22 000 years. The LGM simulation was run with a model resolution of 2.5° latitude × 3.75° longitude and was forced with CO_2 (Joos and Spahni, 2008) and temperature and precipitation fields. Temperature and precip-

itation anomalies were taken from the transient CCSM3 run TraCE21k (Liu et al., 2009). The TraCE21k anomalies were imposed on the CRU TS 3.1 (Mitchell and Jones, 2005) base climate from 1960 to 1990. Interannual variability thus came from TraCE21k. Temperature anomalies were calculated as absolute and precipitation anomalies as relative values.

The resolution of the LGM simulation was adopted for the future simulations. This ensures a truly seamless transition between the simulations, without unpredictable effects of downscaling on peatland dynamics.

In the original LGM simulation, land use was not considered as the focus of the study was on the natural development and evolution of peatlands since the LGM. To integrate a transient history of land use, the simulation was restarted in the year 1500 with subsequent transient land-use forcing (Hurtt et al., 2020) and otherwise unchanged boundary conditions.

In the year 1975, the midpoint of the base climate period, forcing transitions from TraCE21k to CMIP6 climate anomalies (temperature, precipitation, and cloud cover) (O'Neill et al., 2016, see Fig. 1), whereas the base climate remains unchanged. From this point on, simulations are done for each model of a 10-member climate model ensemble (see Sect. 2.5). Short historical simulations from 1975 to 2014 bridge the gap between the LGM simulation and the start of the CMIP6 scenarios with anomalies taken from the CMIP6 historical simulation of the climate model ensemble.

Simulations corresponding to three different CMIP6 scenarios start from the year 2015. One strong-mitigation scenario (SSP1-2.6), one middle-of-the-road scenario (SSP2-4.5) and one high-emission scenario (SSP5-8.5) were selected to represent the scenario range. The standard CMIP6 scenarios end in the year 2100. To investigate the delayed long-term responses of peatlands, the forcing is extended into the future with a detrended version of the last 30 years of each time series repeated over almost 5000 years until the year 7000. The trend correction was done per grid cell and month and with respect to the end of the time series. Scenario CO_2 forcing was adopted from Meinshausen et al. (2020). Land-use forcing is taken from the Land-Use Harmonization (LUH2) project (see Fig. 2g–i, Hurtt et al., 2020).

CMIP6 also includes extended versions of the scenarios SSP1-2.6 and SSP5-8.5 that range until 2300. At the time of this study, however, only three climate models had provided output for these extended scenarios. Climate projections of these three models alone are not representative of the full CMIP6 scenario. They were, however, included in the 10-member climate model ensemble used here (see Sect. 2.5 and Fig. S1) and additional simulations with transient climate and CO_2 forcing until 2300 were performed to compare results to the standard simulations.

To disentangle future changes in peatlands that are induced by changes in climate, CO_2, and land use up to 2014 from those induced by future changes in these drivers, we performed an additional simulation with constant boundary conditions at 2014 levels for each ensemble member. Here climate forcing was extended with a detrended version of the last 30 years of the historical forcing. Similarly, a control simulation was performed with constant boundary conditions after 1500 to show the undisturbed model state. These simulations reveal the committed changes in peatland area and carbon induced by the deglacial changes prior to the preindustrial state at 1500 and the changes over the historical period until 2014 respectively.

2.4 Driver contributions

To determine the different driver contributions to the changes in peatland variables, additional factorial simulations were performed for all scenarios and climate model ensemble members. For each standard simulation, there are five factorial simulations with one of the five transient forcings (temperature, precipitation, cloud cover, CO_2, and land use) kept constant at 2014.

The driver contribution to the anomaly of peatland variables was determined as the difference between the standard run anomaly and the anomaly in the respective factorial run. The contribution from already committed changes due to past climate and land-use change was determined as the anomalies in the simulations with overall constant forcing after 2014 (see Sect. 2.3). The residual of the difference between the sum of all contributions and the standard run anomaly was identified as the contributions from non-linear interactions and other factors not considered in the analysis. Cloud cover was found to have only a minimal effect on the considered peat variables in the LPX-Bern, and thus for further analysis its contribution was added to the other/non-linear category.

As a second step, driver contributions were classified as driving contributions (same sign as peatland variable anomaly) and dampening contributions (opposite sign as peatland variable anomaly) and re-normalized respectively. Figures show only the driving contributions of the respective positive and negative peatland variable anomalies.

2.5 Climate model selection

We chose a subset of 10 climate models out of a CMIP6 ensemble of 22 models (see Figs. 2a–f and S1) that at the time (June 2020) provided monthly output for all necessary forcing variables – precipitation, near-surface temperature, and cloud cover – and for all considered experiments – historical, SSP1-2.6, SSP2-4.5, and SSP5-8.5. Climate model output was downloaded from the earth system grid database. One additional model, the Community Integrated Earth System Model (CIESM), had to be excluded from the CMIP6 ensemble as it showed a discontinuity in the precipitation data between the historical and the scenario simulations.

Three models, IPSL-CM6A-LR, MRI-ESM2-0, and CanESM5, were included in the subset a priori as they were

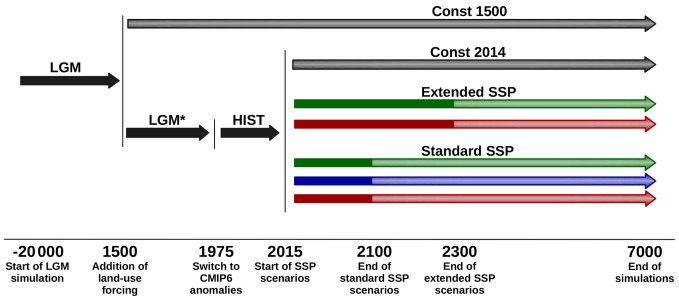

Figure 1. Diagram of the simulation setup. A transient simulation from the LGM to 1975 and with additional land-use forcing after 1500 (LGM*) is followed by short historical simulations until 2014 (HIST) and subsequent standard and extended Shared Socioeconomic Pathway (SSP) scenario simulations forced by CMIP6 climate anomalies. After the end of the transient forcing (solid arrows), SSP scenarios are continued with constant forcing (light color arrows). Additional commitment simulations with constant boundary conditions start at 1500 and 2014.

the only ones that also provided output for both of the extended SSP1-2.6 and SSP5-8.5 scenarios (see Sect. 2.3). The other seven were chosen for the ensemble subset to optimally represent the full CMIP6 ensemble as a whole. The optimization targets of ensemble total range, interquartile range, and median, were defined with respect to the anomalies (from 1961–1990 to 2071–2100) in precipitation and temperature as the most important forcings to the LPX-Bern. The optimization was inspired by McSweeney and Jones (2016). A total of 2000 randomly drawn subsets were ranked according to the distance of the subset to the targets with normalized scores calculated and averaged over all individual grid cells, months, scenarios, and variables. The rating of the best-performing subsets was further improved by a careful hand-picked combination, resulting in the final subset including the climate models referenced in Table 1.

This subset performs best when calculated both over the total land area and over the simulated peatland area alone. Over land, temperature anomaly total range, interquartile range, and median differ between the ensemble subset and the full ensemble by 0.25, −0.18, and 0.02 °C respectively, with larger distance at higher-emission scenarios. Averaged over the simulated peatland area at 1975, the distances are 0.28, −0.31, and 0.03 °C respectively. For precipitation, anomaly total range, interquartile range, and median differ between full ensemble and ensemble subset by 9.7, 0.64, and −0.15 mm over all land area and 7.3, 0.54, and −0.49 mm over the peatland area respectively. The optimization procedure thus yielded an ensemble subset representative of the full CMIP6 ensemble, although, given the number of possible combinations, optimization could be improved further with further sampling.

2.6 Present-day model state

There are still considerable uncertainties connected to estimates of the global area covered by peatlands and the amount of organic carbon stored within them. Estimates for northern peatland area, using various methods ranging from inventory based to machine learning, lie between 2.4 and 4.0 million square kilometers (Mkm^2) (Yu et al., 2010; Loisel et al., 2017; Xu et al., 2018b; Hugelius et al., 2020). For tropical peatlands, which are still much less studied than northern peatlands, peatland area estimates have increased in recent years following the discovery of large new peatland complexes, such as in the Congo Basin (Dargie et al., 2017), and due to new methodologies trying to account for potentially undiscovered peatlands (Gumbricht et al., 2017). Earlier estimates of tropical peatland area thus range from 0.37 to 0.44 Mkm^2 (Yu et al., 2010; Page et al., 2011) and more recent estimates from 1.0 to 1.7 Mkm^2 (Gumbricht et al., 2017; Xu et al., 2018b). Peatland areas simulated by LPX in the year 1975, the end of the transient simulation from the LGM, are within the range of literature estimates with a global, northern (> 30° N), and tropical (30° S to 30° N) peatland area of 3.8, 2.8, and 1.0 Mkm^2 respectively. Global peatland area is shifted more towards the tropics as in most estimates. However, most major peatland complexes seen in global peatland maps, e.g., PEATMAP (Xu et al., 2018b, see Fig. 3), are captured well. Major regional differences exist in Africa, where LPX-Bern fails to simulate the large Congo Basin peatland complex. Peatland area is also underestimated in northern Europe. In North America the model overestimates peatland area in Alaska and Quebec and underestimates peatland extent in western Canada.

Estimates of global peatland carbon are directly dependent on peatland area estimates and thus also come with a large uncertainty range. Northern peatlands have been esti-

Table 1. Ensemble of CMIP6 earth system models used to force the LPX-Bern. Output data were used for monthly precipitation, surface temperature, and cloud cover from the "r1i1p1f1" variant of the respective historical simulations and future scenarios SSP1-2.6, SSP2-4.5, and SSP5-8.5

Model	Model reference	Data reference
CAMS-CSM1-0	Rong et al. (2018)	Rong (2019a, b)
GFDL-ESM4	Dunne et al. (2020)	Krasting et al. (2018); John et al. (2018)
CanESM5	Swart et al. (2019a)	Swart et al. (2019b, c)
EC-Earth3	Döscher et al. (2021)	EC-Earth Consortium (EC-Earth) (2019a, b)
INM-CM5-0	Volodin et al. (2017)	Volodin et al. (2019a, b)
IPSL-CM6A-LR	Boucher et al. (2020)	Boucher et al. (2018, 2019)
MPI-ESM1-2-LR	Mauritsen et al. (2019)	Wieners et al. (2019b, a)
MRI-ESM2-0	Yukimoto et al. (2019a)	Yukimoto et al. (2019b, c)
KACE-1-0-G	Lee et al. (2020)	Byun et al. (2019b, a)
NorESM2-LM	Seland et al. (2020)	Seland et al. (2019a, b)

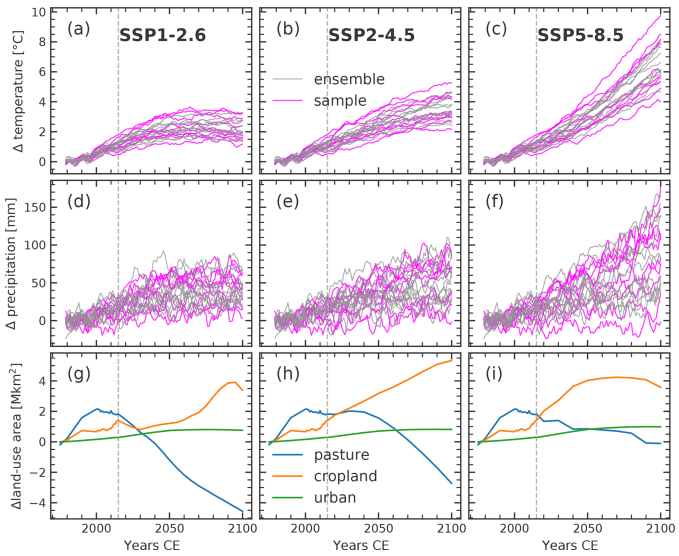

Figure 2. Global surface air temperature **(a–c)**, precipitation **(d–f)**, and land-use area **(g–i)** anomalies for the 1961-1990 average for three CMIP6 scenarios: SSP1-2.6 **(a, d, g)**, SSP2-4.5 **(b, e, h)**, SSP5-8.5 **(c, f, i)**. Magenta lines show anomalies of the climate model ensemble subset applied to force LPX-Bern versus the rest of the CMIP6 ensemble in gray. Dashed vertical gray lines show the year 2015 from which the future scenarios diverge. Pasture, cropland, and urban land-use areas amount to 31.2, 14.4, and 0.3 Mkm^2 during the 1961–1990 baseline period respectively.

mated to store 270 to 604 gigatons of carbon (GtC), using various methods and area estimates (see Yu, 2012, and Yu et al., 2014, for a review). For tropical peatlands, estimates of organic carbon storage range from 44 to 92 GtC in earlier estimates (Yu et al., 2010; Page et al., 2011) and increase as a result of larger assumed areas in recent estimates from 70 to 288 GtC (Dargie et al., 2017; Ribeiro et al., 2021). In the year 1975, peatlands simulated by the LPX-Bern have accumulated about 441 GtC of soil organic carbon globally. From this, northern and tropical peatlands make up 319 and 121 GtC respectively. Simulated carbon stocks thus lie within the literature estimates but again with a distribution shifted more towards the tropics than most estimates suggest.

Throughout the 22 000 years of the transient simulation up to the year 1975, peatland area was highly dynamic with today's peatlands gradually expanding but also

large paleo-peatlands vanishing over time (Müller and Joos, 2020). There, similarly as described in Sect. 2.2, the carbon from former peatlands was tracked through subsequent land classes until its decay. At 1975 LPX-Bern gives a total of 195 GtC of peat carbon leftover from former peatlands on land, with 165 GtC in northern latitudes and 28 GtC in the tropics. Total peat carbon is thus simulated to be 612 GtC. Very little is known about the amount and location of peat leftover and buried from former peatlands, although various deposits have been found (Treat et al., 2019). Peat carbon lost due to past or future sea-level rise is not considered in this study.

Unlike the original LGM simulation in Müller and Joos (2020), here land use and land-use change is considered since the year 1500, with land-use areas being able to expand onto peatlands (see Sect. 2.3). Up to 1975 about 0.42 Mkm^2 of peatland area and 50 GtC of peatland carbon are lost from active peatlands due to land-use change in the simulation. Carbon loss is reduced to about 5 GtC when considering total peat carbon, which does not assume an immediate loss but a slow decay in former peatlands. Leifeld et al. (2019) estimate that about 0.51 Mkm^2 of peatland area and 22 ± 5 GtC of peatland carbon was lost globally from 1850 to 2015 due to drainage and land-use conversion of peatlands, which is in rough agreement with the simulated values (see also Sect. 3.1.1).

3 Results and discussion

3.1 Historical and committed changes

3.1.1 Historical 1975–2014

The gap between the end of the transient LGM run in 1975 and the beginning of the future scenarios in 2015 is bridged by short historical simulations. These are forced with climate anomalies from the 10 ensemble climate models (see Sect. 2.3). During this short period, climate anomalies already drift apart substantially between the different climate models (see Fig. 2). Differences in climate forcing are propagated to differences in peatland responses. Averaged over 1995–2014 simulated global peatland area varies between 3.6–3.8 Mkm^2. Legacy effects and accelerating climate change lead to a reduction in peatland area with respect to 1975 in most simulations, resulting in a median of 3.7 Mkm^2. A part of this reduction (median: -0.1 Mkm^2) is also attributable to an increase in land-use area, which claims an additional 0.06 Mkm^2 from 1975 to 2014.

The respective carbon stored in global peatlands is simulated to be 423 (419–432) GtC, with changes mostly a result of the peatland area changes. Changes in total peat carbon, including carbon in former peatlands (see Sect. 2.2), also are mostly negative but small, with global peat carbon stocks at 611 (610–612) GtC.

3.1.2 Committed 2015–2300

Past changes in climate and land use have long-lasting effects on global peatlands that are superimposed on changes induced by future disturbances. To disentangle the effects of past and future changes in drivers, simulations with constant 2014 boundary conditions were made for each climate model ensemble member. These "commitment" simulations reveal the delayed response to disturbances in the past and thus represent the committed changes independent of the future scenario for climate, land use, and CO_2 (Figs. 4, 5, and S2).

In most commitment simulations, global peatland area continues to decrease and reaches a new equilibrium until 2300. Gross changes reveal, however, also regions of local peatland expansion (Fig. 4). Northeastern Canada, northern Europe, and East Asia are regions with large losses, whereas northwestern Canada, northeastern Asia, and Southeast Asia see an increase in peatland area up to 2300.

Peatland carbon decreases together with global area in most simulations, with the new peatland area showing lower carbon density as lost areas. Total peat carbon, depending on the overall balance of accumulation and decay rather than on peatland area dynamics, is changing only slightly but is declining in 8 out of 10 simulations. Taken together, the simulations suggest a small to moderate peat carbon loss to the atmosphere over the next 300 years given 2014 conditions. Uncertainties, however, are large. The spread between the simulations increases significantly after 2014 despite boundary conditions being kept constant. In the year 2300, the simulated global peatland area anomaly relative to 1995–2014 averages ranges from -13 % to $+4$ %, with a median of -4 % and interquartile range (IQR) from -6 % to -2 % (Table 2). Global carbon stored in active peatlands and global total peat carbon are simulated to change by -9 (total range: -16 to -0; IQR: -10 to -7) % and -1 (-2 to $+1$; -1 to -0) % respectively. The increasing uncertainty highlights how relatively small differences in forcing can propagate and result in large long-term ecosystem and carbon cycle uncertainties.

3.1.3 Committed after 2300

Some simulated peatland responses to historical changes in climate and land use are delayed even beyond 2300. Between about 2700 and 3500 all simulations see a rapid peatland expansion. At 3500 the global peatland area anomaly compared to 1995–2014 averages is $+8$ (-1 to $+16$; $+5$ to $+11$) %. With that, peatland area is simulated even larger than at present but with a dramatically shifted global and regional distribution. The delayed peatland expansion is limited to the northern highest latitudes and the tropics. The resulting peatland distribution at 3500 shows loss of sizable parts of today's northern peatlands, with new peatlands partly expanding into permafrost regions and the tropics.

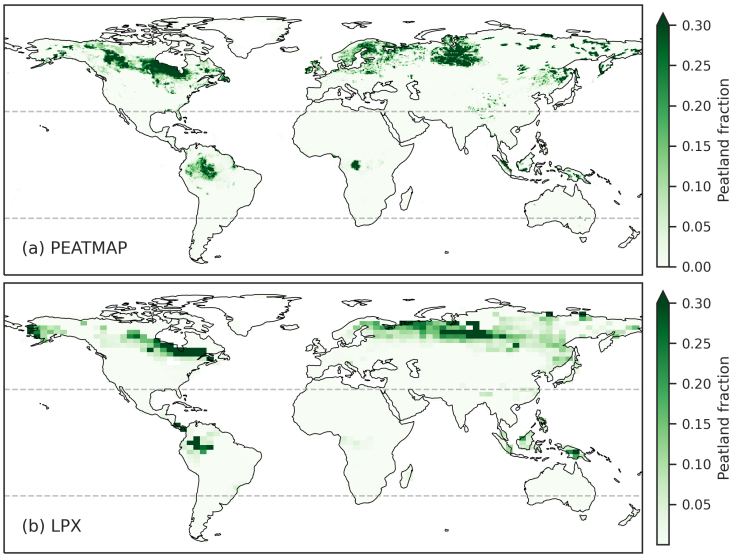

Figure 3. Global peatland area fraction as **(a)** estimated by PEATMAP (Xu et al., 2018b), shown here in a $0.5^\circ \times 0.5^\circ$ gridded version, and **(b)** simulated by LPX in the year 1975 after a transient simulation from the Last Glacial Maximum.

Table 2. Median and corresponding interquartile range (IQR) in parentheses of relative anomalies for simulated peatland area, peatland carbon, and total peat carbon as defined in Sect. 2.2. Medians and the IQR are given relative to 1995–2014 averages. IQR boundaries are listed in Table S1. Values are rounded to integer values. Northern latitudes are defined as $> 30^\circ$ N and tropical latitudes as 30° S–30° N. For the reference period, simulated median peatland area, carbon, and total peat carbon is 3.7 Mkm^2, 423 GtC, and 611 GtC for global peatlands; 2.7 Mkm^2, 301 GtC, and 500 GtC for northern peatlands; and 1 Mkm^2, 121 GtC, and 142 GtC for tropical peatlands respectively

	Δ peatland area [%]			Δ peatland carbon [%]			Δ total peat carbon [%]		
	2100	2300	3500	2100	2300	3500	2100	2300	3500
Global									
Committed	−3 (4)	−4 (4)	+8 (5)	−7 (3)	−9 (3)	+4 (6)	−0 (0)	−1 (1)	+1 (4)
SSP1−2.6	−7 (5)	−4 (17)	+16 (22)	−14 (8)	−12 (21)	+7 (26)	−0 (1)	−0 (3)	+3 (14)
SSP2−4.5	−11 (10)	−23 (19)	0 (27)	−19 (11)	−33 (22)	−17 (31)	−0 (1)	−2 (4)	−4 (18)
SSP5−8.5	−14 (9)	−29 (13)	−2 (27)	−22 (10)	−43 (16)	−29 (20)	−1 (1)	−5 (6)	−17 (21)
Northern									
Committed	−8 (4)	−11 (6)	−4 (5)	−10 (4)	−12 (4)	−1 (4)	+0 (0)	−0 (0)	−0 (2)
SSP1−2.6	−15 (12)	−18 (28)	−8 (25)	−19 (10)	−18 (30)	−5 (35)	−0 (1)	−1 (3)	−2 (14)
SSP2−4.5	−22 (15)	−41 (29)	−31 (31)	−26 (15)	−47 (30)	−37 (37)	−0 (1)	−3 (4)	−14 (19)
SSP5−8.5	−28 (9)	−61 (20)	−54 (30)	−32 (12)	−65 (16)	−61 (27)	−1 (1)	−7 (6)	−32 (25)
Tropical									
Committed	+9 (7)	+14 (10)	+37 (8)	−0 (3)	+2 (5)	+21 (8)	−0 (1)	−1 (1)	+5 (4)
SSP1−2.6	+14 (11)	+27 (19)	+66 (26)	+2 (3)	+5 (8)	+32 (21)	+0 (1)	−0 (5)	+13 (16)
SSP2−4.5	+14 (10)	+34 (15)	+84 (19)	−1 (2)	+2 (6)	+32 (13)	−1 (1)	−1 (4)	+13 (10)
SSP5−8.5	+19 (9)	+60 (34)	+143 (31)	−0 (4)	+7 (13)	+56 (31)	−1 (1)	+1 (9)	+28 (28)

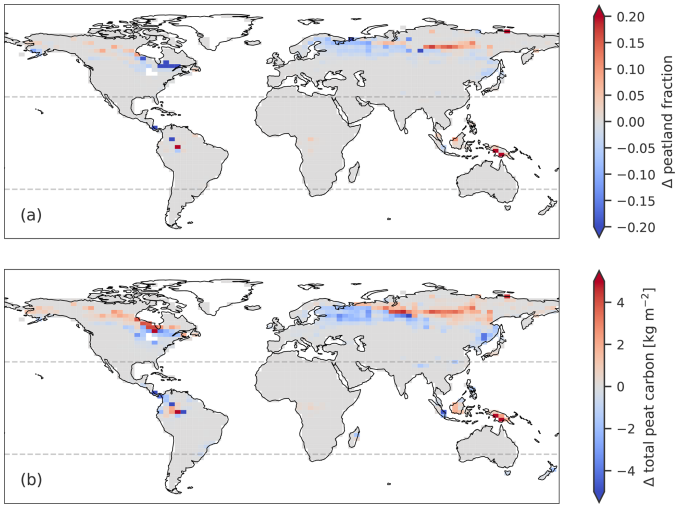

Figure 4. Median anomalies for the simulations with constant 2014 forcing at 2300 in **(a)** peatland area fraction and **(b)** total peat carbon as defined in Sect. 2.2. Anomalies are calculated between 20-year averages spanning 1995–2014 and 2291–2310.

Carbon accumulation within old, as well as newly formed, active peatlands continues over millennia, reaching a global peatland carbon stock of $+4\,(-4$ to $+16$; $+1$ to $+8)\,\%$ in the year 3500 compared to 1995–2014 averages, illustrating a large long-term accumulation potential (Fig. S2).

For global total peat carbon, the expansion in peatland area also results in a trend reversal in most simulations. The large accumulation in the newly established peatlands helps to shift the balance from decay-dominated to accumulation-dominated. At 3500 total peat carbon is simulated at $+1\,(-5$ to $+7$; -1 to $+2)\,\%$ compared to 1995–2014 averages and continues to increase with continued accumulation until the end of the simulation.

3.1.4 1500 control simulation

An additional simulation with constant 1500 CE boundary conditions, and thus with only limited land use and no industrial climate change, shows that without major disturbance peatland area remains stable, with only a small increase of 2 % over the whole 5500 years of simulation (Figs. 5 and S2). Carbon shows a stronger positive trend reflecting the still large accumulation potential of undisturbed global peatlands, with an increase of 22 % and 17 % for peatland and total peat carbon respectively. Millennium-scale accumulation rates, however, are larger in simulations with constant 2014 boundary conditions, due to higher productivity in high latitudes and newly emerging peatlands. This indicates that despite an initial loss peat carbon storage under 2014 conditions could exceed storage under 1500 conditions but only after millennia of ecosystem transformations and renewed carbon accumulation. Another study investigating the fate of permafrost peatland carbon in the circum-Arctic region comes to similar conclusions about the future long-term storage capacity of peatlands (Swindles et al., 2015).

3.2 Future projections

3.2.1 Standard scenarios

2015–2300

The standard CMIP6 scenarios provide transient climate anomalies from 2015 to 2100, after which boundary conditions are held constant. Until the end of the century, global peatland area, peatland carbon, and total peat carbon are simulated to decline (Table 2). This decline is larger than committed changes alone and increases with increasing scenario-based emissions for all three variables (Figs. 5 and 6). These results suggest a clear relationship between future emissions pathways and resulting peatland area and carbon losses until the end of the century.

From 2100 to 2300, global peatland area, peatland carbon, and total peat carbon continue to decrease for scenarios SSP2–4.5 and SSP5–8.5 despite constant boundary conditions after 2100 (Table 2). Only under the strong-mitigation scenario SSP1–2.6 do most simulations show an increase in peatland area and partly in carbon compared to 2100. Medi-

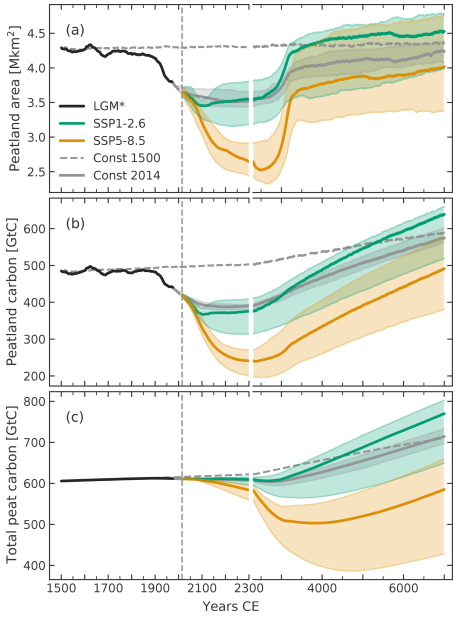

Figure 5. Simulated continued transient evolution after the LGM run (LGM*) of **(a)** global peatland area, **(b)** global peatland carbon, and **(c)** global total peat carbon as defined in Sect. 2.2 under the SSP1–2.6 and SSP5–8.5 scenarios and under constant 1500 and 2014 forcing. SSP2–4.5 is not plotted to increase readability. Lines and shading for SSP1–2.6, SSP5–8.5, and constant 1500 forcing show ensemble medians and interquartile ranges respectively. The dashed vertical line indicates the year 2014. Note the change in the time axis after the year 2300.

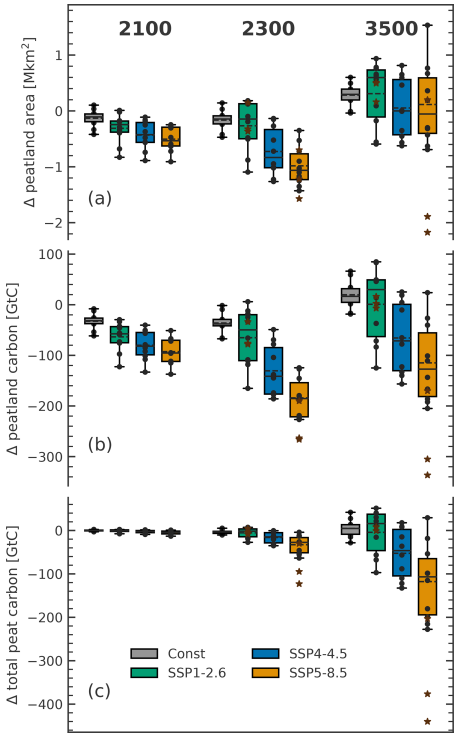

Figure 6. Boxplots of anomalies in **(a)** global peatland area, **(b)** global peatland carbon, and **(c)** global total peat carbon as defined in Sect. 2.2 for simulations under three future scenarios and constant 2014 forcing. Black dots indicate the individual simulations forced with different climate model anomalies. Boxes indicate the interquartile range, whiskers the total range, solid lines the median, and dashed lines the mean. Brown stars indicate additional simulations forced with extended versions of scenario SSP1–2.6 and SSP5–8.5. Anomalies are calculated between 20-year averages (2091–2110, 2291–2310, and 3491–3510) and the reference period 1995–2014.

ans are similar to the simulations under constant 2014 forcing. However, the uncertainty, represented by the spread between the simulations, is larger in the SSP scenarios than in the commitment simulations. This uncertainty increases with time for all scenarios.

Spatial anomaly patterns at 2300 for the strong-mitigation scenario SSP1–2.6 (Fig. 7) are similar to the committed changes (Fig. 4). The regions of peatland area loss are northeastern Canada, northern Europe, central Russia, and East Asia, and peatland area increases can be found in northwestern Canada, northeastern Asia, and Southeast Asia. Losses and gains are further amplified with respect to the committed changes. Thus, the increase in global area after 2100 in SSP1–2.6 is not due to a recovery of lost peatlands but rather due to a stronger increase of peat area in the regions of local peatland expansion.

The higher the scenario-based emissions are, the more extensive the regions of peatland area and carbon loss in the northern high latitudes become and the more reduced the regions of gains are. In the high-emission scenario SSP5–8.5, losses dominate most of the northern high latitudes (Fig. 8). Small regions of area gains remain in northeastern Asia but with weakened expansion compared to lower-emission scenarios. The northern peatland area is simulated to reduce by 18 %, 41 %, and up to 61 % until 2300 under SSP1–2.6, SSP2–4.5, and SSP5–8.5 respectively. These results suggest that large parts of today's northern peatlands might be at risk under future climate change. In the tropics, this trend is reversed, with area expansion in South America and Southeast

Asia amplified under higher-emission scenarios. Although net area gains in the tropics are substantial, carbon anomalies remain small and at 2100 only positive for the strong-mitigation scenario, indicating a strong concurrent increase in heterotrophic respiration.

Taken together these results suggest a likely net loss of global peatland area as well as carbon until the end of the century, driven mostly by northern peatlands, even under the strongest mitigation scenario and continued net loss up to 2300 for the scenarios SSP2–4.5 and SSP5–8.5, with climate assumed to remain constant after 2100. This is in contrast to another recent modeling study investigating future northern peatland area and carbon dynamics. Qiu et al. (2020) used the ORCHIDEE-PEAT DGVM model, with similar TOPMODEL-driven peatland area dynamics as the LPX-Bern and forced by IPSL-CM5A-LR and GFDL-ESM2M model climate to simulate northern peatland dynamics from 1861–2099. They found a strong positive trend in northern peatland area and together with a sustained sink also in peatland carbon over the whole historical period and the two investigated scenarios RCP2.6 and RCP6.0. They identified the main driver of this trend as an internal feedback between grid cell water table position and peatland area, which is independent of the climate forcing. This feedback is also part of the LPX-Bern implementation; however, here it does not lead to a strong sustained historical or future increase in northern peatland area, illustrated by the relatively stable control simulation under constant 1500 boundary conditions (Fig. 5). On the contrary, here it amplifies the simulated negative trend (see Sect. 3.3). One of the main reasons for the different behaviors might be the spinup procedure, which is very different in both cases. Whereas Qiu et al. (2020) used an idealized spinup with constant climate conditions, the spinup in this study corresponds to a full transient simulation. Other factors could be the different parametrization and implementation details. Despite the differences in projected net peatland area trends, there are also regional agreements. Qiu et al. (2020) found central and northern Europe to be regions of future peatland loss, especially given the warmer IPSL-CM5A-LR forcing, and northeastern Asia to be a region of particularly strong peatland expansion, partly matching regional patterns presented here. For central Russia, the simulated dynamics partly agree with another modeling study. Alexandrov et al. (2016) projected the potential future peatland area in western Siberia using an impeded drainage model and MPI-ESM climate anomalies. They found a strong increase in potential area north of 60° N and a strong decrease south of 60° N. A similar response pattern can be found in the simulations forced with MPI-ESM1-2-LR climate anomalies and weaker also in the ensemble medians but only up to the SSP2–4.5 scenario, after which losses dominate over western Siberia.

Peatland area dynamics translate directly and indirectly into the simulated carbon dynamics. In the strong-mitigation scenario, the simulated net loss of northern peatland carbon and total peat carbon is mainly a result of the northern peatland dynamics rather than of declining carbon accumulation rates. Figure 7b shows that the net ecosystem production (NEP) of active peatlands, which represents the net carbon uptake from the atmosphere per year, changes only slightly until 2300, with decreases throughout the tropics and in parts of the northern latitudes. Regional increases in NEP are simulated in central and eastern Europe as well as East Asia. The same is true for the SSP2–4.5 scenario but with slightly larger decreases in the northern mid-latitudes. Under the high-emission scenario SSP5–8.5, simulated NEP decreases strongly in North America, Europe, and western Asia, with most mid- to high-latitude active peatlands turning from a carbon sink to a carbon source and thus contributing directly to the net carbon loss. Regionally NEP increases are simulated again mostly in East Asia, with larger increases compared to SSP1–2.6. (Fig. 8b). It has to be noted that in the case of regional peatland expansion NEP might increase independent of environmental drivers, simply due to the dilution of soil carbon. The results are in broad accordance with a previous study conducted with an older version of the LPX-Bern. Spahni et al. (2013) conducted transient northern peatland simulations from the LGM up to 2100 with prescribed peatland area using CMIP5 future climate anomalies together with the LPX-Bern version 1.0. They found mean northern peatland NEP to slightly decrease over time under the RCP2.6 scenario and strongly decrease under RCP8.5. Qiu et al. (2020), however, simulate net NEP of northern peatlands to increase slightly and peak mid-century before a decline back to roughly 2005 levels at 2099. Regionally, Qiu et al. (2020) project NEP to decline in western Canada, western Europe, and the China–Russia border, especially under the RCP6.0 scenario, but only matching western Canada as a region of NEP decline simulated by LPX-Bern. In both models, northern peatland productivity and soil carbon respiration increase concurrently but balance slightly differently. Chaudhary et al. (2020) investigated past and future carbon accumulation rates (CARs) of northern-high-latitude peatlands up to 2100 using a dynamic vegetation model and similarly found net increases in simulated CARs until the mid-century and declining rates thereafter, which are most pronounced under the RCP8.5 scenario. They found Siberian and highest-latitude peatlands to potentially increase their CARs, whereas northern European and North American mid-latitude peatlands were most vulnerable to carbon sink decreases or even carbon loss, roughly matching regions of NEP increases and decreases simulated by LPX-Bern. Gallego-Sala et al. (2018) used data-derived relationships between CARs and climate variables for global future projections. They found a latitude-dependent response, with CARs increasing continuously until 2300 in high latitudes and decreasing in low latitudes. Under a high-emission scenario, CARs switched in mid-latitudes from an increasing to a decreasing trend with rising temperatures. Changes in peatland NEP simulated by LPX-Bern have a less-latitude-dependent pattern but also project carbon uptake to decrease

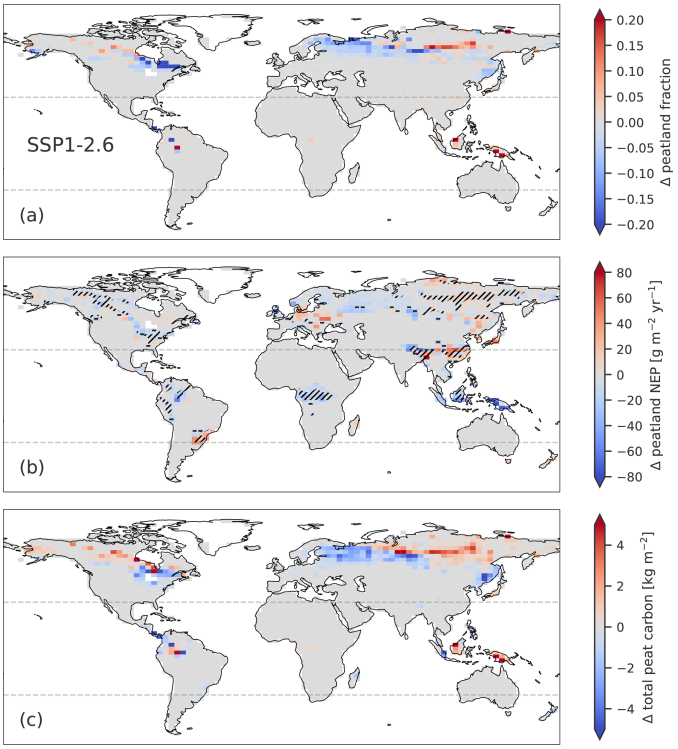

Figure 7. Simulated median anomalies under the SSP1–2.6 scenario in the year 2300 in **(a)** peatland area fraction, **(b)** peatland NEP, and **(c)** total peat carbon as defined in Sect. 2.2. Anomalies are calculated between 20-year averages spanning 1995–2014 and 2291–2310. Grid cells where NEP becomes negative are marked with a minus. Hatched areas in panel **(b)** indicate a positive area anomaly, which in the model can lead to an increase in NEP through the dilution of soil carbon and a corresponding reduction in soil carbon respiration per area

most strongly in the tropics and large parts of the mid-latitudes, with widespread switching to net carbon sources. Large increases in the northern-high-latitude peatland NEP, however, are only simulated in East Asia and parts of eastern Europe.

3.2.2 After 2300

The continuation of the simulations for several millennia under constant boundary conditions reveals the delayed long-term responses of peatlands to the previous changes in forcing. Similar to the committed changes, the future scenarios see a delayed rapid expansion in global peatland area between about 2700 and 3500 CE (Figs. 5, 6, and Table 2). Regionally this expansion is dominated by new peatlands in tropical South Asia, with smaller contributions in the highest northern latitudes and Africa. The expansion in South Asia increases in magnitude under increasing emission scenarios. This leads to a large overlap between the uncertainty ranges of the different scenarios after 3500. The median of global peatland area anomaly in 2300, however, is substantially higher for SSP1–2.6 than for the other scenarios and for constant 2014 climate. Medians of global peatland area in the higher-emission scenarios SSP2–4.5 and SSP5–8.5 remain below the levels given by 2014 boundary conditions for the whole time of the simulation, despite the large delayed expansion.

Carbon storage in old and new active peatlands increases continuously after 2300, with similar rates for all scenarios, preserving the large differences in total peatland carbon stocks formed in previous centuries. The peatland expansion after about 2700 also results in a trend reversal in total peat carbon which continues to increase thereafter. Rates of

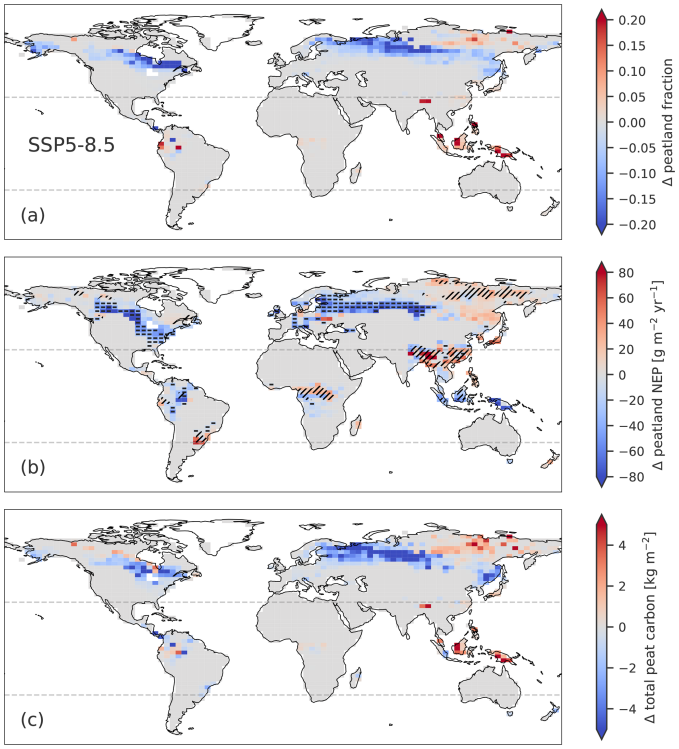

Figure 8. As Fig. 7 but for the SSP5–8.5 scenario.

global carbon sequestration are larger than rates under constant 1500 or 2014 conditions, which are most pronounced in the SSP1–2.6 scenario. Towards the end of the simulation, total peat carbon storage in SSP1–2.6 exceeds carbon stocks under constant 1500 conditions. This reflects higher mean productivity of the remaining and newly formed peatlands under moderately warmer and wetter conditions and with a higher atmospheric CO_2 concentration.

Taken together, the long-term response of global peatlands to future climate change suggests that under strongly limited future climate change and after negative effects dominating over centuries, potential global peatland area and peat carbon could increase compared to today and even compared to pre-industrial levels on a millennial timescale. Higher-emission scenarios, however, show a negative effect on global peatland area and a reduced peat carbon storage potential persisting for millennia compared to constant 2014 conditions. Uncertainties towards the end of the simulations, indicated by the ensemble spread, however, become very large.

3.2.3 Extended scenarios

The assumption of stable climate and atmospheric CO_2 levels over millennia after 2100 is a highly idealized one and not suited for predictions. The extended simulations are rather intended to reveal delayed responses and long-lasting effects in the slow-reacting peatland system. Depending on the future emission pathway, global temperature and atmospheric CO_2 are expected to either decline, stabilize, or dramatically increase beyond 2100 (see Sect. 3.2.3). Continued ocean and land uptake of CO_2 and heat will shape the future climate, sea level, and atmosphere for centuries to millennia after greenhouse gas emissions stop (Frölicher and Joos, 2010; Zickfeld et al., 2013; Frölicher et al., 2014; Clark et al., 2016). Additionally, possible tipping points in the earth system could abruptly change the trajectory of the climate system (Lenton et al., 2008). Learning about the long-term responses to disturbances of key parts of the climate system, such as peat-

lands and their large carbon stocks, is an important part of understanding future earth system responses as a whole.

To additionally investigate the effect of transient boundary conditions from 2100 to 2300, additional simulations were performed for 3 of the 10 ensemble models that provided climate output for the extended scenarios SSP1–2.6 and SSP5–8.5 (see Sect. 2). Results are compared to simulations with standard scenarios in Figs. 9 and 6. For the extended SSP1–2.6 scenario, global mean temperatures begin to decline again after peaking at about 2100 together with atmospheric CO_2 concentrations (Fig. S1). This leads to a weakening of the long-term peatland response compared to constant 2100 conditions in all three simulations. Simulations forced with climate anomalies from the IPSL and CanESM models, with relatively large climate sensitivities, show negative global peatland area and carbon variable anomalies up to 2100. After 2100, the extended scenario mitigates the external pressure, and long-term losses in peatland area and carbon are lower than under continued 2100 conditions. The simulation forced with MRI climate anomalies, with a relatively small climate sensitivity, on the other hand, sees a positive global peatland area anomaly at 2100 and thus shows less global peatland area and long-term peatland carbon storage under the extended scenario, compared to constant 2100 conditions.

The extended SSP5–8.5 scenario forces global temperatures and atmospheric CO_2 to increase drastically until 2300 (Fig. S2). Mean global temperatures over land reach 24–34 °C at 2300 with an atmospheric CO_2 concentration of 2162 ppm. Under these extreme conditions all simulations show a reduction in global peatland area and carbon compared to constant 2100 conditions. The simulations forced with the IPSL and CanESM models lose practically all high- and mid-latitude peatlands as well as the Amazon basin complex until the end of the simulation. This results in a peatland carbon and total peat carbon reduction of about 50 %–60 %. Old and newly established peatlands that remain until the end of the simulations are mostly located in tropical South Asia, Southeast Asia, and coastal regions of South America. The responses in the simulation forced with climate anomalies from the less sensitive MRI model are less extreme but also show a significant reduction in global peatland area and carbon compared to constant 2100 conditions.

The models that provided the extended scenario output are not representative of the ensemble or the full CMIP6 ensemble as a whole. The additional simulations, however, make clear, that the consideration of transient climate after 2100 can change simulated long-term peatland responses strongly, depending on the emission pathway. If the discussed differences in the peatland response to constant and transient forcing after 2100 are similar for all climate models, assumptions can be made about how the ensemble results would change in the case of transient climate until 2300. Transiently extending SSP1–2.6 would likely lead to an overall weaker peatland response, leading to a reduced model spread and less peat carbon loss in the ensemble median. For the SSP5–8.5 we would expect a larger loss of peatland area and carbon over the whole ensemble, shifting medians to larger negative anomalies. As the end of the 21st century approaches steadily, the main focus of future projections and climate policy remains on the next few decades up to 2100. To better understand the long-term effects of past and future emissions on global peatlands and to assess their potentially large feedbacks on future climate, the horizon of the future must be expanded beyond 2100. Scenarios extended to 2300 should be elevated to standard practice for future climate projections.

3.3 Driver contributions

A factorial analysis was used to attribute the positive and negative changes in peatland variables to individual forcing drivers (see Sect. 2.4). Figure 10 shows the calculated mean driver contributions to the global gross positive and negative anomalies in peatland area, peatland carbon, and total peat carbon.

Increases in peatland area up to 2300, both in the high and low latitudes, are driven mostly by committed changes (constant 2014 conditions) and an increase in regional precipitation. In northern permafrost regions, this is further strengthened given strong mitigation and moderately rising temperatures resulting in longer growing seasons and larger water retention (Fig. A1). Suggested pathways of permafrost peatlands after thaw are still debated but include rapid degradation (Avis et al., 2011; Turetsky et al., 2020), collapse followed by long-term recovery (Jones et al., 2017; Magnússon et al., 2020; Swindles et al., 2015), and increased carbon accumulation (Estop-Aragonés et al., 2018), depending on multiple factors such as thaw velocity and local hydrology.

Simulated peatland area losses are driven mostly by committed changes and increasing temperatures. Higher temperatures lead to an increase in evapotranspiration, especially in boreal peatlands (Helbig et al., 2020b), and thus a decrease in the regional water balance which is not compensated for despite a potential concurrent increase in annual precipitation. This corresponds to the already observed decade-to-century-long drying trends in northern Europe (Swindles et al., 2019; Zhang et al., 2020) and eastern Canada peatlands (Pellerin and Lavoie, 2003; Pinceloup et al., 2020; Beauregard et al., 2020), regions of large simulated committed area loss, which is found to result in negative effects on carbon accumulation rates and strong trends of woody encroachment. These trends are expected to continue and amplify under future climate change.

In the LPX-Bern, a decreasing water balance can lead to a positive feedback on the retreating water table. A long-term drawdown of the mean grid cell water table leads to a reduction in peatland area, which in turn reduces the mean grid cell water table further. In some cases, this can lead to a much larger reduction in peatland area than would be the result of the initial disturbance. In reality a lot of complex and of-

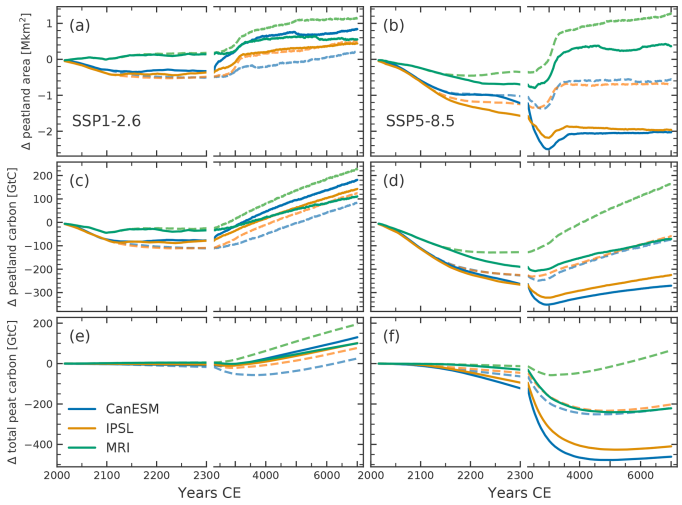

Figure 9. Simulated anomalies of **(a–b)** global peatland area, **(c–d)** global peatland carbon, and **(e–f)** global total peat carbon as defined in Sect. 2.2 for three models providing output for the extended future scenarios SSP1–2.6 **(a, c, e)** and SSP5–8.5 **(b, d, f)**. Solid lines show simulations with extended scenario forcing, evolving transiently until 2300. Dashed lines show simulations with standard scenario forcing, transient only until 2100. Note the change in the time axis after the year 2300

ten still poorly understood both positive and negative hydrological feedbacks control the peatland water table position in response to disturbances (Morris et al., 2011; Waddington et al., 2015). The simplified structure of DGVMs like the LPX-Bern cannot mirror these complex interactions, and thus this strong internal feedback needs to be interpreted with caution. However, although peatlands, in some cases, have been found to be relatively resilient with respect to limited disturbances (Cole et al., 2015; Swindles et al., 2016; Page and Baird, 2016), there could be possible tipping points that could lead to fast vegetation and ecosystem transitions under strong persisting disturbance (Eppinga et al., 2009; Heijmans et al., 2013; Page and Baird, 2016).

Peatland carbon and total peat carbon dynamics up to 2300 are dominated by committed and temperature-driven losses. The decline in peatland area directly reduces global peatland carbon and indirectly affects the total peat carbon balance by reducing overall accumulation. At the same time, global decay in active as well as in former peatlands is increased by the higher temperatures. Peatland NEP in the northern high latitudes is also driven in large parts by committed changes and increasing temperatures which can both increase or decrease NEP given the balance between respiration and productivity and their effect on permafrost (Figs. A1 and A2). Increasing CO_2, precipitation, and non-linear interactions between the drivers have strong positive effects on NEP in East Asia. In the tropics, the negative trend in NEP is mostly driven by the higher temperatures and non-linear effects.

Up to 2300, land-use change and atmospheric CO_2 have a comparatively small impact on the global scale. Increasing CO_2 concentrations have a positive effect on carbon accumulation which is progressively larger with increasing emission scenarios. This also translates into a moderate peatland area gain at 2300. Effects of land-use change are negative for all peatland variables but remain small. One reason for this small impact might be that only net land-use area increases are considered to affect peatlands in the model. The global net increase in land-use area, however, is much smaller in the future scenarios, than for the historical period (Sect. 2.6). Especially in regions where peatlands are directly targeted for land-use conversion, such as in Indonesia (Dommain et al., 2018; Hoyt et al., 2020), our approach might significantly underestimate the negative effect of land-use change.

The late expansion after 2300 is driven by peatlands newly establishing in model grid cells with no previous peatland presence. In some grid cells, the historical and future climate change and atmospheric CO_2 rise lead to the fulfillment of criteria for peatland establishment, targeting the peatland water and carbon balance. The more the boundary conditions change under future scenarios, the more grid cells, especially in the tropics, become able to support peatlands (see Sect. 3.2.2). Initiation of new peatlands in the tropics is mostly driven by CO_2 fertilization nudging the carbon bal-

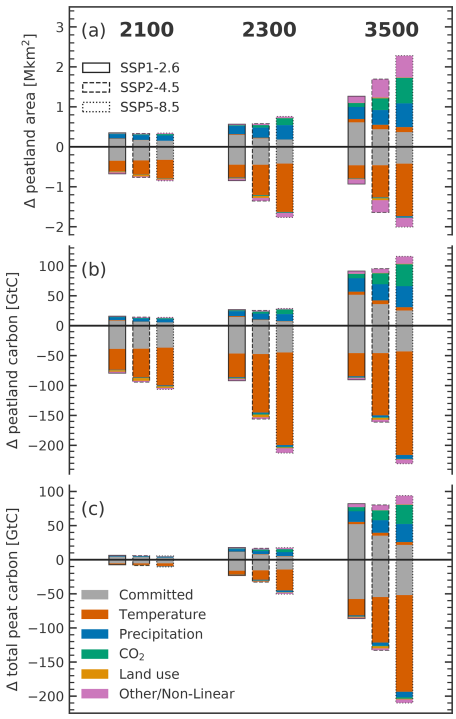

Figure 10. Mean driver contributions to gross positive and negative anomalies since 2014 in **(a)** global peatland area, **(b)** global peatland carbon, and **(c)** global total peat carbon as defined in Sect. 2.2. Anomalies for all three future scenarios are with respect to 2014. Committed driving contributions can decrease, i.e., switching from driving to dampening, if the anomaly in the respective grid cell changes sign under the different scenarios

ance over the initiation thresholds (Fig. A3). In northeastern Asia, the temperature rise is the most prominent initiation driver, whereas in northwestern Canada mostly precipitation increases drive the initiation of new peatlands. In the model, newly established peatlands start from a small seed, and their growth is restricted to 1 % of their size per year. They thus reach noticeable size only centuries after their initial establishment. Outside of the model world, the speed of lateral expansion of growing peatlands depends on multiple factors, including local topography, hydrology, and peatland type (Charman, 2002; Ruppel et al., 2013). Topography can constrain lateral expansion velocities. Depending on terrain slopes, peat accumulation can be limited to a small area or depression for centuries to millennia until the peat column grows tall enough or expand quickly over a flat plain (Bauer et al., 2003; Loisel et al., 2013; Broothaerts et al., 2014; Le Stum-Boivin et al., 2019). This heterogeneity and complexity in lateral expansion of newly established peatlands is not represented by the model used here. The magnitude and timing of the simulated late expansion should therefore be taken with care. However, the results suggest that historical and future climate change might create the potential for newly forming peatlands in regions where conditions have been mostly unsuitable before.

3.4 Climate forcing uncertainty

The spread between simulations forced with climate anomalies from the different CMIP6 climate models indicates a large climate-anomaly-related uncertainty in simulated peatland variables. This is in line with previous studies that also found a large uncertainty propagation from climate variables to peatland and carbon cycle variables in general (Stocker et al., 2013; Ahlström et al., 2017; Qiu et al., 2020; Müller and Joos, 2020).

The magnitude of uncertainties is regionally different, with large uncertainties in the northern high latitudes for peatland area (Fig. S3) and total peat carbon (Fig. S4) and in the mid-latitudes for peatland NEP (Fig. S5). The climate variables driving the uncertainty depend on the region and peatland variable in question. Linear regressions for each grid cell were used to investigate how the differences between the model climate anomalies translate to the simulated peatland variables. Differences in northern-high-latitude peatland area between simulations were found to be dominantly a factor of climate model temperature. Warmer anomalies resulted in less peatland area in most grid cells, except for northeastern Asia, where warmer temperatures facilitate peat expansion in some grid cells (Fig. S3). In the tropics, the difference in precipitation is the best predictor for most grid cells, with anomalies from wetter models resulting in larger peatlands. Total peat carbon, determined by the balance between total accumulation and total decay of peat carbon, shows a similar regional pattern (Fig. S4). Northern-high- and mid-latitude peat carbon is reduced with higher temperature anomalies as the area for accumulation declines and heterotrophic respiration increases. In the tropics precipitation remains the dominant predictor, increasing the accumulation area and limiting respiration. For peatland NEP, precipitation minus evapotranspiration, as a measure of the moisture balance, resulted in a larger number of grid cells with significant (regression p value < 0.05) results compared to temperature or precipitation alone (Fig. S5). Climate models resulting in a more positive water balance mostly also resulted in a higher peatland NEP due to the controls of peatland water table depth on both productivity and respiration. In permafrost regions, also temperature on its own is a strong positive factor for simulated peatland NEP.

The results show that the differences in peatland responses to different climate forcings can be explained mostly by the

same drivers and mechanisms as the transient changes (discussed in Sect. 3.3). They also reveal the large dependence of peatland and carbon cycle projections on key properties of climate models. Further constraining model climate sensitivity is thus essential to reduce uncertainty in carbon cycle projections. Here the climate model ensemble subset was selected to best represent the full CMIP6 ensemble and with this the fullest possible range of projections. However, model performance compared to different targets is highly variable (Harrison et al., 2014), and different ensemble subset selections or weighted ensemble medians might be preferable in future work, depending on the focus.

The simulations presented here are also subject to other large but less quantifiable uncertainties. Keeping the forcing constant after 2100 or 2300 is an idealization with true climate dynamics depending on highly uncertain factors such as future social and economic dynamics and potential tipping points. Structural and parameter uncertainties, not only in the peat module, but through all components of the model, are unavoidable in simplified global models such as the LPX-Bern, especially on regional and local scales. Implementation of peatlands in DGVMs is still in its early stages, and comprehensive model comparison and structural uncertainty evaluation are still mostly lacking. With the inclusion of peatlands into more and more DGVMs and earth system models, comparative studies might identify the most promising model developments and thus pave the way for more robust peatland and carbon cycle projections.

4 Conclusions

The dynamic global vegetation model LPX-Bern was used to estimate committed and projected mid- to long-term future changes in global peatland area and carbon under three different climate and land-use scenarios. A previously published transient simulation from the Last Glacial Maximum to the present (Müller and Joos, 2020) was used as the starting point for the future projections, accounting for the transient history and potential legacy effects of today's and former peatlands. LPX-Bern was forced by climate anomalies from 10 different CMIP6 earth system models, selected to optimally represent the full CMIP6 ensemble range. Peat carbon dynamics were analyzed for carbon in active peatlands (*peatland carbon*) and peat carbon in all land classes including former peatlands (*total peat carbon*), representing two land–atmosphere interaction bounding cases.

Averaged over 1995–2014, median global peatland area, peatland carbon, and total peat carbon are simulated to be 3.7 Mkm^2, 423 GtC, and 611 GtC respectively. This puts the modeled peatlands within the range of literature estimates but with a heavier weight on tropical peatlands than most estimates suggest. Simulations with constant 2014 boundary conditions revealed committed losses of northern peatland area (median: $-8\,\%$) and peatland carbon (median: $-10\,\%$) until the end of the century and beyond, with losses in Europe and eastern Canada partly compensated for by peatland area expansion in eastern Asia, the western part of North America, and the tropics. These results suggest that past climate and land-use change has already led to regional changes in the environmental conditions that put a large part of today's northern peatlands at risk while potentially improving conditions for others. With higher-emission scenarios, global net losses in peatland area and carbon are increased with increases in losses in the northern latitudes and increasing gains in the tropics. Under the SSP1–2.6, SSP2–4.5, and SSP5–8.5 scenario, assuming constant climate, CO_2, and land-use forcing after 2100, the northern peatland area is simulated to decrease by a median of $-18\,\%$, $-41\,\%$, and $-61\,\%$ until 2300 respectively, with concomitant decreases in northern peatland carbon ($-18\,\%$, $-47\,\%$, and $-65\,\%$) and total peat carbon ($-1\,\%$, $-3\,\%$, and $-7\,\%$). These results illustrate the extent to which today's northern peatlands and their large carbon stocks are at risk from future climate change. Estimated peat carbon loss here depends on the assumed emission bounding case and could be large if the carbon is quickly released to the atmosphere (*peatland carbon*) or moderate to small if the carbon decays only slowly after ecosystem transformation (*total peat carbon*). To reduce this persisting uncertainty, additional research focus on the fate of carbon in former peatlands is needed, leading to dedicated model parameterizations for this carbon pool. In our simulations, higher future emissions are clearly tied to a larger potential loss of peatland area and carbon, highlighting the role of fast emission reduction for peatland protection. While direct human disturbances of peatlands through drainage and land-use conversion can be partly mitigated by prompt peatland restoration and legal protection, indirect disturbances from anthropogenic climate change can only be limited by drastically cutting future emissions.

All simulations showed delayed peatland responses beyond 2300 under constant climate and environmental forcing, most notably a delayed peatland expansion in grid cells with no prior peatland presence. This delayed peatland expansion is especially pronounced in the tropics and the highest northern latitudes. Although the timing and magnitude of this expansion are most likely strongly model dependent, it illustrates the potential for new peat initiation in regions that were formerly unsuited for peat development. Towards the end of the simulations, medians for simulated global peatland area, peatland carbon, and total peat carbon in the strong-mitigation scenario exceed the ones of the 1500 and 2014 commitment simulations. The millennial-scale potential for global peatland area and peat carbon storage is thus simulated to be larger under strongly mitigated climate change than under pre-industrial or present-day conditions. This potential, however, is only realized after centuries to millennia of dominating negative effects, with large permanent losses of northern peatland area, peat carbon, and ecosystem services provided by them. For the higher-

emission scenarios, globally aggregated negative changes in area and carbon persist until the end of the simulation.

Additional simulations with extended SSP scenario climate forcing from three different climate models showed that continuing transient forcing along a scenario trajectory can substantially change the simulated results. Extending the SSP1–2.6 scenario to 2300 with global temperature anomalies decreasing again after 2100 led to a reduction in the response, positive or negative, relative to the standard scenario. The extension of SSP5–8.5 on the other hand leads to a drastically increased loss of peatland area and carbon due to the extreme increases in mean global temperature until 2300. Assuming similar results when extended scenarios would be used for the whole ensemble, model spread and median peat carbon loss are expected to be smaller under SSP1–2.6, and median loss of peatland area and carbon is expected to be substantially larger under SSP5–8.5. These results highlight the importance of extended emission pathways to project long-term effects of anthropogenic climate change not only on peatlands but on the carbon cycle and the climate system as a whole. As the current century grows shorter the next phase of CMIP should aim to extend projections beyond the end of the century as a standard practice.

Driver contributions to future changes were analyzed using factorial simulations. Besides committed changes, increasing temperature was identified as the main driver of peatland area and carbon losses, and increasing precipitation was identified as the main driver of gains. After 2300, influences of CO_2 and non-linear interactions on peat initiation become more apparent, when peatland area begins to expand more widely. Cloud cover was found to have only small influences on global peatland variables. Future changes in the net area under land use are small ($< 11\,\%$) in the scenarios compared to the historical changes and have a small impact on global peatlands in our simulations. Here a simplified assumption was taken, with peatlands being affected by land-use change proportional to their size. However, this might not be the case if peatlands are directly targeted for conversion to land-use areas. Future studies might try to integrate specific peatland–land-use conversion scenarios to better quantify the effect of potential future land-use conversion within a global modeling framework.

The spread between the simulations forced with different climate anomalies from the 10 ensemble climate models reveals that a large uncertainty is propagated from the climate anomalies to the global peatland and carbon cycle variables. Depending on the region, uncertainty was propagated mostly by temperature, precipitation, or a combination of both. The uncertainty increases with time even after climate forcing is kept constant due to the long response timescales important for peatlands. Even in the case of the 2014 commitment simulations, which only see 40 years of slightly diverging climate anomalies, uncertainties grow large over time. This shows that small differences in climate forcing can propagate to large long-term differences in peatland and carbon cycle variables. In future studies, uncertainties could be reduced by including a skill criterion into the climate model ensemble selection or the subsequent ensemble analysis. Structural model uncertainties are harder to quantify but could potentially be equally large. A focus of future work must be to quantify these structural uncertainties in peatland model intercomparison projects and continue model development towards simple but robust formulations for dynamic peatlands on a global scale. Given the large and diverse uncertainties involved, the results presented here should be interpreted as a model analysis of potential risks, their transient evolution, environmental drivers, and uncertainties rather than as robust predictions.

The climate and the terrestrial carbon cycle in the simulations presented in this study are uncoupled. The results, however, suggest potentially large feedbacks between the simulated changes in global peatlands and the global carbon cycle and climate system. Carbon released to the atmosphere would additionally warm the climate, leading to a positive feedback. Every 100 GtC released from peatlands would cause a warming of about 0.2 °C (Allen et al., 2009). Other feedbacks not considered here include changes in the methane source, surface energy balance, and surface albedo. Changing surface albedo and energy balance might lead to warming given a transition from moss-dominated boreal peatlands to a dense forest (Helbig et al., 2020a), but it is strongly dependent on the actual vegetation succession. Decreasing methane emissions from reduced northern peatlands could be compensated for or even superseded by increased emissions from expanding tropical peatlands. In addition, methane emissions increase with temperature (Turetsky et al., 2014). The sign of the methane feedback, therefore, is dependent on multiple factors. The absence of these potentially important feedbacks between peatlands and the climate system in the state-of-the-art future projections such as produced by the CMIP is a potential limit to formulating adequate climate policy. Future work should focus on the production of fully coupled peatland–climate simulations to assess the magnitude of the potential feedbacks, as well as the integration of peatland modules into the next generation of earth system and integrated assessment models (Loisel et al., 2021).

Taken together our study provides long-term future projections of global peatland area and carbon, based on a transient spinup since the Last Glacial Maximum, and accompanied by an in-depth analysis of future scenarios, drivers, and uncertainties. It suggests that large parts of northern peatlands are at risk of both committed and future climate change and highlights the need for strong-mitigation and protection efforts. The large uncertainties found call for continued model development and refinement. The long response timescales and potentially large climate feedbacks of peatlands stress the need for century-to-millennial-scale coupled climate–peatland simulations.

Appendix A

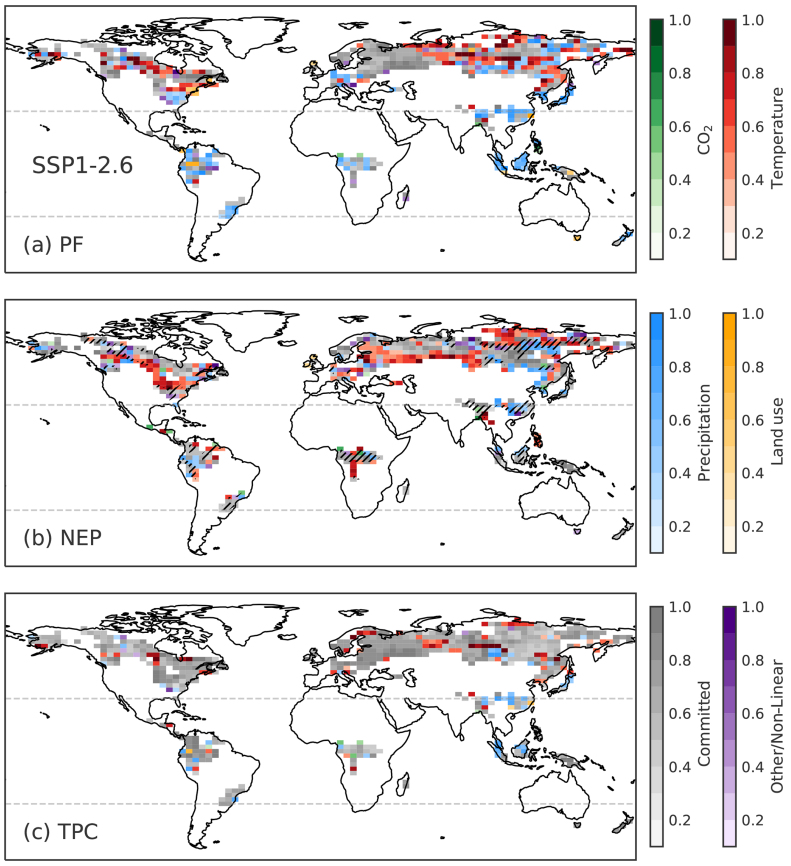

Figure A1. Dominant driver contributions to SSP1-2.6 anomalies at 2300 in **(a)** peatland area fraction (PF), **(b)** peatland NEP, and **(c)** total peat carbon (TPC). Colors indicate the most important driver and color shade the contribution of the respective driver on a scale from 0 (no contribution) to 1 (only contributor). Anomalies are calculated with respect to 1995–2014 averages.

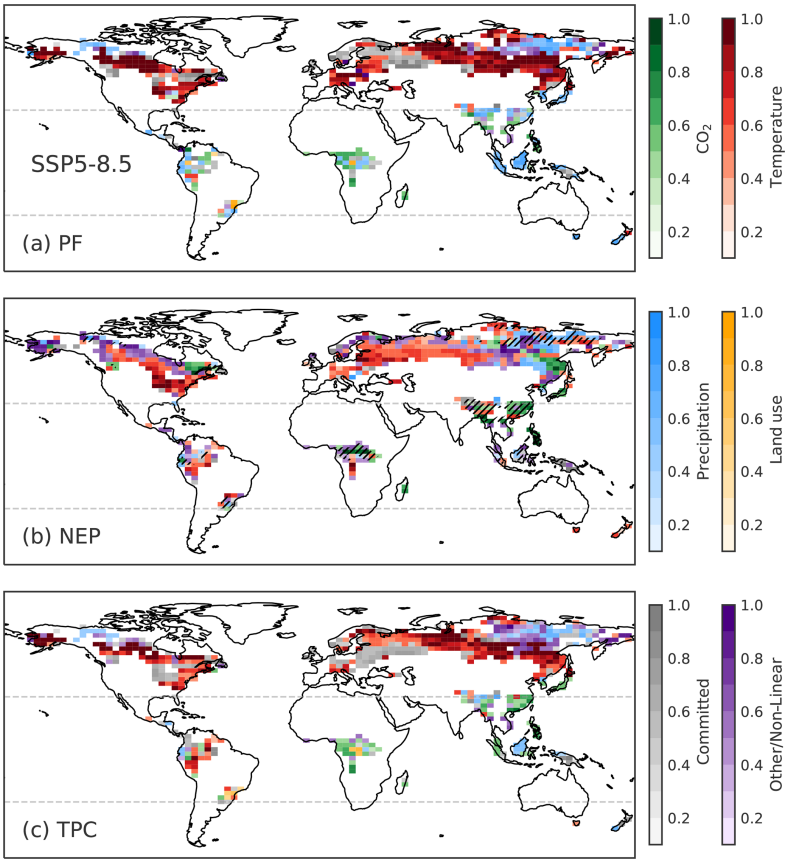

Figure A2. As Fig. A1 but for the SSP5–8.5 scenario.

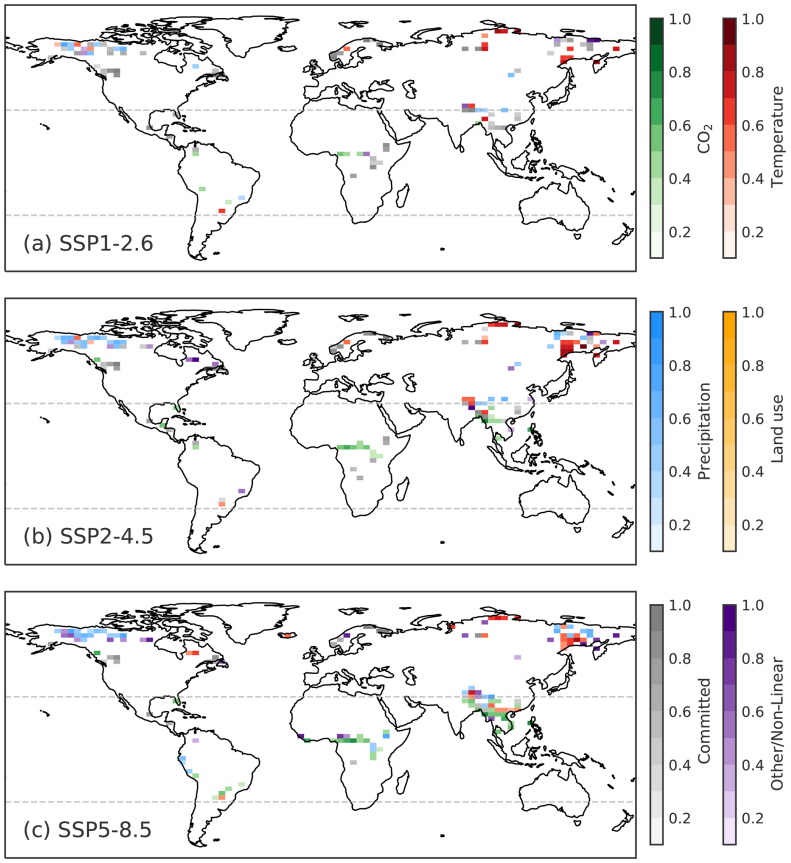

Figure A3. Dominant driver contributions to peatland area at 3500 in grid cells with no peatland presence before the year 1500 for **(a)** SSP1–2.6, **(b)** SSP2–4.5, and **(c)** SSP5–8.5. Colors indicate the most important driver and color shade the contribution of the respective driver on a scale from 0 (no contribution) to 1 (only contributor).

Data availability. The Supplement with additional figures and tables is available below. LPX-Bern model output for variables and simulations presented here is available for download under https://doi.org/10.5281/zenodo.4627681 (Müller and Joos, 2021).

Supplement. The supplement related to this article is available online at: https://doi.org/10.5194/bg-18-3657-2021-supplement.

Author contributions. JM and FJ designed the study. JM performed the simulations and the analyses in consultation with FJ. JM prepared the figures and wrote the paper with input from FJ.

Competing interests. The authors declare that they have no conflict of interest.

Acknowledgements. This project received funding from the Swiss National Science Foundation and from the European Union's Horizon 2020 research and innovation program under the project COMFORT (Our common future ocean in the Earth system – quantifying coupled cycles of carbon, oxygen, and nutrients for determining and achieving safe operating spaces with respect to tipping points) and under the project 4C (Climate-Carbon Interactions in the Current Century). The work reflects only the authors' view; the European Commission and their executive agency are not responsible for any use that may be made of the information the work contains. This study was undertaken as part of C-PEAT, a working group of the Past Global Changes (PAGES) project, which in turn received support from the Swiss Academy of Sciences and the Chinese Academy of Sciences. We thank Sebastian Lienert, Renato Spahni, and Benjamin Stocker for their contributions to the development of LPX-Bern. We acknowledge the World Climate Research Programme's Working Group on Coupled Modelling, which is responsible for CMIP, and the climate modeling groups for producing and making available their model output.

Financial support. This research has been supported by the Schweizerischer Nationalfonds zur Förderung der Wissenschaftlichen Forschung (grant nos. 200020-172476 and 200020_200511) and the European Commission, Horizon 2020 (project COMFORT, grant no. 820989; and project 4C, grant no. 821003).

Review statement. This paper was edited by Alexey V. Eliseev and reviewed by Thomas Kleinen and one anonymous referee.

References

Ahlström, A., Schurgers, G., and Smith, B.: The large influence of climate model bias on terrestrial carbon cycle simulations, Environ. Res. Lett., 12, 014004, https://doi.org/10.1088/1748-9326/12/1/014004, 2017.

Alexandrov, G. A., Brovkin, V. A., and Kleinen, T.: The influence of climate on peatland extent in Western Siberia since the Last Glacial Maximum, Sci. Rep., 6, 6–11, https://doi.org/10.1038/srep24784, 2016.

Allen, M. R., Frame, D. J., Huntingford, C., Jones, C. D., Lowe, J. A., Meinshausen, M., and Meinshausen, N.: Warming caused by cumulative carbon emissions towards the trillionth tonne, Nature, 458, 1163–1166, https://doi.org/10.1038/nature08019, 2009.

Avis, C. A., Weaver, A. J., and Meissner, K. J.: Reduction in areal extent of high-latitude wetlands in response to permafrost thaw, Nat. Geosci., 4, 444–448, https://doi.org/10.1038/ngeo1160, 2011.

Bauer, I. E., Gignac, L. D., and Vitt, D. H.: Development of a peatland complex in boreal western Canada: Lateral site expansion and local variability in vegetation succession and long-term peat accumulation, Can. J. Bot., 81, 833–847, https://doi.org/10.1139/b03-076, 2003.

Beauregard, P., Lavoie, M., and Pellerin, S.: Recent Gray Birch (Betula populifolia) Encroachment in Temperate Peatlands of Eastern North America, Wetlands, 40, 351–364, https://doi.org/10.1007/s13157-019-01186-3, 2020.

Beven, K. J. and Kirkby, M. J.: A physically based, variable contributing area model of basin hydrology, Hydrol. Sci. Bull., 24, 43–69, https://doi.org/10.1080/02626667909491834, 1979.

Blodau, C.: Carbon cycling in peatlands — A review of processes and controls, Environ. Rev., 10, 111–134, https://doi.org/10.1139/a02-004, 2002.

Boucher, O., Denvil, S., Levavasseur, G., Cozic, A., Caubel, A., Foujols, M.-A., Meurdesoif, Y., Cadule, P., Devilliers, M., Ghattas, J., Lebas, N., Lurton, T., Mellul, L., Musat, I., Mignot, J., and Cheruy, F.: IPSL IPSL-CM6A-LR model output prepared for CMIP6 CMIP historical, Version 20200601, https://doi.org/10.22033/ESGF/CMIP6.5195, 2018.

Boucher, O., Denvil, S., Levavasseur, G., Cozic, A., Caubel, A., Foujols, M.-A., Meurdesoif, Y., Cadule, P., Devilliers, M., Dupont, E., and Lurton, T.: IPSL IPSL-CM6A-LR model output prepared for CMIP6 ScenarioMIP, Version 20200601, https://doi.org/10.22033/ESGF/CMIP6.1532, 2019.

Boucher, O., Servonnat, J., Albright, A. L., Aumont, O., Balkanski, Y., Bastrikov, V., Bekki, S., Bonnet, R., Bony, S., Bopp, L., Braconnot, P., Brockmann, P., Cadule, P., Caubel, A., Cheruy, F., Codron, F., Cozic, A., Cugnet, D., D'Andrea, F., Davini, P., Lavergne, C., Denvil, S., Deshayes, J., Devilliers, M., Ducharne, A., Dufresne, J., Dupont, E., Éthé, C., Fairhead, L., Falletti, L., Flavoni, S., Foujols, M., Gardoll, S., Gastineau, G., Ghattas, J., Grandpeix, J., Guenet, B., Guez, Lionel, E., Guilyardi, E., Guimberteau, M., Hauglustaine, D., Hourdin, F., Idelkadi, A., Joussaume, S., Kageyama, M., Khodri, M., Krinner, G., Lebas, N., Levavasseur, G., Lévy, C., Li, L., Lott, F., Lurton, T., Luyssaert, S., Madec, G., Madeleine, J., Maignan, F., Marchand, M., Marti, O., Mellul, L., Meurdesoif, Y., Mignot, J., Musat, I., Ottlé, C., Peylin, P., Planton, Y., Polcher, J., Rio, C., Rochetin, N., Rousset, C., Sepulchre, P., Sima, A., Swingedouw, D., Thiéblemont, R., Traore, A. K., Vancoppenolle, M., Vial, J., Vialard, J., Viovy, N., and Vuichard, N.: Presentation and Evaluation of the IPSL-CM6A-LR Climate Model, J. Adv. Model. Earth Syst., 12, 1–52, https://doi.org/10.1029/2019MS002010, 2020.

Broothaerts, N., Notebaert, B., Verstraeten, G., Kasse, C., Bohncke, S., and Vandenberghe, J.: Non-uniform and diachronous Holocene floodplain evolution: a case study from the Dijle catchment, Belgium, J. Quaternary Sci., 29, 351–360, https://doi.org/10.1002/jqs.2709, 2014.

Byun, Y.-H., Lim, Y.-J., Shim, S., Sung, H. M., Sun, M., Kim, J., Kim, B.-H., Lee, J.-H., and Moon, H.: NIMS-KMA KACE1.0-G model output prepared for CMIP6 ScenarioMIP, Version 20200601, https://doi.org/10.22033/ESGF/CMIP6.2242, 2019a.

Byun, Y.-H., Lim, Y.-J., Sung, H. M., Kim, J., Sun, M., and Kim, B.-H.: NIMS-KMA KACE1.0-G model output prepared for CMIP6 CMIP historical, Version 20200601, https://doi.org/10.22033/ESGF/CMIP6.8378, 2019b.

Camill, P.: Permafrost thaw accelerates in boreal peatlands during late-20th century climate warming, Clim. Change, 68, 135–152, https://doi.org/10.1007/s10584-005-4785-y, 2005.

Campos, J. R. d. R., Silva, A. C., Slater, L., Nanni, M. R., and Vidal-Torrado, P.: Stratigraphic control and chronology of peat bog deposition in the Serra do Espinhaço Meridional, Brazil, CATENA, 143, 167–173, https://doi.org/10.1016/j.catena.2016.04.009, 2016.

Charman, D.: Peatlands and environmental change, John Wiley & Sons Ltd., UK, 2002.

Charman, D. J., Beilman, D. W., Blaauw, M., Booth, R. K., Brewer, S., Chambers, F. M., Christen, J. A., Gallego-Sala, A., Harrison, S. P., Hughes, P. D. M., Jackson, S. T., Korhola, A., Mauquoy, D., Mitchell, F. J. G., Prentice, I. C., van der Linden, M., De Vleeschouwer, F., Yu, Z. C., Alm, J., Bauer, I. E., Corish, Y. M. C., Garneau, M., Hohl, V., Huang, Y., Karofeld, E., Le Roux, G., Loisel, J., Moschen, R., Nichols, J. E., Nieminen, T. M., MacDonald, G. M., Phadtare, N. R., Rausch, N., Sillasoo, Ü., Swindles, G. T., Tuittila, E.-S., Ukonmaanaho, L., Väliranta, M., van Bellen, S., van Geel, B., Vitt, D. H., and Zhao, Y.: Climate-related changes in peatland carbon accumulation during the last millennium, Biogeosciences, 10, 929–944, https://doi.org/10.5194/bg-10-929-2013, 2013.

Chaudhary, N., Miller, P. A., and Smith, B.: Modelling past, present and future peatland carbon accumulation across the pan-Arctic region, Biogeosciences, 14, 4023–4044, https://doi.org/10.5194/bg-14-4023-2017, 2017.

Chaudhary, N., Westermann, S., Lamba, S., Shurpali, N., Sannel, A. B. K., Schurgers, G., Miller, P. A., and Smith, B.: Modelling past and future peatland carbon dynamics across the pan-Arctic, Glob. Change Biol., 26, 4119–4133, https://doi.org/10.1111/gcb.15099, 2020.

Clark, P. U., Shakun, J. D., Marcott, S. A., Mix, A. C., Eby, M., Kulp, S., Levermann, A., Milne, G. A., Pfister, P. L., Santer, B. D., Schrag, D. P., Solomon, S., Stocker, T. F., Strauss, B. H., Weaver, A. J., Winkelmann, R., Archer, D., Bard, E., Goldner, A., Lambeck, K., Pierrehumbert, R. T., and Plattner, G. K.: Consequences of twenty-first-century policy for multi-millennial climate and sea-level change, Nat. Clim. Change, 6, 360–369, https://doi.org/10.1038/nclimate2923, 2016.

Cole, L. E., Bhagwat, S. A., and Willis, K. J.: Long-term disturbance dynamics and resilience of tropical peat swamp forests, J. Ecol., 103, 16–30, https://doi.org/10.1111/1365-2745.12329, 2015.

Cong, M., Xu, Y., Tang, L., Yang, W., and Jian, M.: Predicting the dynamic distribution of Sphagnum bogs in China under climate change since the last interglacial period, PLoS One, 15, e0230969, https://doi.org/10.1371/journal.pone.0230969, 2020.

Dargie, G. C., Lewis, S. L., Lawson, I. T., Mitchard, E. T., Page, S. E., Bocko, Y. E., and Ifo, S. A.: Age, extent and carbon storage of the central Congo Basin peatland complex, Nature, 542, 86–90, https://doi.org/10.1038/nature21048, 2017.

de Jong, R., Blaauw, M., Chambers, F. M., Christensen, T. R., de Vleeschouwer, F., Finsinger, W., Fronzek, S., Johansson, M., Kokfelt, U., Lamentowicz, M., Le Roux, G., Mauquoy, D., Mitchell, E. A., Nichols, J. E., Samaritani, E., and van Geel, B.: Climate and Peatlands, in: Chang. Clim. Earth Syst. Soc., edited by Dodson, J., Springer Netherlands, Dordrecht, 85–121, https://doi.org/10.1007/978-90-481-8716-4_5, 2010.

Dohong, A., Aziz, A. A., and Dargusch, P.: A review of the drivers of tropical peatland degradation in South-East Asia, Land Use Policy, 69, 349–360, https://doi.org/10.1016/j.landusepol.2017.09.035, 2017.

Dommain, R., Frolking, S., Jeltsch-Thömmes, A., Joos, F., Couwenberg, J., and Glaser, P. H.: A radiative forcing analysis of tropical peatlands before and after their conversion to agricultural plantations, Glob. Change Biol., 24, 5518–5533, https://doi.org/10.1111/gcb.14400, 2018.

Döscher, R., Acosta, M., Alessandri, A., Anthoni, P., Arneth, A., Arsouze, T., Bergmann, T., Bernadello, R., Bousetta, S., Caron, L.-P., Carver, G., Castrillo, M., Catalano, F., Cvijanovic, I., Davini, P., Dekker, E., Doblas-Reyes, F. J., Docquier, D., Echevarria, P., Fladrich, U., Fuentes-Franco, R., Gröger, M., v. Hardenberg, J., Hieronymus, J., Karami, M. P., Keskinen, J.-P., Koenigk, T., Makkonen, R., Massonnet, F., Ménégoz, M., Miller, P. A., Moreno-Chamarro, E., Nieradzik, L., van Noije, T., Nolan, P., O'Donnell, D., Ollinaho, P., van den Oord, G., Ortega, P., Prims, O. T., Ramos, A., Reerink, T., Rousset, C., Ruprich-Robert, Y., Le Sager, P., Schmith, T., Schrödner, R., Serva, F., Sicardi, V., Sloth Madsen, M., Smith, B., Tian, T., Tourigny, E., Uotila, P., Vancoppenolle, M., Wang, S., Wårlind, D., Willén, U., Wyser, K., Yang, S., Yepes-Arbós, X., and Zhang, Q.: The EC-Earth3 Earth System Model for the Climate Model Intercomparison Project 6, Geosci. Model Dev. Discuss. [preprint], https://doi.org/10.5194/gmd-2020-446, in review, 2021.

Dunne, J. P., Horowitz, L. W., Adcroft, A. J., Ginoux, P., Held, I. M., John, J. G., Krasting, J. P., Malyshev, S., Naik, V., Paulot, F., Shevliakova, E., Stock, C. A., Zadeh, N., Balaji, V., Blanton, C., Dunne, K. A., Dupuis, C., Durachta, J., Dussin, R., Gauthier, P. P. G., Griffies, S. M., Guo, H., Hallberg, R. W., Harrison, M., He, J., Hurlin, W., McHugh, C., Menzel, R., Milly, P. C. D., Nikonov, S., Paynter, D. J., Ploshay, J., Radhakrishnan, A., Rand, K., Reichl, B. G., Robinson, T., Schwarzkopf, D. M., Sentman, L. T., Underwood, S., Vahlenkamp, H., Winton, M., Wittenberg, A. T., Wyman, B., Zeng, Y., and Zhao, M.: The GFDL Earth System Model Version 4.1 (GFDL-ESM 4.1): Overall Coupled Model Description and Simulation Characteristics, J. Adv. Model. Earth Syst., 12, 1–56, https://doi.org/10.1029/2019MS002015, 2020.

EC-Earth Consortium (EC-Earth): EC-Earth-Consortium EC-Earth3 model output prepared for CMIP6 CMIP historical, Version 20200601, https://doi.org/10.22033/ESGF/CMIP6.4700, 2019a.

EC-Earth Consortium (EC-Earth): EC-Earth-Consortium EC-Earth3 model output prepared for CMIP6 ScenarioMIP, Version 20200601, https://doi.org/10.22033/ESGF/CMIP6.251, 2019b.

Eppinga, M. B., Rietkerk, M., Wassen, M. J., and De Ruiter, P. C.: Linking habitat modification to catastrophic shifts and vegetation patterns in bogs, Plant Ecol., 200, 53–68, https://doi.org/10.1007/s11258-007-9309-6, 2009.

Estop-Aragonés, C., Cooper, M. D., Fisher, J. P., Thierry, A., Garnett, M. H., Charman, D. J., Murton, J. B., Phoenix, G. K., Treharne, R., Sanderson, N. K., Burn, C. R., Kokelj, S. V., Wolfe, S. A., Lewkowicz, A. G., Williams, M., and Hartley, I. P.: Limited release of previously-frozen C and increased new peat formation after thaw in permafrost peatlands, Soil Biol. Biochem., 118, 115–129, https://doi.org/10.1016/j.soilbio.2017.12.010, 2018.

Estop-Aragonés, C., Olefeldt, D., Abbott, B. W., Chanton, J. P., Czimczik, C. I., Dean, J. F., Egan, J. E., Gandois, L., Garnett, M. H., Hartley, I. P., Hoyt, A., Lupascu, M., Natali, S. M., O'Donnell, J. A., Raymond, P. A., Tanentzap, A. J., Tank, S. E., Schuur, E. A. G., Turetsky, M., and Anthony, K. W.: Assessing the Potential for Mobilization of Old Soil Carbon After Permafrost Thaw: A Synthesis of ^{14}C Measurements From the Northern Permafrost Region, Global Biogeochem. Cy., 34, 1–26, https://doi.org/10.1029/2020GB006672, 2020.

Eyring, V., Bony, S., Meehl, G. A., Senior, C. A., Stevens, B., Stouffer, R. J., and Taylor, K. E.: Overview of the Coupled Model Intercomparison Project Phase 6 (CMIP6) experimental design and organization, Geosci. Model Dev., 9, 1937–1958, https://doi.org/10.5194/gmd-9-1937-2016, 2016.

Ferretto, A., Brooker, R., Aitkenhead, M., Matthews, R., and Smith, P.: Potential carbon loss from Scottish peatlands under climate change, Reg. Environ. Change, 19, 2101–2111, https://doi.org/10.1007/s10113-019-01550-3, 2019.

Frölicher, T. L. and Joos, F.: Reversible and irreversible impacts of greenhouse gas emissions in multi-century projections with the NCAR global coupled carbon cycle-climate model, Clim. Dynam., 35, 1439–1459, https://doi.org/10.1007/s00382-009-0727-0, 2010.

Frölicher, T. L., Winton, M., and Sarmiento, J. L.: Continued global warming after CO_2 emissions stoppage, Nat. Clim. Change, 4, 40–44, https://doi.org/10.1038/nclimate2060, 2014.

Frolking, S. and Roulet, N. T.: Holocene radiative forcing impact of northern peatland carbon accumulation and methane emissions, Glob. Change Biol., 13, 1079–1088, https://doi.org/10.1111/j.1365-2486.2007.01339.x, 2007.

Gajewski, K., Viau, A., Sawada, M., Atkinson, L. J., and Wilson, S.: Sphagnum peatland distribution in North America and Eurasia during the past 21,000 years, Carbon N. Y., 15, 297–310, 2001.

Gallego-Sala, A. V., Charman, D. J., Harrison, S. P., Li, G., and Prentice, I. C.: Climate-driven expansion of blanket bogs in Britain during the Holocene, Clim. Past, 12, 129–136, https://doi.org/10.5194/cp-12-129-2016, 2016.

Gallego-Sala, A. V., Charman, D. J., Brewer, S., Page, S. E., Colin Prentice, I., Friedlingstein, P., Moreton, S., Amesbury, M. J., Beilman, D. W., Bjamp, S., Blyakharchuk, T., Bochicchio, C., Booth, R. K., Bunbury, J., Camill, P., Carless, D., Chimner, R. A., Clifford, M., Cressey, E., Courtney-Mustaphi, C., Vleeschouwer, O., Jong, R., Fialkiewicz-Koziel, B., Finkelstein, S. A., Garneau, M., Githumbi, E., Hribjlan, J., Holmquist, J., M Hughes, P. D., Jones, C., Jones, M. C., Karofeld, E., Klein, E. S., Kokfelt, U., Korhola, A., Lacourse, T., Roux, G., Lamentowicz, M., Large, D., Lavoie, M., Loisel, J., Mackay, H., MacDonald, G. M., Makila, M., Magnan, G., Marchant, R., Marcisz, K., Martamp, A., Cortizas, N., Massa, C., Mathijssen, P., Mauquoy, D., Mighall, T., G Mitchell, F. J., Moss, P., Nichols, J., Oksanen, P. O., Orme, L., Packalen, M. S., Robinson, S., Roland, T. P., Sanderson, N. K., Britta Sannel, A. K., Steinberg, N., Swindles, G. T., Edward Turner, T., Uglow, J., Vamp, M., Bellen, S., Linden, M., Geel, B., Wang, G., Yu, Z., Zaragoza-Castells, J., and Zhao, Y.: Latitudinal limits to the predicted increase of the peatland carbon sink with warming, Nat. Clim. Change, 8, 907–914, https://doi.org/10.1038/s41558-018-0271-1, 2018.

Goldstein, A., Turner, W. R., Spawn, S. A., Anderson-Teixeira, K. J., Cook-Patton, S., Fargione, J., Gibbs, H. K., Griscom, B., Hewson, J. H., Howard, J. F., Ledezma, J. C., Page, S., Koh, L. P., Rockström, J., Sanderman, J., and Hole, D. G.: Protecting irrecoverable carbon in Earth's ecosystems, Nat. Clim. Change, 10, 287–295, https://doi.org/10.1038/s41558-020-0738-8, 2020.

Gorham, E.: The Development of Peat Lands, Q. Rev. Biol., 32, 145–166, https://doi.org/10.1086/401755, 1957.

Gorham, E.: Northern Peatlands: Role in the Carbon Cycle and Probable Responses to Climatic Warming, Ecol. Appl., 1, 182–195, https://doi.org/10.2307/1941811, 1991.

Gorham, E., Lehman, C., Dyke, A., Janssens, J., and Dyke, L.: Temporal and spatial aspects of peatland initiation following deglaciation in North America, Quaternary Sci. Rev., 26, 300–311, https://doi.org/10.1016/j.quascirev.2006.08.008, 2007.

Gorham, E., Lehman, C., Dyke, A., Clymo, D., and Janssens, J.: Long-term carbon sequestration in North American peatlands, Quaternary Sci. Rev., 58, 77–82, https://doi.org/10.1016/j.quascirev.2012.09.018, 2012.

Gumbricht, T., Roman-Cuesta, R. M., Verchot, L., Herold, M., Wittmann, F., Householder, E., Herold, N., and Murdiyarso, D.: An expert system model for mapping tropical wetlands and peatlands reveals South America as the largest contributor, Glob. Change Biol., 23, 3581–3599, https://doi.org/10.1111/gcb.13689, 2017.

Günther, A., Barthelmes, A., Huth, V., Joosten, H., Jurasinski, G., Koebsch, F., and Couwenberg, J.: Prompt rewetting of drained peatlands reduces climate warming despite methane emissions, Nat. Commun., 11, 1–5, https://doi.org/10.1038/s41467-020-15499-z, 2020.

Guo, D. and Wang, H.: CMIP5 permafrost degradation projection:A comparison among different regions, J. Geophys. Res.-Atmos., 121, 4499–4517, https://doi.org/10.1002/2015JD024108, 2016.

Haapalehto, T. O., Vasander, H., Jauhiainen, S., Tahvanainen, T., and Kotiaho, J. S.: The effects of peatland restoration on water-table depth, elemental concentrations, and vegetation: 10 years of changes, Restor. Ecol., 19, 587–598, https://doi.org/10.1111/j.1526-100X.2010.00704.x, 2011.

Halsey, L. A., Vitt, D. H., Gignac, L. D., Bryologist, T., and Summer, N.: Sphagnum-Dominated Peatlands in North America since the Last Glacial Maximum: Their Occurrence and Extent Sphagnum-dominated Peatlands in North America Since the Last Glacial Maximum : Their Occurrence and Extent, Bryologist, 103, 334–352, https://doi.org/10.1639/0007-2745(2000)103[0334:SDPINA]2.0.CO;2, 2000.

Harrison, S. P., Bartlein, P. J., Brewer, S., Prentice, I. C., Boyd, M., Hessler, I., Holmgren, K., Izumi, K., and Willis, K.: Climate model benchmarking with glacial and mid-Holocene climates,

Clim. Dynam., 43, 671–688, https://doi.org/10.1007/s00382-013-1922-6, 2014.

Heijmans, M. M. P. D., van der Knaap, Y. A. M., Holmgren, M., and Limpens, J.: Persistent versus transient tree encroachment of temperate peat bogs: effects of climate warming and drought events, Glob. Change Biol., 19, 2240–2250, https://doi.org/10.1111/gcb.12202, 2013.

Helbig, M., Waddington, J. M., Alekseychik, P., Amiro, B., Aurela, M., Barr, A. G., Black, T. A., Carey, S. K., Chen, J., Chi, J., Desai, A. R., Dunn, A., Euskirchen, E. S., Flanagan, L. B., Friborg, T., Garneau, M., Grelle, A., Harder, S., Heliasz, M., Humphreys, E. R., Ikawa, H., Isabelle, P.-E., Iwata, H., Jassal, R., Korkiakoski, M., Kurbatova, J., Kutzbach, L., Lapshina, E., Lindroth, A., Löfvenius, M. O., Lohila, A., Mammarella, I., Marsh, P., Moore, P. A., Maximov, T., Nadeau, D. F., Nicholls, E. M., Nilsson, M. B., Ohta, T., Peichl, M., Petrone, R. M., Prokushkin, A., Quinton, W. L., Roulet, N., Runkle, B. R. K., Sonnentag, O., Strachan, I. B., Taillardat, P., Tuittila, E.-S., Tuovinen, J.-P., Turner, J., Ueyama, M., Varlagin, A., Vesala, T., Wilmking, M., Zyrianov, V., and Schulze, C.: The biophysical climate mitigation potential of boreal peatlands during the growing season, Environ. Res. Lett., 15, 104004, https://doi.org/10.1088/1748-9326/abab34, 2020a.

Helbig, M., Waddington, J. M., Alekseychik, P., Amiro, B. D., Aurela, M., Barr, A. G., Black, T. A., Blanken, P. D., Carey, S. K., Chen, J., Chi, J., Desai, A. R., Dunn, A., Euskirchen, E. S., Flanagan, L. B., Forbrich, I., Friborg, T., Grelle, A., Harder, S., Heliasz, M., Humphreys, E. R., Ikawa, H., Isabelle, P. E., Iwata, H., Jassal, R., Korkiakoski, M., Kurbatova, J., Kutzbach, L., Lindroth, A., Löfvenius, M. O., Lohila, A., Mammarella, I., Marsh, P., Maximov, T., Melton, J. R., Moore, P. A., Nadeau, D. F., Nicholls, E. M., Nilsson, M. B., Ohta, T., Peichl, M., Petrone, R. M., Petrov, R., Prokushkin, A., Quinton, W. L., Reed, D. E., Roulet, N. T., Runkle, B. R., Sonnentag, O., Strachan, I. B., Taillardat, P., Tuittila, E. S., Tuovinen, J. P., Turner, J., Ueyama, M., Varlagin, A., Wilmking, M., Wofsy, S. C., and Zyrianov, V.: Increasing contribution of peatlands to boreal evapotranspiration in a warming climate, Nat. Clim. Change, 10, 555–560, https://doi.org/10.1038/s41558-020-0763-7, 2020b.

Hergoualc'h, K. and Verchot, L. V.: Stocks and fluxes of carbon associated with land use change in Southeast Asian tropical peatlands: A review, Global Biogeochem. Cy., 25, GB2001, https://doi.org/10.1029/2009GB003718, 2011.

Hopple, A. M., Wilson, R. M., Kolton, M., Zalman, C. A., Chanton, J. P., Kostka, J., Hanson, P. J., Keller, J. K., and Bridgham, S. D.: Massive peatland carbon banks vulnerable to rising temperatures, Nat. Commun., 11, 2373, https://doi.org/10.1038/s41467-020-16311-8, 2020.

Hoyt, A. M., Chaussard, E., Seppalainen, S. S., and Harvey, C. F.: Widespread subsidence and carbon emissions across Southeast Asian peatlands, Nat. Geosci., 13, 435–440, https://doi.org/10.1038/s41561-020-0575-4, 2020.

Hugelius, G., Loisel, J., Chadburn, S., Jackson, R. B., Jones, M., MacDonald, G., Marushchak, M., Olefeldt, D., Packalen, M., Siewert, M. B., Treat, C., Turetsky, M., Voigt, C., and Yu, Z.: Large stocks of peatland carbon and nitrogen are vulnerable to permafrost thaw, P. Natl. Acad. Sci. USA, 117, 20438–20446, https://doi.org/10.1073/pnas.1916387117, 2020.

Humpenöder, F., Karstens, K., Lotze-Campen, H., Leifeld, J., Menichetti, L., Barthelmes, A., and Popp, A.: Peatland protection and restoration are key for climate change mitigation, Environ. Res. Lett., 15, 104093, https://doi.org/10.1088/1748-9326/abae2a, 2020.

Hurtt, G. C., Chini, L., Sahajpal, R., Frolking, S., Bodirsky, B. L., Calvin, K., Doelman, J. C., Fisk, J., Fujimori, S., Klein Goldewijk, K., Hasegawa, T., Havlik, P., Heinimann, A., Humpenöder, F., Jungclaus, J., Kaplan, J. O., Kennedy, J., Krisztin, T., Lawrence, D., Lawrence, P., Ma, L., Mertz, O., Pongratz, J., Popp, A., Poulter, B., Riahi, K., Shevliakova, E., Stehfest, E., Thornton, P., Tubiello, F. N., van Vuuren, D. P., and Zhang, X.: Harmonization of global land use change and management for the period 850–2100 (LUH2) for CMIP6, Geosci. Model Dev., 13, 5425–5464, https://doi.org/10.5194/gmd-13-5425-2020, 2020.

Collins, M., Knutti, R., Arblaster, J., Dufresne, J.-L., Fichefet, T., Friedlingstein, P., Gao, X., Gutowski, W. J., Johns, T., Krinner, G., Shongwe, M., Tebaldi, C., Weaver, A. J., and Wehner, M.: Long-term Climate Change: Projections, Com- mitments and Irreversibility. In: Climate Change 2013: The Physical Science Basis. Contribution of Working Group I to the Fifth Assessment Report of the Intergovernmental Panel on Climate Change, edited by: Stocker, T. F., Qin, D., Plattner, G.-K., Tignor, M., Allen, S. K., Boschung, J., Nauels, A., Xia, Y., Bex, V., and Midgley, P. M., Cambridge University Press, Cambridge, United Kingdom and New York, NY, USA, 2013.

Ise, T., Dunn, A. L., Wofsy, S. C., and Moorcroft, P. R.: High sensitivity of peat decomposition to climate change through water-table feedback, Nat. Geosci., 1, 763–766, https://doi.org/10.1038/ngeo331, 2008.

Jiang, L., Song, Y., Sun, L., Song, C., Wang, X., Ma, X., Liu, C., and Gao, J.: Effects of warming on carbon emission and microbial abundances across different soil depths of a peatland in the permafrost region under anaerobic condition, Appl. Soil Ecol., 156, 103712, https://doi.org/10.1016/j.apsoil.2020.103712, 2020.

John, J. G., Blanton, C., McHugh, C., Radhakrishnan, A., Rand, K., Vahlenkamp, H., Wilson, C., Zadeh, N. T., Dunne, J. P., Dussin, R., Horowitz, L. W., Krasting, J. P., Lin, P., Malyshev, S., Naik, V., Ploshay, J., Shevliakova, E., Silvers, L., Stock, C., Winton, M., and Zeng, Y.: NOAA-GFDL GFDL-ESM4 model output prepared for CMIP6 ScenarioMIP, Version 20200601, https://doi.org/10.22033/ESGF/CMIP6.1414, 2018.

Jones, M. C., Harden, J., O'Donnell, J., Manies, K., Jorgenson, T., Treat, C., and Ewing, S.: Rapid carbon loss and slow recovery following permafrost thaw in boreal peatlands, Glob. Change Biol., 23, 1109–1127, https://doi.org/10.1111/gcb.13403, 2017.

Joos, F. and Spahni, R.: Rates of change in natural and anthropogenic radiative forcing over the past 20,000 years, P. Natl. Acad. Sci. USA, 105, 1425–1430, https://doi.org/10.1073/pnas.0707386105, 2008.

Kimmel, K. and Mander, Ü.: Ecosystem services of peatlands: Implications for restoration, Prog. Phys. Geogr., 34, 491–514, https://doi.org/10.1177/0309133310365595, 2010.

Kleinen, T., Brovkin, V., and Schuldt, R. J.: A dynamic model of wetland extent and peat accumulation: Results for the Holocene, Biogeosciences, 9, 235–248, https://doi.org/10.5194/bg-9-235-2012, 2012.

Kluber, L. A., Johnston, E. R., Allen, S. A., Nicholas Hendershot, J., Hanson, P. J., and Schadt, C. W.: Constraints on microbial communities, decomposition and methane production in deep peat deposits, PLoS One, 15, 1–20, https://doi.org/10.1371/journal.pone.0223744, 2020.

Korhola, A., Ruppel, M., Seppä, H., Väliranta, M., Virtanen, T., and Weckström, J.: The importance of northern peatland expansion to the late-Holocene rise of atmospheric methane, Quaternary Sci. Rev., 29, 611–617, https://doi.org/10.1016/j.quascirev.2009.12.010, 2010.

Krasting, J. P., John, J. G., Blanton, C., McHugh, C., Nikonov, S., Radhakrishnan, A., Rand, K., Zadeh, N. T., Balaji, V., Durachta, J., Dupuis, C., Menzel, R., Robinson, T., Underwood, S., Vahlenkamp, H., Dunne, K. A., Gauthier, P. P. G., Ginoux, P., Griffies, S. M., Hallberg, R., Harrison, M., Hurlin, W., Malyshev, S., Naik, V., Paulot, F., Paynter, D. J., Ploshay, J., Reichl, B. G., Schwarzkopf, D. M., Seman, C. J., Silvers, L., Wyman, B., Zeng, Y., Adcroft, A., Dunne, J. P., Dussin, R., Guo, H., He, J., Held, I. M., Horowitz, L. W., Lin, P., Milly, P. C. D., Shevliakova, E., Stock, C., Winton, M., Wittenberg, A. T., Xie, Y., and Zhao, M.: NOAA-GFDL GFDL-ESM4 model output prepared for CMIP6 CMIP historical, Version 20200601, https://doi.org/10.22033/ESGF/CMIP6.8597, 2018.

Lähteenoja, O., Reátegui, Y. R., Räsänen, M., Torres, D. D. C., Oinonen, M., and Page, S.: The large Amazonian peatland carbon sink in the subsiding Pastaza-Marañón foreland basin, Peru, Glob. Change Biol., 18, 164–178, https://doi.org/10.1111/j.1365-2486.2011.02504.x, 2012.

LAI, D.: Methane Dynamics in Northern Peatlands: A Review, Pedosphere, 19, 409–421, https://doi.org/10.1016/S1002-0160(09)00003-4, 2009.

Lara, M. J., Genet, H., McGuire, A. D., Euskirchen, E. S., Zhang, Y., Brown, D. R. N., Jorgenson, M. T., Romanovsky, V., Breen, A., and Bolton, W. R.: Thermokarst rates intensify due to climate change and forest fragmentation in an Alaskan boreal forest lowland, Glob. Change Biol., 22, 816–829, https://doi.org/10.1111/gcb.13124, 2016.

Largeron, C., Krinner, G., Ciais, P., and Brutel-Vuilmet, C.: Implementing northern peatlands in a global land surface model: Description and evaluation in the ORCHIDEE high-latitude version model (ORC-HL-PEAT), Geosci. Model Dev., 11, 3279–3297, https://doi.org/10.5194/gmd-11-3279-2018, 2018.

Lawrence, D. M., Slater, A. G., and Swenson, S. C.: Simulation of present-day and future permafrost and seasonally frozen ground conditions in CCSM4, J. Clim., 25, 2207–2225, https://doi.org/10.1175/JCLI-D-11-00334.1, 2012.

Le Stum-Boivin, É., Magnan, G., Garneau, M., Fenton, N. J., Grondin, P., and Bergeron, Y.: Spatiotemporal evolution of paludification associated with autogenic and allogenic factors in the black spruce–moss boreal forest of Québec, Canada, Quaternary Res., 91, 650–664, https://doi.org/10.1017/qua.2018.101, 2019.

Lee, J., Kim, J., Sun, M.-A., Kim, B.-H., Moon, H., Sung, H. M., Kim, J., and Byun, Y.-H.: Evaluation of the Korea Meteorological Administration Advanced Community Earth-System model (K-ACE), Asia-Pacific J. Atmos. Sci., 56, 381–395, https://doi.org/10.1007/s13143-019-00144-7, 2020.

Leifeld, J. and Menichetti, L.: The underappreciated potential of peatlands in global climate change mitigation strategies, Nat. Commun., 9, 1071, https://doi.org/10.1038/s41467-018-03406-6, 2018.

Leifeld, J., Wüst-Galley, C., and Page, S.: Intact and managed peatland soils as a source and sink of GHGs from 1850 to 2100, Nat. Clim. Change, 9, 945–947, https://doi.org/10.1038/s41558-019-0615-5, 2019.

Lenton, T. M., Held, H., Kriegler, E., Hall, J. W., Lucht, W., Rahmstorf, S., and Schellnhuber, H. J.: Tipping elements in the Earth's climate system, P. Natl. Acad. Sci. USA, 105, 1786–1793, https://doi.org/10.1073/pnas.0705414105, 2008.

Li, C., Grayson, R., Holden, J., and Li, P.: Erosion in peatlands: Recent research progress and future directions, Earth-Sci. Rev., 185, 870–886, https://doi.org/10.1016/j.earscirev.2018.08.005, 2018.

Lienert, S. and Joos, F.: A Bayesian ensemble data assimilation to constrain model parameters and land-use carbon emissions, Biogeosciences, 15, 2909–2930, https://doi.org/10.5194/bg-15-2909-2018, 2018.

Lindsay, R.: Peatland Classification, in: Wetl. B., Springer Netherlands, Dordrecht, 1515–1528, https://doi.org/10.1007/978-90-481-9659-3_341, 2018.

Liu, Z., Otto-Bliesner, B. L., He, F., Brady, E. C., Tomas, R., Clark, P. U., Carlson, A. E., Lynch-Stieglitz, J., Curry, W., Brook, E., Erickson, D., Jacob, R., Kutzbach, J., and Cheng, J.: Transient simulation of last deglaciation with a new mechanism for bolling-allerod warming, Science, 325, 310–314, https://doi.org/10.1126/science.1171041, 2009.

Loisel, J. and Bunsen, M.: Abrupt Fen-Bog Transition Across Southern Patagonia: Timing, Causes, and Impacts on Carbon Sequestration, Front. Ecol. Evol., 8, 1–19, https://doi.org/10.3389/fevo.2020.00273, 2020.

Loisel, J., Yu, Z., Parsekian, A., Nolan, J., and Slater, L.: Quantifying landscape morphology influence on peatland lateral expansion using ground-penetrating radar (GPR) and peat core analysis, J. Geophys. Res.-Biogeo., 118, 373–384, https://doi.org/10.1002/jgrg.20029, 2013.

Loisel, J., van Bellen, S., Pelletier, L., Talbot, J., Hugelius, G., Karran, D., Yu, Z., Nichols, J., and Holmquist, J.: Insights and issues with estimating northern peatland carbon stocks and fluxes since the Last Glacial Maximum, Earth-Sci. Rev., 165, 59–80, https://doi.org/10.1016/j.earscirev.2016.12.001, 2017.

Loisel, J., Gallego-Sala, A. V., Amesbury, M. J., Magnan, G., Anshari, G., Beilman, D. W., Benavides, J. C., Blewett, J., Camill, P., Charman, D. J., Chawchai, S., Hedgpeth, A., Kleinen, T., Korhola, A., Large, D., Mansilla, C. A., Müller, J., van Bellen, S., West, J. B., Yu, Z., Bubier, J. L., Garneau, M., Moore, T., Sannel, A. B., Page, S., Väliranta, M., Bechtold, M., Brovkin, V., Cole, L. E., Chanton, J. P., Christensen, T. R., Davies, M. A., De Vleeschouwer, F., Finkelstein, S. A., Frolking, S., Gałka, M., Gandois, L., Girkin, N., Harris, L. I., Heinemeyer, A., Hoyt, A. M., Jones, M. C., Joos, F., Juutinen, S., Kaiser, K., Lacourse, T., Lamentowicz, M., Larmola, T., Leifeld, J., Lohila, A., Milner, A. M., Minkkinen, K., Moss, P., Naafs, B. D., Nichols, J., O'Donnell, J., Payne, R., Philben, M., Piilo, S., Quillet, A., Ratnayake, A. S., Roland, T. P., Sjögersten, S., Sonnentag, O., Swindles, G. T., Swinnen, W., Talbot, J., Treat, C., Valach, A. C., and Wu, J.: Expert assessment of future vulnerability of the global peatland carbon sink, Nat. Clim. Change, 11, 70–77, https://doi.org/10.1038/s41558-020-00944-0, 2021.

MacDonald, G. M., Beilman, D. W., Kremenetski, K. V., Sheng, Y., Smith, L. C., and Velichko, A. A.: Rapid Early Development of Circumarctic Peatlands and Atmospheric CH_4 and CO_2 Variations, Science, 314, 285–288, https://doi.org/10.1126/science.1131722, 2006.

Magnússon, R. Í., Limpens, J., Huissteden, J., Kleijn, D., Maximov, T. C., Rotbarth, R., Sass-Klaassen, U., and Heijmans, M. M. P. D.: Rapid Vegetation Succession and Coupled Permafrost Dynamics in Arctic Thaw Ponds in the Siberian Lowland Tundra, J. Geophys. Res.-Biogeo., 125, 1–20, https://doi.org/10.1029/2019JG005618, 2020.

Mamet, S. D., Chun, K. P., Kershaw, G. G., Loranty, M. M., and Peter Kershaw, G.: Recent Increases in Permafrost Thaw Rates and Areal Loss of Palsas in the Western Northwest Territories, Canada, Permafrost Periglac., 28, 619–633, https://doi.org/10.1002/ppp.1951, 2017.

Mauritsen, T., Bader, J., Becker, T., Behrens, J., Bittner, M., Brokopf, R., Brovkin, V., Claussen, M., Crueger, T., Esch, M., Fast, I., Fiedler, S., Fläschner, D., Gayler, V., Giorgetta, M., Goll, D. S., Haak, H., Hagemann, S., Hedemann, C., Hohenegger, C., Ilyina, T., Jahns, T., Jimenéz-de-la-Cuesta, D., Jungclaus, J., Kleinen, T., Kloster, S., Kracher, D., Kinne, S., Kleberg, D., Lasslop, G., Kornblueh, L., Marotzke, J., Matei, D., Meraner, K., Mikolajewicz, U., Modali, K., Möbis, B., Müller, W. A., Nabel, J. E. M. S., Nam, C. C. W., Notz, D., Nyawira, S., Paulsen, H., Peters, K., Pincus, R., Pohlmann, H., Pongratz, J., Popp, M., Raddatz, T. J., Rast, S., Redler, R., Reick, C. H., Rohrschneider, T., Schemann, V., Schmidt, H., Schnur, R., Schulzweida, U., Six, K. D., Stein, L., Stemmler, I., Stevens, B., Storch, J., Tian, F., Voigt, A., Vrese, P., Wieners, K., Wilkenskjeld, S., Winkler, A., and Roeckner, E.: Developments in the MPI-M Earth System Model version 1.2 (MPI-ESM1.2) and Its Response to Increasing CO_2, J. Adv. Model. Earth Syst., 11, 998–1038, https://doi.org/10.1029/2018MS001400, 2019.

McSweeney, C. F. and Jones, R. G.: How representative is the spread of climate projections from the 5 CMIP5 GCMs used in ISI-MIP?, Clim. Serv., 1, 24–29, https://doi.org/10.1016/j.cliser.2016.02.001, 2016.

Meinshausen, M., Nicholls, Z. R. J., Lewis, J., Gidden, M. J., Vogel, E., Freund, M., Beyerle, U., Gessner, C., Nauels, A., Bauer, N., Canadell, J. G., Daniel, J. S., John, A., Krummel, P. B., Luderer, G., Meinshausen, N., Montzka, S. A., Rayner, P. J., Reimann, S., Smith, S. J., van den Berg, M., Velders, G. J. M., Vollmer, M. K., and Wang, R. H. J.: The shared socioeconomic pathway (SSP) greenhouse gas concentrations and their extensions to 2500, Geosci. Model Dev., 13, 3571–3605, https://doi.org/10.5194/gmd-13-3571-2020, 2020.

Minayeva, T. Y. and Sirin, A. A.: Peatland biodiversity and climate change, Biol. Bull. Rev., 2, 164–175, https://doi.org/10.1134/s207908641202003x, 2012.

Mitchell, T. D. and Jones, P. D.: An improved method of constructing a database of monthly climate observations and associated high-resolution grids, Int. J. Climatol., 25, 693–712, https://doi.org/10.1002/joc.1181, 2005.

Moore, P. D.: The ecology of peat-forming processes: a review, Int. J. Coal Geol., 12, 89–103, https://doi.org/10.1016/0166-5162(89)90048-7, 1989.

Morris, P. J., Belyea, L. R., and Baird, A. J.: Ecohydrological feedbacks in peatland development: A theoretical modelling study, J. Ecol., 99, 1190–1201, https://doi.org/10.1111/j.1365-2745.2011.01842.x, 2011.

Morris, P. J., Swindles, G. T., Valdes, P. J., Ivanovic, R. F., Gregoire, L. J., Smith, M. W., Tarasov, L., Haywood, A. M., and Bacon, K. L.: Global peatland initiation driven by regionally asynchronous warming, P. Natl. Acad. Sci. USA, 115, 4851–4856, https://doi.org/10.1073/pnas.1717838115, 2018.

Müller, J. and Joos, F.: Global peatland area and carbon dynamics from the Last Glacial Maximum to the present – a process-based model investigation, Biogeosciences, 17, 5285–5308, https://doi.org/10.5194/bg-17-5285-2020, 2020.

Müller, J. and Joos, F.: Committed and projected future changes in global peatlands – continued transient model simulations since the Last Glacial Maximum, Zenodo [Dataset], https://doi.org/10.5281/zenodo.4627681, 2021.

Nugent, K. A., Strachan, I. B., Roulet, N. T., Strack, M., Frolking, S., and Helbig, M.: Prompt active restoration of peatlands substantially reduces climate impact, Environ. Res. Lett., 14, 124030, https://doi.org/10.1088/1748-9326/ab56e6, 2019.

Olefeldt, D., Goswami, S., Grosse, G., Hayes, D., Hugelius, G., Kuhry, P., McGuire, A. D., Romanovsky, V. E., Sannel, A., Schuur, E., and Turetsky, M. R.: Circumpolar distribution and carbon storage of thermokarst landscapes, Nat. Commun., 7, 13043, https://doi.org/10.1038/ncomms13043, 2016.

O'Neill, B. C., Tebaldi, C., Van Vuuren, D. P., Eyring, V., Friedlingstein, P., Hurtt, G., Knutti, R., Kriegler, E., Lamarque, J. F., Lowe, J., Meehl, G. A., Moss, R., Riahi, K., and Sanderson, B. M.: The Scenario Model Intercomparison Project (ScenarioMIP) for CMIP6, Geosci. Model Dev., 9, 3461–3482, https://doi.org/10.5194/gmd-9-3461-2016, 2016.

Packalen, M. S., Finkelstein, S. A., and McLaughlin, J. W.: Carbon storage and potential methane production in the Hudson Bay Lowlands since mid-Holocene peat initiation, Nat. Commun., 5, 1–8, https://doi.org/10.1038/ncomms5078, 2014.

Page, S. and Baird, A.: Peatlands and Global Change: Response and Resilience, Annu. Rev. Environ. Resour., 41, 35–57, https://doi.org/10.1146/annurev-environ-110615-085520, 2016.

Page, S. E. and Hooijer, A.: In the line of fire: The peatlands of Southeast Asia, Philos. Trans. R. Soc. B, 371, https://doi.org/10.1098/rstb.2015.0176, 2016.

Page, S. E., Rieley, J. O., and Banks, C. J.: Global and regional importance of the tropical peatland carbon pool, Glob. Change Biol., 17, 798–818, https://doi.org/10.1111/j.1365-2486.2010.02279.x, 2011.

Payette, S., Delwaide, A., Caccianiga, M., and Beauchemin, M.: Accelerated thawing of subarctic peatland permafrost over the last 50 years, Geophys. Res. Lett., 31, 1–4, https://doi.org/10.1029/2004GL020358, 2004.

Pellerin, S. and Lavoie, C.: Recent expansion of jack pine in peatlands of southeastern Québec: A paleoecological study, Écoscience, 10, 247–257, https://doi.org/10.1080/11956860.2003.11682772, 2003.

Pinceloup, N., Poulin, M., Brice, M.-H., and Pellerin, S.: Vegetation changes in temperate ombrotrophic peatlands over a 35 year period, PLoS One, 15, e0229146, https://doi.org/10.1371/journal.pone.0229146, 2020.

Posa, M. R. C., Wijedasa, L. S., and Corlett, R. T.: Biodiversity and conservation of tropical peat swamp forests, Bioscience, 61, 49–57, https://doi.org/10.1525/bio.2011.61.1.10, 2011.

Qiu, C., Zhu, D., Ciais, P., Guenet, B., Krinner, G., Peng, S., Aurela, M., Bernhofer, C., Brümmer, C., Bret-Harte, S., Chu, H., Chen, J., Desai, A. R., Dušek, J., Euskirchen, E. S., Fortuniak, K., Flanagan, L. B., Friborg, T., Grygoruk, M., Gogo, S., Grünwald, T., Hansen, B. U., Holl, D., Humphreys, E., Hurkuck, M., Kiely, G., Klatt, J., Kutzbach, L., Largeron, C., Laggoun-Défarge, F., Lund, M., Lafleur, P. M., Li, X., Mammarella, I., Merbold, L., Nilsson, M. B., Olejnik, J., Ottosson-Löfvenius, M., Oechel, W., Parmentier, F. J. W., Peichl, M., Pirk, N., Peltola, O., Pawlak, W., Rasse, D., Rinne, J., Shaver, G., Peter Schmid, H., Sottocornola, M., Steinbrecher, R., Sachs, T., Urbaniak, M., Zona, D., and Ziemblinska, K.: ORCHIDEE-PEAT (revision 4596), a model for northern peatland CO_2, water, and energy fluxes on daily to annual scales, Geosci. Model Dev., 11, 497–519, https://doi.org/10.5194/gmd-11-497-2018, 2018.

Qiu, C., Zhu, D., Ciais, P., Guenet, B., and Peng, S.: The role of northern peatlands in the global carbon cycle for the 21st century, Glob. Ecol. Biogeogr., 29, 956–973, https://doi.org/10.1111/geb.13081, 2020.

Ribeiro, K., Pacheco, F. S., Ferreira, J. W., de Sousa-Neto, E. R., Hastie, A., Krieger Filho, G. C., Alvalá, P. C., Forti, M. C., and Ometto, J. P.: Tropical peatlands and their contribution to the global carbon cycle and climate change, Glob. Change Biol., 27, 489–505, https://doi.org/10.1111/gcb.15408, 2021.

Rong, X.: CAMS CAMS_CSM1.0 model output prepared for CMIP6 CMIP historical, Version 20200601, https://doi.org/10.22033/ESGF/CMIP6.9754, 2019a.

Rong, X.: CAMS CAMS-CSM1.0 model output prepared for CMIP6 ScenarioMIP, Version 20200601, https://doi.org/10.22033/ESGF/CMIP6.11004, 2019b.

Rong, X., Li, J., Chen, H., Xin, Y., Su, J., Hua, L., Zhou, T., Qi, Y., Zhang, Z., Zhang, G., and Li, J.: The CAMS Climate System Model and a Basic Evaluation of Its Climatology and Climate Variability Simulation, J. Meteorol. Res., 32, 839–861, https://doi.org/10.1007/s13351-018-8058-x, 2018.

Ruppel, M., Väliranta, M., Virtanen, T., and Korhola, A.: Post-glacial spatiotemporal peatland initiation and lateral expansion dynamics in North America and northern Europe, Holocene, 23, 1596–1606, https://doi.org/10.1177/0959683613499053, 2013.

Rydin, H. and Jeglum, J. K.: The Biology of Peatlands, Oxford University Press, https://doi.org/10.1093/acprof:osobl/9780199602995.001.0001, 2013.

Sawada, M., Viau, A. E., and Gajewski, K.: The biogeography of aquatic macrophytes in North America since the Last Glacial Maximum, J. Biogeogr., 30, 999–1017, https://doi.org/10.1046/j.1365-2699.2003.00866.x, 2003.

Schuldt, R. J., Brovkin, V., Kleinen, T., and Winderlich, J.: Modelling Holocene carbon accumulation and methane emissions of boreal wetlands-an Earth system model approach, Biogeosciences, 10, 1659–1674, https://doi.org/10.5194/bg-10-1659-2013, 2013.

Seland, Ø., Bentsen, M., Olivié, D., Toniazzo, T., Gjermundsen, A., Graff, L. S., Debernard, J. B., Gupta, A. K., He, Y.-c., Kirkevåg, A., Schwinger, J., Tjiputra, J., Aas, K. S., Bethke, I., Fan, Y., Griesfeller, J., Grini, A., Guo, C., Ilicak, M., Karset, I. H. H., Landgren, O., Liakka, J., Moseid, K. O., Nummelin, A., Spensberger, C., Tang, H., Zhang, Z., Heinze, C., Iversen, T., and Schulz, M.: Overview of the Norwegian Earth System Model (NorESM2) and key climate response of CMIP6 DECK, historical, and scenario simulations, Geosci. Model Dev., 13, 6165–6200, https://doi.org/10.5194/gmd-13-6165-2020, 2020.

Seland, Ø., Bentsen, M., Oliviè, D. J. L., Toniazzo, T., Gjermundsen, A., Graff, L. S., Debernard, J. B., Gupta, A. K., He, Y., Kirkevåg, A., Schwinger, J., Tjiputra, J., Aas, K. S., Bethke, I., Fan, Y., Griesfeller, J., Grini, A., Guo, C., Ilicak, M., Karset, I. H. H., Landgren, O. A., Liakka, J., Moseid, K. O., Nummelin, A., Spensberger, C., Tang, H., Zhang, Z., Heinze, C., Iversen, T., and Schulz, M.: NCC NorESM2-LM model output prepared for CMIP6 CMIP historical, Version 20200601, https://doi.org/10.22033/ESGF/CMIP6.8036, 2019a.

Seland, Ø., Bentsen, M., Oliviè, D. J. L., Toniazzo, T., Gjermundsen, A., Graff, L. S., Debernard, J. B., Gupta, A. K., He, Y., Kirkevåg, A., Schwinger, J., Tjiputra, J., Aas, K. S., Bethke, I., Fan, Y., Griesfeller, J., Grini, A., Guo, C., Ilicak, M., Karset, I. H. H., Landgren, O. A., Liakka, J., Moseid, K. O., Nummelin, A., Spensberger, C., Tang, H., Zhang, Z., Heinze, C., Iversen, T., and Schulz, M.: NCC NorESM2-LM model output prepared for CMIP6 ScenarioMIP, Version 20200601, https://doi.org/10.22033/ESGF/CMIP6.604, 2019b.

Sitch, S., Smith, B., Prentice, I. C., Arneth, A., Bondeau, A., Cramer, W., Kaplan, J. O., Levis, S., Lucht, W., Sykes, M. T., Thonicke, K., and Venevsky, S.: Evaluation of ecosystem dynamics, plant geography and terrestrial carbon cycling in the LPJ dynamic global vegetation model, Glob. Change Biol., 9, 161–185, https://doi.org/10.1046/j.1365-2486.2003.00569.x, 2003.

Spahni, R., Joos, F., Stocker, B. D., Steinacher, M., and Yu, Z. C.: Transient simulations of the carbon and nitrogen dynamics in northern peatlands: From the Last Glacial Maximum to the 21st century, Clim. Past, 9, 1287–1308, https://doi.org/10.5194/cp-9-1287-2013, 2013.

Stocker, B. D., Roth, R., Joos, F., Spahni, R., Steinacher, M., Zaehle, S., Bouwman, L., Xu-Ri, and Prentice, I. C.: Multiple greenhouse-gas feedbacks from the land biosphere under future climate change scenarios, Nat. Clim. Chang., 3, 666–672, https://doi.org/10.1038/nclimate1864, 2013.

Stocker, B. D., Feissli, F., Strassmann, K. M., Spahni, R., and Joos, F.: Past and future carbon fluxes from land use change, shifting cultivation and wood harvest, Tellus B, 66, https://doi.org/10.3402/tellusb.v66.23188, 2014a.

Stocker, B. D., Spahni, R., and Joos, F.: DYPTOP: A cost-efficient TOPMODEL implementation to simulate sub-grid spatio-temporal dynamics of global wetlands and peatlands, Geosci. Model Dev., 7, 3089–3110, https://doi.org/10.5194/gmd-7-3089-2014, 2014b.

Stocker, B. D., Yu, Z., Massa, C., and Joos, F.: Holocene peatland and ice-core data constraints on the timing and magnitude of CO_2 emissions from past land use, P. Natl. Acad. Sci. USA, 114, 1492–1497, https://doi.org/10.1073/pnas.1613889114, 2017.

Swart, N. C., Cole, J. N. S., Kharin, V. V., Lazare, M., Scinocca, J. F., Gillett, N. P., Anstey, J., Arora, V., Christian, J. R., Hanna, S., Jiao, Y., Lee, W. G., Majaess, F., Saenko, O. A., Seiler, C., Seinen, C., Shao, A., Sigmond, M., Solheim, L., von Salzen, K., Yang, D., and Winter, B.: The Canadian Earth System Model version 5 (CanESM5.0.3), Geosci. Model Dev., 12, 4823–4873, https://doi.org/10.5194/gmd-12-4823-2019, 2019a.

Swart, N. C., Cole, J. N. S., Kharin, V. V., Lazare, M., Scinocca, J. F., Gillett, N. P., Anstey, J., Arora, V., Christian, J. R.,

Jiao, Y., Lee, W. G., Majaess, F., Saenko, O. A., Seiler, C., Seinen, C., Shao, A., Solheim, L., von Salzen, K., Yang, D., Winter, B., and Sigmond, M.: CCCma CanESM5 model output prepared for CMIP6 CMIP historical, Version 20200601, https://doi.org/10.22033/ESGF/CMIP6.3610, 2019b.

Swart, N. C., Cole, J. N. S., Kharin, V. V., Lazare, M., Scinocca, J. F., Gillett, N. P., Anstey, J., Arora, V., Christian, J. R., Jiao, Y., Lee, W. G., Majaess, F., Saenko, O. A., Seiler, C., Seinen, C., Shao, A., Solheim, L., von Salzen, K., Yang, D., Winter, B., and Sigmond, M.: CCCma CanESM5 model output prepared for CMIP6 ScenarioMIP, Version 20200601, https://doi.org/10.22033/ESGF/CMIP6.1317, 2019c.

Swindles, G. T., Morris, P. J., Mullan, D., Watson, E. J., Turner, T. E., Roland, T. P., Amesbury, M. J., Kokfelt, U., Schoning, K., Pratte, S., Gallego-Sala, A., Charman, D. J., Sanderson, N., Garneau, M., Carrivick, J. L., Woulds, C., Holden, J., Parry, L., and Galloway, J. M.: The long-term fate of permafrost peatlands under rapid climate warming, Sci. Rep., 5, 1–6, https://doi.org/10.1038/srep17951, 2015.

Swindles, G. T., Morris, P. J., Wheeler, J., Smith, M. W., Bacon, K. L., Edward Turner, T., Headley, A., and Galloway, J. M.: Resilience of peatland ecosystem services over millennial timescales: Evidence from a degraded British bog, J. Ecol., 104, 621–636, https://doi.org/10.1111/1365-2745.12565, 2016.

Swindles, G. T., Morris, P. J., Mullan, D. J., Payne, R. J., Roland, T. P., Amesbury, M. J., Lamentowicz, M., Turner, T. E., Gallego-Sala, A., Sim, T., Barr, I. D., Blaauw, M., Blundell, A., Chambers, F. M., Charman, D. J., Feurdean, A., Galloway, J. M., Gałka, M., Green, S. M., Kajukało, K., Karofeld, E., Korhola, A., Lamentowicz, Ł., Langdon, P., Marcisz, K., Mauquoy, D., Mazei, Y. A., McKeown, M. M., Mitchell, E. A. D., Novenko, E., Plunkett, G., Roe, H. M., Schoning, K., Sillasoo, Ü., Tsyganov, A. N., van der Linden, M., Väliranta, M., and Warner, B.: Widespread drying of European peatlands in recent centuries, Nat. Geosci., 12, 922–928, https://doi.org/10.1038/s41561-019-0462-z, 2019.

Swinnen, W., Broothaerts, N., and Verstraeten, G.: Modelling long-term blanket peatland development in eastern Scotland, Biogeosciences, 16, 3977–3996, https://doi.org/10.5194/bg-16-3977-2019, 2019.

Talbot, J., Richard, P., Roulet, N., and Booth, R.: Assessing long-term hydrological and ecological responses to drainage in a raised bog using paleoecology and a hydrosequence, J. Veg. Sci., 21, 143–156, https://doi.org/10.1111/j.1654-1103.2009.01128.x, 2010.

Treat, C. C., Kleinen, T., Broothaerts, N., Dalton, A. S., Dommain, R., Douglas, T. A., Drexler, J. Z., Finkelstein, S. A., Grosse, G., Hope, G., Hutchings, J., Jones, M. C., Kuhry, P., Lacourse, T., Lähteenoja, O., Loisel, J., Notebaert, B., Payne, R. J., Peteet, D. M., Sannel, A. B. K., Stelling, J. M., Strauss, J., Swindles, G. T., Talbot, J., Tarnocai, C., Verstraeten, G., Williams, C. J., Xia, Z., Yu, Z., Väliranta, M., Hättestrand, M., Alexanderson, H., and Brovkin, V.: Widespread global peatland establishment and persistence over the last 130,000 y, P. Natl. Acad. Sci. USA, 116, 201813305, https://doi.org/10.1073/pnas.1813305116, 2019.

Turetsky, M. R., Kotowska, A., Bubier, J., Dise, N. B., Crill, P., Hornibrook, E. R., Minkkinen, K., Moore, T. R., Myers-Smith, I. H., Nykänen, H., Olefeldt, D., Rinne, J., Saarnio, S., Shurpali, N., Tuittila, E. S., Waddington, J. M., White, J. R., Wickland, K. P., and Wilmking, M.: A synthesis of methane emissions from 71 northern, temperate, and subtropical wetlands, Glob. Change Biol., 20, 2183–2197, https://doi.org/10.1111/gcb.12580, 2014.

Turetsky, M. R., Benscoter, B., Page, S., Rein, G., Van Der Werf, G. R., and Watts, A.: Global vulnerability of peatlands to fire and carbon loss, Nat. Geosci., 8, 11–14, https://doi.org/10.1038/ngeo2325, 2015.

Turetsky, M. R., Abbott, B. W., Jones, M. C., Anthony, K. W., Olefeldt, D., Schuur, E. A., Grosse, G., Kuhry, P., Hugelius, G., Koven, C., Lawrence, D. M., Gibson, C., Sannel, A. B. K., and McGuire, A. D.: Carbon release through abrupt permafrost thaw, Nat. Geosci., 13, 138–143, https://doi.org/10.1038/s41561-019-0526-0, 2020.

Voigt, C., Marushchak, M. E., Mastepanov, M., Lamprecht, R. E., Christensen, T. R., Dorodnikov, M., Jackowicz-Korczyński, M., Lindgren, A., Lohila, A., Nykänen, H., Oinonen, M., Oksanen, T., Palonen, V., Treat, C. C., Martikainen, P. J., and Biasi, C.: Ecosystem carbon response of an Arctic peatland to simulated permafrost thaw, Glob. Change Biol., 25, 1746–1764, https://doi.org/10.1111/gcb.14574, 2019.

Volodin, E., Mortikov, E., Gritsun, A., Lykossov, V., Galin, V., Diansky, N., Gusev, A., Kostrykin, S., Iakovlev, N., Shestakova, A., and Emelina, S.: INM INM-CM5-0 model output prepared for CMIP6 CMIP historical, Version 20200601, https://doi.org/10.22033/ESGF/CMIP6.5070, 2019a.

Volodin, E., Mortikov, E., Gritsun, A., Lykossov, V., Galin, V., Diansky, N., Gusev, A., Kostrykin, S., Iakovlev, N., Shestakova, A., and Emelina, S.: INM INM-CM5-0 model output prepared for CMIP6 ScenarioMIP, Version 20200601, https://doi.org/10.22033/ESGF/CMIP6.12322, 2019b.

Volodin, E. M., Mortikov, E. V., Kostrykin, S. V., Galin, V. Y., Lykossov, V. N., Gritsun, A. S., Diansky, N. A., Gusev, A. V., and Iakovlev, N. G.: Simulation of the present-day climate with the climate model INMCM5, Clim. Dynam., 49, 3715–3734, https://doi.org/10.1007/s00382-017-3539-7, 2017.

Waddington, J. M., Morris, P. J., Kettridge, N., Granath, G., Thompson, D. K., and Moore, P. A.: Hydrological feedbacks in northern peatlands, Ecohydrology, 8, 113–127, https://doi.org/10.1002/eco.1493, 2015.

Wang, S., Zhuang, Q., Lähteenoja, O., Draper, F. C., and Cadillo-Quiroz, H.: Potential shift from a carbon sink to a source in Amazonian peatlands under a changing climate, P. Natl. Acad. Sci. USA, 115, 12407–12412, https://doi.org/10.1073/pnas.1801317115, 2018.

Wania, R., Ross, I., and Prentice, I. C.: Integrating peatlands and permafrost into a dynamic global vegetation model: 2. Evaluation and sensitivity of vegetation and carbon cycle processes, Global Biogeochem. Cy., 23, GB3015, https://doi.org/10.1029/2008GB003413, 2009a.

Wania, R., Ross, I., and Prentice, I. C.: Integrating peatlands and permafrost into a dynamic global vegetation model: 1. Evaluation and sensitivity of physical land surface processes, Global Biogeochem. Cy., 23, 1–19, https://doi.org/10.1029/2008GB003412, 2009b.

Warren, M., Frolking, S., Dai, Z., and Kurnianto, S.: Impacts of land use, restoration, and climate change on tropical peat carbon stocks in the twenty-first century: implications for climate mitigation, Mitig. Adapt. Strateg. Glob. Change, 22, 1041–1061, https://doi.org/10.1007/s11027-016-9712-1, 2017.

Wibisana, A. G. and Setyorini, S. N.: Peatland Protection in Indonesia: Toward the Right Direction?, in: Springer Clim., Springer International Publishing, 301–328, https://doi.org/10.1007/978-3-030-55536-8_15, 2021.

Wieners, K.-H., Giorgetta, M., Jungclaus, J., Reick, C., Esch, M., Bittner, M., Gayler, V., Haak, H., de Vrese, P., Raddatz, T., Mauritsen, T., von Storch, J.-S., Behrens, J., Brovkin, V., Claussen, M., Crueger, T., Fast, I., Fiedler, S., Hagemann, S., Hohenegger, C., Jahns, T., Kloster, S., Kinne, S., Lasslop, G., Kornblueh, L., Marotzke, J., Matei, D., Meraner, K., Mikolajewicz, U., Modali, K., Müller, W., Nabel, J., Notz, D., Peters, K., Pincus, R., Pohlmann, H., Pongratz, J., Rast, S., Schmidt, H., Schnur, R., Schulzweida, U., Six, K., Stevens, B., Voigt, A., and Roeckner, E.: MPI-M MPIESM1.2-LR model output prepared for CMIP6 ScenarioMIP, Version 20200601, https://doi.org/10.22033/ESGF/CMIP6.793, 2019a.

Wieners, K.-H., Giorgetta, M., Jungclaus, J., Reick, C., Esch, M., Bittner, M., Legutke, S., Schupfner, M., Wachsmann, F., Gayler, V., Haak, H., de Vrese, P., Raddatz, T., Mauritsen, T., von Storch, J.-S., Behrens, J., Brovkin, V., Claussen, M., Crueger, T., Fast, I., Fiedler, S., Hagemann, S., Hohenegger, C., Jahns, T., Kloster, S., Kinne, S., Lasslop, G., Kornblueh, L., Marotzke, J., Matei, D., Meraner, K., Mikolajewicz, U., Modali, K., Müller, W., Nabel, J., Notz, D., Peters, K., Pincus, R., Pohlmann, H., Pongratz, J., Rast, S., Schmidt, H., Schnur, R., Schulzweida, U., Six, K., Stevens, B., Voigt, A., and Roeckner, E.: MPI-M MPI-ESM1.2-LR model output prepared for CMIP6 CMIP historical, Version 20200601, https://doi.org/10.22033/ESGF/CMIP6.6595, 2019b.

Wilson, R. M., Hopple, A. M., Tfaily, M. M., Sebestyen, S. D., Schadt, C. W., Pfeifer-Meister, L., Medvedeff, C., McFarlane, K. J., Kostka, J. E., Kolton, M., Kolka, R., Kluber, L. A., Keller, J. K., Guilderson, T. P., Griffiths, N. A., Chanton, J. P., Bridgham, S. D., and Hanson, P. J.: Stability of peatland carbon to rising temperatures, Nat. Commun., 7, 13723, https://doi.org/10.1038/ncomms13723, 2016.

Xu, H., Lan, J., Sheng, E., Liu, Y., Liu, B., Yu, K., Ye, Y., Cheng, P., Qiang, X., Lu, F., and Wang, X.: Tropical/Subtropical Peatland Development and Global CH_4 during the Last Glaciation, Sci. Rep., 6, 30431, https://doi.org/10.1038/srep30431, 2016.

Xu, J., Morris, P. J., Liu, J., and Holden, J.: Hotspots of peatland-derived potable water use identified by global analysis, Nat. Sustain., 1, 246–253, https://doi.org/10.1038/s41893-018-0064-6, 2018a.

Xu, J., Morris, P. J., Liu, J., and Holden, J.: PEATMAP: Refining estimates of global peatland distribution based on a meta-analysis, CATENA, 160, 134–140, https://doi.org/10.1016/j.catena.2017.09.010, 2018b.

Xu-Ri, Prentice, I. C., Spahni, R., and Niu, H. S.: Modelling terrestrial nitrous oxide emissions and implications for climate feedback, New Phytol., 196, 472–488, https://doi.org/10.1111/j.1469-8137.2012.04269.x, 2012.

Young, D. M., Baird, A. J., Morris, P. J., and Holden, J.: Simulating the long-term impacts of drainage and restoration on the ecohydrology of peatlands, Water Resour. Res., 53, 6510–6522, https://doi.org/10.1002/2016WR019898, 2017.

Yu, Z.: Holocene carbon flux histories of the world's peatlands: Global carbon-cycle implications, The Holocene, 21, 761–774, https://doi.org/10.1177/0959683610386982, 2011.

Yu, Z., Loisel, J., Brosseau, D. P., Beilman, D. W., and Hunt, S. J.: Global peatland dynamics since the Last Glacial Maximum, Geophys. Res. Lett., 37, 1–5, https://doi.org/10.1029/2010GL043584, 2010.

Yu, Z., Loisel, J., Turetsky, M. R., Cai, S., Zhao, Y., Frolking, S., MacDonald, G. M., and Bubier, J. L.: Evidence for elevated emissions from high-latitude wetlands contributing to high atmospheric CH_4 concentration in the early Holocene, Global Biogeochem. Cy., 27, 131–140, https://doi.org/10.1002/gbc.20025, 2013.

Yu, Z., Loisel, J., Charman, D. J., Beilman, D. W., and Camill, P.: Holocene peatland carbon dynamics in the circum-Arctic region: An introduction, The Holocene, 24, 1021–1027, https://doi.org/10.1177/0959683614540730, 2014.

Yu, Z. C.: Northern peatland carbon stocks and dynamics: A review, Biogeosciences, 9, 4071–4085, https://doi.org/10.5194/bg-9-4071-2012, 2012.

Yukimoto, S., Kawai, H., Koshiro, T., Oshima, N., Yoshida, K., Urakawa, S., Tsujino, H., Deushi, M., Tanaka, T., Hosaka, M., Yabu, S., Yoshimura, H., Shindo, E., Mizuta, R., Obata, A., Adachi, Y., and Ishii, M.: The Meteorological Research Institute Earth System Model Version 2.0, MRI-ESM2.0: Description and Basic Evaluation of the Physical Component, J. Meteorol. Soc. Jpn. Ser. II, 97, 931–965, https://doi.org/10.2151/jmsj.2019-051, 2019a.

Yukimoto, S., Koshiro, T., Kawai, H., Oshima, N., Yoshida, K., Urakawa, S., Tsujino, H., Deushi, M., Tanaka, T., Hosaka, M., Yoshimura, H., Shindo, E., Mizuta, R., Ishii, M., Obata, A., and Adachi, Y.: MRI MRI-ESM2.0 model output prepared for CMIP6 CMIP historical, Version 20200601, https://doi.org/10.22033/ESGF/CMIP6.6842, 2019b.

Yukimoto, S., Koshiro, T., Kawai, H., Oshima, N., Yoshida, K., Urakawa, S., Tsujino, H., Deushi, M., Tanaka, T., Hosaka, M., Yoshimura, H., Shindo, E., Mizuta, R., Ishii, M., Obata, A., and Adachi, Y.: MRI MRI-ESM2.0 model output prepared for CMIP6 ScenarioMIP, Version 20200601, https://doi.org/10.22033/ESGF/CMIP6.638, 2019c.

Zhang, H., Väliranta, M., Piilo, S., Amesbury, M. J., Aquino-López, M. A., Roland, T. P., Salminen-Paatero, S., Paatero, J., Lohila, A., and Tuittila, E.: Decreased carbon accumulation feedback driven by climate-induced drying of two southern boreal bogs over recent centuries, Glob. Change Biol., 26, 2435–2448, https://doi.org/10.1111/gcb.15005, 2020.

Zhong, Y., Jiang, M., and Middleton, B. A.: Effects of water level alteration on carbon cycling in peatlands, Ecosyst. Heal. Sustain., 6, 1806113, https://doi.org/10.1080/20964129.2020.1806113, 2020.

Zickfeld, K., Eby, M., Weaver, A. J., Alexander, K., Crespin, E., Edwards, N. R., Eliseev, A. V., Feulner, G., Fichefet, T., Forest, C. E., Friedlingstein, P., Goosse, H., Holden, P. B., Joos, F., Kawamiya, M., Kicklighter, D., Kienert, H., Matsumoto, K., Mokhov, I. I., Monier, E., Olsen, S. M., Pedersen, J. O., Perrette, M., Philippon-Berthier, G., Ridgwell, A., Schlosser, A., Von Deimling, T. S., Shaffer, G., Sokolov, A., Spahni, R., Steinacher, M., Tachiiri, K., Tokos, K. S., Yoshimori, M., Zeng, N., and Zhao, F.: Long-Term climate change commitment and reversibility: An EMIC intercomparison, J. Clim., 26, 5782–5809, https://doi.org/10.1175/JCLI-D-12-00584.1, 2013.

4.2 Supplementary information

Supplement of Biogeosciences, 18, 3657–3687, 2021
https://doi.org/10.5194/bg-18-3657-2021-supplement

Biogeosciences Open Access EGU

Supplement of

Committed and projected future changes in global peatlands – continued transient model simulations since the Last Glacial Maximum

Jurek Müller and Fortunat Joos

Correspondence to: Jurek Müller (jurek.mueller@climate.unibe.ch)

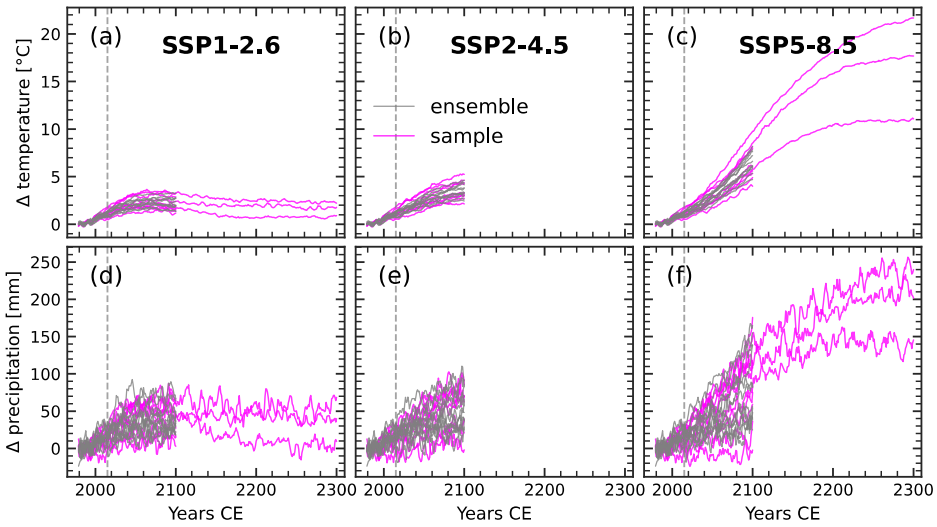

Figure S1:
Global temperature (a-c) and precipitation (d-f) anomalies to the 1961-1990 average for three CMIP6 scenarios: SSP1-2.6 (a,d), SSP2-4.5 (b,e), SSP5-8.5 (c,f) and extended SSP1-2.6 and SSP5-8.5 for three models. Mangenta lines show anomalies of the climate model sample versus the rest of the CMIP6 ensemble in grey. Dashed vertical gray lines show the year 2015 from which the future scenarios diverge

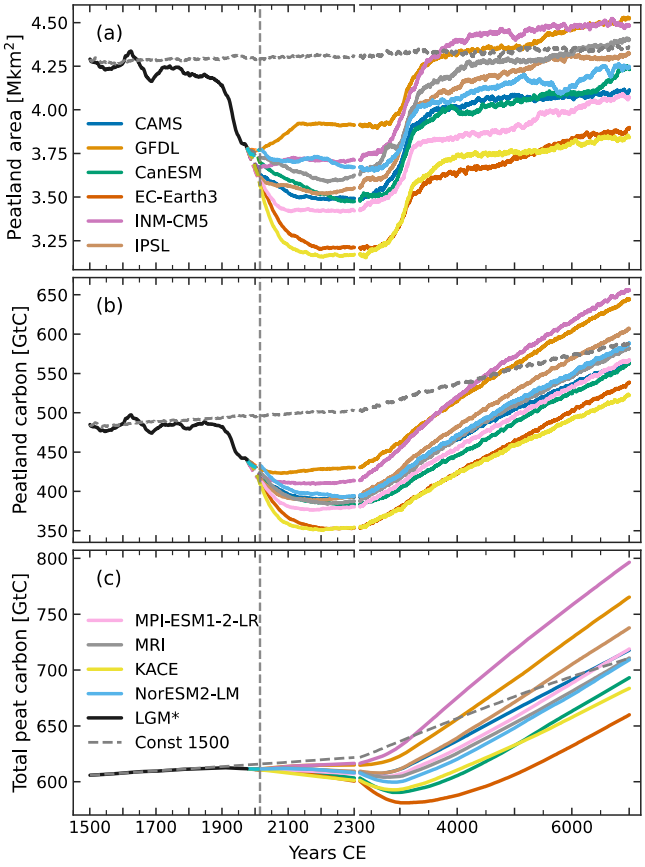

Figure S2:
Simulated continued transient evolution after the LGM run (LGM*) of (a) global peatland area, (b) global peatland carbon, and (c) global total peat carbon under under constant 1500 and 2014 conditions. Shown are ten simulations forced with different climate model anomalies. The dashed vertical line indicates the year 2014. Note the change in the time axis after the year 2300

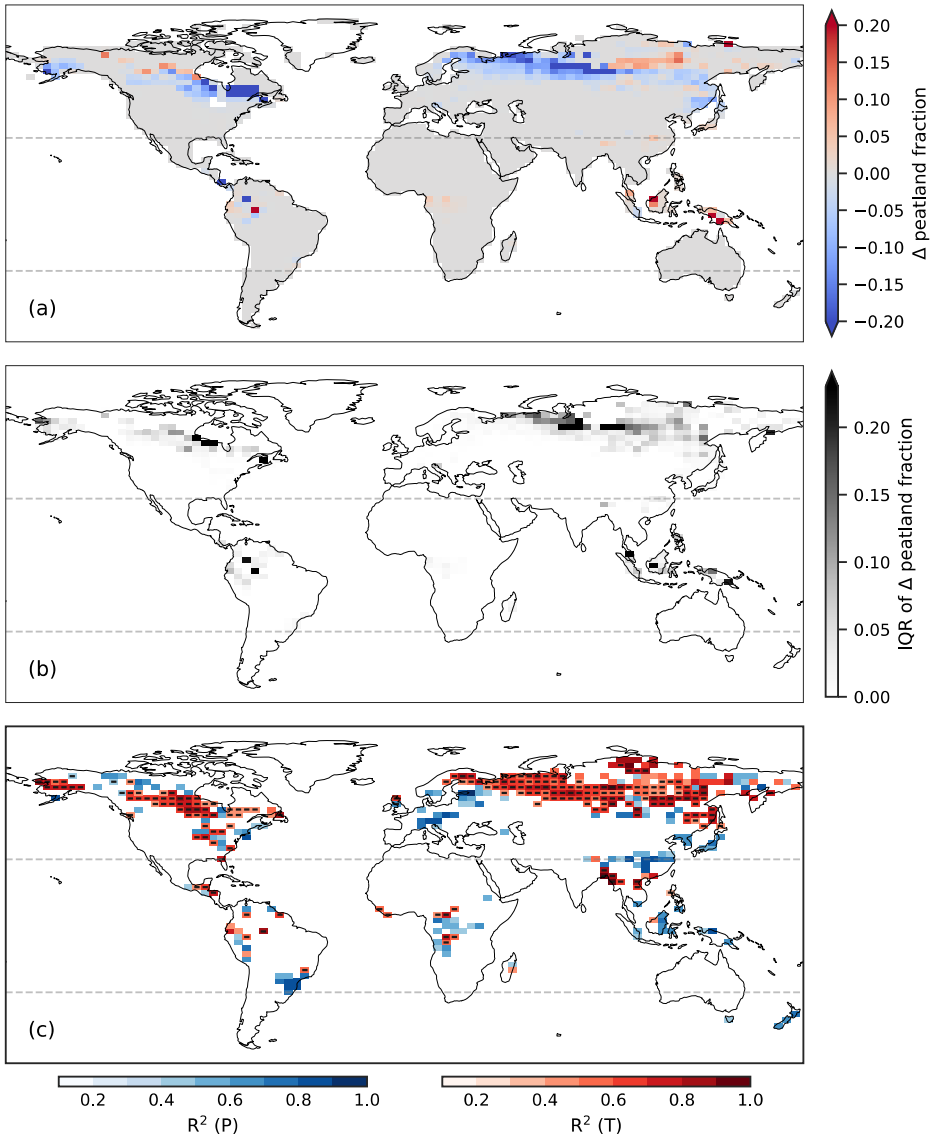

Figure S3:
Year 2300 SSP2-4.5 peatland area fraction anomaly (a) median, (b) inter quartile range and (c) squared correlation coefficient (R^2) for a linear regression between the ten different sample precipitation or temperature values and the resulting peatland fraction in the respective simulation. Plotted in (c) are only cells with significant correlation ($p > 0.05$). Color code in (c) denotes the dominant predictor in the respective cell. Cells with a negative regression slope are marked with a minus

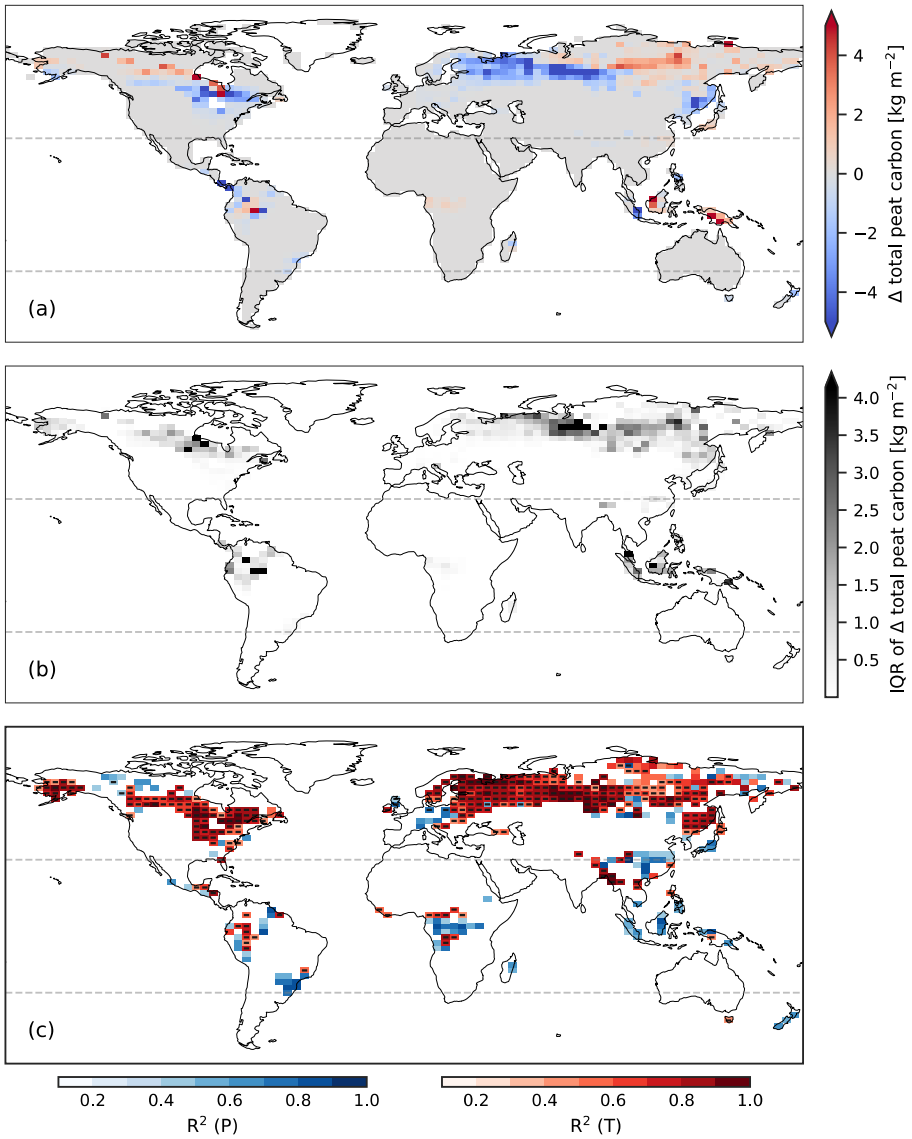

Figure S4:
Year 2300 SSP2-4.5 total peat carbon anomaly (a) median, (b) inter quartile range and (c) squared correlation coefficient (R^2) for a linear regression between the ten different sample precipitation or temperature values and the resulting total peat carbon concentrations in the respective simulation. Plotted in (c) are only cells with significant correlation ($p > 0.05$). Color code in (c) denotes the dominant predictor in the respective cell. Cells with a negative regression slope are marked with a minus

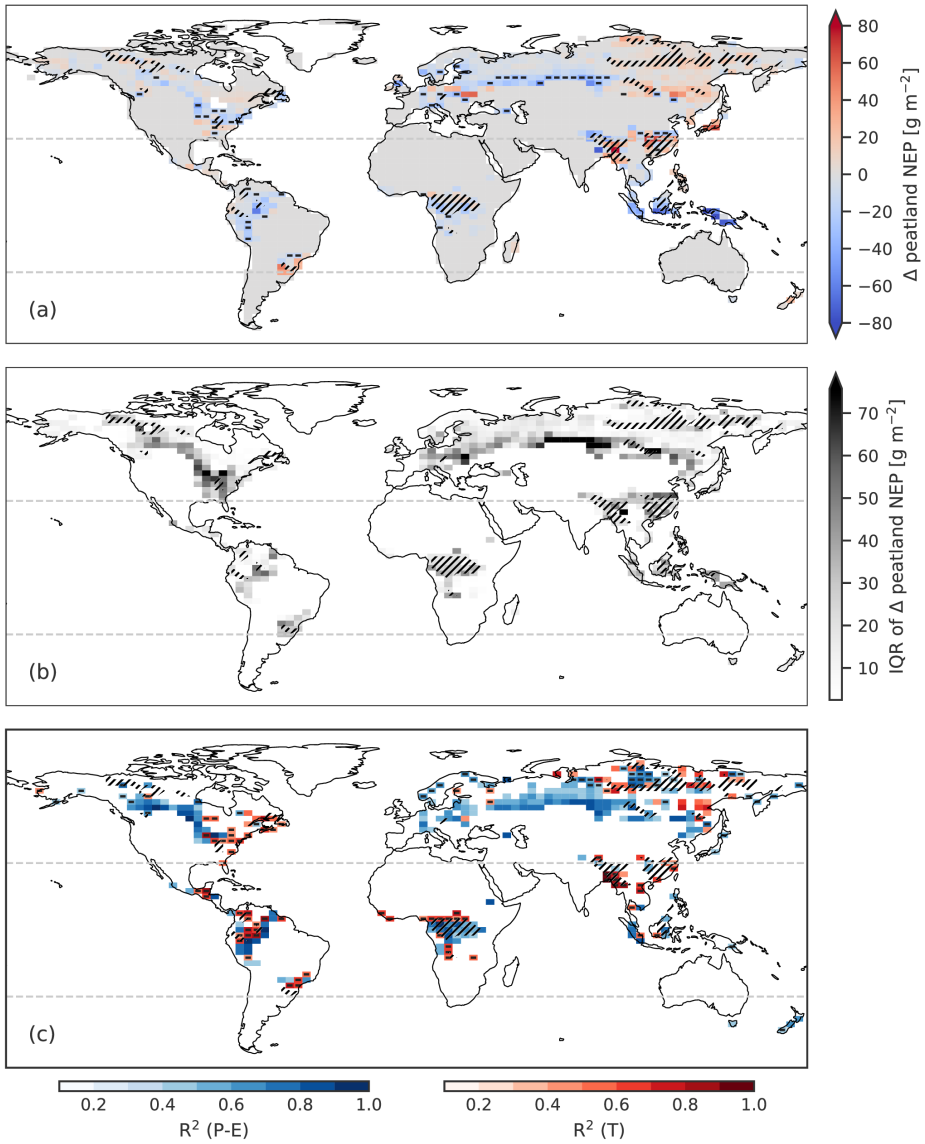

Figure S5:
Year 2300 SSP2-4.5 peatland NEP anomaly (a) median, (b) inter quartile range and (c) squared correlation coefficient (R^2) for a linear regression between the ten different sample precipitation or temperature values and the resulting peatland NEP in the respective simulation. Gridcells where NEP becomes negative are marked with a minus in (a). Plotted in (c) are only cells with significant correlation ($p > 0.05$). Color code in (c) denotes the dominant predictor in the respective cell. Cells with a negative regression slope are marked with a minus. Hatched areas indicate a positive area anomaly, which in the model can lead to an increase in NEP through the dilution of soil carbon

Table S1: Median and corresponding inter quartile range (IQR, encompassing 50% of the results) of relative anomalies for simulated peatland area, peatland carbon and total peat carbon as defined in section 2.2. Medians and the IQR are given relative to 1995-2014 averages. Values are rounded to integer values. Northern latitudes are defined as ¿30°N and tropical latitudes as 30°S-30°N. For the reference period, simulated median peatland area, carbon and total peat carbon is 3.7 Mkm^2, 423 GtC and 611 GtC for global, 2.7 Mkm^2, 301 GtC and 500 GtC for northern, and 1 Mkm^2, 121 GtC and 142 GtC for tropical peatlands respectively

	Δ peatland area [%]			**Δ peatland carbon [%]**			**Δ total peat carbon [%]**		
	2100	2300	3500	2100	2300	3500	2100	2300	3500
Global									
Committed	-3 (-5 – -1)	-4 (-6 – -2)	+8 (+5 – +10)	-7 (-9 – -6)	-9 (-10 – -7)	+4 (+1 – +7)	-0 (-0 – +0)	-1 (-1 – -0)	+1 (-1 – +2)
SSP1-2.6	-7 (-10 – -5)	-4 (-13 – +3)	+16 (-3 – +20)	-14 (-18 – -10)	-12 (-26 – -5)	+7 (-15 – +12)	-0 (-0 – +0)	-0 (-2 – +1)	+3 (-8 – +6)
SSP2-4.5	-11 (-15 – -6)	-23 (-28 – -9)	0 (-12 – +15)	-19 (-23 – -13)	-33 (-42 – -20)	-17 (-31 – +0)	-0 (-1 – -0)	-2 (-5 – -1)	-4 (-17 – +0)
SSP5-8.5	-14 (-17 – 8)	-29 (-33 – -21)	-2 (-11 – +16)	-22 (-27 – -17)	-43 (-53 – -36)	-29 (-43 – -13)	-1 (-1 – -0)	-5 (-8 – -3)	-17 (-32 – -11)
Northern									
Committed	-8 (-9 – -5)	-11 (-14 – -8)	-4 (-6 – -1)	-10 (-12 – -8)	-12 (-15 – -11)	-1 (-4 – -0)	+0 (-0 – +0)	-0 (-1 – -0)	-0 (-1 – +1)
SSP1-2.6	-15 (-22 – -11)	-18 (-32 – -6)	-8 (-22 – +3)	-19 (-26 – -16)	-18 (-38 – -8)	-5 (-28 – +7)	-0 (-0 – +0)	-1 (-2 – +1)	-2 (-10 – +4)
SSP2-4.5	-22 (-27 – -12)	-41 (-54 – -24)	-31 (-44 – -13)	-26 (-33 – -18)	-47 (-59 – -29)	-37 (-54 – -16)	-0 (-1 – +0)	-3 (-5 – -1)	-14 (-25 – -6)
SSP5-8.5	-28 (-32 – -16)	-61 (-70 – -50)	-54 (-67 – -37)	-32 (-37 – -24)	-65 (-73 – -57)	-61 (-75 – -49)	-1 (-1 – -0)	-7 (-10 – -4)	-32 (-47 – -22)
Tropical									
Committed	+9 (+5 – +11)	+14 (+9 – +19)	+37 (+33 – +41)	-0 (-2 – +1)	+2 (-1 – +4)	+21 (+16 – +24)	-0 (-1 – +0)	-1 (-1 – -0)	+5 (+3 – +7)
SSP1-2.6	+14 (+8 – +19)	+27 (+16 – +36)	+66 (+46 – +72)	+2 (-0 – +2)	+5 (+0 – +8)	+32 (+18 – +39)	+0 (-0 – +0)	-0 (-2 – +2)	+13 (+4 – +19)
SSP2-4.5	+14 (+8 – +19)	+34 (+23 – +38)	+84 (+71 – +90)	-1 (-3 – -0)	+2 (+0 – +6)	+32 (+25 – +38)	-1 (-1 – +0)	-1 (-3 – +1)	+13 (+6 – +16)
SSP5-8.5	+19 (+14 – +22)	+60 (+42 – +76)	+143 (+128 – +158)	-0 (-2 – +2)	+7 (+0 – +13)	+56 (+32 – +62)	-1 (-1 – -0)	+1 (-5 – +4)	+28 (+6 – +34)

Chapter 5

Wetland methane emissions through time

5.1 Motivation

Methane is an important greenhouse gas and plays a major role in regulating global temperature (Ciais et al., 2013). Despite its relatively short atmospheric residence time, atmospheric methane concentrations have more than doubled since the pre-industrial period, from about 700 parts per billion (ppb) Schilt et al. (2010) to 1879 ppb in 2020 (Ed Dlugokencky, 2021). Next to anthropogenic methane sources from agriculture, waste management, fossil fuel, and bio-fuel burning, emissions from natural sources have also been increasing. Today, still about a quarter to half of the global methane emissions have natural sources such as wildfires, hydrates, termites, wild animals, open waters, and wetlands (Saunois et al., 2020).

The largest natural sources of methane are wetlands. Waterlogged conditions create an anoxic environment in which methanogenic microorganisms produce methane during the respiration of organic carbon. Understanding the response of wetlands and wetland methane emissions to future climate change is thus an integral part of quantifying climate feedbacks and determining feasible trajectories towards global warming targets (Arneth et al., 2010; Stocker et al., 2013; Zhang et al., 2017b; Dean et al., 2018). Under changing boundary conditions not only emissions per unit wetland area might change, but also wetland area extent and wetland types with large indirect effects on total methane emissions.

Process-based models which dynamically and simultaneously predict wetland area and methane emissions can be a unique tool to project the evolution of future wetland methane emissions (e.g. Gedney et al., 2004; Zhang et al., 2017b). To allow for robust projections, models need to be validated over a multitude of different boundary conditions. The application of models in the paleo setting provides an opportunity to test model behavior under different boundary conditions and can provide valuable insights about the important processes controlling wetland area and methane emissions in the past.

One way to validate model performance in the paleo setting is using ice cores extracted from the ice shields of Antarctica and Greenland. They enable the reconstruction of atmospheric methane concentration over the past 800,000 years by measuring gas trapped in the ice (Loulergue et al., 2008). For the last deglaciation and the following Holocene, the high temporal resolution and accuracy of these records (e.g. Schilt et al., 2010; Mitchell et al., 2013; Baumgartner et al., 2014) allow for the validation of process-based models over a large climatic space (e.g. Hopcroft et al., 2017; Kleinen et al., 2020).

In this chapter, transient simulations from the Last Glacial Maximum (LGM, ∼21 kyrs BP) to the present are presented and analyzed. The results presented here are for the most part based on work dating back to 2017/18. However, for this chapter, the analysis has been updated and extended and all simulations have been redone with the newest version of LPX-Bern (v1.4)

(Lienert & Joos, 2018) and with the methane module as described in section 2.1.2. Note that the updated scaling factors for peatland ($mt_p = 0.157$) and seasonal wetland emissions ($r_i = 0.070$) were used compared to sections 6.1 and 6.2. The setup of the simulations and the model forcing is the same as in chapter 3. Simulated emissions from peatlands, seasonal wetlands, and wet mineral soils are compared to different estimates for present day in section 5.2. In section 5.3, simulated transient wetland emissions since the LGM are presented and compared to ice core data, including a driver attribution analysis. Potential model changes to overcome identified shortcomings are explored in section 5.4. Finally, section 5.5 provides a summary and gives a brief overview over possible future model improvements and the future of the research project.

5.2 Present-day wetland area and emissions

Estimates of wetland area are needed to estimate wetland methane emissions, e.g. with process-based models such as the LPX-Bern. These area estimates, however, are subject to large uncertainties (Hu et al., 2017). Zhang et al. (2017a) compared five commonly used wetland data sets, three of which are static in nature and two dynamic with a monthly time step. To compare the dynamic to the static datasets, the maximum area within a year was averaged over all years within the dataset. They found large differences in wetland extent. Global wetland area ranged from 5.3 to 10.2 million square kilometers (Mkm^2) with tropical wetlands (30° S–30° N) making up about 43 ± 4 %.

Wetland area simulated by the LPX-Bern, defined similarly as peatland area plus the maximum extent of seasonal wetlands averaged over the end of the simulation (1980–1990), is with 8.1 Mkm^2 well within the range of estimates (Fig. 5.1). The proportion of tropical wetlands, however, is with 35 % simulated to be smaller than suggested by the data estimates. When considering only the maximum inundated grid-cell fraction, f_i, determined by the DYPTOP module, wetland extent amounts to 7.4 Mkm^2 of which 36 % are located in the tropics.

Methane emissions from wetlands for the years 2000–2009 are estimated by Saunois et al. (2020) using bottom-up and top-down approaches. The bottom-up estimate range of 102–179 teragram methane per year (Tg yr^{-1}) was derived with multiple global process-based methane models, including the LPX-Bern (see 6.1), and with a maximum wetland area of about 7.6 Mkm^2. The top-down estimates range is with 153–196 Tg yr^{-1} slightly higher than the bottom-up range. In the top-down approach emissions from different sources are optimized to match atmospheric measurements, using prior emission estimates, such as from process-based models, and atmospheric transport and chemistry models (Houweling et al., 2017). Due to their reliance on prior distributions, top-down estimates are not entirely independent from their bottom-up counterparts. A third, independent approach is the up-scaling of emissions measured directly at the source with incubation chambers or eddy co-variance towers (e.g Pangala et al., 2017). Previously mostly applied to regional scales, Peltola et al. (2019) used a similar approach to estimate wetland methane emissions above 45° N in the years 2013 and 2014 to 31–38 Tg yr^{-1}, depending on the wetland distribution map used for upscaling.

Modern methane emission simulated by the LPX-Bern averaged over the end of the transient LGM simulation (1980–1990), are 134 Tg yr^{-1} globally, and 23 Tg yr^{-1} for wetlands above 45° N (Fig. 5.1 (b)). This puts emissions within the range of bottom-up estimates but remains lower than the top-down or up-scaling estimates. However, the time periods compared are slightly different. About 75 % of the global emissions are emitted in the tropics, 23 % in northern extratropics (>30° N), and only 2 % in the southern latitudes. The simulated latitudinal distribution is thus similar as for the bottom-up (<30° N: 79 %, >30° N: 21 %) and top-down (<30° N: 74 %, >30° N: 26 %) estimates reported in Saunois et al. (2020) for the period 2000–2009.

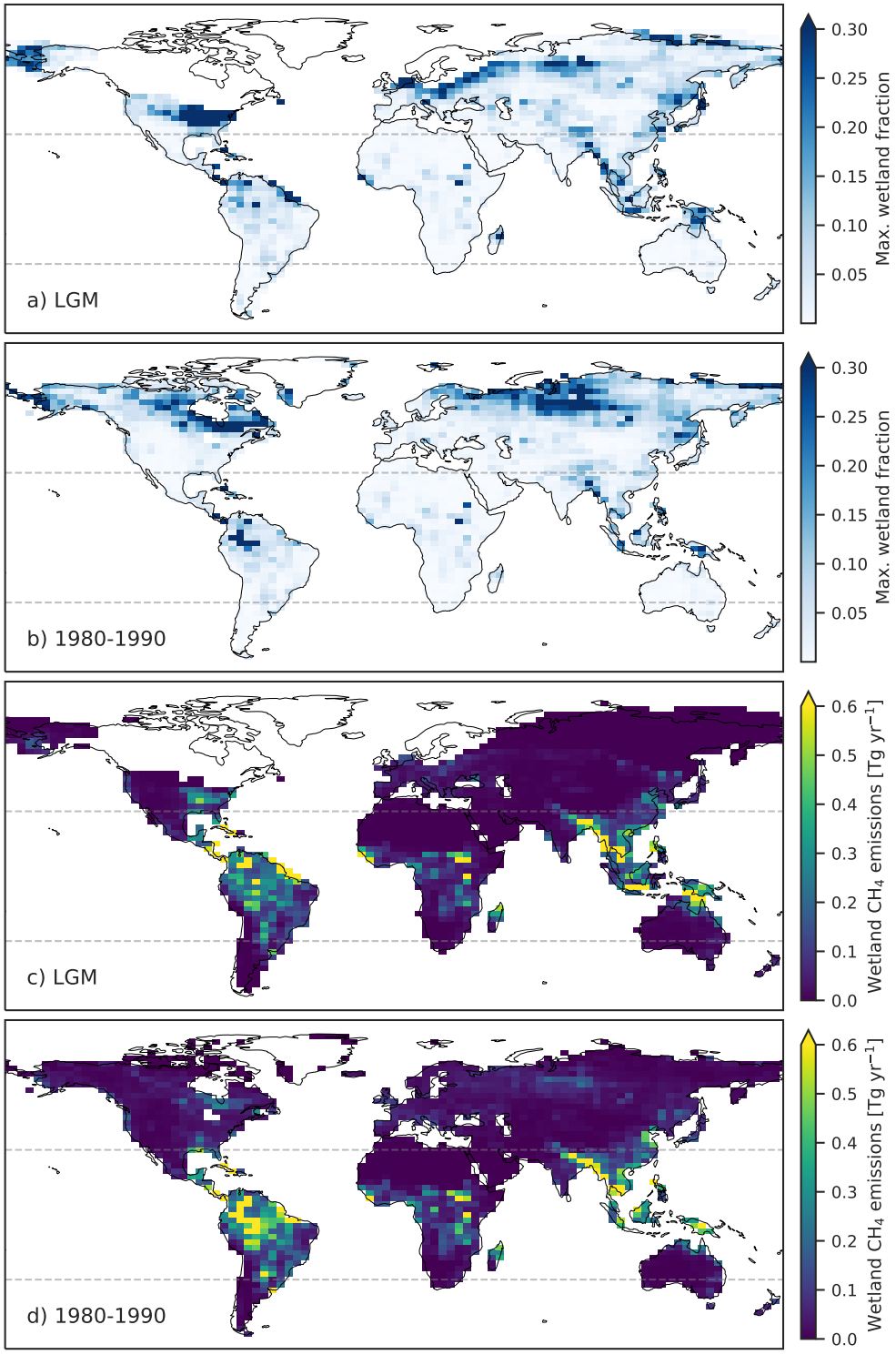

Figure 5.1: Global simulated (a,b) maximum wetland area (peatlands and seasonal wetlands) and (c,d) wetland methane emissions for (a,c) LGM conditions (21 kyrs BP) and (b,d) present day (1980–1990), from a transient simulation spanning from the LGM to the present. Dashed grey lines indicate 30° North and South.

5.3 Methane emissions since the Last Glacial Maximum

5.3.1 Ice core records

Despite its small atmospheric lifetime of about 9–11 years (Prather et al., 2012; Voulgarakis et al., 2013; Maasakkers et al., 2019) methane is well mixed in the lower atmosphere except for a small interpolar difference (Mitchell et al., 2013). Additionally, the largest sink of methane, chemical oxidation through hydroxyl radicals (OH) in the atmosphere, is thought to have changed little from the LGM to today (Levine et al., 2011; Murray et al., 2014), implying a relatively stable atmospheric lifetime. The variability in atmospheric concentrations reconstructed from ice cores can thus be interpreted as representative of global atmospheric dynamics, driven primarily by changes in the strength of sources. Ice-core records reveal a complex and intriguing variability in the atmospheric methane concentration since the Last Glacial Maximum (Fig. 5.2 (a)).

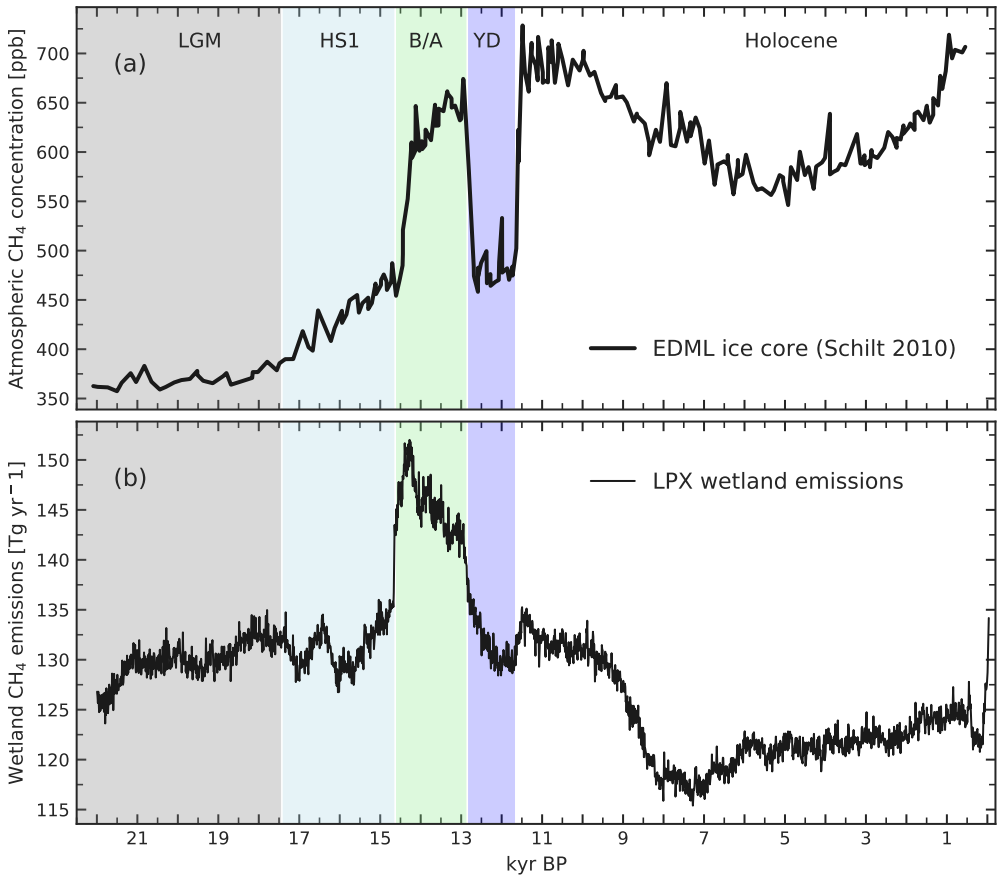

Figure 5.2: (a) Measured atmospheric methane concentration from the EDML ice-core (Schilt et al., 2010) in ppb and (b) simulated wetland methane emission by the LPX over the past 22 thousand years. Background shading indicates the Last Glacial Maximum (LGM) period, the Heinrich Stadial 1 (HS1) Northern Hemisphere cold phase, the Bølling-Allerød (BA) Northern Hemisphere warm phase, and the Younger Dryas (YD) Northern Hemisphere cold phase.

The transition from the last glacial to the beginning of the Holocene was characterized by strong warming, changes in ocean circulation, and increases in atmospheric CO_2 concentrations (Masson-Delmotte et al., 2013). During the termination, the Atlantic Meridional Overturning Circulation (AMOC) experienced multiple phases of reduced and strengthened states, leading to northern hemisphere (NH) cold and warm periods due to changes in the ocean heat transport (Stocker & Johnsen, 2003; Rasmussen et al., 2014). The concurrent changes in the low- to high-latitude temperature gradient led to northward (small gradient) and southward (large

gradient) shifts of the Intertropical Convergence Zone (ITCZ) and with it to shifts in the high precipitation zones in the tropics (McGee et al., 2014; Shi & Yan, 2019; Cao et al., 2019). The changes in ocean heat transport and atmospheric circulation also affected the Asian and African monsoon systems and their related precipitation patterns (e.g. Shi & Yan, 2019; He et al., 2021). The TraCE21k climate anomalies used as forcing for the LPX-Bern simulations presented here, capture the discussed climate variability well (Liu et al., 2009).

From the LGM (∼21 kyrs BP) to the pre-industrial period (0.25–1 kyrs BP) atmospheric methane concentration almost doubled, from about 370 ppb to about 705 ppb (Fig. 5.2 (a) Schilt et al., 2010). Concentrations started rising with the onset of Heinrich-Stadial 1 (HS1, 17.43–14.63 kyr BP), a period of reduced AMOC and a NH cold period, thought to be triggered by iceberg discharge (Ng et al., 2018). The following Bølling-Allerød (BA, 14.63–12.85 kyr BP) NH warm period is thought to have followed an abrupt strengthening of the AMOC, transporting heat from the southern to the northern hemisphere (McManus et al., 2004). At the onset of the BA, atmospheric methane concentrations abruptly increased to about 600 ppb and continued to steadily rise until its end to about 650 ppb (Fig. 5.2 (a)). The BA was interrupted by the Younger Dryas (YD, 12.85–11.65 kyr BP), another NH cold period with reduced AMOC, in which NH climate briefly returned to almost glacial levels (Renssen et al., 2015). Atmospheric methane concentrations abruptly fell back to pre-BA levels and remained reduced until the onset of the Holocene (Fig. 5.2 (a)). There, again accompanied by a strengthening of the AMOC, atmospheric methane concentrations quickly rose back to about 680 ppb. Despite the relatively stable climate during the following Holocene (Mayewski et al., 2004), atmospheric methane concentrations continued to change significantly. From the onset of the Holocene, concentrations continually decreased to a mid-Holocene minimum of about 570 ppb at about 6–5 kyrs BP. The subsequent increase brings atmospheric concentrations back to early Holocene levels of 705 ppb in the pre-industrial period (Fig. 5.2 (a)).

5.3.2 Simulated emissions

As LPX-Bern does not simulate all natural methane sources, the measured atmospheric concentrations can not be compared directly to simulated atmospheric concentrations. However, as wetlands are the largest methane source and in absence of strong changes in methane sinks, methane emissions from global wetlands should show the same variability as the atmospheric concentrations measured in ice cores. The wetland emissions simulated transiently since the LGM by the LPX-Bern, show some of these characteristics while lacking important others (Fig. 5.2 (b)).

Simulated global wetland emissions during the HS1 show fluctuations but no general positive trend. Figure 5.3 shows the simulated global, northern extratropical, and tropical emissions from peatlands, seasonal wetlands, and wet mineral soils. It reveals that a positive trend is present for emissions from northern extratropical wetlands throughout the whole HS1. However, simulated global emissions are dominated by emissions from tropical seasonal wetlands, which decrease from 16.5–16 kyrs BP with a slow recovery thereafter.

The period best reproduced by the model is the BA, with an abrupt increase and decrease in simulated emissions at its beginning and end, but with a decreasing instead of an increasing trend during the BA itself (Fig. 5.2). The simulated abrupt increase at the beginning of the BA is mostly driven by emissions from tropical seasonal wetlands (Fig. 5.3 (b)). This is in line with isotopic evidence from ice cores suggesting tropical wetlands as the likely drivers of the sharp emission increases at the beginning of the BA and the Holocene (Bock et al., 2017). Sea-level rise and subsequent flooding of continental shelves was also proposed to have contributed to these abrupt changes (Ridgwell et al., 2012). A contribution might also have come from extensive melt water-driven wetland expansion in the North American mid-latitudes (Byun et al., 2021).

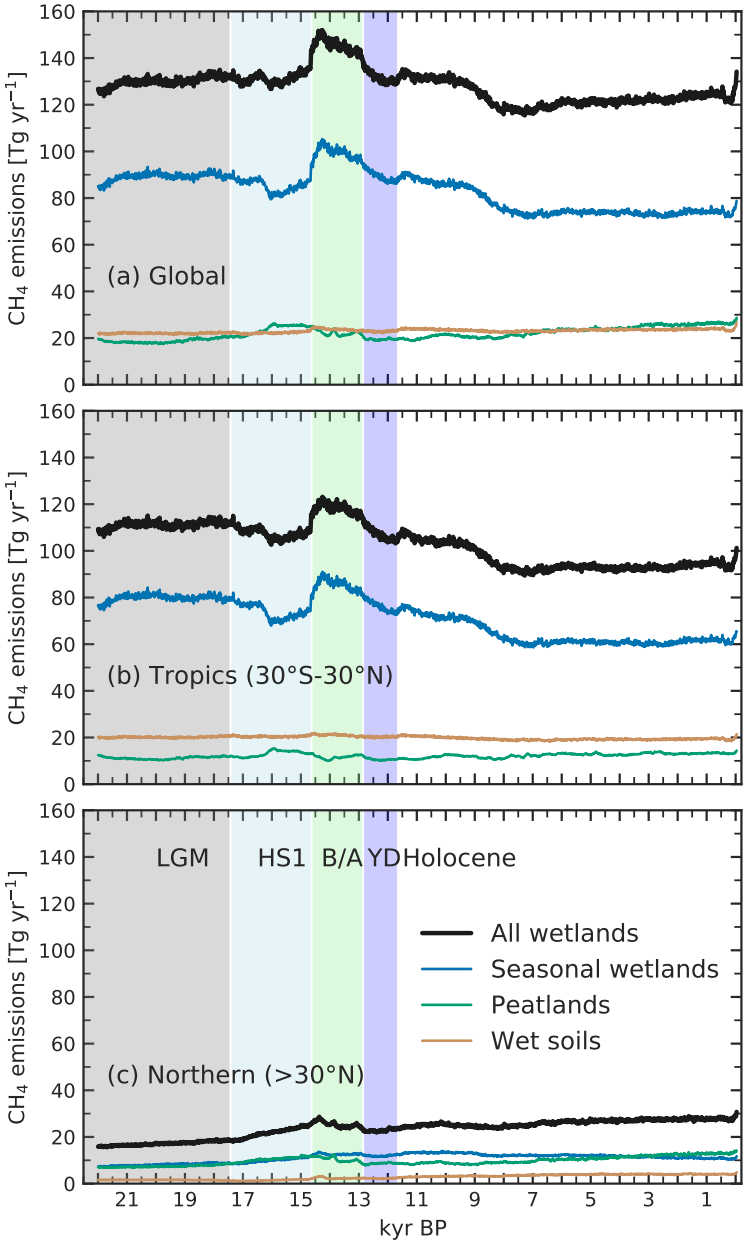

Figure 5.3: Simulated (a) global, (b) tropical (30° S–30° N), and (c) northern (>30° N) wetland emissions from seasonally inundated wetlands, peatlands, and wet mineral soils. Background shading same as in figure 5.2.

Meltwater from the Laurentide ice sheet abruptly decreased at the onset of the YD reducing these wetlands and their methane emissions.

The fast decrease in simulated global emissions at the transition from BA to YD is driven by peatland emissions especially in the northern extratropics, whereas emissions from tropical seasonal wetlands continue the negative trend during the BA throughout the YD (Fig. 5.3). The simulated emissions in the YD are thus characterized by a negative trend rather than sustained low emissions, as suggested by the ice core record. At the transition from the YD to the Holocene, simulated global emissions see a small increase, driven again by tropical seasonal wetlands, but generally remain at LGM levels (Fig. 5.3 (a,b)).

Similar to the ice core records, simulated Holocene wetland emissions decrease towards the mid-Holocene with a following recovery towards the pre-industrial period. Different to the measured atmospheric concentrations, however, simulated emissions decrease rapidly between

10–8 kyrs BP with an emission minimum between 8–7 kyrs BP instead of 6–5 kyrs BP and a linear recovery thereafter (Fig. 5.2). The emission reduction in the early Holocene is driven by reduced emissions from tropical seasonal wetlands (Fig. 5.3 (b)). The subsequent increase of late Holocene emissions stems from increasing peatland emission, especially in the northern extratropics (Fig. 5.3 (c)). Beck et al. (2018) used the small interpolar difference in methane concentrations and isotopes measured between ice cores from Antarctica and Greenland to estimate the hemispheric distribution of sources over the Holocene. They suggest a decline in northern latitude peatland emissions during the early Holocene (11–8 ka BP) due to fen to bog transitions, which are not represented within the LPX-Bern. In the mid-Holocene (8–5.5 kyrs BP), emissions are suggested to reduce mostly in the tropics, partly matching simulated emissions. For the subsequent late Holocene (5.5–1 kyrs BP) methane rise, previously, a potentially important role of northern peatlands was proposed (Korhola et al., 2010), similar to the simulated results. However, according to Beck et al. (2018), tropical emissions are most likely to have driven the late Holocene (5.5–1 kyrs BP) methane rise. The latter conclusion is also supported by another interpolar difference study by Mitchell et al. (2013), who use high-resolution interpolar difference measurements for the late Holocene.

Chappellaz et al. (1997) used the interpolar difference to estimate the latitudinal distribution of sources over the Holocene within three boxes. They found no general trend in source distribution with the tropical share ranging between about 50 to 64 % during the Holocene. For the PI period, Chappellaz et al. (1997) found about 64 % of emissions originating in the tropics, 29 % in the northern, and 6 % in the southern extratropics and thus a distribution shifted more to the northern and southern latitudes than the estimates for present day. This indicates a relative overestimation of tropical sources during the Holocene by LPX-Bern, with simulated values ranging between 76–80 %, despite a good model agreement to present-day estimates (Fig. 5.4).

5.3.3 LGM-PI methane rise

The most notable model-data mismatch is the lack of a substantial increase in emissions from the LGM (21 kyrs BP) to the pre-industrial period (PI, 1–0.25 kyrs BP) or the early Holocene. Instead of the expected near doubling of emissions (+90 %), simulated wetland emissions at the beginning of the Holocene remain at LGM levels (+2 %) and even fall below that during the PI period (–4.5 %). Figure 5.3 shows that this general trend is the combined effect of emissions from tropical wetlands that reduce from LGM to PI by about –16 %, driven mostly by seasonal wetlands, and an LGM-PI emission increase of +68 % in the northern extratropics, driven mostly by peatland emissions. This entails a reduction of the tropical share of simulated global emissions from 86 % at LGM to 76 % at PI (Fig. 5.4 (a)). Isotopic measurements from ice cores identify tropical wetlands as the main drivers of the LGM-PI increase in atmospheric methane concentration (Bock et al., 2017). The simulated decreasing trend in tropical wetland emissions is thus opposite to the expected one. When including simulated emissions from wildfires, which increase with available biomass, the simulated LGM-PI emission anomaly increases slightly to –3.3 %. Other sources not explicitly considered here, such as wild animals and termites might have also increased over the termination, but only play a secondary role in driving atmospheric methane concentrations (Saunois et al., 2020). Previous suggestions of substantial release of methane from hydrates and other geological sources (Etiope et al., 2008) have been dismissed based isotopic evidence (Bock et al., 2017). Methane emissions from inland waters, like lakes and rivers, however, are a still mostly uncertain but potentially large emission source which is not considered here (Walter et al., 2007; DelSontro et al., 2018).

Previous modeling studies investigating the LGM methane cycle have also struggled to achieve the full expected increase of methane emissions from LGM to PI of about 90 % without

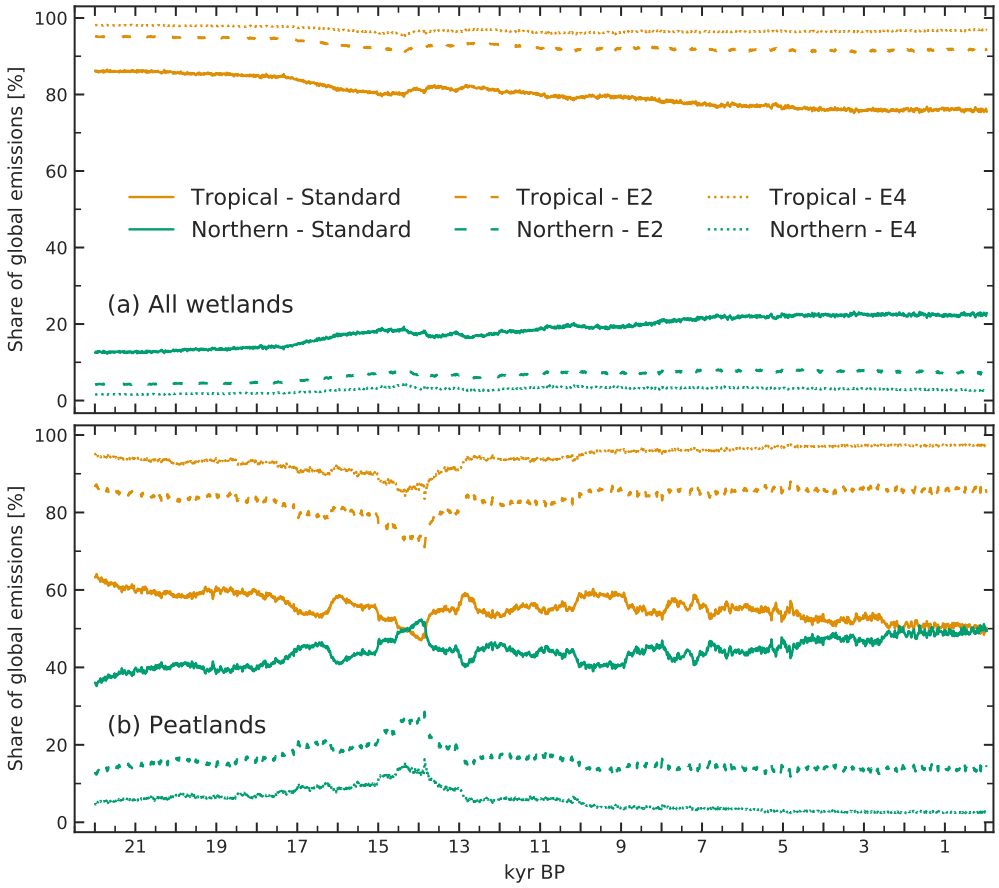

Figure 5.4: Relative proportion of tropical (30° S–30° N) and northern (>30° N) simulated (a) total wetland and (b) peatland emissions for the standard setup and two sensitivity simulations with additional temperature dependence of the CH_4/CO_2 production ratio, with a Q_{10} equivalent of $Q_{10} \approx 2$ (E2) and $Q_{10} \approx 4$ (E4).

assuming changes in the atmospheric sink. Kaplan (2002) found a mostly CO_2 driven 30 % increase in wetland methane emissions from LGM to PI, despite a slightly larger wetland area during the LGM. Valdes et al. (2005) simulated an LGM to PI increase of global wetland emissions of 37 % with the largest increase, however, stemming from northern latitude wetlands. Kaplan et al. (2006) simulated wetland methane emissions from the LGM to the present in 19 timeslices. They found a similar evolution of wetland emissions as simulated by LPX-Bern, with an LGM-PI difference in emissions of about 0 % and an emission maximum during the BA at 13 kyrs BP. Weber et al. (2010) used climate output from multiple models participating in the Palaeoclimate Modelling Intercomparison Project Phase 2 (PMIP2) to diagnose wetland methane emissions, resulting in a range of relative emission increases from LGM to PI of 41–72 %, with generally larger increases in northern extratropics than in the tropics. Singarayer et al. (2011) simulated atmospheric methane concentrations in 65 time slices spanning the past 130 kyrs using a global circulation model (GCM) coupled to a DGVM and an atmospheric chemistry model, however, with no changes to the glacial land-sea mask. They found an increase between LGM and early Holocene wetland emissions of about 58 % and an increase of about 46 % from LGM to PI. Finally, Hopcroft et al. (2017) simulated changes in the LGM methane cycle, considering emissions from wetlands, wildfires, termites, oceans and hydrates. They found a total emission increase of 49–72 %. Wetland methane emissions were simulated to increase by about 72 %.

These examples reveal the simulation of the LGM methane cycle as a long standing and ongoing challenge for process-based models. In a recent study, Kleinen et al. (2020) provide the first demonstration that the atmospheric concentration increase from LGM to PI can be

explained by changes in source strength alone. They performed six timeslice simulations from the LGM to the present day and simulated emissions from wetlands, wildfires and termites as well as the methane uptake by soils. They find an LGM-PI increase of total emissions of 113 %, with wetland emissions increasing by 103 %. Their investigation into the underlying drivers using factorial simulations, revealed the atmospheric CO_2 and temperature increase to have the largest effect on wetland emissions. CO_2 fertilization alone lead to a 24 % increase in emissions. Rising temperatures led to increased emissions indirectly by increases in vegetation productivity and soil respiration and directly through the temperature dependence of methane production, with the latter contributing about 16 % to the methane rise (Kleinen et al., 2020). Changes in the available land area through ice sheet retreat and sea-level rise were identified as a third main driver leading to an LGM-PI increase in northern wetland area and a decrease in the tropics.

Identifying the key drivers for methane emissions simulated by LPX-Bern and comparing them to results from the previous modeling studies discussed above might reveal potential model deficits that lead to the lack in a simulated LGM-PI methane rise.

5.3.4 Driver contributions

To reveal the underlying environmental drivers for the changes in simulated wetland methane emissions discussed above, factorial simulations were used. Five factorial simulations were performed, where atmospheric CO_2, temperature, precipitation, orbital forcing, and the land-sea-ice mask were kept constant at LGM levels respectively. Figure 5.5 shows the driver contribution calculated for the relative emission anomaly since the LGM. At any given time, the respective driver contribution was calculated as the difference between the relative emission anomaly of the respective factorial simulation and the standard simulation. The residual between all calculated driver contributions and the standard run was identified as contributions from non-linear effects.

During the HS1, shifts in precipitation patterns lead to a reduction of tropical seasonal wetland emissions, where the source area responds more quickly to changes in precipitation (Fig. 5.5 (b)). The emission reduction at about 16 kyrs BP is dampened by non-linear effects in the tropics and precipitation-driven emission increases in the northern extratropics (Fig. 5.5 (b,c)). Rising atmospheric CO_2 levels during the HS1 lead to increases in emissions over all source types and latitudes, by increasing plant productivity and substrate availability (Fig. 5.5). Despite low Greenland temperatures during HS1, temperatures in the TraCE21k simulation start to rise throughout large parts of the northern hemisphere, especially in Asia. Rising temperatures lead to rising emissions from the northern extratropics until the BA onset (Fig. 5.5 (c)). The large emission variability throughout the BA and YD is mostly forced by precipitation changes in the tropics following shifts in the ITCZ, except for the YD onset which is dominated by northern peatlands responding to abrupt changes in precipitation and temperature (Fig. 5.5).

These deglacial changes are superimposed on a strong emission decrease due to sea-level rise and the subsequent loss of strongly emitting seasonal wetlands. Most of these are located on tropical exposed continental shelves (Fig. 5.5 (b)). Emissions from additional land areas in the northern extratropics, that become available after ice sheet retreat, can only marginally compensate for the emissions lost in the tropics (Fig. 5.5 (c)). The effect of increasing temperatures in the northern extratropics varies. In the high latitudes, wetland expansion and the increase in primary productivity and soil respiration lead to a rise in emissions. In the mid latitudes, however, wetland area decreases due to the temperature-driven loss of large wetland complexes in eastern North America (see also chapter 3), leading to a net negative effect of temperature on emissions after about 14.5 kyrs BP.

At the onset of the Holocene, emissions increase due to increases in precipitation and CO_2 across latitudes (Fig. 5.5). The early Holocene is dominated by further emission reductions due

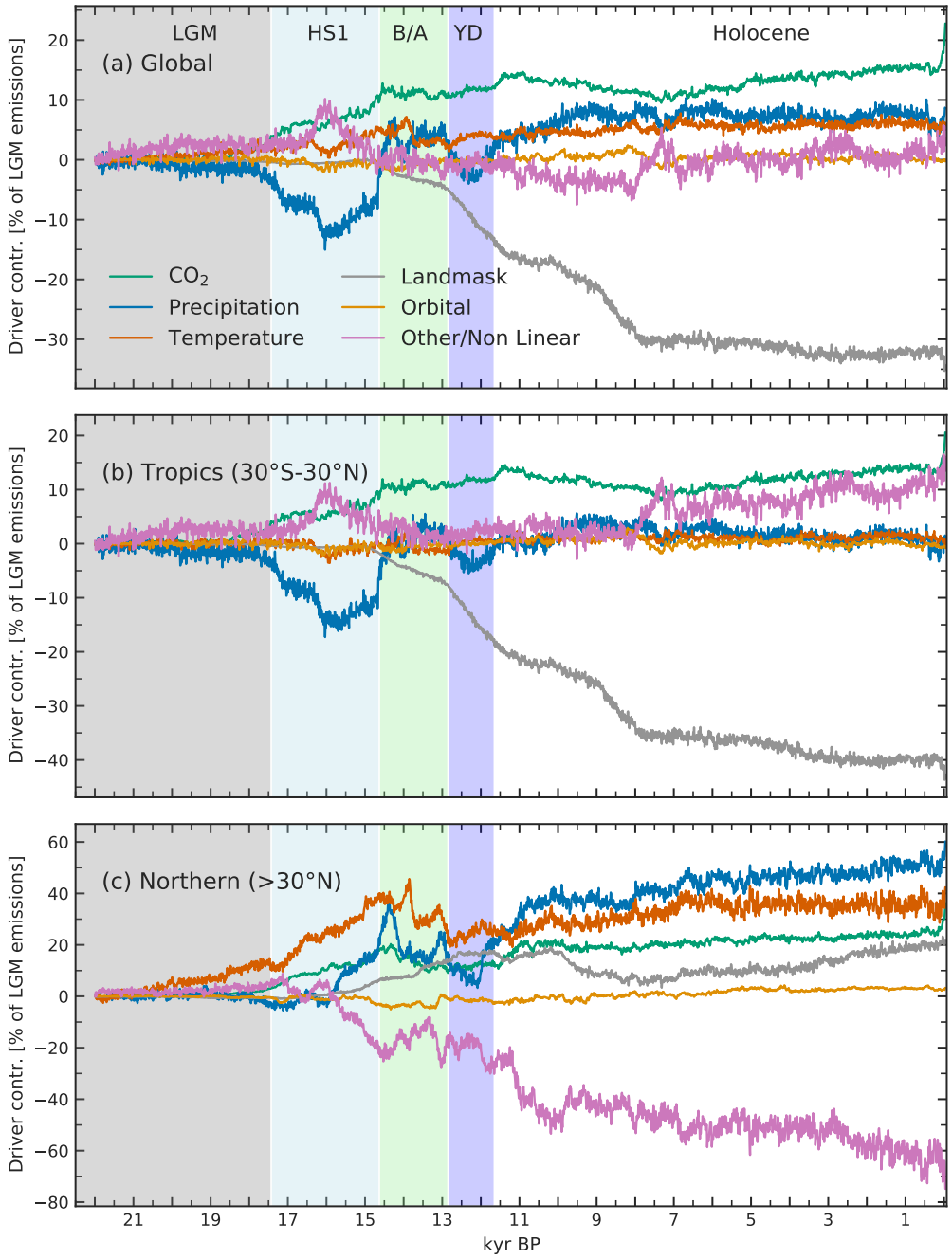

Figure 5.5: Driver contributions to the change in simulated (a) global, (b) tropical (30° S–30° N), and (c) northern (>30° N) wetland emissions since the LGM. Contributions are calculated using factorial simulations and are given in percent of LGM emissions averaged over 21.5–19.5 kyrs BP. Background shading same as in figure 5.2.

to sea-level rise, now also impacting emissions from the northern extratropics, but dampened by continued positive contributions from precipitation increases. The CO_2 contribution during the Holocene follows the atmospheric concentrations which have a mid-Holocene minimum and start rising again towards the late Holocene. The continued expansion of peatlands into North America after ice sheet retreat leads to a continually increasing contribution from land area changes in the northern extratropics. The effect of the orbital forcing, here only affecting available photosynthetic radiation, and of temperature changes in the tropics, remain small throughout the simulations (Fig. 5.5).

Non-linear contributions play a continually large negative role in the northern extratropics (Fig. 5.5 (c)). Their dynamic is anticorrelated with the calculated contribution from precipitation, suggesting non-linear interactions between precipitation and other environmental drivers. Precipitation is a strong determinant of wetland area extent. The available source area, however, limits the effect that other factors like CO_2 and temperature can have on total emissions. The precipitation effect as calculated here thus includes double-counting of all other contributions that affect the additional wetland areas emerging due to increased precipitation. Similar double-counting exists for other drivers potentially affecting wetland area, such as changes in the land-sea-ice mask or temperature, which through changes in evapotranspiration also has an indirect effect on the water balance. For a more thorough future analysis, a strategy might be found to minimize such double counting. This could potentially include additional factorial simulations with all but one forcing fixed at pre-industrial levels and factorial simulations isolating the effect of wetland area changes.

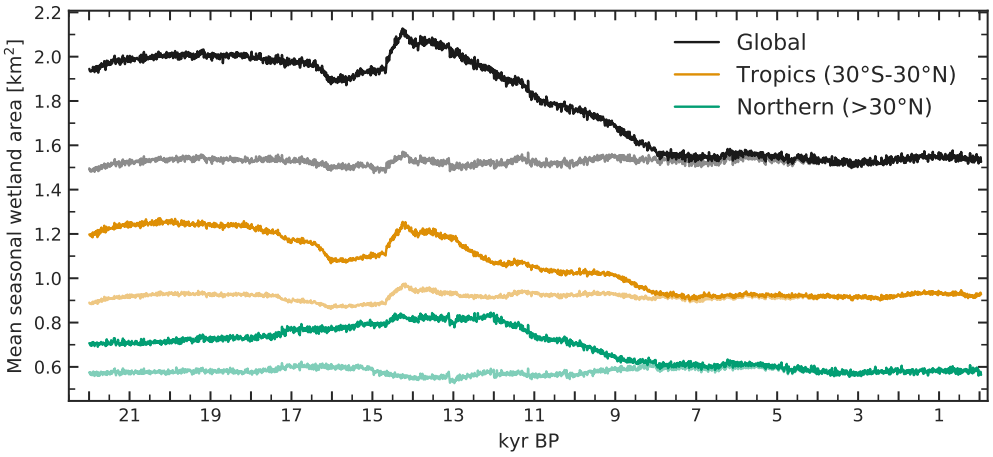

Figure 5.6: Mean simulated area of seasonal wetlands (not including peatlands), in the standard setup (thick lines) and without wetlands on continental shelves (soft lines)

The driver contributions to the methane emissions anomaly at PI reveal possible reasons for the lack of the LGM-PI methane rise in the simulations. Although there are considerable positive contributions from increasing CO_2, precipitation, and temperature, they are largely canceled out by the loss of emissions due to the flooding of tropical continental shelves (Fig. 5.5). During the LGM, DYPTOP predicts large wetlands on the shelves in Sundaland, North of Australia, and the northern coast of South America, accompanied by large methane emissions (Fig. 5.1 (a)). The subsequent sea-level rise thus leads to a large net loss of emission source area throughout the termination and the early Holocene (Fig. 5.6). The extent of paleo wetlands on these shelves is largely unknown, however, deep river systems could have limited wetland extent through effective drainage (Dommain et al., 2014). Other studies that struggled to reproduce the full LGM-PI methane rise also predicted large wetland areas on tropical continental shelves, strongly affecting LGM methane emissions (Kaplan, 2002; Kaplan et al., 2006; Valdes et al., 2005; Weber et al., 2010). Kleinen et al. (2020), however, managed to simulate a considerable LGM-PI methane rise, despite a decreasing source area in the tropics following sea-level rise. Their reduction in mean tropical wetland area (–13 %) is, however, substantially smaller than the one simulated by the LPX-Bern (–25 %, for seasonal wetlands).

Other factors for the lack of a simulated LGM-PI methane rise could be too small positive contributions from rising temperature and CO_2. The CO_2 contribution for emission anomalies from LGM to PI here is simulated at 15 % and the temperature contribution at 6 %, compared to 24 % from CO_2 and 16 % from the direct temperature dependence of methane production alone in Kleinen et al. (2020). Part of this difference can be explained by the lack of an explicit

temperature dependence of the methane production (see section 2.1.2). Similarly, LPX-Bern is known to have a relatively low sensitivity of primary production to atmospheric CO_2 changes (Lienert & Joos, 2018). In the following section, potential LPX-Bern adjustments are discussed addressing some of these issues, namely the temperature dependence of methane emissions and the simulation of wetland area.

5.4 Model investigations

In pursuit of reducing the model-data mismatch, particularly concerning the lack of an LGM-PI rise in simulated emissions, some sensitivity and model investigations were performed. In the driver analysis in section 5.3.4, the absence of an explicit temperature dependence of the methane production and the large deglacial loss of tropical shelf wetland area, were identified as two of the potential sources of the model-data mismatch. Below, in section 5.4.1, a simple implementation for a temperature dependence of the CH_4/CO_2 production ratio is added to the LPX-Bern, and results from additional simulations are compared to the standard simulation. In section 5.4.2, the DYPTOP implementation is slightly changed and parameters newly tuned to potentially reduce seasonal wetland area during the LGM, especially on the tropical continental shelves.

5.4.1 Temperature dependence

Methane emissions from wetlands were found to be more sensitive to temperature changes than their concurrent CO_2 emissions (Yvon-Durocher et al., 2014; Turetsky et al., 2014). The CH_4/CO_2 emission ratio, which is a constant factor in LPX-Bern, thus should be assumed as temperature-dependent. In chapter 2, a simple implementation of a temperature modifier for the CH_4/CO_2 ratio for seasonal wetlands, peatlands, and wet mineral soils is described, which is used for the sensitivity runs presented here. The modifier, m_T, is determined, analogous to the temperature modifiers for soil respiration, by an Arrhenius equation following Lloyd & Taylor (1994). The two free parameters of the modified Q_{10} relationship are T_{ref}, the reference temperature at which $m_T = 1$, and E_o which determines the slope of the function. T_{ref} is here taken at 20° C, similar to the calculation for soil respiration. For E_o values were determined that roughly correspond to Q_{10} values, to facilitate interpretation and comparability to other studies. Other methane models with a Q_{10} relationship for the CH_4/CO_2 emission ratio have Q_{10} values ranging between 1.5 and 4 (Xu et al., 2016), while observed Q_{10} values have an even larger range from 1.7 to 15.8, depending on wetland type and soil depth (Turetsky et al., 2014). Here, the Arrhenius function used in LPX-Bern was fitted against the Q_{10} relationships with $Q_{10} \approx 2$ and $Q_{10} \approx 4$, resulting in $E_o = 298$ and $E_o = 679.9$ respectively. For now, these parameter values simply serve as a sensitivity test. For full integration into LPX-Bern, ideally, the parameters should be determined using appropriate site data.

Figure 5.7 shows the anomaly of wetland methane emissions relative to the LGM for the standard simulation and the two sensitivity simulations with $E_o = 298$ (further referred to as E2) and $E_o = 679.9$ (further referred to as E4). Due to the additional temperature dependence, the temperature variability has a stronger imprint on global wetland emissions, especially in the case of E4. At the beginning of the BA, an emission overshoot and a subsequent reduction during the Older Dryas (14 kyrs BP) emerge following the temperature profile. Similarly, emission reductions during the YD are more pronounced with larger temperature sensitivity.

The LGM-PI emissions anomaly is increased from –4.5 % in the standard run to +1 % for E2 and +17 % for E4. The additional temperature effect on the LGM-PI emission anomaly in E2 is with about 6 % much smaller than the contribution of 16 % reported in Kleinen et al. (2020), who have an even weaker temperature dependence for the CH_4/CO_2 production ratio,

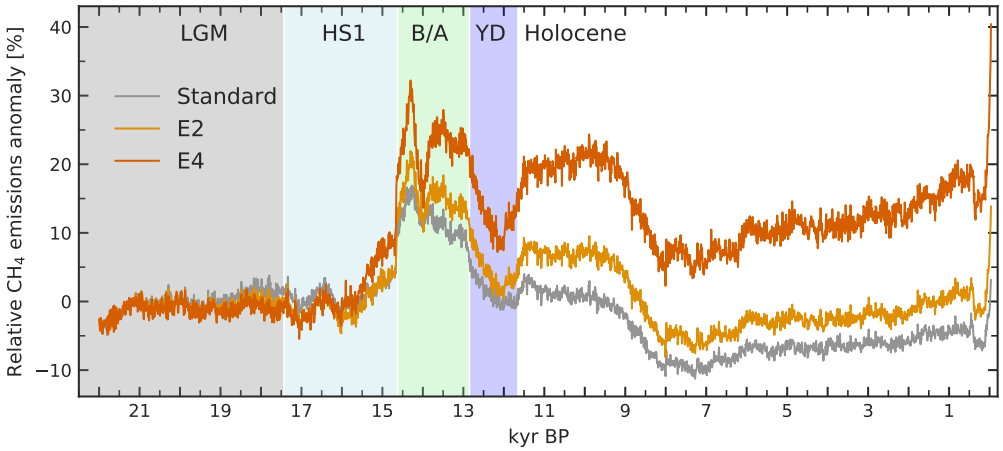

Figure 5.7: Methane emission anomaly relative to the LGM (21 kyrs BP) for the standard setup and two sensitivity simulations with additional temperature dependence of the CH_4/CO_2 production ratio, with a Q_{10} equivalent of $Q_{10} \approx 2$ (E2) and $Q_{10} \approx 4$ (E4). Background shading same as in figure 5.2.

with a Q_{10} of 1.8, in their model. One reason for these different results lies in the difference in climate forcing. The MPI-ESM used in Kleinen et al. (2020) simulates an LGM-PI anomaly of global temperature of 4.4 Kelvin (K) while the transient TraCE21k simulation used as forcing for the LPX-Bern (Liu et al., 2009) shows a global temperature anomaly of only 3.8 K. In the tropics, where most methane emissions originate, the temperature anomaly is 3.1 K and 2.1 K for MPI-ESM and TraCE21k respectively. Temperature anomalies above land could differ even more. Similar as discussed in chapter 3, uncertainties in climate anomalies are propagated to large uncertainties in simulated past methane emissions.

Another reason for the relatively weak temperature effect in LPX-Bern could be the latitudinal distribution of wetland emissions. Higher latitudes experience larger temperature anomalies over the termination, leading to less sensitive responses of global emissions to the global mean temperature change the more of the global emissions originate from lower latitudes. Despite a similar distribution of wetlands, emissions in the LPX-Bern standard simulation have more weight in the tropics than in Kleinen et al. (2020). At PI LPX-Bern simulates 76 % of global emissions in the tropics versus 66 % in Kleinen et al. (2020) and 86 % versus 71 % at LGM. Due to the temperature gradient between low and high latitudes, the distribution is even more skewed towards the tropics when adding the additional temperature dependence, with 92 % (E2) and 97 % (E4) of emissions originating in the tropics at PI (Fig. 5.4 (a)).

The large weight of tropical emissions after introducing the additional temperature dependence is unrealistic and conflicts with estimates throughout the Holocene (Chappellaz et al., 1997; Saunois et al., 2020). In the current setup, peatland emissions make up only a small portion of total wetland emissions. As the majority of peatlands are located in the northern extratropics, a re-balancing of the relative strength of different sources could influence the latitudinal distribution. However, the additional temperature dependence also skews the distribution of peatland emissions by increasing the tropical emission share at PI from 50 % (standard) to 86 % (E2) and 97 % (E4). Thus, even when taking only peatland emissions into account, the tropical share would be overestimated after including the additional CH_4/CO_2 production ratio temperature dependence. Potential changes to the calculation of the temperature modifier could help to avoid the concentration of emissions in the tropics. Methanogenic microorganisms in high and low latitudes might have adapted to very different temperature regimes and thus different values of T_{ref} might be needed for different latitudes. Similarly, the temperature dependence of methane emissions was found to vary greatly between ecosystem types (Turetsky et al., 2014), possibly warranting different parameter sets for different source categories. These changes,

however, would introduce new parameters that would need to be well constrained by observations to avoid over-fitting. The most direct way to reduce the share of tropical emissions would be to reduce the respective source area in the tropics. However, as discussed in 5.2, for present-day conditions the relative size of tropical wetland area is already underestimated in LPX-Bern. In the next section, sensitivity studies into the DYPTOP module are discussed that could potentially reduce tropical seasonal wetland area, especially during the LGM.

5.4.2 Alternative DYPTOP formulation

In section 5.3, the large loss of tropical seasonal wetland area from LGM to PI was identified as one of the main reasons for the small simulated LGM to PI anomaly in wetland methane emissions. During LGM conditions, LPX-Bern simulates large seasonal wetlands and peatlands on the exposed continental shelves in Sundaland, North of Australia, and the northern coast of South America. The sub-grid topographic information used in DYPTOP (ETOPO1, 2013) identifies them as mostly flat surfaces. The extent of wetlands on these shelves during the LGM, however, is not well known and data is sparse due to their location on the seafloor. However, in sediment cores from the Sunda Shelf, little evidence is found for widespread peatland presence during the LGM (Hanebuth et al., 2011). Furthermore, Dommain et al. (2014) suggests that the Sunda Shelf might have been effectively drained by a deep-cut river system, preventing the formation of large wetlands, and suggest that peatland formation only started in response to sea-level rise. This evidence thus suggests that the wetland extent simulated on tropical continental shelves might be overestimated by LPX-Bern.

As the largest source of emissions, the simulated loss of tropical emissions is dominated by seasonal wetlands. To potentially reduce simulated seasonal wetland area in the tropics during the LGM, especially on the continental shelves, and thus decreasing the loss of tropical seasonal wetland area from LGM to PI, an alternative formulation of the DYPTOP module and its underlying TOPMODEL parametrization was tested. The standard implementation of the DYPTOP module, which dynamically determines the grid-cell fraction of seasonal wetlands and peatlands, is described in section 2.1.2.1. In the TOPMODEL parametrization by Stocker et al. (2014), sub-grid pixels with a compound topographic index (CTI) that are below a threshold $CTI_{min} = 12$ are assumed to be 'unfloodable'. The CTI include information about slope and catchment area of the sub-grid pixel, with larger CTI indicating potentially larger water collection. The argument for introducing a minimum threshold for CTI values was that the topography in the respective sub-grid pixel would be too steep, and any water would quickly run off. However, there are also implementations of the TOPMODEL approach that use a threshold in the opposite direction. Gedney & Cox (2003) and Kleinen et al. (2012) argue that sub-grid pixels with a CTI larger than an upper threshold, CTI_{max}, collect so much water that they form permanent flow systems or lakes, rather than wetlands.

Figure 5.8 shows the sub-grid CTI values and 'unfloodable' sub-grid pixels, given a maximum or a minimum threshold, for three exemplary LPX-Bern grid cells located in flat regions with large simulated wetland extent at PI or LGM: the Hudson Bay Lowlands (HBL), the West Siberian Lowlands (WSL) and the Sunda shelf (SS). While wetland area in these grid cells is only minimally restricted when using the previous threshold of $CTI_{min} = 12$, restrictions increase drastically when imposing an alternative upper threshold, here set to $CTI_{max} = 17.2$ as derived below. Restrictions to flooding in the HBL and WSL grid cells, however, mostly seem to follow patterns of open water. Sub-grid pixels in the HBL grid cell with $CTI > CTI_{max}$, for example, mostly seem to cover the James Bay and the river channels leading into it. At the same time, the majority of the SS grid cell would be defined as 'unfloodable' when using the upper CTI threshold, restricting wetland area on the continental shelf.

This alternative approach was thus identified as a potential way to limit simulated seasonal

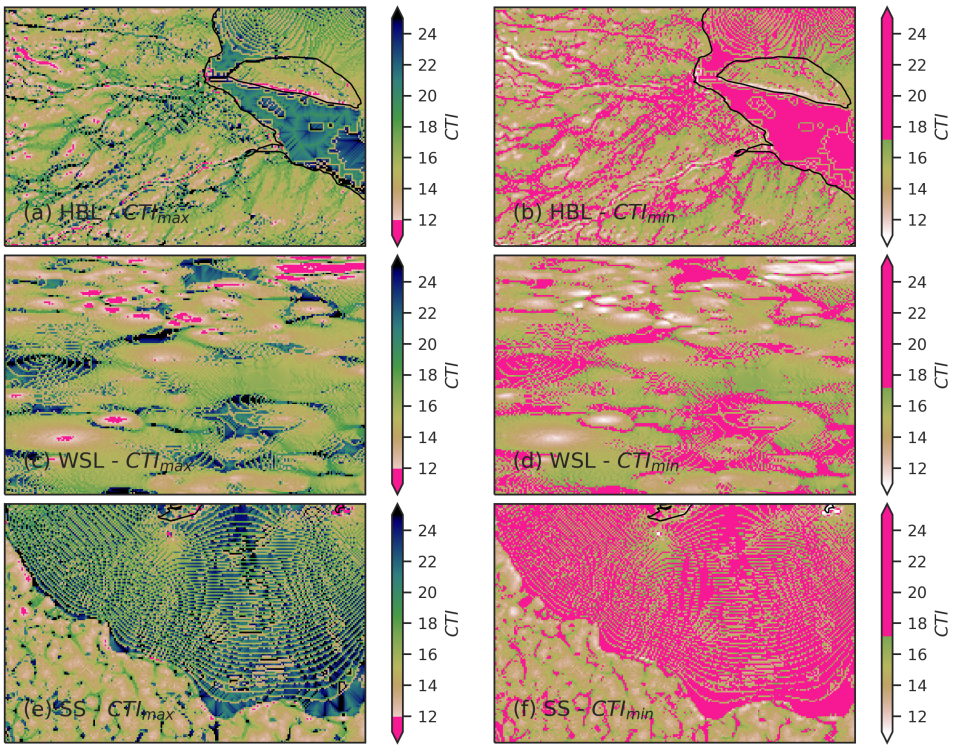

Figure 5.8: Sub-grid CTI values for three LPX-Bern grid cells in (a-b) the Hudson Bay Lowlands (52.5° N, 82.5° W), (c-d) the Western Siberian Lowlands (72.5° N, 63.75° E), and (e-f) the Sunda Shelf (7.5° N, 105° E). The coordinates denote the center point of the respective model grid cells. Pink colored sub grid pixels are assumed to be 'unfloodable' (a,c,e) in the standard DYPTOP formulation with $CTI_{min} = 12$ and (b,d,f) the alternative formulation with $CTI_{max} = 17.2$.

wetland extent on the mostly flat continental shelves, while potentially retaining realistic wetland prediction in today's major wetland regions.

To test this approach the threshold for 'unfloodable' sub-grid pixels was changed from CTI_{min} to CTI_{max} and the two TOPMODEL parameters M (equation 2.2) and CTI_{max} were re-tuned. The tuning was done with the goal to minimize the LGM-PI reduction in the mean area of tropical seasonal wetlands while mostly preserving present-day seasonal wetland area with respect to mean extent and latitudinal distribution. Due to the peatland-water-table feedback, peatlands were not included in this step but addressed separately afterwards. To reduce computational costs, the LPX-Bern uses asymmetric sigmoid functions that are fitted for each grid cell to the relationships between the grid cell water table and the inundated grid cell fraction that follows from equation 2.2. The fitting was performed using different values for M and CTI_{max} and, in contrast to Stocker et al. (2014), after the exclusion of sub-grid pixels with $CTI > CTI_{max}$. Upon closer inspection, the asymmetric sigmoid functions had worse fits to the TOPMODEL relationship than in the standard setup. This could be the result of choosing to perform the fitting after the exclusion of CTI values instead of before, which might need to be reconsidered in the future. The fitted functions were then used together with simulated water table depths from two LPX-Bern simulations under LGM and PI conditions to offline evaluate the predicted wetland area given different for M and CTI_{max}. The parameter values tested ranged from 2.5–8 for M and from 15–22 for CTI_{max}, with additional iterations narrowing the parameter space.

The results revealed different latitude-dependent sensitivities of mean seasonal wetland area to the sampled parameters. Mean wetland area generally decreased with M. At the same time, lower values for M led to more positive LGM-PI anomalies for mean wetland area over all

latitudes. Higher values for CTI_{max} led to increases in the simulated mean seasonal wetland area, as more and more sub-grid pixels are counted as floodable. When CTI_{max} is reduced the relative LGM-PI wetland anomaly in the tropics becomes more positive, but more negative for the northern extratropics. Additionally, the variability of monthly wetland area reduces in the northern extratropics with decreasing CTI_{max}. Low values for both M and CTI_{max} thus would maximize the relative LGM-PI wetland area anomaly in the tropics, however, with potential changes to the extent of global seasonal wetlands and with a potentially reduced variability and relative LGM-PI anomaly in the northern extratropics. The optimal parameter set was found with $M = 3$ and $CTI_{max} = 17.2$. With this parameter set, LGM-PI anomalies of seasonal wetland area increased both in the tropics (–16 % versus –25 % with the standard setup) and the northern extratropics (3.5 % versus 2.9 %). Mean seasonal wetland area in the tropics is roughly conserved at PI (+3 % relative to the standard setup), and slightly more increased in the northern extratropics (13.5 %). Due to the introduction of CTI_{max}, the variability of the northern seasonal wetland area is reduced, with 17 % smaller standard deviation for monthly values over the PI period (1–0.25 kyrs BP) than in the standard setup.

The TOPMODEL output is used to determine potential peatland area, as the grid-cell fraction that is flooded at least N months in the previous 31 years, with $N = 18$ in the standard setup (see also section 2.1.1). With N unchanged, the reduction of variability for seasonal wetland area in the northern extratropics under the alternative TOPMODEL formulation thus would lead to a significant decrease in diagnosed northern peatland area (–26 % at PI relative to the standard setup). Therefore, in a second step, N was re-tuned so that simulated PI peatland area in the northern extratropics matches the results from the standard setup, which were shown to fit within the range of estimates for present-day peatland area (see 3). Tropical peatland area is less well constrained and thus not considered as a target here. Furthermore, northern extratropics showed a higher sensitivity of simulated peatland area to changes in N. Full transient simulations from LGM to PI, with values for N ranging from 8–18, were performed and $N = 8$ was identified as the best match value. With this, the northern extratropical PI peatland area decreases by –1 % compared to the standard setup. The addition of peatlands changes the simulated seasonal wetland area compared to the results discussed above, through their prioritization in grid-cell flooding and their feedback on the water table (see section 2.1.2.1). Table 5.1 provides an overview over the differences between the standard setup and the final alternative DYPTOP formulation (from now on referred to as ALTTOP), concerning DYPTOP parameters, wetland area, and methane emissions.

Figure 5.9 shows that ALTTOP indeed considerably reduces emissions from tropical continental shelves in Sundaland, North of Australia, and the northern coast of South America during the LGM (see also Fig. 5.1). The alternative DYPTOP formulation, however, changes emissions globally. As the model changes relate to the sub-grid topography, which is assumed to be constant, regional patterns of changes in emissions are similar for the LGM and present day. Emissions with ALTTOP are increased relative to the standard setup in China, central Africa, southern Europe, southwestern North America, and western and eastern South America. They constitute regions with rougher terrain, where the previous threshold of CTI_{min} limited seasonal wetland extent. Similarly, mostly flat regions, such as central South America, South-East Asia, and parts of Africa, see emission reductions under the upper CTI threshold with ALTTOP.

Present-day emissions in the northern extratropics mostly follow the distribution of peatlands. Although the total northern peatland area is conserved with ALTTOP, it is much more distributed than in the standard setup. Peatland area and wetland methane emissions are reduced in the large peatland complexes of the HBL and WSL and increased mostly in Europe and East Asia (Fig. 5.9). Compared to PEATMAP, a recent compilation of known global peatlands (Xu et al., 2018), peatlands in Northern Asia are overestimated in the standard setup. With ALTTOP this mismatch increases except for the WSL, where peatland area now is slightly

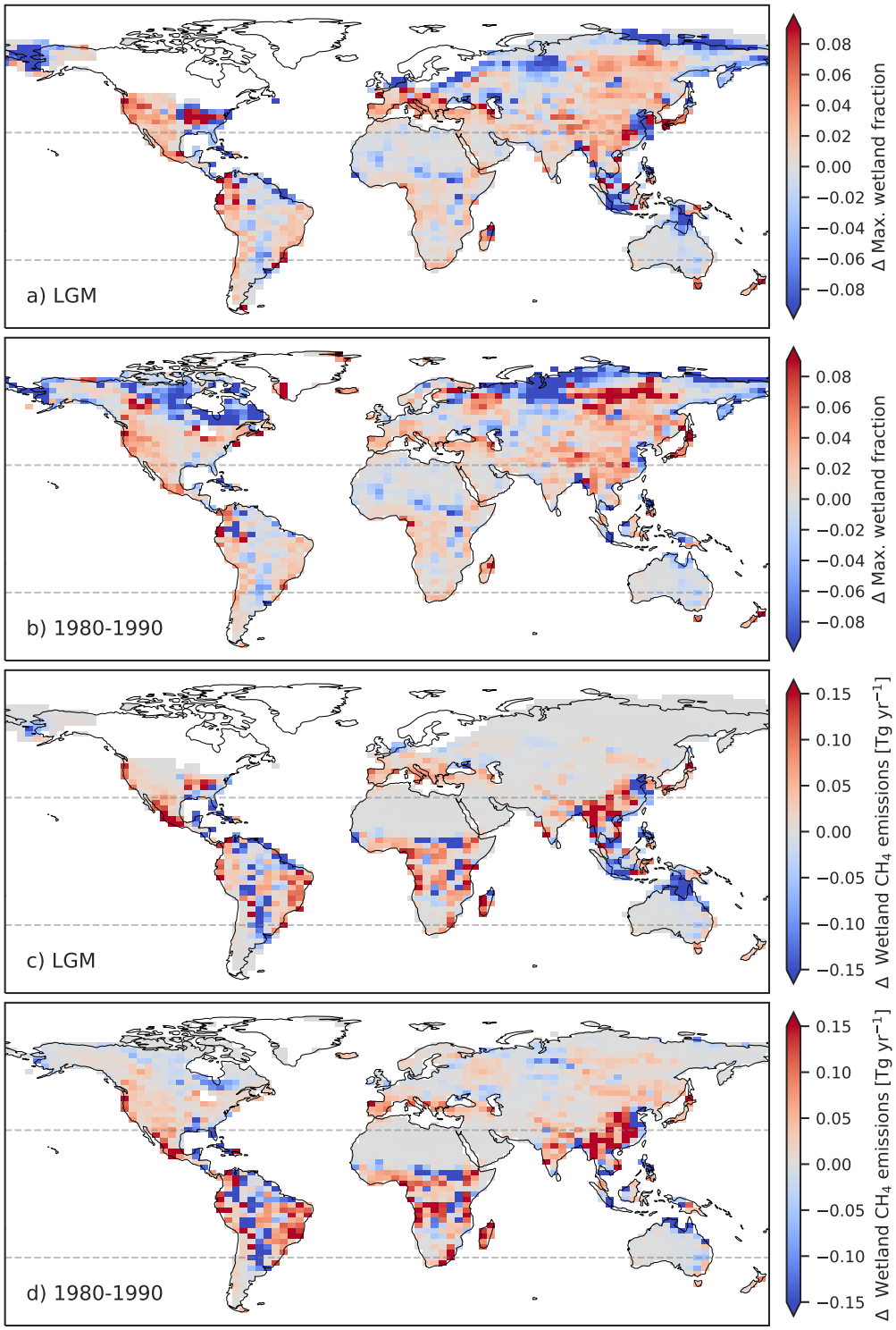

Figure 5.9: Difference of simulated (a,b) maximum wetland area and (c,d) wetland methane emissions between the alternative DYPTOP formulation (ALTTOP) and the standard setup (a,c) during the LGM and (b,d) at present. Dashed grey lines indicate 30° North and South.

Table 5.1: DYPTOP parameter values and simulated results for the standard setup and the alternative DYPTOP formulation (ALTTOP). Shown are LGM and PI values together with the corresponding relative LGM-PI anomaly for global, northern (>30° N), and tropical (30° S–30° N) monthly mean seasonal wetland area, peatland area, and yearly wetland methane emissions.

	Standard			**ALTTOP**		
Parameter						
M	8			3		
CTI_{min}	12			-		
CTI_{max}	-			17.2		
N	18			8		
	LGM	PI	LGM-PI [%]	LGM	PI	LGM-PI [%]
Global						
Seasonal wetland area [Mkm^2]	2.0	1.5	–22.1	1.9	1.7	–14.2
Peatland area [Mkm^2]	2.7	4.3	+62.8	3.0	4.2	+38.0
CH_4 emissions [Tg yr^{-1}]	130.0	124	–4.5	115.9	125.8	+8.5
Northern						
Seasonal wetland area [Mkm^2]	0.7	0.6	–17.6	0.8	0.7	–16.2
Peatland area [Mkm^2]	1.4	3.1	+114.8	1.6	3.1	+89.9
CH_4 emissions [Tg yr^{-1}]	16.5	27.8	+68.1	19.5	32.0	+64.0
Tropical						
Seasonal wetland area [Mkm^2]	1.2	0.9	–25.0	1.0	0.9	–12.9
Peatland area [Mkm^2]	1.2	1.2	+1.0	1.3	1.0	–22.6
CH_4 emissions [Tg yr^{-1}]	111.9	94.4	–15.6	95.2	92.0	–3.3

underestimated. The mismatch to PEATMAP also increases in North America, where peatland area is significantly underestimated with ALTTOP, however, regional improvements in simulated peatland distribution can be seen in the reduction of peatland area in eastern Canada and increases in western Canada. In the tropics, ALTTOP brings peatland area closer to PEATMAP estimates compared to the standard setup, with area reductions in South-East Asia and South America, and area increases in central Africa.

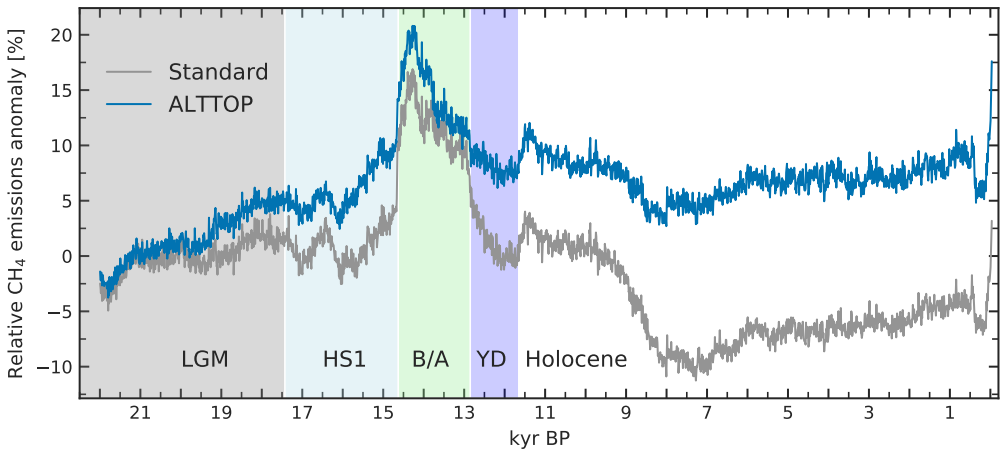

Figure 5.10: Wetland methane emission anomaly relative to the LGM (21 kyrs BP) for the standard setup and the alternative DYPTOP formulation (ALTTOP).

Due to the emission reduction from the continental shelves, the alternative DYPTOP formulation leads to an increase of wetland methane emissions from LGM to PI of +8.5 %

compared to the –4.5 % in the standard setup (Fig. 5.10 and Table 5.1), with a slightly reduced share of tropical emissions compared to the standard setup, of 82 % at LGM and 73 % at PI. The transient evolution of wetland emissions with ALTTOP shows the first increase in emissions before the HS1 from about 19–18 kyrs BP which is not mirrored in the ice core record (Fig. 5.2 (b)). The rest of the dynamics are similar to the standard setup, however, with substantially dampened losses due to sea-level rise and a less pronounced emission reduction at the end of the BA.

Taken together, the investigation into the DYPTOP formulation showed that an upper threshold for sub-grid CTI values can limit wetland prediction on continental shelves during the LGM, reducing the loss of wetland emissions in the tropics due to sea-level rise. Predictions of the resulting present-day wetland and peatland distributions, depending on the region, move towards or away from observational estimates, but remain consistent on a global scale. Here, parameters were tuned against standard setup results, but for a potential full integration into the LPX-Bern, parameters should be tuned against observational estimates of wetland and peatland area. Argumentations for both, an upper and a lower version of the CTI threshold, have convincingly been made in previous studies. Following the encouraging results presented here, a DYPTOP version could be tested in the future which includes both thresholds at the same time.

5.5 Conclusion

In this chapter, simulated wetland area and wetland methane emissions were presented and analyzed using transient and factorial simulations from the LGM to the present. Present-day global wetland area and wetland methane emission simulated by LPX-Bern were found to be well within the range of literature estimates. Simulated global emissions were dominated by tropical seasonal wetlands matching present-day latitudinal source distributions estimates. The transient evolution of simulated past wetland emissions showed some features of the atmospheric methane variability measured in ice cores, most notably, abrupt changes in emissions at the transitions between northern hemisphere cold and warm periods. However, simulated methane emissions failed to reproduce the general positive trend, with sources expected to almost double from LGM to PI. Emission increases at the onset of the BA and the early Holocene were found to be dominated by tropical seasonal wetlands and driven by increases in precipitation, consistent with isotopic evidence. The abrupt decrease of emissions at the transition from BA to YD was found to originate in the northern extratropics, driven by abrupt decreases in temperature and precipitation. The emission variability in the early Holocene was dominated by a decrease of emissions from tropical seasonal wetlands due to sea-level rise and the subsequent flooding of continental shelves. Peatland and wetland expansion into northern high latitudes in the late Holocene led to a partial recovery of simulated global emissions towards the PI period. The lack of a simulated positive emission anomaly from LGM to PI was found to be the result of large sea-level-driven emission losses from seasonal wetlands on continental shelves canceling the moderate emission increases due to rising atmospheric CO_2, temperature, and precipitation.

Two model investigations were performed with the goal of potentially reducing the model-data mismatch regarding the simulated LGM-PI emission anomaly. The weak indirect temperature dependence of wetland methane emissions was supplemented with an additional explicit temperature dependence of the CH_4/CO_2 emission ratio. The effect of the additional temperature dependence was dampened by the latitudinal emission distribution, which was skewed towards the tropics due to the latitudinal temperature gradient. The concentration of emissions into low latitudes, which see limited warming compared to high latitudes, resulted in a reduced sensitivity to mean global temperature changes. Redistribution of emissions can not be achieved

by re-balancing the strength of relative sources but would either require a latitudinal shift in source area or a more adaptive implementation of the additional temperature dependence.

To reduce the potentially overestimated seasonal wetland area on tropical continental shelves during the LGM, an alternative formulation of the DYPTOP module was tested. Following previous modeling studies, the threshold on sub-grid topography which limits wetland extent in rough terrain (with low CTI values) was changed to a threshold that limits wetland extent on very flat terrain (with high CTI values), such as continental shelves. DYPTOP parameters were then tuned to minimize seasonal wetland area during the LGM, while roughly reproducing standard setup results for PI. Transient simulations with the resulting ALTTOP setup showed a moderate increase in the relative LGM-PI emission anomaly, due to the reduced emission loss from sea-level rise. Compared to peatland area estimates, ALTTOP improved the predicted peatland area at PI in the tropics and worsened it in the northern extratropics, however, with regional exceptions. Over the full simulation, the tropical emission share was slightly smaller compared to the standard setup.

The model investigations showed that neither the additional temperature dependence nor the alternative DYPTOP formulation can solve the model-data mismatch on their own and that they introduce additional challenges that need to be addressed. The solution most likely lies in a combination of these and other approaches. Indeed there might be potential synergies between the two approaches explored here. The reduction of the tropical emission share when using ALTTOP could partly compensate for the effects from adding the temperature dependence. Combining ALTTOP with E2, the temperature sensitivity roughly corresponding to a Q_{10} of 2, leads to a relative LGM-PI emission anomaly of 14.8 % with a tropical emission share of 90 % at PI. The resulting tropical emission share is still overestimated but smaller than when adding the additional temperature dependence alone. The synergy could potentially be increased further by introducing thresholds for both, large and small CTI values, simultaneously, which could further reduce wetland area in the tropics. However, the resulting wetland area would need to be validated against observational estimates, which indicate an already slightly underestimated tropical wetland area. Furthermore, it is clear that beyond the approaches discussed here, additional factors are needed to achieve the full expected LGM-PI emission anomaly.

The sensitivity of vegetation to changes in atmospheric CO_2 could be one of those factors. Although CO_2 fertilization since the LGM has the largest positive effect on simulated methane emissions, the effect remains small compared to other modeling studies. Future model investigations should strive to test the simulated fertilization effect against observations and find appropriate model adjustments if necessary. Another change that might positively influence the LGM-PI wetland area and methane emission anomaly concerns the basin map used to calculate the TOPMODEL relationship (Equation 2.2). In the current setup, this basin map is constant in time and spans the maximum land area, including the continental shelves. Adjusting this map for each time step of the transient land-sea-ice mask would lead to decreasing CTI basin averages following the flooding of the flat continental shelves and thus to an increase in wetland area on the remaining land with rising sea level. This adjustment would require fit functions to be calculated for each time step of the land-sea-ice mask. Finally, a quantification of the uncertainty stemming from the climate forcing, similar to the investigations in chapter 3, can reveal the effect of different assumed climate anomalies.

Other model changes might improve the methane module of LPX-Bern in general. Emissions from seasonal wetlands, make up by far the largest share of the simulated global emissions but are calculated with the most simple parametrization. Expanding the implementation of seasonal wetland emissions with more mechanistic parametrizations of methane production and transport might greatly improve simulated emissions compared to observations. This model development could build on the previous work by Ringeval et al. (2014), who implemented a

representation of tropical floodplains and their methane cycle using the LPX-Bern, however, without a subsequent integration into the main development version of the LPX-Bern. Another potential future model development is the inclusion of the atmospheric methane concentration as model input. Currently, a constant present-day value of 1800 ppb is used as a boundary condition for methane diffusion in peatland soils and the calculation of methane uptake by dry mineral soils. Introducing transient atmospheric methane concentrations as model forcing, such as provided by Köhler et al. (2017), could improve the consistency of simulated methane emissions and sinks in paleo as well as future settings. Finally, key parameters of the LPX-Bern methane module should be re-tuned after each adjustment, relying on additional site data and regional budgets, as discussed in section 2.1.2.3. Furthermore, global scaling factors might need to be determined separately depending on the model resolution, land-sea-ice mask and dynamic or prescribed wetland area used.

Bibliography

Arneth, A., Harrison, S. P., Zaehle, S., Tsigaridis, K., Menon, S., Bartlein, P. J., Feichter, J., Korhola, A., Kulmala, M., O'Donnell, D., Schurgers, G., Sorvari, S., & Vesala, T., 2010. Terrestrial biogeochemical feedbacks in the climate system, *Nat. Geosci.*, 3(8), 525–532.

Baumgartner, M., Kindler, P., Eicher, O., Floch, G., Schilt, A., Schwander, J., Spahni, R., Capron, E., Chappellaz, J., Leuenberger, M., Fischer, H., & Stocker, T. F., 2014. NGRIP CH4 concentration from 120 to 10 kyr before present and its relation to a δ15N temperature reconstruction from the same ice core, *Clim. Past*, 10(2), 903–920.

Beck, J., Bock, M., Schmitt, J., Seth, B., Blunier, T., & Fischer, H., 2018. Bipolar carbon and hydrogen isotope constraints on the Holocene methane budget, *Biogeosciences*, 15(23), 7155–7175.

Bock, M., Schmitt, J., Beck, J., Seth, B., Chappellaz, J., & Fischer, H., 2017. Glacial/interglacial wetland, biomass burning, and geologic methane emissions constrained by dual stable isotopic CH4 ice core records, *Proc. Natl. Acad. Sci.*, 114(29), E5778–E5786.

Byun, E., Sato, H., Cowling, S. A., & Finkelstein, S. A., 2021. Extensive wetland development in mid-latitude North America during the Bølling-Allerød, *Nat. Geosci.*, 14(1), 30–35.

Cao, J., Wang, B., & Ma, L., 2019. Attribution of Global Monsoon Response to the Last Glacial Maximum Forcings, *J. Clim.*, 32(19), 6589–6605.

Chappellaz, J., Blunier, T., Kints, S., Dällenbach, A., Barnola, J.-M., Schwander, J., Raynaud, D., & Stauffer, B., 1997. Changes in the atmospheric CH 4 gradient between Greenland and Antarctica during the Holocene, *J. Geophys. Res. Atmos.*, 102(D13), 15987–15997.

Ciais, P., Sabine, C., Bala, G., Bopp, L., Brovkin, V., Canadell, J., Chhabra, A., DeFries, R., Galloway, J., Heimann, M., Jones, C., Quéré, C. L., Myneni, R., Piao, S., & Thornton, P., 2013. Carbon and Other Biogeochemical Cycles, in *Clim. Chang. 2013 Phys. Sci. Basis Work. Gr. I Contrib. to Fifth Assess. Rep. Intergov. Panel Clim. Chang.*, pp. 465–570, eds Stocker, T., Qin, D., Plattner, G.-K., Tignor, M., Allen, S., Boschung, J., Nauels, A., Xia, Y., Bex, V., & Midgley, P., Cambridge University Press, Cambridge.

Dean, J. F., Middelburg, J. J., Röckmann, T., Aerts, R., Blauw, L. G., Egger, M., Jetten, M. S. M., de Jong, A. E. E., Meisel, O. H., Rasigraf, O., Slomp, C. P., in 't Zandt, M. H., & Dolman, A. J., 2018. Methane feedbacks to the global climate system in a warmer world, *Rev. Geophys.*, pp. 207–250.

DelSontro, T., Beaulieu, J. J., & Downing, J. A., 2018. Greenhouse gas emissions from lakes and impoundments: Upscaling in the face of global change, *Limnol. Oceanogr. Lett.*, 3(3), 64–75.

Dommain, R., Couwenberg, J., Glaser, P. H., Joosten, H., & Suryadiputra, I. N. N., 2014. Carbon storage and release in Indonesian peatlands since the last deglaciation, *Quat. Sci. Rev.*, 97, 1–32.

Ed Dlugokencky, 2021. NOAA/GML (www.esrl.noaa.gov/gmd/ccgg/trends_ch4/).

Etiope, G., Milkov, A. V., & Derbyshire, E., 2008. Did geologic emissions of methane play any role in Quaternary climate change?, *Glob. Planet. Change*, 61(1-2), 79–88.

ETOPO1, 2013. NOAA National Geophysical Data Center. 2009: ETOPO1 1 Arc-Minute Global Relief Model. NOAA National Centers for Environmental Information. Accessed April 2013.

Gedney, N. & Cox, P. M., 2003. The Sensitivity of Global Climate Model Simulations to the Representation of Soil Moisture Heterogeneity, *J. Hydrometeorol.*, 4(6), 1265–1275.

Gedney, N., Cox, P. M., & Huntingford, C., 2004. Climate feedback from wetland methane emissions, *Geophys. Res. Lett.*, 31(20), 1–4.

Hanebuth, T. J., Voris, H. K., Yokoyama, Y., Saito, Y., & Okuno, J., 2011. Formation and fate of sedimentary depocentres on Southeast Asia's Sunda Shelf over the past sea-level cycle and biogeographic implications, *Earth-Science Rev.*, 104(1-3), 92–110.

He, C., Liu, Z., Otto-Bliesner, B. L., Brady, E. C., Zhu, C., Tomas, R., Clark, P. U., Zhu, J., Jahn, A., Gu, S., Zhang, J., Nusbaumer, J., Noone, D., Cheng, H., Wang, Y., Yan, M., & Bao, Y., 2021. Hydroclimate footprint of pan-Asian monsoon water isotope during the last deglaciation, *Sci. Adv.*, 7(4), 1–12.

Hopcroft, P. O., Valdes, P. J., O'Connor, F. M., Kaplan, J. O., & Beerling, D. J., 2017. Understanding the glacial methane cycle, *Nat. Commun.*, 8, 14383.

Houweling, S., Bergamaschi, P., Chevallier, F., Heimann, M., Kaminski, T., Krol, M., Michalak, A. M., & Patra, P., 2017. Global inverse modeling of CH4 sources and sinks: An overview of methods, *Atmos. Chem. Phys.*, 17(1), 235–256.

Hu, S., Niu, Z., & Chen, Y., 2017. Global Wetland Datasets: a Review, *Wetlands*, 37(5), 807–817.

Kaplan, J. O., 2002. Wetlands at the Last Glacial Maximum: Distribution and methane emissions, *Geophys. Res. Lett.*, 29(6), 3–1–3–4.

Kaplan, J. O., Folberth, G., & Hauglustaine, D. A., 2006. Role of methane and biogenic volatile organic compound sources in the late glacial and Holocene fluctuations of atmospheric methane concentrations, *Global Biogeochem. Cycles*, 20(2).

Kleinen, T., Brovkin, V., & Schuldt, R. J., 2012. A dynamic model of wetland extent and peat accumulation: Results for the Holocene, *Biogeosciences*, 9(1), 235–248.

Kleinen, T., Mikolajewicz, U., & Brovkin, V., 2020. Terrestrial methane emissions from the Last Glacial Maximum to the preindustrial period, *Clim. Past*, 16(2), 575–595.

Köhler, P., Nehrbass-Ahles, C., Schmitt, J., Stocker, T. F., & Fischer, H., 2017. A 156 kyr smoothed history of the atmospheric greenhouse gases CO2, CH4, and N2O and their radiative forcing, *Earth Syst. Sci. Data*, 9(1), 363–387.

Korhola, A., Ruppel, M., Seppä, H., Väliranta, M., Virtanen, T., & Weckström, J., 2010. The importance of northern peatland expansion to the late-Holocene rise of atmospheric methane, *Quat. Sci. Rev.*, 29(5-6), 611–617.

Levine, J. G., Wolff, E. W., Jones, A. E., Sime, L. C., Valdes, P. J., Archibald, A. T., Carver, G. D., Warwick, N. J., & Pyle, J. A., 2011. Reconciling the changes in atmospheric methane sources and sinks between the Last Glacial Maximum and the pre-industrial era, *Geophys. Res. Lett.*, 38(23), 2–7.

Lienert, S. & Joos, F., 2018. A Bayesian ensemble data assimilation to constrain model parameters and land-use carbon emissions, *Biogeosciences*, 15(9), 2909–2930.

Liu, Z., Otto-Bliesner, B. L., He, F., Brady, E. C., Tomas, R., Clark, P. U., Carlson, A. E., Lynch-Stieglitz, J., Curry, W., Brook, E., Erickson, D., Jacob, R., Kutzbach, J., & Cheng, J., 2009. Transient simulation of last deglaciation with a new mechanism for bolling-allerod warming, *Science*, 325(5938), 310–314.

Lloyd, J. & Taylor, J. A., 1994. On the temperature-dependence of soil respiration, *Funct. Ecol.*, 8(3), 315–323.

Loulergue, L., Schilt, A., Spahni, R., Masson-Delmotte, V., Blunier, T., Lemieux, B., Barnola, J.-M., Raynaud, D., Stocker, T. F., & Chappellaz, J., 2008. Orbital and millennial-scale features of atmospheric CH4 over the past 800,000 years, *Nature*, 453(7193), 383–386.

Maasakkers, J. D., Jacob, D. J., Sulprizio, M. P., Scarpelli, T. R., Nesser, H., Sheng, J.-X., Zhang, Y., Hersher, M., Bloom, A. A., Bowman, K. W., Worden, J. R., Janssens-Maenhout, G., & Parker, R. J., 2019. Global distribution of methane emissions, emission trends, and OH concentrations and trends inferred from an inversion of GOSAT satellite data for 2010–2015, *Atmos. Chem. Phys. Discuss.*, pp. 1–36.

Masson-Delmotte, V., Schulz, M., Abe-Ouchi, A., Beer, J., Ganopolski, A., Rouco, J. G., Jansen, E., Lambeck, K., Luterbacher, J., Naish, T., Osbor, T., Otto-Bliesner, B., Quinn, T., Ramesh, R., Rojas, M., Shao, X., & Timmermann, A., 2013. Information from Paleoclimate Archives, in *Clim. Chang. 2013 Phys. Sci. Basis. Contrib. Work. Gr. I to Fifth Assess. Rep. Intergov. Panel Clim. Chang.*, pp. 383–464, eds Stocker, T., D. Qin, G.-K. P., Tignor, M., Allen, S., Boschung, J., Nauels, A., Xia, Y., Bex, V., & Midgley, P., Cambridge University Press, Cambridge.

Mayewski, P. A., Rohling, E. E., Stager, J. C., Karlén, W., Maasch, K. A., Meeker, L. D., Meyerson, E. A., Gasse, F., van Kreveld, S., Holmgren, K., Lee-Thorp, J., Rosqvist, G., Rack, F., Staubwasser, M., Schneider, R. R., & Steig, E. J., 2004. Holocene climate variability, *Quat. Res.*, 62(3), 243–255.

McGee, D., Donohoe, A., Marshall, J., & Ferreira, D., 2014. Changes in ITCZ location and cross-equatorial heat transport at the Last Glacial Maximum, Heinrich Stadial 1, and the mid-Holocene, *Earth Planet. Sci. Lett.*, 390, 69–79.

McManus, J. F., Francois, R., Gherardi, J.-M., Keigwin, L. D., & Brown-Leger, S., 2004. Collapse and rapid resumption of Atlantic meridional circulation linked to deglacial climate changes, *Nature*, 428(6985), 834–837.

Mitchell, L., Brook, E., Lee, J. E., Buizert, C., & Sowers, T., 2013. Constraints on the Late Holocene Atmospheric Methane Budget, *Science*, 342(November), 964–967.

Murray, L. T., Mickley, L. J., Kaplan, J. O., Sofen, E. D., Pfeiffer, M., & Alexander, B., 2014. Factors controlling variability in the oxidative capacity of the troposphere since the Last Glacial Maximum, *Atmos. Chem. Phys.*, 14(7), 3589–3622.

Ng, H. C., Robinson, L. F., McManus, J. F., Mohamed, K. J., Jacobel, A. W., Ivanovic, R. F., Gregoire, L. J., & Chen, T., 2018. Coherent deglacial changes in western Atlantic Ocean circulation, *Nat. Commun.*, 9(1), 1–10.

Pangala, S. R., Enrich-Prast, A., Basso, L. S., Peixoto, R. B., Bastviken, D., Hornibrook, E. R., Gatti, L. V., Marotta, H., Calazans, L. S. B., Sakuragui, C. M., Bastos, W. R., Malm, O., Gloor, E., Miller, J. B., & Gauci, V., 2017. Large emissions from floodplain trees close the Amazon methane budget, *Nature*, 552(7684), 230–234.

Peltola, O., Vesala, T., Gao, Y., Räty, O., Alekseychik, P., Aurela, M., Chojnicki, B., Desai, A. R., Dolman, A. J., Euskirchen, E. S., Friborg, T., Göckede, M., Helbig, M., Humphreys, E., Jackson, R. B., Jocher, G., Joos, F., Klatt, J., Knox, S. H., Kutzbach, L., Lienert, S., Lohila, A., Mammarella, I., Nadeau, D. F., Nilsson, M. B., Oechel, W. C., Peichl, M., Pypker, T., Quinton, W., Rinne, J., Sachs, T., Samson, M., Schmid, H. P., Sonnentag, O., Wille, C., Zona, D., & Aalto, T., 2019. Monthly Gridded Data Product of Northern Wetland Methane Emissions Based on Upscaling Eddy Covariance Observations, *Earth Syst. Sci. Data Discuss.*, pp. 1–50.

Prather, M. J., Holmes, C. D., & Hsu, J., 2012. Reactive greenhouse gas scenarios: Systematic exploration of uncertainties and the role of atmospheric chemistry, *Geophys. Res. Lett.*, 39(9), 6–10.

Rasmussen, S. O., Bigler, M., Blockley, S. P., Blunier, T., Buchardt, S. L., Clausen, H. B., Cvijanovic, I., Dahl-Jensen, D., Johnsen, S. J., Fischer, H., Gkinis, V., Guillevic, M., Hoek, W. Z., Lowe, J. J., Pedro, J. B., Popp, T., Seierstad, I. K., Steffensen, J. P., Svensson, A. M., Vallelonga, P., Vinther, B. M., Walker, M. J., Wheatley, J. J., & Winstrup, M., 2014. A stratigraphic framework for abrupt climatic changes during the Last Glacial period based on three synchronized Greenland ice-core records: refining and extending the INTIMATE event stratigraphy, *Quat. Sci. Rev.*, 106, 14–28.

Renssen, H., Mairesse, A., Goosse, H., Mathiot, P., Heiri, O., Roche, D. M., Nisancioglu, K. H., & Valdes, P. J., 2015. Multiple causes of the Younger Dryas cold period, *Nat. Geosci.*, 8(12), 946–949.

Ridgwell, A., Maslin, M., & Kaplan, J. O., 2012. Flooding of the continental shelves as a contributor to deglacial CH4 rise, *J. Quat. Sci.*, 27(8), 800–806.

Ringeval, B., Houweling, S., Van Bodegom, P. M., Spahni, R., Van Beek, R., Joos, F., & Röckmann, T., 2014. Methane emissions from floodplains in the Amazon Basin: Challenges in developing a process-based model for global applications, *Biogeosciences*, 11(6), 1519–1558.

Saunois, M., Stavert, A. R., Poulter, B., Bousquet, P., Canadell, J. G., Jackson, R. B., Raymond, P. A., Dlugokencky, E. J., Houweling, S., Patra, P. K., Ciais, P., Arora, V. K., Bastviken, D., Bergamaschi, P., Blake, D. R., Brailsford, G., Bruhwiler, L., Carlson, K. M., Carrol, M., Castaldi, S., Chandra, N., Crevoisier, C., Crill, P. M., Covey, K., Curry, C. L., Etiope, G., Frankenberg, C., Gedney, N., Hegglin, M. I., Höglund-Isaksson, L., Hugelius, G., Ishizawa, M., Ito, A., Janssens-Maenhout, G., Jensen, K. M., Joos, F., Kleinen, T., Krummel, P. B., Langenfelds, R. L., Laruelle, G. G., Liu, L., Machida, T., Maksyutov, S., McDonald, K. C., McNorton, J., Miller, P. A., Melton, J. R., Morino, I., Müller, J., Murguia-Flores, F., Naik, V., Niwa, Y., Noce, S., O'Doherty, S., Parker, R. J., Peng, C., Peng, S., Peters, G. P., Prigent, C., Prinn, R., Ramonet, M., Regnier, P., Riley, W. J., Rosentreter, J. A., Segers, A., Simpson, I. J., Shi, H., Smith, S. J., Steele, L. P., Thornton, B. F., Tian, H., Tohjima, Y., Tubiello, F. N., Tsuruta, A., Viovy, N., Voulgarakis, A., Weber, T. S., van Weele, M., van der Werf, G. R., Weiss, R. F., Worthy, D., Wunch, D., Yin, Y., Yoshida, Y., Zhang, W., Zhang, Z., Zhao, Y., Zheng, B., Zhu, Q., Zhu, Q., & Zhuang, Q., 2020. The Global Methane Budget 2000-2017, *Earth Syst. Sci. Data*, 12(3), 1561–1623.

Schilt, A., Baumgartner, M., Schwander, J., Buiron, D., Capron, E., Chappellaz, J., Loulergue, L., Schüpbach, S., Spahni, R., Fischer, H., & Stocker, T. F., 2010. Atmospheric nitrous oxide during the last 140,000 years, *Earth Planet. Sci. Lett.*, 300(1-2), 33–43.

Shi, J. & Yan, Q., 2019. Evolution of the Asian-African Monsoonal Precipitation over the last 21 kyr and the Associated Dynamic Mechanisms, *J. Clim.*, 32(19), 6551–6569.

Singarayer, J. S., Valdes, P. J., Friedlingstein, P., Nelson, S., & Beerling, D. J., 2011. Late Holocene methane rise caused by orbitally controlled increase in tropical sources, *Nature*, 470(7332), 82–85.

Stocker, B. D., Roth, R., Joos, F., Spahni, R., Steinacher, M., Zaehle, S., Bouwman, L., Xu-Ri, & Prentice, I. C., 2013. Multiple greenhouse-gas feedbacks from the land biosphere under future climate change scenarios, *Nat. Clim. Chang.*, 3(7), 666–672.

Stocker, B. D., Spahni, R., & Joos, F., 2014. DYPTOP: A cost-efficient TOPMODEL implementation to simulate sub-grid spatio-temporal dynamics of global wetlands and peatlands, *Geosci. Model Dev.*, 7(6), 3089–3110.

Stocker, T. F. & Johnsen, S. J., 2003. A minimum thermodynamic model for the bipolar seesaw, *Paleoceanography*, 18(4), 1–9.

Turetsky, M. R., Kotowska, A., Bubier, J., Dise, N. B., Crill, P., Hornibrook, E. R., Minkkinen, K., Moore, T. R., Myers-Smith, I. H., Nykänen, H., Olefeldt, D., Rinne, J., Saarnio, S., Shurpali, N., Tuittila, E. S., Waddington, J. M., White, J. R., Wickland, K. P., & Wilmking, M., 2014. A synthesis of methane emissions from 71 northern, temperate, and subtropical wetlands, *Glob. Chang. Biol.*, 20(7), 2183–2197.

Valdes, P. J., Beerling, D. J., & Jonhson, C. E., 2005. The ice age methane budget, *Geophys. Res. Lett.*, 32(2), 1–4.

Voulgarakis, A., Naik, V., Lamarque, J. F., Shindell, D. T., Young, P. J., Prather, M. J., Wild, O., Field, R. D., Bergmann, D., Cameron-Smith, P., Cionni, I., Collins, W. J., Dalsøren, S. B., Doherty, R. M., Eyring, V., Faluvegi, G., Folberth, G. A., Horowitz, L. W., Josse, B., MacKenzie, I. A., Nagashima, T., Plummer, D. A., Righi, M., Rumbold, S. T., Stevenson, D. S., Strode, S. A., Sudo, K., Szopa, S., & Zeng, G., 2013. Analysis of present day and future OH and methane lifetime in the ACCMIP simulations, *Atmos. Chem. Phys.*, 13(5), 2563–2587.

Walter, K. M., Smith, L. C., & Chapin, F. S., 2007. Methane bubbling from northern lakes: Present and future contributions to the global methane budget, *Philos. Trans. R. Soc. A Math. Phys. Eng. Sci.*, 365(1856), 1657–1676.

Weber, S. L., Drury, A. J., Toonen, W. H., & Van Weele, M., 2010. Wetland methane emissions during the last glacial maximum estimated from PMIP2 simulations: Climate, vegetation, and geographic controls, *J. Geophys. Res. Atmos.*, 115(6), 1–13.

Xu, J., Morris, P. J., Liu, J., & Holden, J., 2018. PEATMAP: Refining estimates of global peatland distribution based on a meta-analysis, *CATENA*, 160(September 2017), 134–140.

Xu, X., Yuan, F., Hanson, P. J., Wullschleger, S. D., Thornton, P. E., Riley, W. J., Song, X., Graham, D. E., Song, C., & Tian, H., 2016. Reviews and syntheses: Four decades of modeling methane cycling in terrestrial ecosystems, *Biogeosciences*, 13(12), 3735–3755.

Yvon-Durocher, G., Allen, A. P., Bastviken, D., Conrad, R., Gudasz, C., St-Pierre, A., Thanh-Duc, N., & Del Giorgio, P. A., 2014. Methane fluxes show consistent temperature dependence across microbial to ecosystem scales, *Nature*, 507(7493), 488–491.

Zhang, B., Tian, H., Lu, C., Chen, G., Pan, S., Anderson, C., & Poulter, B., 2017a. Methane emissions from global wetlands: An assessment of the uncertainty associated with various wetland extent data sets, *Atmos. Environ.*, 165, 310–321.

Zhang, Z., Zimmermann, N. E., Stenke, A., Li, X., Hodson, E. L., Zhu, G., Huang, C., & Poulter, B., 2017b. Emerging role of wetland methane emissions in driving 21st century climate change, *Proc. Natl. Acad. Sci.*, 114(36), 201618765.

Chapter 6

Selected other contributions

Simulations performed with the LPX-Bern also contributed to cooperative studies that investigate the terrestrial carbon and methane cycle (e.g. Saunois et al., 2020; Qiu et al., 2021). These studies typically focus on aggregated model-ensemble statistics rather than on results from individual models. This chapter presents a detailed analysis of the LPX-Bern contribution to two selected international studies and compares the results from LPX-Bern to the respective model ensembles. In section 6.1, the contribution to the assessment of the global methane budget (Saunois et al., 2020) as part of the Global Carbon Project is discussed and additional simulations are presented. Section 6.2 presents the LPX-Bern results from a model inter-comparison project that investigates future changes in the carbon balance of northern peatlands under different future scenarios (Qiu et al., 2021) and compares results to LPX-Bern simulation from chapter 4.

Other contributions that here are not discussed in detail include investigations on nitrous oxide emissions and the glacial nitrogen cycle (Joos et al., 2020) and community expert assessments of past and future changes in peatland carbon stocks as part of the Past Global Changes (PAGES) working group C-PEAT. Additionally, extended versions of the LPX-Bern simulations from Saunois et al. (2020) were used in Aalto et al. (2021) to analyze temperature and precipitation responses of wetland methane emissions and as prior for atmospheric inversions.

6.1 LPX-Bern in the global methane budget

The Global Methane Budget 2000–2017

M. Saunois, A. R. Stavert, B. Poulter, P. Bousquet, J. G. Canadell, R. B. Jackson, P. A. Raymond, E. J. Dlugokencky, S. Houweling, P. K. Patra, P. Ciais, V. K. Arora, D. Bastviken, P. Bergamaschi, D. R. Blake, G. Brailsford, L. Bruhwiler, K. M. Carlson, M. Carrol, S. Castaldi, N. Chandra, C. Crevoisier, P. M. Crill, K. Covey, C. L. Curry, G. Etiope, C. Frankenberg, N. Gedney, M. I. Hegglin, L. Höglund-Isaksson, G. Hugelius, M. Ishizawa, A. Ito, G. Janssens-Maenhout, K. M. Jensen, F. Joos, T. Kleinen, P. B. Krummel, R. L. Langenfelds, G. G. Laruelle, L. Liu, T. Machida, S. Maksyutov, K. C. McDonald, J. McNorton, P. A. Miller, J. R. Melton, I. Morino, **J. Müller**, F. Murguia-Flores, V. Naik, Y. Niwa, S. Noce, S. O'Doherty, R. J. Parker, C. Peng, S. Peng, G. P. Peters, C. Prigent, R. Prinn, M. Ramonet, P. Regnier, W. J. Riley, J. A. Rosentreter, A. Segers, I. J. Simpson, H. Shi, S. J. Smith, L. P. Steele, B. F. Thornton, H. Tian, Y. Tohjima, F. N. Tubiello, A. Tsuruta, N. Viovy, A. Voulgarakis, T. S. Weber, M. van Weele, G. R. van der Werf, R. F. Weiss, D. Worthy, D. Wunch, Y. Yin1, Y. Yoshida, W. Zhang, Z. Zhang, Y. Zhao, B. Zheng, Q. Zhu, Q. Zhu, and Q. Zhuang

Published in *Earth System Science Data*, Volume 12, 1561–1623, 2020.

6.1.1 Introduction

The global methane budget published in Saunois et al. (2016) and Saunois et al. (2020) is part of the Global Carbon Project and is a key community-synthesis publication that aims at providing a comprehensive overview of the present-day methane cycle, encompassing estimates of all anthropogenic and natural sources and sinks. It expands and builds on previous efforts to quantify global methane fluxes (Kirschke et al., 2013). This continually updated publication includes ensemble-style bottom-up and top-down estimates for methane emissions from different sources. The bottom-up estimates are based on process-based models or upscaling with prescribed wetland area, while the top-down estimates rely on atmospheric inversions (see section 1.3.2 for a more detailed definition).

Despite continued efforts, bottom-up and top-down estimates for total natural sources show substantial differences, with bottom-up estimates being almost 30 % larger than top-down estimates and with no overlap between both estimated ranges (Saunois et al., 2020). This state is reflective of the large uncertainties that are still connected to the estimates for natural methane sources such as termites, geological sources, wetlands, and other freshwater systems such as lakes, ponds, and rivers. In the past, special focus has been put on reconciling the bottom-up and top-down emissions from natural wetlands.

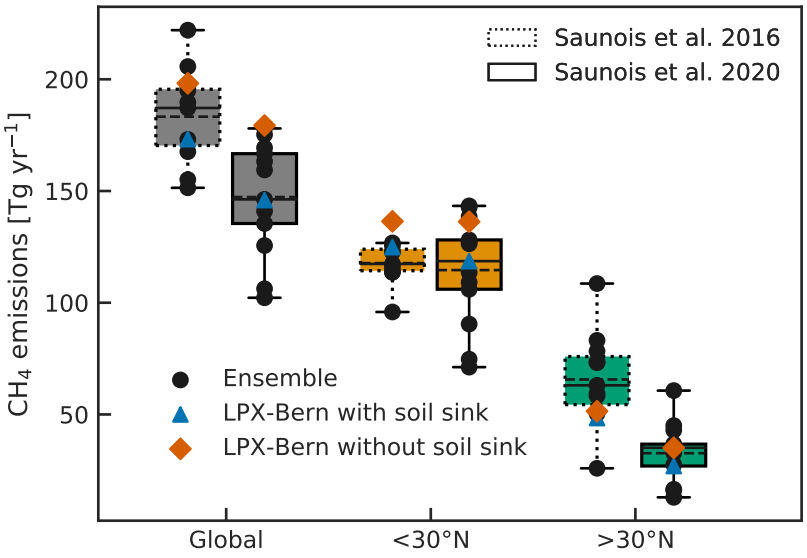

Figure 6.1: Boxplots of global, northern (>30° N), and tropical and southern (<30° N) wetland methane emissions from the model ensembles in Saunois et al. (2016) (dotted boxes) and Saunois et al. (2016) (solid boxes). Boxes indicate the interquartile range, whiskers the total range, solid horizontal lines the median, and dashed horizontal lines the mean. Black markers show emissions from individual ensemble members, blue markers show LPX-Bern results as reported in the global methane budgets with the global methane sink in dry mineral soils subtracted from the emissions, and orange markers show the respective LPX-Bern results without subtraction of the soil sink.

In Saunois et al. (2016), bottom-up estimates for 2000–2009 range from 151–222 teragrams of methane per year (Tg yr^{-1}), about 17 Tg yr^{-1} larger than the corresponding top-down estimates ranging from 125–204 Tg yr^{-1} (Fig. 6.1). In an effort to reduce double counting of freshwater sources in the bottom-up estimates, an updated wetland dataset was used for Saunois et al. (2020) to force the process-based models, which explicitly excluded open waters such as lakes and rivers and rice paddies. This led to a substantially reduced bottom-up estimate range of

102–179 Tg yr^{-1} (Fig. 6.1). However, at the same time, top-down estimates of wetland emissions increased to 153–196 Tg yr^{-1}, increasing the gap between top-down and bottom-up estimates to about 30 Tg yr^{-1} with top-down estimates now generally larger than their bottom-up counterparts. Top-down approaches are more robust than bottom-up approaches with respect to estimates of the total natural methane budget due to atmospheric constraints. However, source attribution in top-down approaches can be much more uncertain. One factor in the persisting mismatch might be that posterior distributions for wetland emissions include also emissions from spatially neighboring open water sources, while for the bottom-up estimate great care was taken to exclude them as best as possible (Saunois et al., 2020). A second potential factor concerns the handling of the simulated soil sink which is discussed later in this chapter.

Since wetland area is still one of the largest contributors to the wetland emission uncertainty (Zhang et al., 2017), Saunois et al. (2020) also reported bottom-up estimates with wetland area determined prognostically by process-based models. These range between 125–218 Tg yr^{-1} for 2008–2017. However, Saunois et al. (2020) does not provide any further analysis of these results or a comparison to the estimates with prescribed wetland area.

LPX-Bern results were included both in the bottom-up estimates of wetland methane emissions in Saunois et al. (2016), as one of 11 land surface models, and in Saunois et al. (2020), as one of 13 models. The contribution to Saunois et al. (2020) was created in the framework of this thesis. The following sections will give a short overview of the simulation setup in Saunois et al. (2016) and Saunois et al. (2020) and will provide a more detailed analysis of the LPX-Bern results produced for Saunois et al. (2020) including a detailed comparison between simulated emissions with prescribed and prognostically determined wetland area. Additionally, results from LPX-Bern are compared to the model ensemble and to the previous LPX-Bern results produced for Saunois et al. (2016).

6.1.2 Simulation setup

The simulations for Saunois et al. (2016) and Saunois et al. (2020) were performed with LPX-Bern version 1.0 (Spahni et al., 2013) and version 1.4 (Lienert & Joos, 2018) respectively, both on a $0.5° \times 0.5°$ model grid resolution. For Saunois et al. (2020) the LPX-Bern methane module was newly calibrated as described in section 2.1.2.3. Note that here different scaling factors for peatland ($mt_p = 0.197$) and seasonal wetland emissions ($r_i = 0.058$) were used compared to chapter 5.

The simulation protocol for Saunois et al. (2016) and Saunois et al. (2020) included a model spinup under pre-industrial conditions followed by a transient simulation from 1901 until 2017. Models were forced with the CRU reconstructed climate fields. Wetland area in Saunois et al. (2016) was prescribed as recycled monthly values from the SWAMPS-GLWD wetland area dataset (Poulter et al., 2017) which combines remote sensing with traditional inventory data sets and spans the years 2000–2012. The wetland area dataset used in Saunois et al. (2020), WAD2M (Wetland Area Dynamics for Methane Modeling; Zhang et al., 2021), spans the years 2000–2017 and is a further development in wetland mapping, where special care was taken to exclude permanent open water bodies such as lakes and rivers. Prior to 2000, the wetland datasets are cyclically repeated.

As LPX-Bern distinguishes between methane emissions from peatlands and other wetlands (see section 2.1.2), peatland area was also prescribed. Simulations for Saunois et al. (2016) used the peatland map from Tarnocai et al. (2007) which only covers northern peatlands. For Saunois et al. (2020), PEATMAP was used, a global compilation of known peatlands (Xu et al., 2018). To remain consistent with respect to emission source area, emissions from peatlands were only calculated where the prescribed wetland area and peatland area overlapped.

For Saunois et al. (2020), an additional simulation was performed where wetland and peatland area were determined prognostically based on the LPX-Bern DYPTOP module (Stocker et al., 2013, see section 2.1.1 for details). Results for the prognostic simulations from 7 out of the 13 process-based models were only reported briefly in Saunois et al. (2020) with simulated emissions ranging from 125–218 Tg yr^{-1} between 2008–2017. Results from the prognostic LPX-Bern simulation are compared in more detail to the diagnostic simulation (with prescribed wetlands) in the following section.

6.1.3 Results

The global wetland emissions simulated by LPX-Bern for 2000–2009 reported in Saunois et al. (2016) and Saunois et al. (2020) were 173.2 Tg yr^{-1} and 146.0 Tg yr^{-1} respectively. Figure 6.1 shows that LPX-Bern results reported for Saunois et al. (2020) (blue marker) are close to the ensemble mean for global emissions and emissions from tropical and southern wetlands, but on the lower side for emissions from northern wetlands. For Saunois et al. (2016), reported LPX-Bern emissions are lower than the ensemble means for global and northern emissions and higher for emissions from below 30° N.

However, the values reported in these publications are the simulated net emissions with the simulated global methane sink in dry mineral soils subtracted from the actual wetland methane emissions. The actual global wetland methane emissions simulated by LPX-Bern between 2000–2009 (orange markers in figure 6.1) are 198.2 Tg yr^{-1} and 179.3 Tg yr^{-1} respectively with a concurrent simulated global soil sink of 24.98 Tg yr^{-1} and 33.35 Tg yr^{-1}. The subtraction of the soil sink was likely not unique to LPX-Bern but potentially extended to other models that simulate explicitly both wetland emissions and the soil sink. The subtraction of the soil sink leads to inconsistencies, with net emissions reported as wetland emissions and parallel reporting of bottom-up estimates for the global soil sink. At the same time, top-down inversion estimates explicitly represent the soil sink in their prior and posterior distributions and do not include the soil sink in their reported wetland emissions. This different treatment of bottom-up and top-down estimates for wetland methane emissions could be one of the reasons for their persisting mismatch, which constitutes about 30 Tg yr^{-1} in Saunois et al. (2020) corresponding roughly to the there reported bottom-up (11–49 Tg yr^{-1}) and top-down (27–41 Tg yr^{-1}) estimates for the global soil sink.

Table 6.1: Maximum yearly prescribed (diagnostic) and simulated (prognostic) global, tropical/southern (<30° N), and northern (>30° N) total wetland, seasonal wetland, and peatland area together with their respective simulated methane emissions between 2000–2009, from the LPX-Bern contribution to Saunois et al. (2020). Emissions are given in units of teragrams methane per year (Tg yr^{-1}). Peatland area in the diagnostic case only refers to the overlap between prescribed datasets for peatland area (PEATMAP) and wetland area (WAD2M), which was used to calculate methane emissions from peatlands.

	Diagnostic			**Prognostic**		
	Global	<30° N	>30° N	Global	<30° N	>30° N
Total wetland area [Mkm^2]	7.65	3.31	3.97	10.43	4.68	5.48
Seas. wetl. area [Mkm^2]	5.32	2.64	1.64	4.42	2.09	2.15
Peatland area [Mkm^2]	2.33	0.67	2.33	6.02	2.59	3.33
CH_4 emissions [Tg yr^{-1}]	179.3	136.3	35.1	153.6	112.0	36.1
Seas. wetl. CH_4 emissions [Tg yr^{-1}]	134.5	105.0	22.5	71.4	57.0	10.8
Peatland CH_4 emissions [Tg yr^{-1}]	17.9	10.2	7.6	58.4	37.2	20.1

For Saunois et al. (2020), additional simulations with prognostic wetland area prediction were performed with 7 out of the 13 models, including the LPX-Bern. The maximum yearly

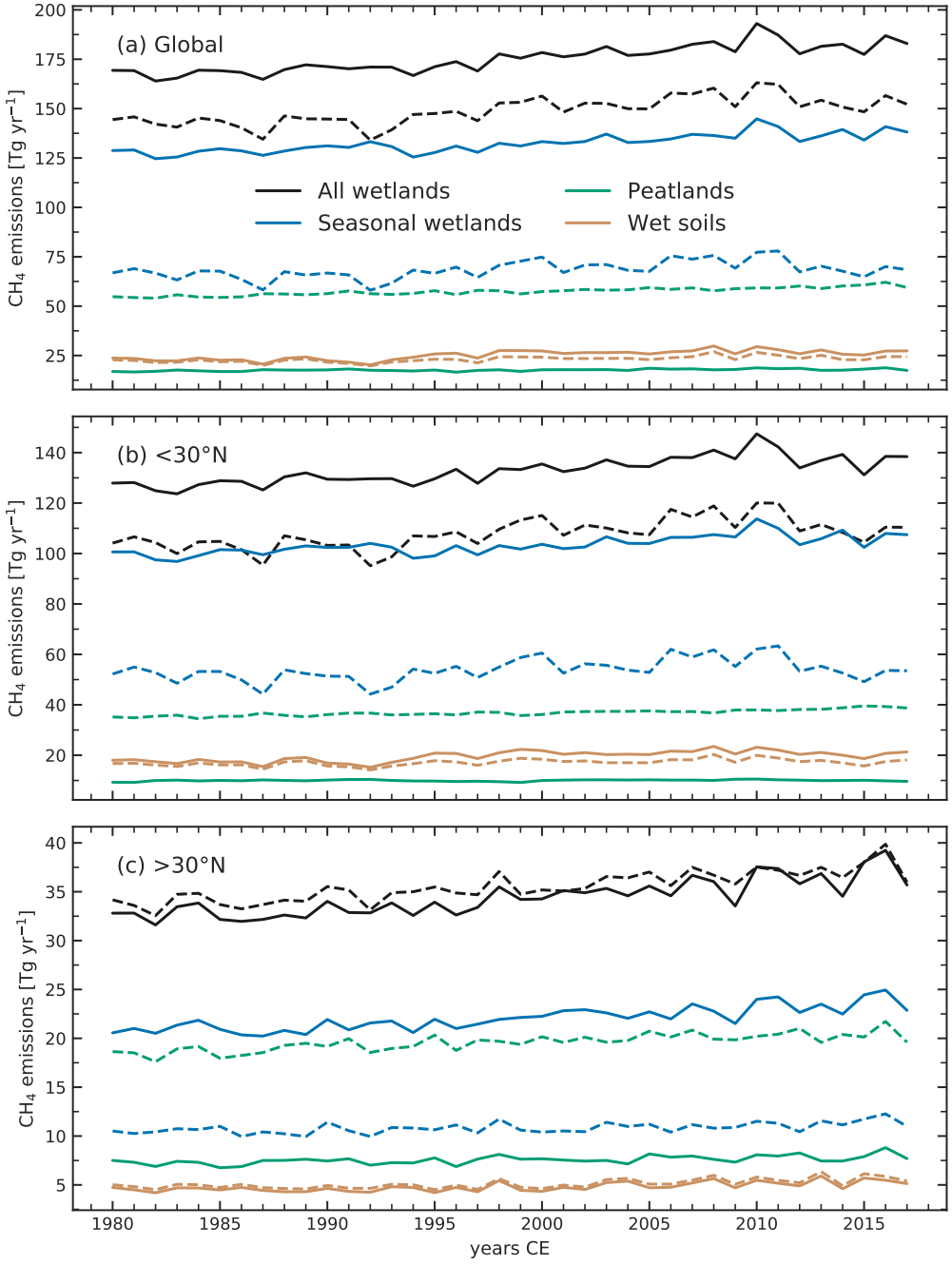

Figure 6.2: Simulated mean annual methane emissions from (a) global, (b) tropical and southern (<30° N), and (c) northern (>30° N) wetlands between 1980–2017 from the diagnostic (solid lines) and prognostic (dashed lines) LPX-Bern simulation. Shown are emissions from peatlands (green), seasonal wetlands (blue), wet mineral soils (brown), and all source categories combined (black).

wetland area between 2000–2009 predicted by LPX-Bern in the prognostic simulation was 36 % larger than the prescribed WAD2M wetland area (see table 6.1). Most of the prognostically determined wetland area consisted of peatlands (6 Mkm^2), while only about 2.3 Mkm^2 of the prescribed wetland area overlapped with the prescribed PEATMAP and thus was treated as methane-emitting peatlands (see section 6.1.2). In contrast to the peatland area, the emission source area of seasonal wetlands is slightly smaller in the prognostic simulation with 4.4 Mkm^2 compared to 5.3 Mkm^2 in the diagnostic simulation (Table 6.1). The low per-area-emissions from peatlands in LPX-Bern together with the reduced seasonal wetland area in the prognostic run

led to net global emissions of about 153.6 Tg yr^{-1} between 2000–2009, which is smaller than in the diagnostic run. Figure 6.2 and table table 6.1 show that emissions are reduced mostly in the tropics where the increase in emissions from peatlands can only partly compensate for the reduction in emissions from seasonal wetlands. For northern wetlands (>30° N), however, net emissions for the diagnostic and prognostic simulations are very similar with emissions from peatlands dominating in the prognostic run and emissions from seasonal wetland dominating in the diagnostic run.

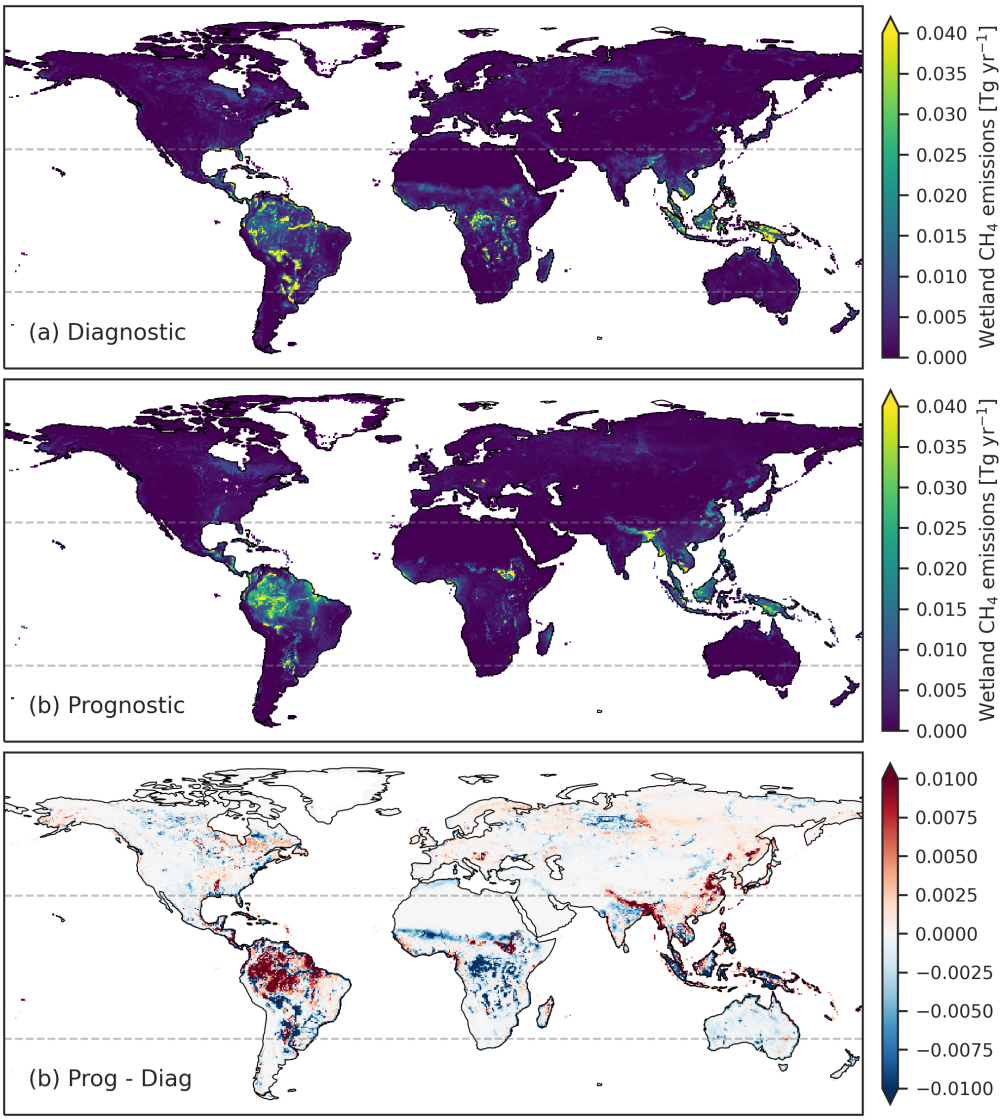

Figure 6.3: Mean annual wetland methane emissions per grid cell simulated by LPX-Bern on a 0.5° × 0.5° grid between 2000–2009 for (a) the diagnostic simulation, (b) the prognostic simulation, and (c) the difference between prognostic and diagnostic simulation. Dashed grey lines indicate 30° North and South.

Figure 6.3 shows the global emission distribution from the diagnostic and prognostic simulations averaged over 2000–2009. Both show the largest emissions in the tropics, however with differences in the regional distribution. In the Amazon basin, the prognostic run shows larger and more spatially-distributed emissions than the diagnostic run, reflecting larger predicted wetland areas than in the prescribed dataset (Fig. 6.3 (b)). Larger wetland emissions are also simulated in northern India, Bangladesh, Myanmar, and eastern China, where the large wetland areas predicted by the prognostic simulation correspond to areas of extensive rice cultivation

which are masked out in WAD2M. Emissions from tropical Africa are substantially smaller in the prognostic simulation due to the small predicted wetland area. There, LPX-Bern is known to underestimate wetland- and peatland area (see also chapter 5). Emissions from the prognostic run are also lower in South East Asia, except on small islands where WAD2M is not defined. These lower emissions in South East Asia are partly due to differences in the source type, with larger fractions of peatlands in the prognostic than diagnostic run.

Cumulative methane emissions from northern wetlands (>30° N) are very similar in the prognostic and diagnostic simulation (Fig. 6.2 (c) and table 6.1) but regional emission distributions differ slightly. The prognostic run shows larger emissions over northern East Asia, East Canada, and Alaska than the run with prescribed wetland area. These correspond to regions where LPX-Bern overestimates peatland area compared to literature estimates (see also chapter 3). Larger emissions are also simulated in Europe, especially in the Balkan region, possibly reflecting historic wetland drainage, which is neglected in the prognostic wetland prediction but implicit in the prescribed contemporary wetland dataset. With prognostic wetlands, fewer emissions are predicted for the Western Siberian Lowland (WSL) and parts of western Canada where less extensive wetlands and peatlands are simulated than suggested in WAD2M.

6.1.4 Conclusion

Taken together, the detailed analysis of the LPX-Bern contributions to Saunois et al. (2016) and Saunois et al. (2020) reveals that bottom-up and top-down estimates in these publications are treated inconsistently with respect to the global soil sink, at least in case of the LPX-Bern contribution. Comparing the diagnostic and prognostic simulations shows that, overall, dynamically simulating wetland area yields similar global-scale results as when wetland area is prescribed. However, locally methane emissions can differ greatly, especially in regions of poor prognostic wetland prediction, such as tropical Africa, and in regions with large anthropogenic disturbance.

6.2 Model inter-comparison of the future peat carbon response

Emerging role of northern peatlands in the future greenhouse gas balance

C. Qiu, P. Ciais, D. Zhu, B. Guenet, J. Chang, N. Chaudhary, T. Kleinen, X. Li, **J. Müller**, Y. Xi, W. Zhang, A. Ballantyne, S. C. Brewer, V. Brovkin, D. J. Charman, A. Gustafson, A. V. Gallego-Sala, T. Gasser, J. Holden, F. Joos, M. J. Kwon, R. Lauerwald, P. A. Miller, S. Peng, S. Page, B. Smith, B. D. Stocker, A. B. K. Sannel, E. Salmon, G. Schurgers, N. J. Shurpali, D. Wårlind, and S. Westermann

in preparation.

6.2.1 Introduction

As long-term carbon stores and important methane sources, peatlands contribute to short-term and long-term changes to the global energy budget. Quantifying the feedbacks between climate and peatlands thus is important for determining future climate trajectories and developing effective mitigation policies (Loisel et al., 2021). Different data-informed and modeling approaches have been used in the past to quantify potential responses of peatland soil respiration (e.g Ise et al., 2008), carbon accumulation (e.g Charman et al., 2015; Gallego-Sala et al., 2018; Chaudhary et al., 2020), water table dynamics (e.g Swindles et al., 2019), and methane emissions (e.g Ma et al., 2017) to past and future changes in temperature, atmospheric CO_2, and the moisture balance. However, uncertainties about the sign and magnitude of future peatland feedbacks are still large, with conflicting results about key factors such as carbon accumulation rates (e.g. Qiu et al., 2020; Müller & Joos, 2021) and the fate of permafrost peat carbon (e.g. Hugelius et al., 2020; Estop-Aragonés et al., 2018).

Studies using process-based models such as the LPX-Bern have to account for multiple sources of uncertainty from uncertainties in the calibration and input data to structural model uncertainty. To account for uncertainties in the climate forcing used for peatlands projections, some studies use input from multiple different climate scenarios or climate models (e.g. Qiu et al., 2020; Müller & Joos, 2021, see also chapter 4). Quantifying structural model uncertainty is typically harder and often relies on model inter-comparison projects, where multiple models with different process implementations are used for simulations following an identical simulation protocol. Such model inter-comparisons have been done for the modeling of historic and present-day wetland area and wetland methane emissions (e.g. Melton et al., 2013; Saunois et al., 2020, see also section 6.1), but have been so far absent for future projections of peatland carbon dynamics and concurrent methane emissions.

In Qiu et al. (2021), the authors present the first peatland model inter-comparison project investigating future peatland-climate feedbacks and quantifying structural uncertainty based on five state-of-the-art peatland and methane models, including the LPX-Bern. However, models are forced only with climate input from a single climate model and peatland area is assumed to be constant. Their focus lies on northern peatlands as most models only include parametrizations for boreal peatlands. They find that, when assuming a constant peatland area, northern peatlands will stay climate-neutral until 2300 under the strong mitigation scenario, RCP2.6. This is the result of a sustained carbon uptake which compensates for the effect of sustained moderate methane emissions. However, under the high emission scenario, RCP8.5, northern peatlands are projected to switch from carbon sinks to sources in the next 100–150 years, with strong concurrent increases in peatland methane emissions, leading to an estimated additional warming of 0.09–0.49 °C in 2300.

The results from Qiu et al. (2021) are partly in contrast to LPX-Bern results presented in Müller & Joos (2021, chapter 4,). Bern-LPX simulations with prognostic peatland area suggest a long-term net peat carbon loss to be likely even under the strong mitigation scenario SSP1-2.6. Potential reasons for these differences will be discussed in this chapter. Section 6.2.2 will give a quick overview of the different simulation setups of both studies and the methods used to calculate the results. In section 6.2.3, LPX-Bern results and the respective estimates for climate and model-structure-related uncertainties from both studies are compared, including unpublished simulated peatland methane emissions from simulations in Müller & Joos (2021).

6.2.2 Methods

Five peatland models participated in Qiu et al. (2021), including the LPX-Bern. The LPX-Bern simulations for both Qiu et al. (2021) and Müller & Joos (2021) were performed with the

LPX-Bern v1.4 (Lienert & Joos, 2018) using the peatland- and methane modules described in chapter 2. Note that here a different scaling factors for peatland methane emissions ($mt_p = 0.197$) was used compared to chapter 5. Simulations for Qiu et al. (2021) were performed with a $1^\circ \times 1^\circ$ model resolution and prescribed northern peatland area from PEATMAP (Xu et al., 2018), while simulations for Müller & Joos (2021) were performed with a courser resolution ($3.75^\circ \times 2.5^\circ$) and prognostically calculated peatland area.

In Qiu et al. (2021), all models were subject to the same simulation protocol and model forcing. Bias-corrected climate fields from the IPSL-CM5A-LR global circulation model contribution to ISIMIP2b (Frieler et al., 2017) were used as climate fields. Bias-correction was done with respect to the period 1979–2013. Models were spun up in an idealized fashion, with 10,000 years of repeated 1961–1990 climate and constant pre-industrial atmospheric CO_2 concentrations, followed by 100 years of repeated 1901–1920 climate. A historic simulation with transient forcing from 1861–2005 is then followed by two transient scenario simulations from 2006–2299 following the RCP2.6 and RCP8.5 scenarios extended to 2300.

The simulation setup in Müller & Joos (2021) is described in detail in chapter 4. Simulations were continued from a previously-published transient simulation with dynamic peatland area which started at the Last Glacial Maximum (Müller & Joos, 2020, chapter 3), allowing the consideration of the dynamic history of present-day and former peatlands. From 1975–2100 simulations with transient climate and land-use forcing were done using climate fields from 10 different CMIP6 models that were bias-corrected for the period 1960–1990. For 3 out of the 10 climate models, additional simulations were forced with transient climate forcing until 2300. The respective CMIP6 future scenarios SSP1-2.6 and SSP5-8.5 correspond roughly to the CMIP5 scenarios RCP2.6 and RCP8.5. The model ensemble for Müller & Joos (2021) included simulations forced with IPSL-CM6A-LR output, which is the next generation of the model used in Qiu et al. (2021).

In the following section, the integrated net carbon balance (NCB) of northern peatlands simulated by LPX-Bern in Qiu et al. (2021) and Müller & Joos (2021) is compared. Due to the dynamic area calculation in Müller & Joos (2021), NCB, in this case, was defined as the balance between the total accumulation of carbon into the catotelm of active peatlands and the total heterotrophic respiration of peat carbon in active and former peatlands. It thus represents the net change of the variable 'total peat carbon' as defined in chapter 3. The NCB calculated in this way depends among others on the amount of peat carbon left from former peatlands which vanished during the deglaciation.

6.2.3 Data comparison

The ensembles of Qiu et al. (2021) (further on referred to as QIU) and Müller & Joos (2021) (further on referred to as MJ) arrive at slightly different present-day (1975–1995) northern peatland states due to the differences in the simulation protocols. Mean peatland carbon storage is 572 GtC in QIU and 313 GtC in MJ and the prescribed and prognostically determined mean peatland areas are 3.2 Mkm^2 and 2.7 Mkm^2, respectively. While the total carbon storage in QIU varied drastically between peatland models (200–870 GtC), the respective LPX-Bern simulation is with 304 GtC comparable to the LPX-Bern simulations in MJ. The lower carbon storage despite the larger peatland area can be attributed to the idealized spinup procedure for QIU.

At present-day, simulations from all models in QIU show a net accumulation of peat carbon (mean 0.1 GtC yr^{-1}), while most LPX-Bern simulations in MJ show a very small peat carbon loss (mean –0.004 GtC yr^{-1}; Fig. 6.4). The negative NCB in MJ is a result of the additional consideration of legacy peat carbon that is left from former peatlands which have been buried during the deglaciation. Excluding legacy peat carbon that is older than 1975 from the NCB

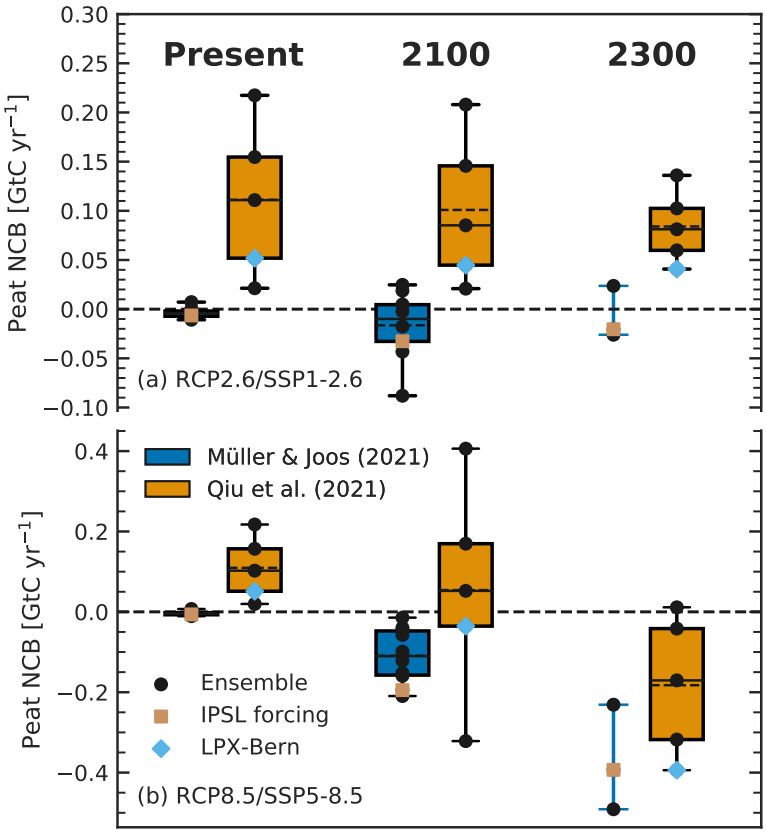

Figure 6.4: Uncertainty ranges of the annual peat carbon balance (NCB) north of 30° N for (a) RCP2.6/SSP1-2.6 and (b) RCP8.5/SSP5-8.5 in Qiu et al. (2021) (blue) and Müller & Joos (2021) (orange) averaged over 1979–2013 (present), 2091–2110, and 2281–2300. The ensemble from Qiu et al. (2021) consists of 5 different peatland models with prescribed peatland area and the ensemble from Müller & Joos (2021) consists of 10 LPX-Bern simulations forced with different climate anomalies. For the simulations from Qiu et al. (2021), transient RCP2.6 and RCP8.5 scenario climate forcing from the IPSL-CM5A-LR was used. For the simulations from Müller & Joos (2021), transient SSP1-2.6 and SSP5-8.5 scenario climate forcing from 10 different climate models were used until 2100 and from a sub-set of 3 climate models until 2300, including the IPSL-CM6A-LR. Boxes indicate the interquartile range, whiskers the total range, solid horizontal lines the median, and dashed horizontal lines the mean. For the simulations in Müller & Joos (2021) at 2300, only the range is shown (blue whiskers), due to the small ensemble size. Black markers show emissions from individual ensemble members, blue markers show LPX-Bern results in the ensemble from Qiu et al. (2021), and orange markers show the simulation forced with IPSL-CM6A-LR climate in the ensemble from Müller & Joos (2021).

calculation leads to a slightly positive mean NCB of 0.01 GtC yr^{-1} (Fig. 6.5) which is, however, still substantially smaller than simulated in QIU. The generally larger NCB in QIU compared to MJ is mostly the result of a substantially wetter climate forcing.

Although the precipitation forcings in both studies are bias-corrected towards monthly values of present-day observations, differences exist in the respective gridded data products that were used for bias correction. For MJ, the Climatic Research Unit (CRU) TS 3.1 climatology Harris et al. (2014) was used which is a global gridded observation data set. The climate forcing used in QIU was originally prepared for the Inter-Sectoral Impact Model Intercomparison Project (ISIMIP2b) (Frieler et al., 2017). Their bias correction was performed using the gridded WFDEI-GPCC dataset which is based on the ERA-Interim reanalysis product and is specifically designed as a meteorological forcing data set (Weedon et al., 2014). The monthly precipitation totals in WFDEI-GPCC itself are bias-corrected towards the Global Precipitation Climatology Centre (GPCC) gridded observational data, which is comparable to the CRU products but includes more measurement stations. However, mean annual precipitation over land above >30° N between 1979–2013 is about 50 mm larger in WFDEI-GPCC compared to both the CRU

and GPCC products. This offset in annual precipitation translates into similar offsets between the bias-corrected precipitation forcings used in QIU and MJ and contributes to the differences in the simulated NCB (Fig. 6.4).

The offset in NCB leads to differences in the integrated carbon stock changes, however, projected ensemble trends in NCB mostly agree between QIU and MJ, with mean NCB changing only slightly over time under the respective strong mitigation scenarios RCP2.6 and SSP1-2.6 (Fig. 6.4 (a)), whereas substantial decreases in NCB are projected for the respective large emission scenarios RCP8.5 and SSP5-8.5 with both studies suggesting net release of peat carbon until 2300 (Fig. 6.4 (b)).

Figure 6.4 shows that the uncertainty range for the simulated NCB in MJ, given by the spread between simulations forced with different climate anomalies, is small at present-day and increases as the different climate forcings diverge with time, corresponding to the results presented in chapter 4. In contrast, the uncertainty ranges in QIU, given by the spread between simulations with different peatland models show no specific time dependence and are large for all time periods. Comparing uncertainties between QIU and MJ suggests that uncertainties stemming from uncertain climate forcing are smaller than the structural uncertainties rooted in the model parametrizations, but increase with time and become comparable in size for projections beyond the end of the century.

Within the MJ ensemble, the simulation forced with IPSL-CM6A-LR climate anomalies is on the lower side of the simulated NBC range for all scenarios and periods (Fig. 6.4). Similarly, within the QIU ensemble, the simulation with LPX-Bern is on the lower end of the simulated NCB range. These results suggest that both ensemble estimates might be biased towards low NCB, as MJ and QIU exclusively rely on LPX-Bern and IPSL forcing respectively.

The two simulations from MJ and QIU which both are performed with the LPX-Bern and are forced with IPSL climate anomalies are the most suitable for direct comparison (blue and brown markers in figure 6.4). As the climate scenarios differ slightly between the studies with respect to the warming rates and maximum warming, figure 6.5 shows simulated annual NCB of both simulations with respect to the forced mean temperature anomaly. The simulations show similar features as the respective ensembles with a moisture-driven offset in present-day NCB between QIU and MJ and a slightly negative present-day NCB in the MJ simulation due to the deglacial legacy carbon.

The QIU simulation shows a larger interannual variability than the MJ simulation (Fig. 6.5). The smaller variability in MJ results from the slightly different NCB calculation which only considers fluxes in and out of the slow soil carbon pools and thus represents long-term changes in the peat carbon storage, whereas the calculation in QIU includes short-term fluctuations in vegetation and acrotelm carbon. The inter-annual variability of NCB in the QIU simulation increases with increased warming, driven by the increased variability in annual precipitation.

In the strong mitigation scenarios RCP2.6 and SSP1-2.6, surface air temperatures stabilize at about 2050 and slightly decrease afterward. Apart from the increase in interannual variability under warmer climates, the QIU simulation shows no clear trend in simulated NCB for this scenario (Fig. 6.5 (a)). The MJ simulation on the other hand shows NCB slightly decreasing with warming above about 2 °C, with sustained lower levels even after temperatures decrease again. This hysteresis behavior is linked to a permanent loss of northern peatland area in the MJ simulation which reaches about 0.6 Mkm^2 at 2100 and which does not recover even with decreasing temperatures. Part of this change is a response to climate and land-use change prior to 1975 as is discussed in chapter 4.

In the large emission scenarios RCP8.5 and SSP5-8.5, temperatures increase drastically until 2300 with faster and larger warming in the SSP5-8.5 scenario. Both the MJ and QIU simulations show strong decreases in simulated NCB with warming above about 4 °C, with both

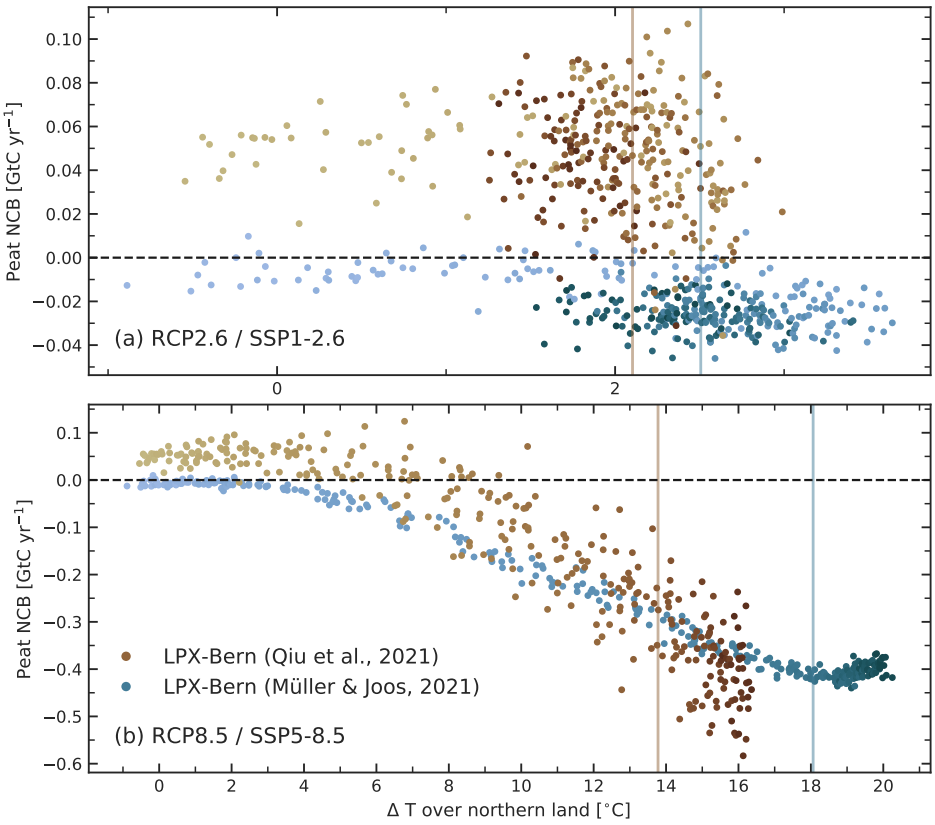

Figure 6.5: Annual peat carbon balance (NCB) north of 30° N with respect to the forced temperature anomaly over northern lands (>30° N) compared to 1975–1995 for (a) RCP2.6/SSP1-2.6 and (b) RCP8.5/SSP5-8.5 simulated by LPX-Bern with prescribed peatland area in Qiu et al. (2021) (brown) and with dynamic peatland area in Müller & Joos (2021) (blue). For the simulation from Qiu et al. (2021), transient RCP2.6 and RCP8.5 scenario climate forcing from the IPSL-CM5A-LR was used. For the simulation from Müller & Joos (2021), transient SSP1-2.6 and SSP5-8.5 scenario climate forcing from the IPSL-CM6A-LR was used. The darkness of the colors indicates the passage of time with darker colors representing later years. Vertical brown and blue lines indicate the temperature anomaly averaged over 2190–2210. Note the difference in x and y scales between (a) and (b).

simulations agreeing on a net loss of peat carbon after about 2100 (Fig. 6.5 (b)). The QIU simulation shows a stronger decrease towards the end of the simulation than MJ, potentially reflecting the additional loss of vegetation and acrotelm carbon under large warming. After 2200, warming in the SSP5-8.5 scenario slows down, leading to a stabilization of simulated NCB in the MJ simulation. With continued large carbon loss, NCB starts to get slightly more positive, approaching a new equilibrium. Warming in the RCP8.5 slows later than in SSP5-8.5 with simulated NCB only stabilizing after about 2270.

The net effect of peatlands on the radiative balance of the atmosphere includes peatland methane emissions which are also discussed in Qiu et al. (2021). They find peatland methane emissions to remain relatively stable under RCP2.6 and to substantially increases under RCP8.5. Qiu et al. (2021) used a spatial bias-correction to compare methane emissions between models, however, in the following, LPX-Bern results are presented prior to this bias-correction.

Figure 6.6 compares northern peatland methane emissions between the two QIU and MJ simulations that are both performed with the LPX-Bern and forced with IPSL climate. In the strong mitigation scenarios RCP2.6 and SSP1-2.6, both simulations show increased emissions with warming, however, with a stronger emission increase in the QIU simulation (Fig. 6.6 (a)). Methane emission increases due to increases in vegetation productivity and heterotrophic

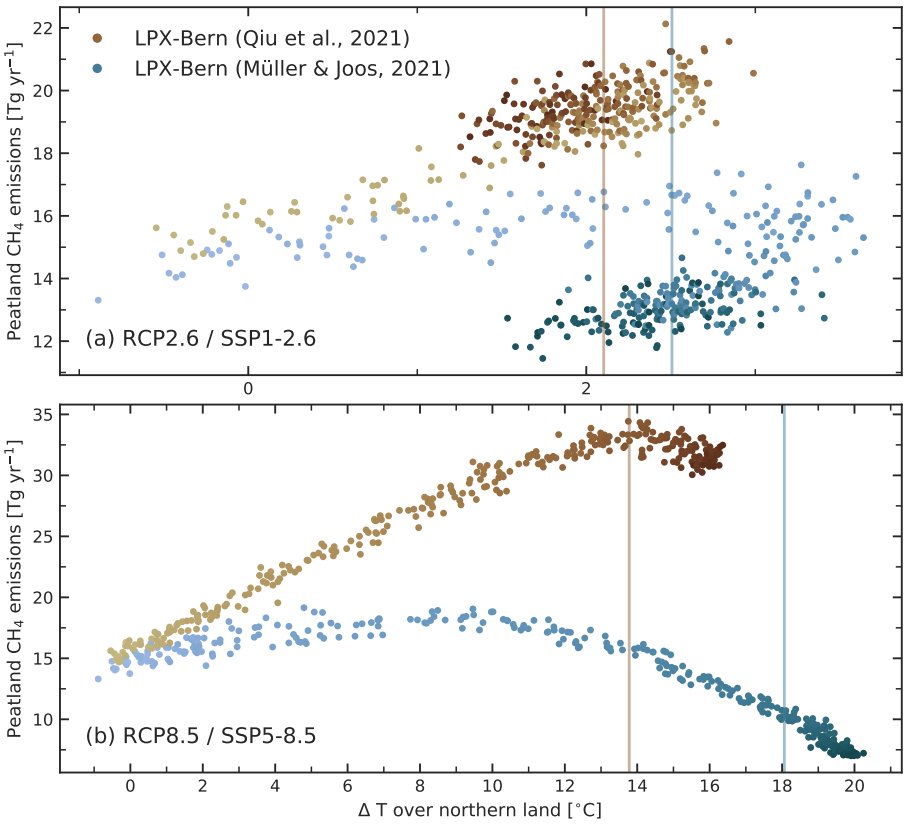

Figure 6.6: Same as figure 6.5 but for simulated annual methane emissions from northern peatlands (>30° N).

respiration are dampened in the MJ simulation due to peatland area losses. This persistent area loss also leads to a hysteresis behavior, similar to the one seen in the simulated NCB, resulting in emissions decreasing below present-day levels after 2050.

In the large emission scenarios RCP8.5 and SSP5-8.5, the MJ simulation shows increasing northern peatland methane emissions up to about 10 °C of warming, corresponding roughly to the end of the century in the SSP5-8.5 scenario. After that, the negative effect of the continued loss in peatland area and the increased drying dominate over any positive effects from increases in vegetation productivity and soil respiration, leading to a decline in peatland methane emissions. The QIU simulation on the other hand, due to the lack of peatland loss, shows strongly increasing peatland emissions up to a warming of about 14 °C corresponding to the year 2200 in the RCP8.5 scenario. The following decline is potentially driven by reduced substrate availability and continued drying. Qiu et al. (2021) speculate that nitrogen limitation of the peatland vegetation could be a limiting factor for the substrate availability, as only models with a dynamic nitrogen cycle, including the LPX-Bern, showed a decrease in peatland emissions after 2200.

6.2.4 Conclusion

Taken together, the comparison of the future projections from Qiu et al. (2021) and Müller & Joos (2021) revealed the dependence of the results on the treatment of peatland area, spinup procedure, and the choice of the bias-correction target for the climate forcing. Lower NCB and methane emissions are projected if peatland area is calculated dynamically, with large area losses predicted under future warming. Structural model uncertainty is the largest contributor to the uncertainty for simulated present-day NCB, with contributions from uncertain climate forcing becoming comparable in future projections.

Bibliography

Aalto, T., Tsuruta, A., Mäkelä, J., Müller, J., Tenkanen, M., Burke, E., Chadburn, S., Gao, Y., Kangasaho, V., Kleinen, T., Lee, H., Leppänen, A., Markkanen, T., Materia, S., Miller, P., Peano, D., Peltola, O., Raivonen, M., Saunois, M., Wårlind, D., & Zaehle, S., 2021. Air temperature and precipitation constraining the modelled wetland methane emissions in a boreal region in Northern Europe, *in preparation*.

Charman, D. J., Amesbury, M. J., Hinchliffe, W., Hughes, P. D., Mallon, G., Blake, W. H., Daley, T. J., Gallego-Sala, A. V., & Mauquoy, D., 2015. Drivers of Holocene peatland carbon accumulation across a climate gradient in northeastern North America, *Quat. Sci. Rev.*, 121, 110–119.

Chaudhary, N., Westermann, S., Lamba, S., Shurpali, N., Sannel, A. B. K., Schurgers, G., Miller, P. A., & Smith, B., 2020. Modelling past and future peatland carbon dynamics across the pan-Arctic, *Glob. Chang. Biol.*, 26(7), 4119–4133.

Estop-Aragonés, C., Cooper, M. D., Fisher, J. P., Thierry, A., Garnett, M. H., Charman, D. J., Murton, J. B., Phoenix, G. K., Treharne, R., Sanderson, N. K., Burn, C. R., Kokelj, S. V., Wolfe, S. A., Lewkowicz, A. G., Williams, M., & Hartley, I. P., 2018. Limited release of previously-frozen C and increased new peat formation after thaw in permafrost peatlands, *Soil Biol. Biochem.*, 118(August 2017), 115–129.

Frieler, K., Lange, S., Piontek, F., Reyer, C. P., Schewe, J., Warszawski, L., Zhao, F., Chini, L., Denvil, S., Emanuel, K., Geiger, T., Halladay, K., Hurtt, G., Mengel, M., Murakami, D., Ostberg, S., Popp, A., Riva, R., Stevanovic, M., SuzGBRi, T., Volkholz, J., Burke, E., Ciais, P., Ebi, K., Eddy, T. D., Elliott, J., Galbraith, E., Gosling, S. N., Hattermann, F., Hickler, T., Hinkel, J., Hof, C., Huber, V., Jägermeyr, J., Krysanova, V., Marcé, R., Müller Schmied, H., Mouratiadou, I., Pierson, D., Tittensor, D. P., Vautard, R., Van Vliet, M., Biber, M. F., Betts, R. A., Leon Bodirsky, B., Deryng, D., Frolking, S., Jones, C. D., Lotze, H. K., Lotze-Campen, H., Sahajpal, R., Thonicke, K., Tian, H., & Yamagata, Y., 2017. Assessing the impacts of 1.5Â°C global warming - Simulation protocol of the Inter-Sectoral Impact Model Intercomparison Project (ISIMIP2b), *Geosci. Model Dev.*, 10(12), 4321–4345.

Gallego-Sala, A. V., Charman, D. J., Brewer, S., Page, S. E., Colin Prentice, I., Friedlingstein, P., Moreton, S., Amesbury, M. J., Beilman, D. W., Bjamp, S., Blyakharchuk, T., Bochicchio, C., Booth, R. K., Bunbury, J., Camill, P., Carless, D., Chimner, R. A., Clifford, M., Cressey, E., Courtney-Mustaphi, C., Vleeschouwer, O., Jong, R., Fialkiewicz-Koziel, B., Finkelstein, S. A., Garneau, M., Githumbi, E., Hribjlan, J., Holmquist, J., M Hughes, P. D., Jones, C., Jones, M. C., Karofeld, E., Klein, E. S., Kokfelt, U., Korhola, A., Lacourse, T., Roux, G., Lamentowicz, M., Large, D., Lavoie, M., Loisel, J., Mackay, H., MacDonald, G. M., Makila, M., Magnan, G., Marchant, R., Marcisz, K., Martamp, A., Cortizas, N., Massa, C., Mathijssen, P., Mauquoy, D., Mighall, T., G Mitchell, F. J., Moss, P., Nichols, J., Oksanen, P. O., Orme, L., Packalen, M. S., Robinson, S., Roland, T. P., Sanderson, N. K., Britta Sannel, A. K., Steinberg, N., Swindles, G. T., Edward Turner, T., Uglow, J., Vamp, M., Bellen, S., Linden, M., Geel, B., Wang, G., Yu, Z., Zaragoza-Castells, J., & Zhao, Y., 2018. Latitudinal limits to the predicted increase of the peatland carbon sink with warming, *Nat. Clim. Chang.*, 8(October), 907–914.

Harris, I., Jones, P. D., Osborn, T. J., & Lister, D. H., 2014. Updated high-resolution grids of monthly climatic observations - the CRU TS3.10 Dataset, *Int. J. Climatol.*, 34(3), 623–642.

Hugelius, G., Loisel, J., Chadburn, S., Jackson, R. B., Jones, M., MacDonald, G., Marushchak, M., Olefeldt, D., Packalen, M., Siewert, M. B., Treat, C., Turetsky, M., Voigt, C., & Yu, Z., 2020. Large stocks of peatland carbon and nitrogen are vulnerable to permafrost thaw, *Proc. Natl. Acad. Sci. U. S. A.*, 117(34), 20438–20446.

Ise, T., Dunn, A. L., Wofsy, S. C., & Moorcroft, P. R., 2008. High sensitivity of peat decomposition to climate change through water-table feedback, *Nat. Geosci.*, 1(11), 763–766.

Joos, F., Spahni, R., D. Stocker, B., Lienert, S., Müller, J., Fischer, H., Schmitt, J., Colin Prentice, I., Otto-Bliesner, B., & Liu, Z., 2020. N2O changes from the Last Glacial Maximum to the preindustrial - Part 2: Terrestrial N2O emissions and carbon-nitrogen cycle interactions, *Biogeosciences*, 17(13), 3511–3543.

Kirschke, S., Bousquet, P., Ciais, P., Saunois, M., Canadell, J. G., Dlugokencky, E. J., Bergamaschi, P., Bergmann, D., Blake, D. R., Bruhwiler, L., Cameron-Smith, P., Castaldi, S., Chevallier, F., Feng, L., Fraser, A., Heimann, M., Hodson, E. L., Houweling, S., Josse, B., Fraser, P. J., Krummel, P. B., Lamarque, J.-F., Langenfelds, R. L., Le Quéré, C., Naik, V., O'Doherty, S., Palmer, P. I., Pison, I., Plummer, D., Poulter, B., Prinn, R. G., Rigby, M., Ringeval, B., Santini, M., Schmidt, M., Shindell, D. T., Simpson, I. J., Spahni, R., Steele, L. P., Strode, S. A., Sudo, K., Szopa, S., van der Werf, G. R., Voulgarakis, A., van Weele, M., Weiss, R. F., Williams, J. E., & Zeng, G., 2013. Three decades of global methane sources and sinks, *Nat. Geosci.*, 6(10), 813–823.

Lienert, S. & Joos, F., 2018. A Bayesian ensemble data assimilation to constrain model parameters and land-use carbon emissions, *Biogeosciences*, 15(9), 2909–2930.

Loisel, J., Gallego-Sala, A. V., Amesbury, M. J., Magnan, G., Anshari, G., Beilman, D. W., Benavides, J. C., Blewett, J., Camill, P., Charman, D. J., Chawchai, S., Hedgpeth, A., Kleinen, T., Korhola, A., Large, D., Mansilla, C. A., Müller, J., van Bellen, S., West, J. B., Yu, Z., Bubier, J. L., Garneau, M., Moore, T., Sannel, A. B., Page, S., Väliranta, M., Bechtold, M., Brovkin, V., Cole, L. E., Chanton, J. P., Christensen, T. R., Davies, M. A., De Vleeschouwer, F., Finkelstein, S. A., Frolking, S., Gałka, M., Gandois, L., Girkin, N., Harris, L. I., Heinemeyer, A., Hoyt, A. M., Jones, M. C., Joos, F., Juutinen, S., Kaiser, K., Lacourse, T., Lamentowicz, M., Larmola, T., Leifeld, J., Lohila, A., Milner, A. M., Minkkinen, K., Moss, P., Naafs, B. D., Nichols, J., O'Donnell, J., Payne, R., Philben, M., Piilo, S., Quillet, A., Ratnayake, A. S., Roland, T. P., Sjögersten, S., Sonnentag, O., Swindles, G. T., Swinnen, W., Talbot, J., Treat, C., Valach, A. C., & Wu, J., 2021. Expert assessment of future vulnerability of the global peatland carbon sink, *Nat. Clim. Chang.*, 11(1), 70–77.

Ma, S., Jiang, J., Huang, Y., Shi, Z., Wilson, R. M., Ricciuto, D., Sebestyen, S. D., Hanson, P. J., & Luo, Y., 2017. Data-Constrained Projections of Methane Fluxes in a Northern Minnesota Peatland in Response to Elevated CO 2 and Warming, *J. Geophys. Res. Biogeosciences*, 122(11), 2841–2861.

Melton, J. R., Wania, R., Hodson, E. L., Poulter, B., Ringeval, B., Spahni, R., Bohn, T., Avis, C. A., Beerling, D. J., Chen, G., Eliseev, A. V., Denisov, S. N., Hopcroft, P. O., Lettenmaier, D. P., Riley, W. J., Singarayer, J. S., Subin, Z. M., Tian, H., Zürcher, S., Brovkin, V., van Bodegom, P. M., Kleinen, T., Yu, Z. C., & Kaplan, J. O., 2013. Present state of global wetland extent and wetland methane modelling: conclusions from a model inter-comparison project (WETCHIMP), *Biogeosciences*, 10(2), 753–788.

Müller, J. & Joos, F., 2020. Global peatland area and carbon dynamics from the Last Glacial Maximum to the present - a process-based model investigation, *Biogeosciences*, 17(21), 5285–5308.

Müller, J. & Joos, F., 2021. Committed and projected future changes in global peatlands - continued transient model simulations since the Last Glacial Maximum, *Biogeosciences*, 18(12), 3657–3687.

Poulter, B., Bousquet, P., Canadell, J. G., Ciais, P., Peregon, A., Saunois, M., Arora, V. K., Beerling, D. J., Brovkin, V., Jones, C. D., Joos, F., Gedney, N., Ito, A., Kleinen, T., Koven, C. D., McDonald, K., Melton, J. R., Peng, C., Peng, S., Prigent, C., Schroeder, R., Riley, W. J., Saito, M., Spahni, R., Tian, H., Taylor, L., Viovy, N., Wilton, D., Wiltshire, A., Xu, X., Zhang, B., Zhang, Z., & Zhu, Q., 2017. Global wetland contribution to 2000-2012 atmospheric methane growth rate dynamics, *Environ. Res. Lett.*, 12(9), 094013.

Qiu, C., Zhu, D., Ciais, P., Guenet, B., & Peng, S., 2020. The role of northern peatlands in the global carbon cycle for the 21st century, *Glob. Ecol. Biogeogr.*, 29(5), 956–973.

Qiu, C., Ciais, P., Zhu, D., Guenet, B., Chang, J., Chaudhary, N., Kleinen, T., Li, X., Müller, J., Xi, Y., Zhang, W., Ballantyne, A., Brewer, S. C., Brovkin, V., Charman, D. J., Gustafson, A., Gallego-Sala, A. V., Gasser, T., Holden, J., Joos, F., Kwon, M. J., Lauerwal, R., & Westermann, S., 2021. Emerging role of northern peatlands in the future greenhouse gas balance, *in preparation*.

Saunois, M., Bousquet, P., Poulter, B., Peregon, A., Ciais, P., Canadell, J. G., Dlugokencky, E. J., Etiope, G., Bastviken, D., Houweling, S., Janssens-Maenhout, G., Tubiello, F. N., Castaldi, S., Jackson, R. B., Alexe, M., Arora, V. K., Beerling, D. J., Bergamaschi, P., Blake, D. R., Brailsford, G., Brovkin, V., Bruhwiler, L., Crevoisier, C., Crill, P., Covey, K., Curry, C., Frankenberg, C., Gedney, N., Höglund-Isaksson, L., Ishizawa, M., Ito, A., Joos, F., Kim, H. S., Kleinen, T., Krummel, P., Lamarque, J. F., Langenfelds, R., Locatelli, R., Machida, T., Maksyutov, S., McDonald, K. C., Marshall, J., Melton, J. R., Morino, I., Naik, V., O'Doherty, S., Parmentier, F. J. W., Patra, P. K., Peng, C., Peng, S., Peters, G. P., Pison, I., Prigent, C., Prinn, R., Ramonet, M., Riley, W. J., Saito, M., Santini, M., Schroeder, R., Simpson, I. J., Spahni, R., Steele, P., Takizawa, A., Thornton, B. F., Tian, H., Tohjima, Y., Viovy, N., Voulgarakis, A., Van Weele, M., Van Der Werf, G. R., Weiss, R., Wiedinmyer, C., Wilton, D. J., Wiltshire, A., Worthy, D., Wunch, D., Xu, X., Yoshida, Y., Zhang, B., Zhang, Z., & Zhu, Q., 2016. The global methane budget 2000-2012, *Earth Syst. Sci. Data*, 8(2), 697–751.

Saunois, M., Stavert, A. R., Poulter, B., Bousquet, P., Canadell, J. G., Jackson, R. B., Raymond, P. A., Dlugokencky, E. J., Houweling, S., Patra, P. K., Ciais, P., Arora, V. K., Bastviken, D., Bergamaschi, P., Blake, D. R., Brailsford, G., Bruhwiler, L., Carlson, K. M., Carrol, M., Castaldi, S., Chandra, N., Crevoisier, C., Crill, P. M., Covey, K., Curry, C. L., Etiope, G., Frankenberg, C., Gedney, N., Hegglin, M. I., Höglund-Isaksson, L., Hugelius, G., Ishizawa, M., Ito, A., Janssens-Maenhout, G., Jensen, K. M., Joos, F., Kleinen, T., Krummel, P. B., Langenfelds, R. L., Laruelle, G. G., Liu, L., Machida, T., Maksyutov, S., McDonald, K. C., McNorton, J., Miller, P. A., Melton, J. R., Morino, I., Müller, J., Murguia-Flores, F., Naik, V., Niwa, Y., Noce, S., O'Doherty, S., Parker, R. J., Peng, C., Peng, S., Peters, G. P., Prigent, C., Prinn, R., Ramonet, M., Regnier, P., Riley, W. J., Rosentreter, J. A., Segers, A., Simpson, I. J., Shi, H., Smith, S. J., Steele, L. P., Thornton, B. F., Tian, H., Tohjima, Y., Tubiello, F. N., Tsuruta, A., Viovy, N., Voulgarakis, A., Weber, T. S., van Weele, M., van der Werf, G. R., Weiss, R. F., Worthy, D., Wunch, D., Yin, Y., Yoshida, Y., Zhang, W., Zhang, Z., Zhao, Y., Zheng, B., Zhu, Q., Zhu, Q., & Zhuang, Q., 2020. The Global Methane Budget 2000-2017, *Earth Syst. Sci. Data*, 12(3), 1561–1623.

Spahni, R., Joos, F., Stocker, B. D., Steinacher, M., & Yu, Z. C., 2013. Transient simulations of the carbon and nitrogen dynamics in northern peatlands: From the Last Glacial Maximum to the 21st century, *Clim. Past*, 9(3), 1287–1308.

Stocker, B. D., Roth, R., Joos, F., Spahni, R., Steinacher, M., Zaehle, S., Bouwman, L., Xu-Ri, & Prentice, I. C., 2013. Multiple greenhouse-gas feedbacks from the land biosphere under future climate change scenarios, *Nat. Clim. Chang.*, 3(7), 666–672.

Swindles, G. T., Morris, P. J., Mullan, D. J., Payne, R. J., Roland, T. P., Amesbury, M. J., Lamentowicz, M., Turner, T. E., Gallego-Sala, A., Sim, T., Barr, I. D., Blaauw, M., Blundell, A., Chambers, F. M., Charman, D. J., Feurdean, A., Galloway, J. M., Gałka, M., Green, S. M., Kajukało, K., Karofeld, E., Korhola, A., Lamentowicz, Ł., Langdon, P., Marcisz, K., Mauquoy, D., Mazei, Y. A., McKeown, M. M., Mitchell, E. A. D., Novenko, E., Plunkett, G., Roe, H. M., Schoning, K., Sillasoo, Ü., Tsyganov, A. N., van der Linden, M., Väliranta, M., & Warner, B., 2019. Widespread drying of European peatlands in recent centuries, *Nat. Geosci.*, 12(11), 922–928.

Tarnocai, C., Swanson, D., Kimble, J., & Broll, G., 2007. Northern Circumpolar Soil Carbon Database, Digital Database, Research Branch, Agriculture and Agri-Food Canada, Ottawa, Canada, http://wms1.agr.gc.ca/NortherCircumpolar/ northercircumpolar.zip (last access: 12 April 2011).

Weedon, G. P., Balsamo, G., Bellouin, N., Gomes, S., Best, M. J., & Viterbo, P., 2014. The WFDEI meteorological forcing data set: WATCH Forcing Data methodology applied to ERA-Interim reanalysis data, *Water Resour. Res.*, 50(9), 7505–7514.

Xu, J., Morris, P. J., Liu, J., & Holden, J., 2018. PEATMAP: Refining estimates of global peatland distribution based on a meta-analysis, *CATENA*, 160(September 2017), 134–140.

Zhang, B., Tian, H., Lu, C., Chen, G., Pan, S., Anderson, C., & Poulter, B., 2017. Methane emissions from global wetlands: An assessment of the uncertainty associated with various wetland extent data sets, *Atmos. Environ.*, 165, 310–321.

Zhang, Z., Fluet-Chouinard, E., Jensen, K., McDonald, K., Hugelius, G., Gumbricht, T., Carroll, M., Prigent, C., Bartsch, A., & Poulter, B., 2021. Development of the global dataset of Wetland Area and Dynamics for Methane Modeling (WAD2M), *Earth Syst. Sci. Data*, 13(5), 2001–2023.

Chapter 7

Outlook

The research presented in this thesis provides the basis for many future research opportunities. This chapter will discuss some of the potential research avenues including possible future developments of the LPX-Bern model.

An ongoing research project, which will be continued beyond this thesis, concerns the improvement of the LPX-Bern wetland and methane module and the simulation of wetland methane emissions since the LGM. First results of that project are discussed in chapter 5. The described model adjustments concerning the alternative TOPMODEL formulation and the temperature dependence of the methane production will be further developed. The aim is to reduce the mismatch between simulated methane emissions and observational evidence. LPX-Bern simulates only a small change in emissions from LGM to pre-industrial, whereas the ice-core data (Schilt et al., 2010b) implies a near-doubling of emissions in light of a stable atmospheric sink (Levine et al., 2011; Murray et al., 2014). Additionally, all further model developments and investigations could be based on the new land-sea-ice mask discussed in the appendix.

As discussed in chapter 5, an additional TOPMODEL formulation should be tested, with a combination of thresholds limiting wetland area on rough or steep terrain, such as in the standard setup of the LPX-Bern (Stocker et al., 2014), and on flat or floodable terrain, such as described in chapter 5. Additionally, transiently updated mapping of the hydrological basins and the sub-grid topography of the available land fraction when using the new land-sea-ice mask could be used to calculate TOPMODEL parameters for each time step of the land-sea-ice mask, allowing for sea-level rise to exert a positive feedback on the coastal wetland area expansion as suggested in (Dommain et al., 2014). The wetland area from model versions with different thresholds and parameter settings should be validated against the new WAD2M wetland dataset (Zhang et al., 2021). Introducing an additional temperature dependence of the wetland methane production led to a fraction of tropical emissions that is too large compared to observations, as discussed in chapter 5. If this model-data mismatch persists with the updated wetland distribution, further adjustments of the additional temperature dependence would be needed. Potentially necessary adjustments could include wetland type or latitudinal-dependent parametrizations.

It may further be necessary to increase the sensitivity of the net primary productivity (NPP) to atmospheric CO_2 in LPX-Bern to simulate a near-doubling in wetland methane emissions from the LGM to the pre-industrial period. This sensitivity is known to be on the lower side of estimates Lienert & Joos (2018). A comparison of the simulated CO_2 fertilization effect to data from remote sensing (e.g. Zhu et al., 2016), and field experiments with artificially elevated CO_2 (e.g. Terrer et al., 2021), can reveal the extent of existing model biases and facilitate potential model adjustments.

The model developments addressing the temperature dependence of the wetland methane

production and the sensitivity of NPP to CO_2 and the use of the new land-sea-ice mask would require a re-calibration of the methane module similar as described in section 2.1.2.3. However, the calibration should rely on additional seasonal site data beyond the limited data used for calibration in section 2.1.2.3. New compilations of flux-tower (Knox et al., 2019) and chamber measurements (Calabrese et al., 2021) of wetland methane emissions allow for site-level calibration across different wetland types and latitudes, including the tropics.

Finally, after arriving at a model which qualitatively reproduces the deglacial ice-core records in transient simulations, a detailed analysis of the transient dynamics of wetland sources and their drivers could shed light on the glacial methane cycle. This analysis would contribute to the growing literature about this topic, where so far only results from timeslice simulations are published (e.g. Singarayer et al., 2011; Kleinen et al., 2020). A new generation of transient climate model simulations over the deglaciation from the fourth phase of the Paleoclimate Modelling Intercomparison Project (PMIP4) (Swinnen et al., 2019) provides new opportunities to investigate the deglacial dynamics not only of wetland methane emissions but also of peatland dynamics. For a long time, the TraCE21k climate forcing (Liu et al., 2009), which was used to force the LPX-Bern in chapters 3 to 5, was the only available transient and fully coupled global circulation model simulation over the deglaciation. The upcoming PMIP4 simulations would allow for LPX-Bern ensemble simulations that could enable transient uncertainty estimates based on the different climate anomalies and increase the robustness of our understanding of past wetland dynamics.

There are also opportunities to extend LPX-Bern simulations of wetlands and their methane emissions further back in time and investigate their dynamics on glacial-interglacial timescales. Transient climate output from the earth system model of intermediate complexity LOVECLIM (Timmermann & Friedrich, 2016) that spans the past 784 thousand years could be used to perform transient LPX-Bern wetland simulations. The resulting greenhouse gas budgets could be compared to the 800 thousand years covered by the Antarctic ice-core records (Lüthi et al., 2008; Loulergue et al., 2008; Schilt et al., 2010a), potentially yielding insights into the roles of wetlands in past glacial-interglacial cycles. Previous modeling studies have investigated wetland methane emissions (Singarayer et al., 2011) and peatland dynamics (Treat et al., 2019) on glacial-interglacial timescales but the described simulation would be the first-ever transient simulation of both wetland area dynamics and greenhouse gas budgets over the full length of the ice core record.

Another potential research project concerns future projections of peatlands and their methane emissions. Due to their character as large carbon stores and methane sources, the potential carbon cycle feedbacks of peatlands to future climate and land-use change have been a hot topic in recent years. Studies suggest both potential positive and negative future feedbacks depending on the future scenario (e.g. Warren et al., 2017; Gallego-Sala et al., 2018; Wang et al., 2018; Chaudhary et al., 2020; Qiu et al., 2020). The projections of peatland dynamics presented in chapter 4 and section 6.2 show that potential positive feedbacks between peatlands and the physical climate system, although small compared to the anthropogenic disturbance, can become substantial, especially on long timescales. However, there are, as far as I know, no studies that have investigated peatland feedbacks in a coupled peatland-climate setup, which would be crucial to fully quantify the effect of peatlands on future climate projections. This is mostly due to the lack of peatland representation in fully coupled earth system models (Loisel et al., 2021). The potential to couple the LPX-Bern to the ocean-circulation model Bern3D to form a fully coupled earth system model of intermediate complexity is a unique opportunity to explore the net radiative feedbacks of peatlands under different future scenarios. Due to the computational efficiency of the Bern3D-LPX, a wide range of sensitivity analyses for parameters such as the climate sensitivity could be performed. The analysis could further be extended to wetlands and wetland methane emissions in general.

Finally, there is a multitude of further model improvements concerning the LPX-Bern peatland and methane model that might be addressed in the future. A relatively simple addition to the methane module that would greatly increase its consistency in the paleo setting would be the implementation of atmospheric methane concentrations as model input to the soil diffusion routines, using yearly data products such as the one provided by Köhler et al. (2017). Furthermore, the further development of the parametrization for methane emissions from seasonal wetlands has a large potential to improve simulated wetland methane emissions. The existing simple implementation could be replaced with a more realistic one, including methane production, consumption, and transport, similar to the implementation for emissions from peatlands, and building on previous work in Ringeval et al. (2014). A long-term, but at some point likely necessary, model development would be the replacement of the two-layer (acrotelm and catotelm) peatland model in favor of a multi-layer peat representation with a freely variable water table. The two-layer peat model is unable to capture important internal feedbacks (Morris et al., 2011) whereas a multi-layer model, similar to Chaudhary et al. (2017) or Largeron et al. (2018), would not only allow for better representation of some of these feedbacks but also allow for the comparison of simulated accumulation histories and carbon isotopes to peat core data.

Additionally to the above-discussed research topics and model developments, I will continue to contribute to community projects, such as publications from the Past Global Changes (PAGES) working group C-PEAT (e.g. Loisel et al., 2021), international model intercomparison projects, such as the Global Methane Budget (Saunois et al., 2020), and in-house projects at U. Bern simulating the global carbon and nutrient cycles such as Joos et al. (2020).

Bibliography

Calabrese, S., Garcia, A., Wilmoth, J. L., Zhang, X., & Porporato, A., 2021. Critical inundation level for methane emissions from wetlands, *Environ. Res. Lett.*, 16(4), 044038.

Chaudhary, N., Miller, P. A., & Smith, B., 2017. Modelling past, present and future peatland carbon accumulation across the pan-Arctic region, *Biogeosciences*, 14(18), 4023–4044.

Chaudhary, N., Westermann, S., Lamba, S., Shurpali, N., Sannel, A. B. K., Schurgers, G., Miller, P. A., & Smith, B., 2020. Modelling past and future peatland carbon dynamics across the pan-Arctic, *Glob. Chang. Biol.*, 26(7), 4119–4133.

Dommain, R., Couwenberg, J., Glaser, P. H., Joosten, H., & Suryadiputra, I. N. N., 2014. Carbon storage and release in Indonesian peatlands since the last deglaciation, *Quat. Sci. Rev.*, 97, 1–32.

Gallego-Sala, A. V., Charman, D. J., Brewer, S., Page, S. E., Colin Prentice, I., Friedlingstein, P., Moreton, S., Amesbury, M. J., Beilman, D. W., Bjamp, S., Blyakharchuk, T., Bochicchio, C., Booth, R. K., Bunbury, J., Camill, P., Carless, D., Chimner, R. A., Clifford, M., Cressey, E., Courtney-Mustaphi, C., Vleeschouwer, O., Jong, R., Fialkiewicz-Koziel, B., Finkelstein, S. A., Garneau, M., Githumbi, E., Hribjlan, J., Holmquist, J., M Hughes, P. D., Jones, C., Jones, M. C., Karofeld, E., Klein, E. S., Kokfelt, U., Korhola, A., Lacourse, T., Roux, G., Lamentowicz, M., Large, D., Lavoie, M., Loisel, J., Mackay, H., MacDonald, G. M., Makila, M., Magnan, G., Marchant, R., Marcisz, K., Martamp, A., Cortizas, N., Massa, C., Mathijssen, P., Mauquoy, D., Mighall, T., G Mitchell, F. J., Moss, P., Nichols, J., Oksanen, P. O., Orme, L., Packalen, M. S., Robinson, S., Roland, T. P., Sanderson, N. K., Britta Sannel, A. K., Steinberg, N., Swindles, G. T., Edward Turner, T., Uglow, J., Vamp, M., Bellen, S., Linden, M., Geel, B., Wang, G., Yu, Z., Zaragoza-Castells, J., & Zhao, Y., 2018. Latitudinal limits to the predicted increase of the peatland carbon sink with warming, *Nat. Clim. Chang.*, 8(October), 907–914.

Joos, F., Spahni, R., D. Stocker, B., Lienert, S., Müller, J., Fischer, H., Schmitt, J., Colin Prentice, I., Otto-Bliesner, B., & Liu, Z., 2020. N2O changes from the Last Glacial Maximum to the preindustrial - Part 2: Terrestrial N2O emissions and carbon-nitrogen cycle interactions, *Biogeosciences*, 17(13), 3511–3543.

Kleinen, T., Mikolajewicz, U., & Brovkin, V., 2020. Terrestrial methane emissions from the Last Glacial Maximum to the preindustrial period, *Clim. Past*, 16(2), 575–595.

Knox, S. H., Jackson, R. B., Poulter, B., McNicol, G., Fluet-Chouinard, E., Zhang, Z., Hugelius, G., Bousquet, P., Canadell, J. G., Saunois, M., Papale, D., Chu, H., Keenan, T. F., Baldocchi, D., Torn, M. S., Mammarella, I., Trotta, C., Aurela, M., Bohrer, G., Campbell, D. I., Cescatti, A., Chamberlain, S., Chen, J., Chen, W., Dengel, S., Desai, A. R., Euskirchen, E., Friborg, T., Gasbarra, D., Goded, I., Goeckede, M., Heimann, M., Helbig, M., Hirano, T., Hollinger, D. Y., Iwata, H., Kang, M., Klatt, J., Krauss, K. W., Kutzbach, L., Lohila, A., Mitra, B., Morin, T. H., Nilsson, M. B., Niu, S., Noormets, A., Oechel, W. C., Peichl, M., Peltola, O., Reba, M. L., Richardson, A. D., Runkle, B. R., Ryu, Y., Sachs, T., Schäfer, K. V., Schmid, H. P., Shurpali, N., Sonnentag, O., Tang, A. C., Ueyama, M., Vargas, R., Vesala, T., Ward, E. J., Windham-Myers, L., Wohlfahrt, G., & Zona, D., 2019. FluXNET-CH4 synthesis activity objectives, observations, and future directions, *Bull. Am. Meteorol. Soc.*, 100(12), 2607–2632.

Köhler, P., Nehrbass-Ahles, C., Schmitt, J., Stocker, T. F., & Fischer, H., 2017. A 156 kyr smoothed history of the atmospheric greenhouse gases CO2, CH4, and N2O and their radiative forcing, *Earth Syst. Sci. Data*, 9(1), 363–387.

Largeron, C., Krinner, G., Ciais, P., & Brutel-Vuilmet, C., 2018. Implementing northern peatlands in a global land surface model: Description and evaluation in the ORCHIDEE high-latitude version model (ORC-HL-PEAT), *Geosci. Model Dev.*, 11(8), 3279–3297.

Levine, J. G., Wolff, E. W., Jones, A. E., Sime, L. C., Valdes, P. J., Archibald, A. T., Carver, G. D., Warwick, N. J., & Pyle, J. A., 2011. Reconciling the changes in atmospheric methane sources and sinks between the Last Glacial Maximum and the pre-industrial era, *Geophys. Res. Lett.*, 38(23), 2–7.

Lienert, S. & Joos, F., 2018. A Bayesian ensemble data assimilation to constrain model parameters and land-use carbon emissions, *Biogeosciences*, 15(9), 2909–2930.

Liu, Z., Otto-Bliesner, B. L., He, F., Brady, E. C., Tomas, R., Clark, P. U., Carlson, A. E., Lynch-Stieglitz, J., Curry, W., Brook, E., Erickson, D., Jacob, R., Kutzbach, J., & Cheng, J., 2009. Transient simulation of last deglaciation with a new mechanism for bolling-allerod warming, *Science*, 325(5938), 310–314.

Loisel, J., Gallego-Sala, A. V., Amesbury, M. J., Magnan, G., Anshari, G., Beilman, D. W., Benavides, J. C., Blewett, J., Camill, P., Charman, D. J., Chawchai, S., Hedgpeth, A., Kleinen, T., Korhola, A., Large, D., Mansilla, C. A., Müller, J., van Bellen, S., West, J. B., Yu, Z., Bubier, J. L., Garneau, M., Moore, T., Sannel, A. B., Page, S., Väliranta, M., Bechtold, M., Brovkin, V., Cole, L. E., Chanton, J. P., Christensen, T. R., Davies, M. A., De Vleeschouwer, F., Finkelstein, S. A., Frolking, S., Gałka, M., Gandois, L., Girkin, N., Harris, L. I., Heinemeyer, A., Hoyt, A. M., Jones, M. C., Joos, F., Juutinen, S., Kaiser, K., Lacourse, T., Lamentowicz, M., Larmola, T., Leifeld, J., Lohila, A., Milner, A. M., Minkkinen, K., Moss, P., Naafs, B. D., Nichols, J., O'Donnell, J., Payne, R., Philben, M., Piilo, S., Quillet, A., Ratnayake, A. S., Roland, T. P., Sjögersten, S., Sonnentag, O., Swindles, G. T., Swinnen, W., Talbot, J., Treat, C., Valach, A. C., & Wu, J., 2021. Expert assessment of future vulnerability of the global peatland carbon sink, *Nat. Clim. Chang.*, 11(1), 70–77.

Loulergue, L., Schilt, A., Spahni, R., Masson-Delmotte, V., Blunier, T., Lemieux, B., Barnola, J.-M., Raynaud, D., Stocker, T. F., & Chappellaz, J., 2008. Orbital and millennial-scale features of atmospheric CH4 over the past 800,000 years, *Nature*, 453(7193), 383–386.

Lüthi, D., Le Floch, M., Bereiter, B., Blunier, T., Barnola, J. M., Siegenthaler, U., Raynaud, D., Jouzel, J., Fischer, H., Kawamura, K., & Stocker, T. F., 2008. High-resolution carbon dioxide concentration record 650,000-800,000 years before present, *Nature*, 453(7193), 379–382.

Morris, P. J., Waddington, J. M., Benscoter, B. W., & Turetsky, M. R., 2011. Conceptual frameworks in peatland ecohydrology: looking beyond the two-layered (acrotelm-catotelm) model, *Ecohydrology*, 4(1), 1–11.

Murray, L. T., Mickley, L. J., Kaplan, J. O., Sofen, E. D., Pfeiffer, M., & Alexander, B., 2014. Factors controlling variability in the oxidative capacity of the troposphere since the Last Glacial Maximum, *Atmos. Chem. Phys.*, 14(7), 3589–3622.

Qiu, C., Zhu, D., Ciais, P., Guenet, B., & Peng, S., 2020. The role of northern peatlands in the global carbon cycle for the 21st century, *Glob. Ecol. Biogeogr.*, 29(5), 956–973.

Ringeval, B., Houweling, S., Van Bodegom, P. M., Spahni, R., Van Beek, R., Joos, F., & Röckmann, T., 2014. Methane emissions from floodplains in the Amazon Basin: Challenges in developing a process-based model for global applications, *Biogeosciences*, 11(6), 1519–1558.

Saunois, M., Stavert, A. R., Poulter, B., Bousquet, P., Canadell, J. G., Jackson, R. B., Raymond, P. A., Dlugokencky, E. J., Houweling, S., Patra, P. K., Ciais, P., Arora, V. K., Bastviken, D., Bergamaschi, P., Blake, D. R., Brailsford, G., Bruhwiler, L., Carlson, K. M., Carrol, M., Castaldi, S., Chandra, N., Crevoisier, C., Crill, P. M., Covey, K., Curry, C. L., Etiope, G., Frankenberg, C., Gedney, N., Hegglin, M. I., Höglund-Isaksson, L., Hugelius, G., Ishizawa, M., Ito, A., Janssens-Maenhout, G., Jensen, K. M., Joos, F., Kleinen, T., Krummel, P. B., Langenfelds, R. L., Laruelle, G. G., Liu, L., Machida, T., Maksyutov, S., McDonald, K. C., McNorton, J., Miller, P. A., Melton, J. R., Morino, I., Müller, J., Murguia-Flores, F., Naik, V., Niwa, Y., Noce, S., O'Doherty, S., Parker, R. J., Peng, C., Peng, S., Peters, G. P., Prigent, C., Prinn, R., Ramonet, M., Regnier, P., Riley, W. J., Rosentreter, J. A., Segers, A., Simpson, I. J., Shi, H., Smith, S. J., Steele, L. P., Thornton, B. F., Tian, H., Tohjima, Y., Tubiello, F. N., Tsuruta, A., Viovy, N., Voulgarakis, A., Weber, T. S., van Weele, M., van der Werf, G. R., Weiss, R. F., Worthy, D., Wunch, D., Yin, Y., Yoshida, Y., Zhang, W., Zhang, Z., Zhao, Y., Zheng, B., Zhu, Q., Zhu, Q., & Zhuang, Q., 2020. The Global Methane Budget 2000-2017, *Earth Syst. Sci. Data*, 12(3), 1561–1623.

Schilt, A., Baumgartner, M., Blunier, T., Schwander, J., Spahni, R., Fischer, H., & Stocker, T. F., 2010a. Glacial-interglacial and millennial-scale variations in the atmospheric nitrous oxide concentration during the last 800,000 years, *Quat. Sci. Rev.*, 29(1-2), 182–192.

Schilt, A., Baumgartner, M., Schwander, J., Buiron, D., Capron, E., Chappellaz, J., Loulergue, L., Schüpbach, S., Spahni, R., Fischer, H., & Stocker, T. F., 2010b. Atmospheric nitrous oxide during the last 140,000 years, *Earth Planet. Sci. Lett.*, 300(1-2), 33–43.

Singarayer, J. S., Valdes, P. J., Friedlingstein, P., Nelson, S., & Beerling, D. J., 2011. Late Holocene methane rise caused by orbitally controlled increase in tropical sources, *Nature*, 470(7332), 82–85.

Stocker, B. D., Spahni, R., & Joos, F., 2014. DYPTOP: A cost-efficient TOPMODEL implementation to simulate sub-grid spatio-temporal dynamics of global wetlands and peatlands, *Geosci. Model Dev.*, 7(6), 3089–3110.

Swinnen, W., Broothaerts, N., & Verstraeten, G., 2019. Modelling long-term blanket peatland development in eastern Scotland, *Biogeosciences*, 16(20), 3977–3996.

Terrer, C., Phillips, R. P., Hungate, B. A., Rosende, J., Pett-Ridge, J., Craig, M. E., van Groenigen, K. J., Keenan, T. F., Sulman, B. N., Stocker, B. D., Reich, P. B., Pellegrini, A. F., Pendall, E., Zhang, H., Evans, R. D., Carrillo, Y., Fisher, J. B., Van Sundert, K., Vicca, S., & Jackson, R. B., 2021. A trade-off between plant and soil carbon storage under elevated CO2, *Nature*, 591(7851), 599–603.

Timmermann, A. & Friedrich, T., 2016. Late Pleistocene climate drivers of early human migration, *Nature*, 538(7623), 92–95.

Treat, C. C., Kleinen, T., Broothaerts, N., Dalton, A. S., Dommain, R., Douglas, T. A., Drexler, J. Z., Finkelstein, S. A., Grosse, G., Hope, G., Hutchings, J., Jones, M. C., Kuhry, P., Lacourse, T., Lähteenoja, O., Loisel, J., Notebaert, B., Payne, R. J., Peteet, D. M., Sannel, A. B. K., Stelling, J. M., Strauss, J., Swindles, G. T., Talbot, J., Tarnocai, C., Verstraeten, G., Williams, C. J., Xia, Z., Yu, Z., Väliranta, M., Hättestrand, M., Alexanderson, H., & Brovkin, V., 2019. Widespread global peatland establishment and persistence over the last 130,000 y, *Proc. Natl. Acad. Sci.*, 116(11), 201813305.

Wang, S., Zhuang, Q., Lähteenoja, O., Draper, F. C., & Cadillo-Quiroz, H., 2018. Potential shift from a carbon sink to a source in Amazonian peatlands under a changing climate, *Proc. Natl. Acad. Sci.*, 115(49), 12407–12412.

Warren, M., Frolking, S., Dai, Z., & Kurnianto, S., 2017. Impacts of land use, restoration, and climate change on tropical peat carbon stocks in the twenty-first century: implications for climate mitigation, *Mitig. Adapt. Strateg. Glob. Chang.*, 22(7), 1041–1061.

Zhang, Z., Fluet-Chouinard, E., Jensen, K., McDonald, K., Hugelius, G., Gumbricht, T., Carroll, M., Prigent, C., Bartsch, A., & Poulter, B., 2021. Development of the global dataset of Wetland Area and Dynamics for Methane Modeling (WAD2M), *Earth Syst. Sci. Data*, 13(5), 2001–2023.

Zhu, Z., Piao, S., Myneni, R. B., Huang, M., Zeng, Z., Canadell, J. G., Ciais, P., Sitch, S., Friedlingstein, P., Arneth, A., Cao, C., Cheng, L., Kato, E., Koven, C., Li, Y., Lian, X., Liu, Y., Liu, R., Mao, J., Pan, Y., Peng, S., Peuelas, J., Poulter, B., Pugh, T. A., Stocker, B. D., Viovy, N., Wang, X., Wang, Y., Xiao, Z., Yang, H., Zaehle, S., & Zeng, N., 2016. Greening of the Earth and its drivers, *Nat. Clim. Chang.*, 6(8), 791–795.

Appendix A

Implementation of a new land-sea-ice mask

A.1 Motivation

For paleo simulations, the LPX-Bern uses a transient land-sea-ice mask with a grid resolution of 3.75° longitudinal and 2.5° latitudinal. The currently used land-sea-ice mask (Fig. A.1 (a)) is built on the ICE-5G ice-sheet and sea-level reconstruction and spans 21–0 kyrs BP (Peltier, 2004). During a transient simulation, the LPX-Bern grid is updated every 1000 years and is linearly interpolated between updates, with grid cells gradually flooding or emerging. The current implementation only allows for binary land fractions of 0 or 1, with smaller land fractions only occurring during the interpolated transition from one state to the other. Especially on the coasts and in regions dominated by islands such as South East Asia, this leads to an unrealistic distribution of the landmass and potentially to unrealistic rates of land emergence or flooding. In the chapters 3 and 5, the deglacial evolution of wetlands and their methane emissions were shown to depend greatly on the extent of the continental shelf areas and ice sheets and the timing and rate of their change. A more realistic representation of the grid-cell land fraction and its temporal dynamics could thus greatly benefit future investigations of wetland and wetland methane dynamics in the past.

Based on these considerations, a new land-sea-ice mask was prepared to be used as input for the LPX-Bern (Fig. A.1 (b)). In section A.2, the preparation of the new transient land-sea-ice mask is discussed, which is based on ICE-6G-C, an updated ice-sheet and sea-level reconstruction (Argus et al., 2014; Peltier et al., 2015). The new implementation allows for a reduced timestep and land fractions smaller than 1 on coastal as well as inland grid cells. Section A.2 then gives an overview of the necessary code changes for the implementation of the new input into the LPX-Bern. Finally, in section A.4, the new and the old land-sea-ice mask are compared.

A.2 Preparation

The basis for the new transient land-sea-ice mask is the ICE-6G-C global ice-sheet and sea-level reconstruction presented in Argus et al. (2014) and Peltier et al. (2015). The reconstructions have a timestep of 1000 years between 26–21 kyrs BP and a timestep of 500 years between 21 kyrs BP and the present. Its spatial resolution is $1° \times 1°$, except for the reconstructions at 21 kyrs BP and 0 kyrs BP which are available with a 10-minute spatial resolution.

The original files were preprocessed by Sebastian Lienert, including the linearly interpolation of the land-sea-ice mask onto a 500-year temporal resolution between 26–21 kyrs BP, a conservative spatial regridding to the LPX-Bern paleo model grid with a 3.75° longitudinal and 2.5° latitudinal resolution, and the calculation of the available land fraction, corresponding to land that is not

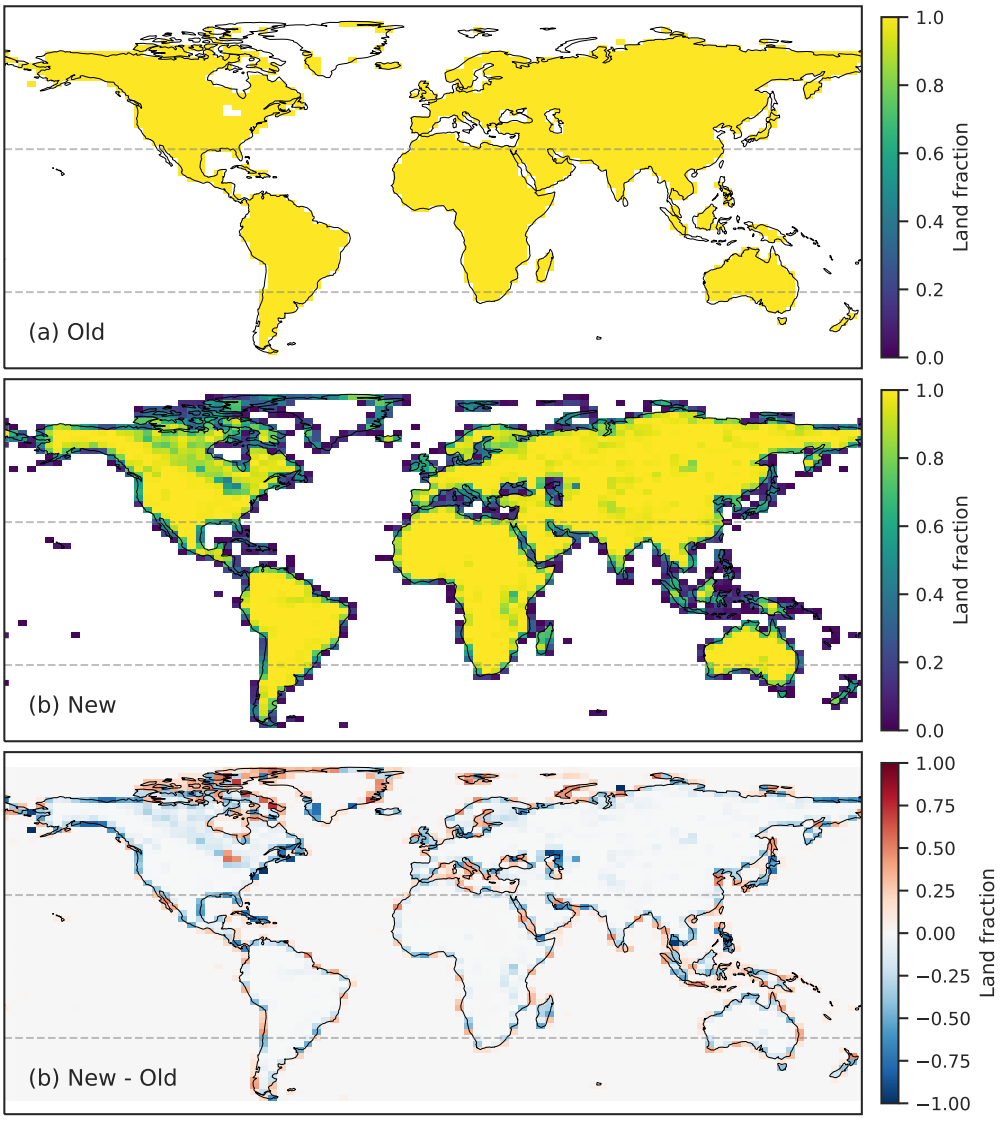

Figure A.1: Present-day land fraction for the 2.5° × 3.75° grid resolution according to the (a) old and (b) new land-sea-ice mask. The difference between new and old mask is shown in (c). Dashed grey lines indicate 30° North and South.

covered by ice or ocean. The spatial regridding results in grid-cell land fractions smaller than 1 along the coasts and ice-sheet borders.

The resulting transient land-sea-ice mask was then combined with information about the present-day inland water distribution to account for variable grid-cell land fractions beyond the coast and ice-sheet borders. First, coast and border cells were identified as grid cells with land fractions smaller than 1 and inland cells as grid cells with land fractions equal to 1 for all timesteps. The present-day inland land fractions were taken from the Land-Use Harmonization (LUH2) project (Hurtt et al., 2020), which in turn uses data from the History Database of the Global Environment (HYDE version 3.2; Goldewijk et al., 2017). The same land fraction data is also used in the present-day land-sea-ice masks for LPX-Bern simulations on higher resolution grids (0.5° × 0.5° or 1° × 1°). Inland land fractions were then regridded from their original 0.25° × 0.25° grid to the target 3.75° × 2.5° resolution and combined with the information about present-day coastal and border land fractions from ICE-6G-C.

To extend the information about inland land fractions back in time, the land fraction for

present-day inland cells was treated as an upper limit for all other timesteps. In this case, the land fraction of a grid cell that emerges from under a retreating ice sheet would be limited to its present-day value. The underlying assumption is that the distribution of inland waters did not change drastically throughout the deglaciation, which, however, does not hold true everywhere. Examples are the large glacial river and lake systems in North America fed by the large meltwater discharge during ice-sheet retreat, which have receded since (Byun et al., 2021) or the wet and dry periods in tropical Africa leading to a temporary greening and wettening of the Sahara and to the temporary drying of large inland lakes (Gasse, 2000). In these cases, land fractions of inland grid cells could be underestimated or overestimated. For grid cells covered by oceans at present-day, the land fraction is not limited for previous timesteps as no inland water estimates exist. In these cases, land fractions could be overestimated in the past.

In a last step, land fractions below 0.01 are set to 0, masking grid cells that only represent small islands or coast fragments to reduce the computational cost. For a transient simulation from 26–0 kyrs BP, this reduces the number of simulated grid cells from 2467 to 2370, which is still a substantial increase compared to the 1831 grid cells simulated using the old land-sea-ice mask.

A.3 Implementation

The LPX-Bern model code differentiates between different spatial resolutions and the respective internal treatment of the land-sea-ice mask input. Transient changes to the simulated land area for paleo simulations are so far only implemented for the $3.75° \times 2.5°$ resolution, for which up to now the old land-sea-ice mask, with a binary land fraction (0 or 1) was used. The largest model code changes thus concern the switch from a binary land fraction input that can either be 0 or 1 to a variable land fraction that ranges between 0–1. The new implementation of the input processing mostly followed the implementation for the model configurations with higher spatial resolution ($0.5° \times 0.5°$ or $1° \times 1°$), which already use a land-sea-ice mask with variable land fractions. However, some additional code changes were necessary to allow for a variable land area and consistent wetland prediction.

In paleo simulations, during the interpolation from one timestep of the land-sea-ice mask to the next, a special land class has been used to represent land that is buried under an ice sheet or flooded by ocean. A given grid cell would gradually transition from fully covered by ice or ocean to fully covered by land or vice versa, with carbon and nutrient pools being transferred to or from the buried land class to conserve the grid-cell carbon and nutrient pools. For the new land-sea-ice mask, the buried land class is now also used outside of the interpolation and covers, at any time, the grid-cell fraction that is not covered by available land. This allows for a consistent treatment and a closed carbon and nutrient budget for the transitions and interpolations between different variable land fractions that might occur multiple times in one cell over the full glaciation. The extended use of the buried land class necessitated its explicit exclusion from calculations elsewhere in the model code. The calculation of the mean grid-cell water table for example, which is used in wetland prediction (see section 2.1.1 or Stocker et al. (2014)), previously averaged surface runoff and water table over all land classes, but now explicitly excludes the buried grid-cell fraction.

Another code adjustment concerning the dynamic wetland prediction had to be made due to the treatment of the sub-grid topography in the TOPMODEL approach described in section 2.1.1 and Stocker et al. (2014). The sub-grid topography of the whole grid cell is used to establish a relationship between the mean grid-cell water table and the flooded grid-cell fraction. In the case of cells with a small grid-cell land fraction, this often leads to predicted wetland fractions that cover all available land, while the sub-grid topography that corresponds to the predicted wetland

area might actually be covered by the ocean or inland open waters. To produce more realistic predicted wetland areas, especially along the coasts, the flooded grid-cell fraction determined by the TOPMODEL approach is now interpreted and treated as the flooded land fraction instead. However, this should only be a temporary solution. A more robust and consistent way of treating this issue would be to use a higher resolution ($1^\circ \times 1^\circ$) version of the transient land-sea-ice mask, which could be constructed in the same way as described in section A.2, to map the parts of the sub-grid topography which should be used in the TOPMODEL calculation of the respective cell of the coarser grid. This would entail calculating separate TOPMODEL parameter sets for each timestep of the land-sea-ice mask which could be combined with a transient basin mapping as mentioned in section 5.5.

The timestep between the land-sea-ice mask updates was previously hardcoded to 1000 years. The respective implementation was now adapted to allow for a variable timestep, which can be provided as a parameter. This also extends to the transition routine which now is capable of linearly interpolating on a variable timestep between different land fractions. This allows for large flexibility in case of future changes to the land-sea-ice mask input, allowing to change the update timestep with only one parameter and for the use of binary as well as variable land fractions without code changes. Indeed, backward compatibility to the old land-sea-ice mask is guaranteed by an optional compiler flag named '_old_lpjgr', which only affects the input read-in and timestep setting.

One drawback of the new land-sea-ice mask is the larger computational cost due to the 29 % increase in simulated grid cells. However, due to the scalable parallelization capabilities of LPX-Bern, the increase in computation time can be partly mitigated if enough resources are available. For longer simulations over multiple glacial-interglacial cycles, the lower threshold on the land fraction (see section A.2) could be increased, further lowering the number of simulated cells. In this case, however, some means would need to be found to project the transient land-sea-ice mask further back in time.

Due to the changes to the available land area and the related direct and indirect effects on the wetland prediction, the respective LPX-Bern wetland and wetland methane modules might need to be recalibrated based on the new land-sea-ice mask before it is used for the investigation of wetland and methane dynamics.

A.4 Comparison

Figure A.1 shows a comparison of the present-day land area in the old and the new land-sea-ice mask. The largest difference can be found at the coasts and surrounding large islands, with a more realistic land distribution in the new mask due to the variable land fractions (Fig. A.1 (c)). The new mask additionally includes grid cells covering small islands and archipelagos which are not represented in the old mask due to their small overall land fraction, such as in South East Asia (Fig. A.1 (b)). Large differences also emerge due to the inclusion of inland waters into the new mask, especially in northern North America, northern Europe, and central Africa where large inland waters reduce the available land fraction.

These differences in coastal and inland land fractions lead to a small (4 %) net reduction in the overall available land area at present-day compared to the old land-sea-ice mask. Figure A.2 shows that the available land area in the new mask is globally smaller over all timesteps. Apart from the higher temporal resolution, the new mask shows various other differences in the transient evolution of the available land area. Globally a qualitative difference can be seen in the land area after the mid-Holocene, where the old mask shows a short rapid increase in land area after 8 kyrs BP while the new land mask suggests a gradual increase over the remaining

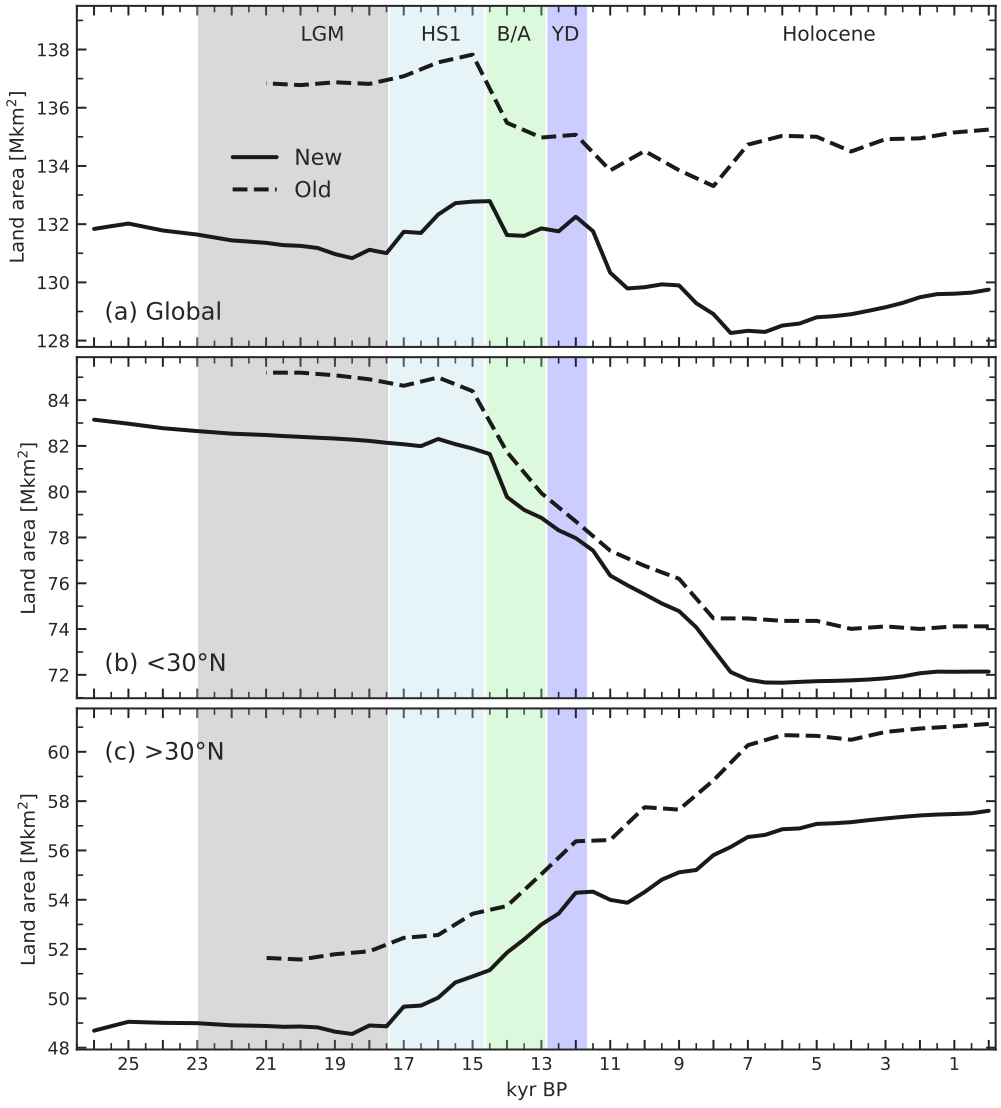

Figure A.2: Transient evolution of the (a) global, (b) >30° N, and <30° N land area according to the old (dashed lines) and new (solid lines) land-sea-ice mask. Background shading indicates the Last Glacial Maximum (LGM) period, the Heinrich Stadial 1 (HS1) Northern Hemisphere cold phase, the Bølling-Allerød (BA) Northern Hemisphere warm phase, and the Younger Dryas (YD) Northern Hemisphere cold phase.

Holocene (Fig. A.2 (a)). This difference could stem from the better representation of the Arctic circle (Fig. A.1 (c)) and the gradual isotopic rebound effect.

Other differences can be seen in the timing of the land loss in the tropics due to sea-level rise, which in the new mask is shifted by about 500 years so that land loss starts and ends later compared to the old mask (Fig. A.2 (b)). A similar temporal shift in the timing of the land emergence due to glacial retreat on the northern hemisphere can be seen during the Holocene, whereas during the termination, the available landmass north of 30° N increases faster in the new mask compared to the old mask (Fig. A.2 (c)).

Future fully transient simulations from the Last Glacial Maximum to the present will reveal how these changes in available land area influence model results.

Bibliography

Argus, D. F., Peltier, W. R., Drummond, R., & Moore, A. W., 2014. The Antarctica component of postglacial rebound model ICE-6G_C (VM5a) based on GPS positioning, exposure age dating of ice thicknesses, and relative sea level histories, *Geophys. J. Int.*, 198(1), 537–563.

Byun, E., Sato, H., Cowling, S. A., & Finkelstein, S. A., 2021. Extensive wetland development in mid-latitude North America during the Bølling-Allerød, *Nat. Geosci.*, 14(1), 30–35.

Gasse, F., 2000. Hydrological changes in the African tropics since the Last Glacial Maximum, *Quat. Sci. Rev.*, 19(1-5), 189–211.

Goldewijk, K. K., Beusen, A., Doelman, J., & Stehfest, E., 2017. Anthropogenic land use estimates for the Holocene - HYDE 3.2, *Earth Syst. Sci. Data*, 9(2), 927–953.

Hurtt, G. C., Chini, L., Sahajpal, R., Frolking, S., Bodirsky, B. L., Calvin, K., Doelman, J. C., Fisk, J., Fujimori, S., Klein Goldewijk, K., Hasegawa, T., Havlik, P., Heinimann, A., Humpenöder, F., Jungclaus, J., Kaplan, J. O., Kennedy, J., Krisztin, T., Lawrence, D., Lawrence, P., Ma, L., Mertz, O., Pongratz, J., Popp, A., Poulter, B., Riahi, K., Shevliakova, E., Stehfest, E., Thornton, P., Tubiello, F. N., van Vuuren, D. P., & Zhang, X., 2020. Harmonization of global land use change and management for the period 850-2100 (LUH2) for CMIP6, *Geosci. Model Dev.*, 13(11), 5425–5464.

Peltier, W., 2004. Global glacial isostasy and the surface of the ice-age eart: The ICE-5G (VM2) Model and GRACE, *Annu. Rev. Earth Planet. Sci.*, 32(1), 111–149.

Peltier, W. R., Argus, D. F., & Drummond, R., 2015. Space geodesy constrains ice age terminal deglaciation: The global ICE-6G_C (VM5a) model, *J. Geophys. Res. Solid Earth*, 120(1), 450–487.

Stocker, B. D., Spahni, R., & Joos, F., 2014. DYPTOP: A cost-efficient TOPMODEL implementation to simulate sub-grid spatio-temporal dynamics of global wetlands and peatlands, *Geosci. Model Dev.*, 7(6), 3089–3110.

Acknowledgements

This work would not have been possible without the people around me supporting and believing in me. The whole KUP has provided me with an incredible working environment and many joyful memories to keep. Special thanks goes to...

...Fortunat Joos for giving me this great opportunity to learn and grow, for the best possible guidance and for always encouraging me with calm and trusting optimism.

...Thomas Stocker for chairing my defense and Hubertus Fischer for agreeing to become my co-supervisor and answering all my naive modeler questions about ice cores.

...Thomas Kleinen agreeing to be my external referee and reviewer of my papers, for taking his time to visit Bern, and for the great scientific and collegial exchange on conferences and workshops.

...Angela Gallego-Sala and Julie Loisel for supporting me from early on and giving me the opportunity to be part of the international C-PEAT community.

...Sebastian for introducing me to the LPX-Bern and teaching me about all its nooks and crannies and for being a great office mate.

...Aurich, Sebastian, and Frerk for proofreading chapters of this thesis.

...Gunnar and Réne for always helping me with my small and large computer troubles.

...Aurich for being the social engine of the KUP and organizing the best social events from Finnish dinners to Dutch culture evenings.

...Doris, Claudia, and Bettina for guiding me through the jungle of Swiss bureaucracy and always taking time to help.

...Gianna, Aurich, Sebastian, Jeemijn, Mathias, Angélique, Michael, Gunnar, Woon Me, Cevi, and many more for not only being amazing colleagues but also for the friendship outside of KUP which allowed me to feel so at home in Bern.

...Cevi, Gianna, Michael, Aurich, Mathias, and more for believing in a better world and demanding it on the streets with me.

...the whole KUP for the welcoming and friendly environment and an amazing time.

...my former and current flat mates who have given me not only a roof over my head but a true home in Bern.

And finally, I want to thank Anita and all my friends and family and everyone who did not get mentioned yet who have supported me through the rough and the easy times with their love and their friendship.

Publications

Papers published: (ordered by date):

[1] **Müller, J.**, Nawrot, M., Menzel, R., and Landgraf, T., 2018. A neural network model for familiarity and context learning during honeybee foraging flights, *Biological Cybernetics*, 112(1–2), 113–126.

[2] Joos, F., Spahni, R., D. Stocker, B., Lienert, S., **Müller, J.**, Fischer, H., Schmitt, J., Colin Prentice, I., Otto-Bliesner, B., and Liu, Z., 2020. N2O changes from the Last Glacial Maximum to the preindustrial – Part 2: Terrestrial N2O emissions and carbon-nitrogen cycle interactions, *Biogeosciences*, 17(13), 3511–3543.

[3] **Müller, J.** and Joos, F., 2020. Global peatland area and carbon dynamics from the Last Glacial Maximum to the present – a process-based model investigation, *Biogeosciences*, 17(21), 5285–5308.

[4] Saunois, M., Stavert, A. R., Poulter, B., Bousquet, P., Canadell, J. G., Jackson, R. B., Raymond, P. A., Dlugokencky, E. J., Houweling, S., Patra, P. K., Ciais, P., Arora, V. K., Bastviken, D., Bergamaschi, P., Blake, D. R., Brailsford, G., Bruhwiler, L., Carlson, K. M., Carrol, M., Castaldi, S., Chandra, N., Crevoisier, C., Crill, P. M., Covey, K., Curry, C. L., Etiope, G., Frankenberg, C., Gedney, N., Hegglin, M. I., Höglund-Isaksson, L. , Hugelius, G., Ishizawa, M., Ito, A., Janssens-Maenhout, G., Jensen, K. M., Joos, F., Kleinen, T., Krummel, P. B., Langenfelds, R. L., Laruelle, G. G., Liu, L., Machida, T., Maksyutov, S., McDonald, K. C., McNorton, J., Miller, P. A., Melton, J. R., Morino, I., **Müller, J.**, Murguia-Flores, F., Naik, V., Niwa, Y., Noce, S., O'Doherty, S., Parker, R. J., Peng, C., Peng, S., Peters, G. P., Prigent, C., Prinn, R., Ramonet, M., Regnier, P., Riley, W. J., Rosentreter, J. A., Segers, A., Simpson, I. J., Shi, H., Smith, S. J., Steele, L. P., Thornton, B. F., Tian, H., Tohjima, Y., Tubiello, F. N., Tsuruta, A., Viovy, N., Voulgarakis, A., Weber, T. S., van Weele, M., van der Werf, G. R., Weiss, R. F., Worthy, D., Wunch, D., Yin, Y., Yoshida, Y., Zhang, W., Zhang, Z., Zhao, Y., Zheng, B., Zhu, Q., Zhu, Q., and Zhuang, Q., 2020. The Global Methane Budget 2000–2017, *Earth System Science Data*, 12(3), 1561–1623.

[5] Loisel, J., Gallego-Sala, A. V., Amesbury, M. J., Magnan, G., Anshari, G., Beilman, D. W., Benavides, J. C., Blewett, J., Camill, P., Charman, D. J., Chawchai, S., Hedgpeth, A., Kleinen, T., Korhola, A., Large, D., Mansilla, C. A., **Müller, J.**, van Bellen, S., West, J. B., Yu, Z., Bubier, J. L., Garneau, M., Moore, T., Sannel ,A. B., Page, S., Väliranta, M., Bechtold, M., Brovkin, V., Cole, L. E., Chanton, J. P., Christensen, T. R., Davies, M. A., De Vleeschouwer, F., Finkelstein, S. A., Frolking, S., Ga lka, M., Gandois, L., Girkin, N., Harris, L. I., Heinemeyer, A., Hoyt, A. M., Jones, M. C., Joos, F., Juutinen, S., Kaiser, K., Lacourse, T., Lamentowicz, M., Larmola, T., Leifeld, J., Lohila, A., Milner, A. M., Minkkinen, K., Moss,

P., Naafs, B. D., Nichols, J., O'Donnell, J., Payne, R., Philben, M., Piilo, S., Quillet, A., Ratnayake, A. S., Roland, T. P., Sjögersten, S.,Sonnentag, O., Swindles, G. T., Swinnen, W., Talbot, J., Treat, C., Valach, A. C., and Wu, J., 2021. Expert assessment of future vulnerability of the global peatland carbon sink, *Nature Climate Change*, 11(1), 70–77.

[6] **Müller, J.** and Joos, F., 2021. Committed and projected future changes in global peatlands – continued transient model simulations since the Last Glacial Maximum, *Biogeosciences*, 18(12), 3657–3687.

Papers in review/preparation:

[7] Qiu, C., Ciais, P., Zhu, D., Guenet, B., Chang, J., Chaudhary, N., Kleinen, T., Li, X., **Müller, J.**, Xi, Y., Zhang, W., Ballantyne, A., Brewer, S. C., Brovkin, V., Charman, D. J., Gustafson, A., Gallego-Sala, A. V., Gasser, T., Holden, J., Joos, F., Kwon, M. J., Lauerwal, R., and Westermann, S., 2021. Emerging role of northern peatlandsin the future greenhouse gas balance, in review at *PNAS*

[8] Aalto, T., Tsuruta, A., Mäkelä, J., **Müller, J.**, Tenkanen, M., Burke, E., Chadburn, S., Gao, Y., Kangasaho, V., Kleinen, T., Lee, H., Leppänen, A., Markkanen, T., Materia, S., Miller, P., Peano, D., Peltola, O., Raivonen, M., Saunois, M., Wårlind, D., and Zaehle, S., 2021 Air temperature and precipitation constraining the modelled wetland methane emissions in a boreal region in Northern Europe, in preparation.

Erklärung

gemäss Art. 18 PromR Phil.-nat. 2019

Name, Vorname:	Müller, Jurek
Matrikelnummer:	17-134-131
Studiengang:	Climate Sciences
	Bachelor ☐ Master ☐ Dissertation ☒
Titel der Arbeit:	Wetlands through time – modeling changes in area and greenhouse gas budgets from the past to the future
Leiter der Arbeit:	Prof. Dr. Fortunat Joos

Ich erkläre hiermit, dass ich diese Arbeit selbständig verfasst und keine anderen als die angegebenen Quellen benutzt habe. Alle Stellen, die wörtlich oder sinngemäss aus Quellen entnommen wurden, habe ich als solche gekennzeichnet. Mir ist bekannt, dass andernfalls der Senat gemäss Artikel 36 Absatz 1 Buchstabe r des Gesetzes über die Universität vom 5. September 1996 und Artikel 69 des Universitätsstatuts vom 7. Juni 2011 zum Entzug des Doktortitels berechtigt ist. Für die Zwecke der Begutachtung und der Überprüfung der Einhaltung der Selbständigkeitserklärung bzw. der Reglemente betreffend Plagiate erteile ich der Universität Bern das Recht, die dazu erforderlichen Personendaten zu bearbeiten und Nutzungshandlungen vorzunehmen, insbesondere die Doktorarbeit zu vervielfältigen und dauerhaft in einer Datenbank zu speichern sowie diese zur Überprüfung von Arbeiten Dritter zu verwenden oder hierzu zur Verfügung zu stellen.

Bern, 03. August 2021

Unterschrift